

LV-2012-112



Landsvirkjun



Námafjall Geothermal Area, Northern Iceland

3D Inversion of MT and TEM Data

Report no: LV-2012-112



Námafjall Geothermal Area, Northern Iceland

3D Inversion of MT and TEM Data



ÍSOR-2012/057

Project no.: 700010

December 2012

Key Page

LV report no: LV-2012-112 **Date:** December 2012

Number of pages: 139+CD **Copies:** 10 **Distribution:** On www.lv.is
 Open
 Limited until

Title: Námafjall Geothermal Area, Northern Iceland. 3D Inversion of MT and TEM Data

Authors/Company: Ragna Karlsdóttir, Andemariam Teklesenbet Beyene and Arnar Már Vilhjálmsson

Project manager: Ásgrímur Guðmundsson (LV) Magnús Ólafsson (ÍSOR)

Prepared for: Prepared by Iceland GeoSurvey (ÍSOR) for Landsvirkjun.

Co operators:

Abstract: A 3D inversion of TEM/MT resistivity data from Námafjall high temperature area shows a conventional resistivity structure for a high temperature system, a low resistivity cap underlain by a high resistivity core. The low resistivity cap reaches surface at Námafjall, where also the highest elevation of the high resistivity core is encountered. Deep seated low resistivity body indicating the heat source of the geothermal system is present under Námafjall geothermal system. An up flow of heat into the system is indicated by two anomalies, one under Námafjall and another south east of Hverfjall. The Námafjall low resistivity anomaly domes up to 1500 m b.sl. under Námafjall mountain and seems to indicate the main up flow zone into the geothermal system. The Hverfjall low resistivity anomaly domes up to 3000 m b.s.l. just south east of Hverfjall and may indicate a second up flow zone into the geothermal system.

Keywords: TEM/MT resistivity survey, resistivity structure of a high temperature system, deep seated low resistivity body, heat source

ISBN no:

Approved by Landsvirkjun's project manager

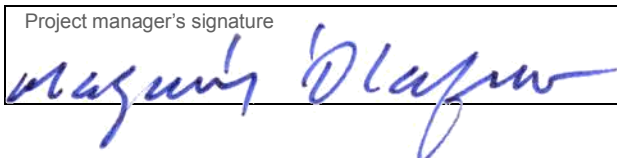
| | |
|--|--------------------|
| Project manager's signature  | Reviewed by GKR |
|--|--------------------|

Table of contents

| | | |
|----------|---|------------|
| 1 | Introduction | 7 |
| 2 | The resistivity survey | 8 |
| 2.1 | The role of resistivity surveying in geothermal exploration..... | 8 |
| 2.2 | Data acquisition..... | 9 |
| 2.3 | Data processing | 11 |
| 3 | 3D inversion | 12 |
| 3.1 | Data preparation | 13 |
| 3.2 | The model grid | 13 |
| 3.3 | Initial and prior models | 16 |
| 3.4 | The inversion | 17 |
| 4 | Comparison of different initial models | 18 |
| 5 | Presentation of the 3D model | 26 |
| 6 | Discussion of the 3D model | 27 |
| 6.1 | Resistivity maps | 27 |
| 6.2 | Resistivity cross sections | 37 |
| 6.3 | EW bound resistivity cross sections (Figure 15)..... | 38 |
| 6.4 | NS bound resistivity cross sections (Figure 15)..... | 49 |
| 7 | Conclusion | 55 |
| 8 | References | 57 |
| | Appendix 1: Resistivity maps | 59 |
| | Appendix 2: East – west resistivity cross sections | 75 |
| | Appendix 3: North – south resistivity cross sections | 105 |
| | Appendix 4: Datafit | 121 |

List of figures

| | | |
|------------|--|----|
| Figure 1. | <i>Hverfjall and Námafjall geothermal field.</i> | 8 |
| Figure 2. | <i>A schematic picture of an MT equipment installation in the field.</i> | 10 |
| Figure 3. | <i>The model grid with 250 m between the vertical planes.</i> | 15 |
| Figure 4. | <i>The model grid</i> | 16 |
| Figure 5. | <i>Comparison of models at 200 m a.sl.</i> | 19 |
| Figure 6. | <i>Comparison of models at 1500 m a.sl.</i> | 20 |
| Figure 7. | <i>Comparison of models at 2000 m a.sl.</i> | 21 |
| Figure 8. | <i>Comparison of models at 2500 m a.sl.</i> | 22 |
| Figure 9. | <i>Comparison of models at 3500 m a.sl.</i> | 23 |
| Figure 10. | <i>Comparison of models at 5000 m a.sl.</i> | 24 |

| | |
|--|----|
| Figure 11. Comparison of models at 8000 m a.sl. | 25 |
| Figure 12. MT and TEM soundings at Námafjall area | 26 |
| Figure 13. Resistivity at 200 m a.sl. | 28 |
| Figure 14. Resistivity at sea level..... | 29 |
| Figure 15. Resistivity at 500 m b.sl. | 30 |
| Figure 16. Resistivity at 1000 m b.sl. | 31 |
| Figure 17. Resistivity at 1000 m b.sl. | 32 |
| Figure 18. Resistivity at 2500 m b.sl. | 33 |
| Figure 19. Resistivity at 5000 m b.sl. | 34 |
| Figure 20. Resistivity at 8000 m b.sl. | 35 |
| Figure 21. Resistivity at 10000 m b.sl. | 36 |
| Figure 22. Resistivity cross sections | 37 |
| Figure 23. Resistivity cross section EW_N4625 down to 5 km b.s.l. | 38 |
| Figure 24. Resistivity cross section EW_N3625 down to 5 km b.s.l. | 39 |
| Figure 25. Resistivity cross section EW_N3375 down to 5 and 15 km b.s.l. | 40 |
| Figure 26. Resistivity cross section EW_N2875 down to 5 and 15 km b.s.l. | 41 |
| Figure 27. Resistivity cross section EW_N2625 down to 5 and 15 km b.s.l. | 42 |
| Figure 28. Resistivity cross section EW_N2375 down to 5 and 15 km b.s.l. | 43 |
| Figure 29. Resistivity cross section EW_N1375 down to 5 and 15 km b.s.l. | 44 |
| Figure 30. Resistivity cross section EW_N625 down to 5 and 15 km b.s.l. | 45 |
| Figure 31. Resistivity cross section EW_N375 down to 5 km b.s.l. | 46 |
| Figure 32. Resistivity cross section EW_N125 down to 5 km b.s.l. | 46 |
| Figure 33. Resistivity cross section EW_N-125 down to 5 15 km b.s.l. | 47 |
| Figure 34. Resistivity cross section EW_N-2875 down to 5 and 15 km b.s.l. | 48 |
| Figure 35. Resistivity cross section EW_N-4625 down to 5 km b.s.l. | 49 |
| Figure 36. Resistivity cross section NS_E-625 down to 5 and 15 km b.s.l. | 50 |
| Figure 37. Resistivity cross section NS_E-125 down to 5 and 15 km b.s.l. | 51 |
| Figure 38. Resistivity cross section NS_E125 down to 5 and 15 km b.s.l. | 52 |
| Figure 39. Resistivity cross section NS_E375 down to 5 and 15 km b.s.l. | 53 |
| Figure 40. Resistivity cross section NS_E875 down to 5 and 15 km b.s.l. | 54 |
| Figure 41. Resistivity cross section NS_E1375 down to 15 km b.s.l. | 55 |

1 Introduction

At the request of Landsvirkjun, ÍSOR applied MT measurements at Námafjall in 2009. Landsvirkjun asked for the minimum amount of MT soundings to determine the resistivity structures at depth under the geothermal system at Námafjall as well as adding TEM and MT soundings south of Námafjall to see if the geothermal system had an extension to south.

The results of 1D inversion of the TEM and MT measurements revealed a deep seated low resistivity layer under Námafjall geothermal field, arching up under the area where most surface manifestations are present, in Námafjall and Hverarönd. The low resistivity layer is centred at 9–10 km depth under most of the geothermal field tilting toward north, as far as the limited amount of soundings can tell. It reaches the depth of about 3 km under Námafjall and Hverarönd (Karlsdóttir, 2011).

The geothermal field takes name after the mountain Námafjall (the mountain by the mines). Sulphur was mined from Námafjall for centuries and exported until the middle of nineteenth century. The main surface manifestations, sulphur and hydrothermally altered rocks are present in the slopes of Námafjall, east of it in Hverarönd and to the west in Bjarnarflag. Hverarönd has a great tourist attraction as it holds an area with colourful surface manifestations, mud pits and steam vents, many of which are old shallow drill holes now covered with stones. The main well field until now is in Bjarnarflag and therefore the name Bjarnarflag is commonly used when referring the geothermal field. In this report, the name Námafjall is used for the gross geothermal field but the name Bjarnarflag applies to the geothermal area west of the Námafjall mountain.

In 2011 ÍSOR added MT measurements at the same location as most of the existing TEM sites in the Námafjall area, as well as extending the survey to south with additional TEM and MT soundings. The data coverage was further improved in 2012, when 11 MT and 5 TEM soundings were added, to accommodate 3D inversion of the data. A total of 69 TEM/MT sounding pairs are available for interpretation.

In this report a 3D inversion model of the MT/TEM data will be discussed. 3D inversion of electromagnetic data enhances the reliable and detailed results than an inversion in terms of layered earth (1D inversion). Improvements in computer technology and software development have made 3D inversion of MT data practical. In this report a 3D interpretation of the static shift corrected MT data will be presented. In order to study the robustness of the results, the 3D inversion was done using different initial models and in this report results from three different initial models are compared to the results of the joint 1D inversion of the TEM and MT data (see Karlsdóttir, 2011).

Knútur Árnason is the supervisor of the application of 3D inversion of resistivity data at ÍSOR. He supervised the preparations of MT data for the 3D inversion at Námafjall. Andemariam Teklesenbet Beyene prepared the data for the 3D inversion and ran the 3D inversion program. Arnar Már Vilhjálmsson wrote the technical part of the report. Ragna Karlsdóttir processed the TEM data and the MT data, performed the joint

inversion of the 1D model, prepared the MT data for the 3D inversion and wrote the report other than the technical part.



Figure 1. *Hverfjall and Námafjall geothermal field.*

2 The resistivity survey

2.1 The role of resistivity surveying in geothermal exploration

The main factors influencing resistivity in rocks are water content, salinity and temperature of the fluid, and the type of hydrothermal alteration of the rocks due to geothermal activity. In essence, water-saturated rocks conduct electrical currents more readily than dry rocks and conductivity increases with increasing temperature up to about 300°C (Violay et al., 2010). Geothermal systems can be distinguished from the surroundings because the electrical conductivity (resistivity) of certain clay minerals (phyllosilicates, such as smectite) found in fractures in the rocks are strongly temperature dependent. The electrical resistivity of the rocks is only weakly influenced by the salinity of the fluid, unless the salinity is very high and approaches that of seawater (Flóvenz et al., 2005).

Surface resistivity surveys of high-temperature geothermal systems in the basaltic rocks of the volcanic zones of Iceland (and where the host rocks are volcanic) always seem to commonly reveal similar resistivity structure which correlates to the distribution of alteration mineralogy. A low resistivity cap is observed on the outer and the upper margins of the reservoirs and is underlain by a more resistive core. Extensive comparison of this resistivity structure to well data has revealed a consistent correlation to the zones of dominant alteration minerals. The low-resistivity cap coincides with the smectite-zeolite zone and the transition to the more resistive core occurs within the mixed layer clay zone. Within the resistive core chlorite and epidote are the dominant alteration minerals. The alteration mineralogy is mostly influenced by temperature. This has the consequence that if the alteration is in equilibrium with present formation temperature, the resistivity structure can be interpreted in terms of

temperature,. The upper boundary of the low-resistivity cap is found where the temperature is in the range of 50–100°C and the transition to the resistive core occurs at temperatures in the range of 230–250°C (Árnason et al., 2000).

The resistivity reflects the hydrothermal alteration caused by the heating of the rocks and reflects the peak temperature experienced by the system, being it at the present or in the past. Thus, resistivity measurements reveal the alteration but do not indicate whether cooling has occurred after the alteration was formed because the resistivity profile only captures the alteration in the formation, irrespective of any later cooling of the system. The resistivity structure reflects the temperature, provided there is equilibrium between alteration and present temperature. In case of cooling the alteration may remain and the resistivity will reflect the temperature at which the alteration was formed. Whether the resistivity (and the alteration) indicates the present temperature of the system will only be confirmed by drilling.

Wherever MT measurements have been conducted in the volcanic zones in Iceland, a deep-seated low-resistivity layer is seen at a 10–15 km depth. The upper boundary (10 Ω m contact) of this low-resistivity layer arches up to a depth as shallow as 2–3 km beneath high-temperature geothermal systems, e.g., in the Krafla area (Mortensen et al., 2009). As the low-resistivity layer is thought to reflect very high temperatures, it is interpreted as providing information about upwelling of heat into geothermal systems. Plume-like low-resistivity anomalies in limited areas beneath the deep low-resistivity layer, as seen in TEM and MT measurements at Upptyppingar (Vilhjálmsón et al., 2008), also support the idea of active up-flow of hot material (magma?).

2.2 Data acquisition

The acquisition of the bulk of the TEM and MT data has been accounted for in a previous report on the joint 1D inversion (Karlsdóttir, 2011) and will only be briefly described here. ÍSOR performed an MT survey of the area and applied 35 soundings at two double profiles across Námafjall mountain in 2009, followed by 1D interpretation of the MT data along with the existing TEM data (Karlsdóttir, 2011). As the results revealed a deep seated low resistivity layer and an extension of the geothermal field towards south, it was decided to cover the Námafjall area with MT soundings in 2011 at all available TEM sites to give a better account of the resistivity structure (26 MT and 10 TEM soundings). After reviewing the results with the new soundings, further 11 MT soundings and 5 TEM soundings were added to the survey in 2012, where 3 of the MT soundings were repeated at previously measured locations. Thus a total of 69 MT/TEM pairs will be used for the 3D inversion.

The MT instruments used in this campaign are from Phoenix Ltd. in Canada (MTU type) and can measure the MT signals in the frequency range up to 1000 Hz and down to 0.00002 Hz (Phoenix Geophysics, 2009). Four sets of MT equipment were used in the field work. One served as a base station for remote reference processing of the data and was located outside the survey area. The remaining three MT units were operated in the investigation area, i.e. moved to a new location every day for recording till the next day, recording for 16–22 hours at each site. Three of the MT units measure five components (E_x , E_y , H_x , H_y and H_z); the base station and two of the others. The fourth

station measures only the electric field, i.e. E_x , E_y . The two component unit is always set up close to a five component site (around 1 km away), and the magnetic field at that site used for the data processing. This approach is chosen if the magnetic field is almost identical at the two stations, valid for short distances.

In 2009 the reference station was set up at Hólásandur, approximately 10 km from Námafjall and in 2012 it was set up in Þrengsli in Hellisheiði, south Iceland, some 300 km away. In 2011, one of the 5 component MT instruments was out of order and no fixed base station was set up. Instead, an MT survey was conducted simultaneously in Þeistareykir and Námafjall and a 5 component station in one survey area was used as a reference for the other 5 component unit in the other survey area.

The MT method

Magneto telluric methods use time variations of the Earth's magnetic field to investigate the resistivity structure of the earth. The time varying magnetic field represents electromagnetic waves that penetrate the earth. By measuring simultaneously the magnetic and electric field variations in the surface, which are coupled through Maxwell's equations, inference can be made about the subsurface resistivity.

The horizontal components of the electric and magnetic fields are determined by measuring voltage in short (~50 m) orthogonal grounded dipoles and induction in orthogonal induction coils, respectively (Figure 2). The field layout defines a coordinate system with one of the dipoles and one of the coils parallel to the x-axis, normally taken to be in magnetic N-S, and the other dipole and coil along the y-axis in magnetic E-W. The magnetic declination is 13 degrees west of north and hence the x-axis is oriented N13°W in the present survey.

The electrical dipoles consist of two non-polarizing electrodes (lead/lead-chloride in this case) connected to the data-logger by cables. The induction coils are normally buried to avoid them from shaking (in the wind) which generates noise to the measurements. The vertical component of the magnetic field is usually also measured by a buried vertical induction coil.

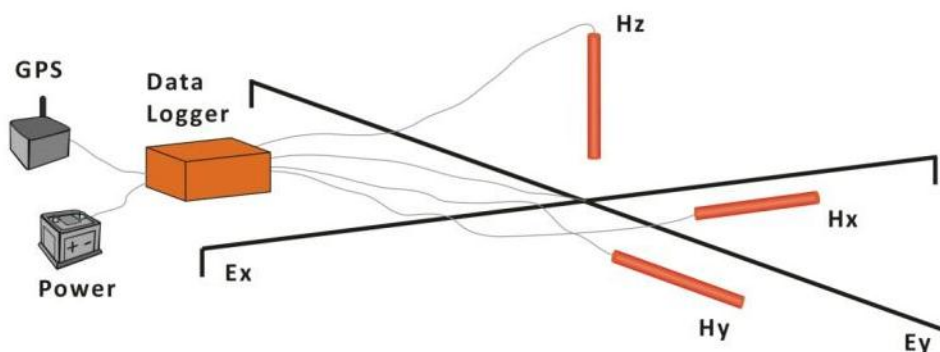


Figure 2. A schematic picture of an MT equipment installation in the field.

The electric and magnetic field variations are measured as a function of time or as time series. The time series are composed (a sum) of harmonic (sinusoidal) components of different periods (frequencies). Short period (high frequency) waves are attenuated at shallow depth and hence do not penetrate deep but the longer the period (lower the frequency) the deeper the waves probe into the earth. In the processing of the MT data the time series are sorted into different frequencies (by Fourier transformation) and the relation between the electric and magnetic fields give information about the resistivity at different depths. MT can therefore penetrate from shallow depths to the depth of several tens of kilometres.

2.3 Data processing

The measured MT time series are Fourier transformed into the frequency domain and the “best” solution that describes the relation between the electrical and magnetic field is found through the following equation:

$$\begin{bmatrix} E_x \\ E_y \end{bmatrix} = \begin{bmatrix} Z_{xx} & Z_{xy} \\ Z_{yx} & Z_{yy} \end{bmatrix} \begin{bmatrix} H_x \\ H_y \end{bmatrix}$$

or in matrix notation:

$$\vec{E} = \mathbf{Z}\vec{H}$$

where, \vec{E} and \vec{H} are the electrical and magnetic field vectors (in the frequency domain) and \mathbf{Z} is a complex impedance tensor which contains information on the subsurface resistivity structure. Programs from Phoenix Geophysics (2005) were used to process the time series using a robust processing method technique (see e.g. Egbert and Booker, 1986) and for editing the results. The output was run through a program developed at ÍSOR, which calculates various MT parameters and produces the results in standard EDI file format (see SEG, 1991). The values of the impedance tensor elements depend on the resistivity structures below and around the site. For a homogeneous and 1D earth $Z_{xy} = -Z_{yx}$ and $Z_{xx} = Z_{yy} = 0$. For a 2D earth, i.e. resistivity varies with depth and in one horizontal direction, it is possible to rotate the coordinate system by mathematical means, such that $Z_{xx} = Z_{yy} = 0$, but $Z_{xy} \neq -Z_{yx}$. For a 3D earth all the impedance tensor elements are different.

From the impedances the apparent resistivity (ρ) and phases (θ) for each frequency are calculated according to

$$\rho_{xy} = 0.2T|Z_{xy}|^2; \theta_{xy} = \arg(Z_{xy})$$

$$\rho_{yx} = 0.2T|Z_{yx}|^2; \theta_{yx} = \arg(Z_{yx})$$

3 3D inversion

The 3D inversion was performed using the inversion program WSINV3DMT written by Prof. Weerachai Siripunvaraporn (Siripunvaraporn et al., 2005; Siripunvaraporn and Egbert, 2009). WSINV3DMT uses finite difference forward algorithm and utilizes a formulation of the inverse problem in the data-space rather than in the model-space. This reduces the dimensionality of the problem dramatically and makes 3D inversion of MT data attainable.

When running a 3D inversion an initial model is required to start the procedure. The initial model can influence the final result but that is further discussed in Section 3.3 and Chapter 4. The process of 3D inversion of MT data is a highly underdetermined problem, i.e. the number of unknown resistivity values is much higher than the number of data values. In the present case the number of data points is 8556 (69 soundings \times 31 periods \times 4 real and imaginary off-diagonal tensor elements, see below) but the model has 151536 unknown resistivity values (in the $74 \times 52 \times 28$ blocks, see below) or almost 13 times the number of data points. The inversion therefore needs to be regularized by imposing constraints on the model (mathematically this means to make the model parameters interdependent in such a way that the number of the actually free parameters is reduced). This can be done by constraining the model parameters to vary smoothly, often referred to as minimum structure or Occam inversion (Constable et al., 1987). Another way of regularizing is using a reference or "prior" model and constrain the inversion model not to deviate too much from the prior model. Using a prior model offers the possibility of fixing some of the model parameters to a priori known values. The inversion code used here aims to minimize a penalty function that consists of a combination of these regularization methods, i.e. minimizes a weighted sums of the 1) difference between measured data and calculated response, 2) the roughness of the model and 3) the deviation from the prior model. Initially, the inversion process quickly adjusts the model to reduce severe misfit of the data. Later on, changes that would further reduce the data misfit are rejected because they make the model deviate too much from the prior model.

The user can adjust the smoothing criteria, but not the weight of the deviation from the prior model. This can constrict the inversion from fitting the measured data adequately, especially if a model that deviates considerably from the prior model is required. Running the inversion in steps, where the initial and prior models are updated at each step (the model that gave the best fit in the previous step), can facilitate the processes of fitting the data. In this way the limitation of the prior model is gradually relaxed until the data fit can no longer be improved.

WSINV3DMT assumes flat surface. This seems to be a limitation, but prior to the inversion, the MT data are corrected for static shift and this correction removes topographic effects in the data to a large extent. The inversion is performed for the complex off-diagonal elements of the MT impedance tensor, i.e. 4 numbers (2 real and 2 imaginary parts) for each period of each sounding. The misfit measure is the RMS misfit of the observed and calculated tensor elements, weighted by the variance of the measured values.

3.1 Data preparation

The processed MT data has the x-axis in true north. In the inversion program the measured data and the model are defined in an internal (local) coordinate system or grid. It is preferable to have one of the grid axis parallel to the dominant electric (resistivity) strike, since the resistivity anomalies are most likely to be aligned in that direction. According to strike analysis of the MT data (not shown in this report) the dominant electric strike is close to the geological strike of N11°E. The internal coordinate system of the model is therefore taken to have x-axis in N11°E and the y-axis in N101°E. The MT impedance tensors were therefore rotated by 24° to the internal system (i.e. 13° to correct for the magnetic declination and then 11° to match the geological strike).

The 3D inversion is performed for the MT tensor elements that may contain static shift. By assuming that the static shift is dominantly due to distortion of the electric field, the tensor can be static shift corrected by the equation:

$$\begin{bmatrix} Z_{xx}^c & Z_{xy}^c \\ Z_{yx}^c & Z_{yy}^c \end{bmatrix} = \begin{bmatrix} C_x & 0 \\ 0 & C_y \end{bmatrix} \begin{bmatrix} Z_{xx} & Z_{xy} \\ Z_{yx} & Z_{yy} \end{bmatrix} ; \quad C_x = \sqrt{1/S_{xy}} \quad ; \quad C_y = \sqrt{1/S_{yx}}$$

where Z^c is the corrected and Z the uncorrected tensor. S_{xy} and S_{yx} are the shift multipliers for apparent resistivity of the xy and yx polarizations, respectively (Árnason et al., 2010). After the rotation of the soundings to the internal coordinate system, a joint 1D inversion was performed of the apparent resistivity and phase for both xy and yx polarizations and the nearby TEM sounding in order to determine the static shift multipliers (Árnason, 2008).

The computational intensity in the inversion is directly proportional to the number of periods to be inverted for. The raw data generally contain 78 different periods ranging from about 0.003 to 2940 s with 13 periods per decade. To reduce the computation cost, the static shift corrected tensor was re-sampled at 31 periods equally spaced on log scale (six values per decade), from 0.0063 to 1000 s. This choice of periods is a “trade off” between computational cost on the one hand and resolution and depth of investigation on the other. For physical consistency, the MT tensor must be a smooth function of the logarithm of the period (Weidelt, 1972). Inverting for six periods per decade is generally considered to give enough resolution. The period range and the resistivity determine the depth range of exploration (the shorter the period and lower the resistivity, the shallower resistivity structures can be resolved and the longer the period and the higher the resistivity, the deeper structures can be resolved).

3.2 The model grid

The model grid is set out so that the dense part of the grid covers the main area of data coverage. The model used for the inversion was run with mesh with 250 m grid pane spacing in the central area of the data coverage.

The 3D model consists of resistivity cubes in a 3D grid mesh defining the internal coordinate system. The origin (centre) of the internal coordinate system is at the UTM

(zone 28) coordinates (in km) 415,6E and 7278,7N (approximately at the centre of the area of interest and data coverage), and with x-axis positive towards N11°E and y-axis positive towards N101°E. The mesh has 75 vertical grid planes (two edges and 73 internal planes) in the x-direction (perpendicular to the x-axis) and 53 vertical (two edges and 51 internal planes) in the y-direction and 29 horizontal grid planes (surface, bottom and 27 horizontal internal planes). The grid is dense in the area of interest with grid plane spacing of 250 m in the area of the data coverage, that is in the range of ± 6 km in the x-direction (SW-NE) and $\pm 3,25$ km in the y-direction (NW-SE). Outside the dense area the grid spacing increases exponentially to the edges at $\pm 137,268$ km and $\pm 134,518$ km in the x- and y-directions, respectively. Figure 3 shows a horizontal slice of the central part of the model grid mesh and the location of the MT soundings in the grid. Red star shows the origin (middle point) of the grid. All resistivity cross sections are named with reference to their position in the grid and are named by distance from origin. A cross section, EW_N2000, refers to the EW cross section that is 2000 m to the north of origin point. Figure 4 shows a larger part of the model grid and the coastal line to the north.

The horizontal grid planes are likewise dense at shallow depth but eventually with exponentially increasing spacing to the bottom at the depth of 160,684 km. The shallowest layer thicknesses are 16, 26, 36, 50, 76, 100, 158, 200 m etc.

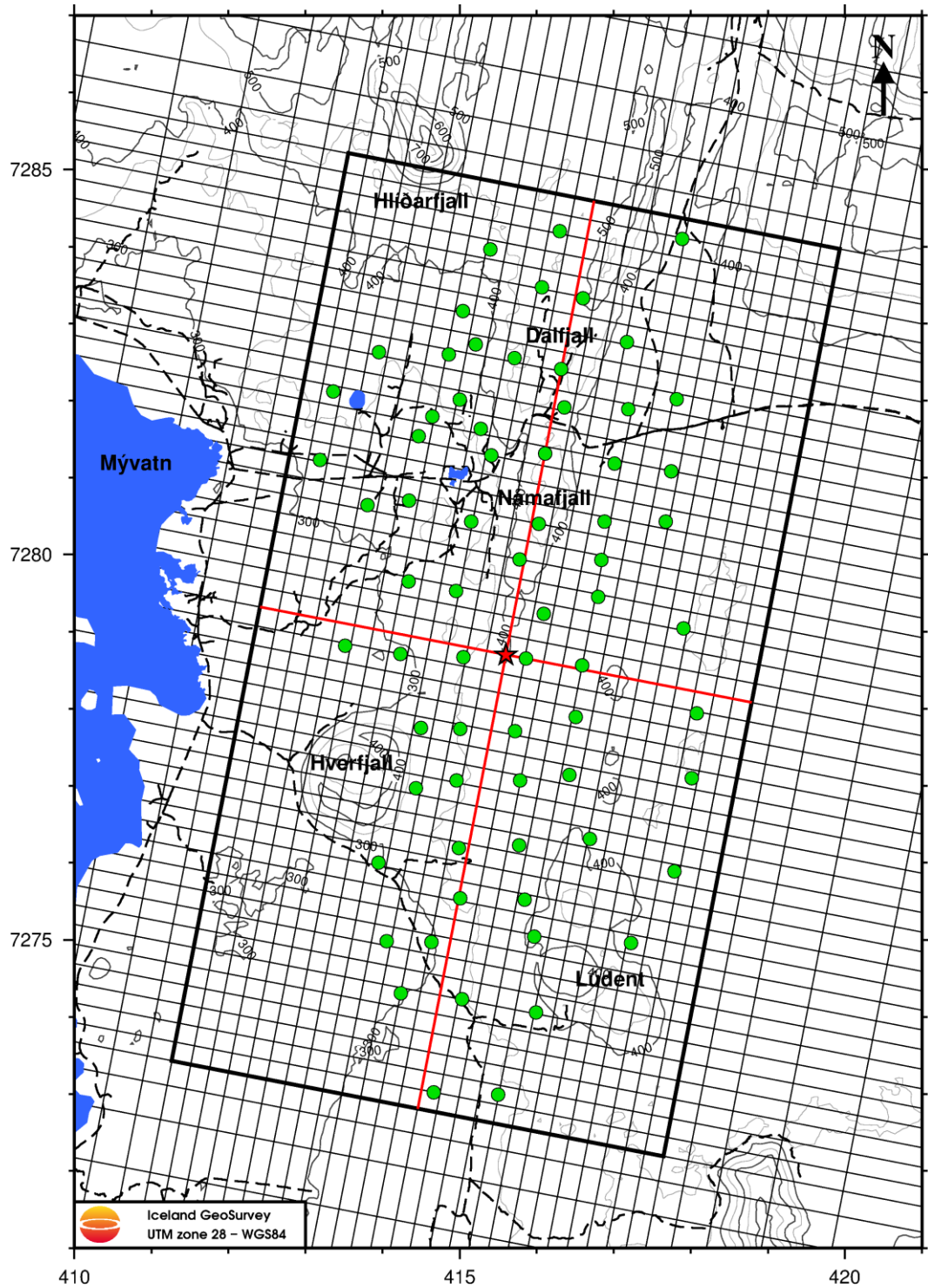


Figure 3. The model grid with 250 m between the vertical planes. The heavy black line marks the area of interest (8 x 12 km). Red star shows the origin and green dots show the MT/TEM sites.

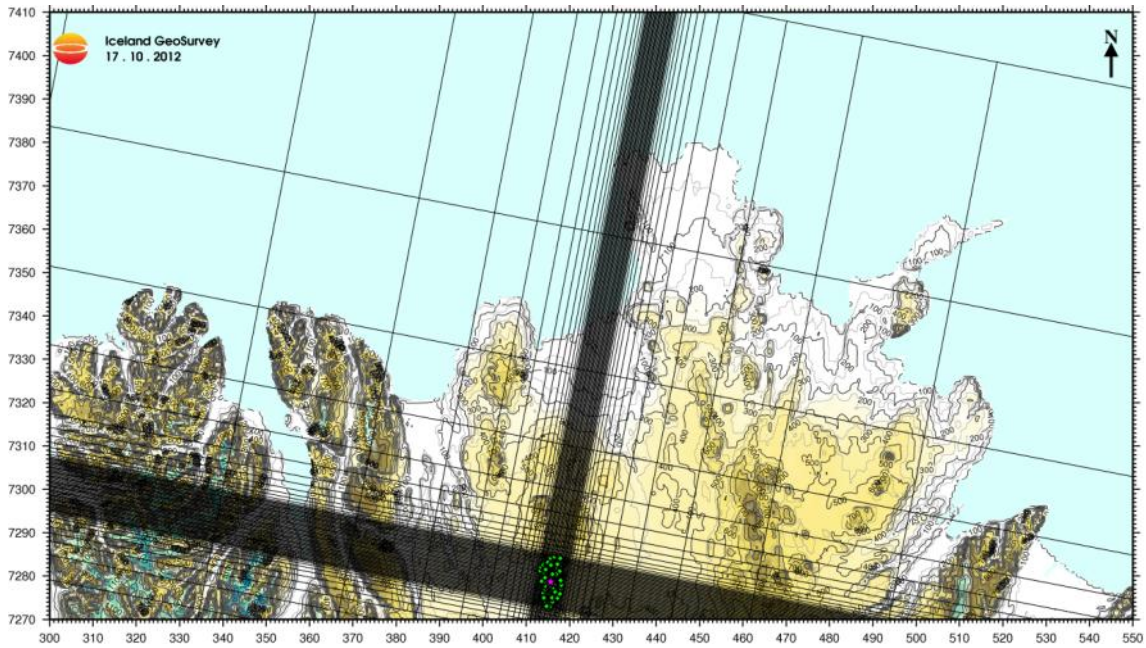


Figure 4. The model grid. The dense grid, shown as grey shade, covers the survey area. MT soundings are marked as green dots.

3.3 Initial and prior models

As discussed earlier, 3D inversion of MT data is a highly underdetermined problem. The inversion is started from an initial model and in order to regularize the inversion, a prior model is used to constrain the deviation of the resulting model from the prior model. As a consequence of this the resulting model will depend on the initial and prior model.

Some components of the prior model can, in some cases be assumed to be known a priori and even fixed in the inversion. In the case of the Námafjall area, the proximity of the sea (ca. 40 km) will probably not have a great influence but will be taken into account as it may have some impact in the MT data, at long periods. The sea has therefore to be taken into account in the inversion and the resistivity of the model cells in the sea were assigned the average resistivity of seawater ($0.3 \Omega\text{m}$) and the inversion is forced to keep it fixed. The proximity to the Mývatn Lake was not considered in the inversion, as the lake is not saline and is very shallow.

To investigate the influences of the initial model on the resulting models, inversions with five distinct initial models were done. In all cases the same model was used as initial and prior model. Out of these five inversions, three results will be discussed in this report:

- (1) A model compiled from joint 1D inversion of individual TEM/MT sounding pairs (Karlisdóttir, 2011).
- (2) A homogeneous half-space model with resistivity $70 \Omega\text{m}$.

- (3) A model compiled from the resulting 3D model from (1) down to 3196 meters depth and a homogeneous half-space of $71 \Omega\text{m}$ below that (referred to as “Final 1D / Homog. Earth, $71 \Omega\text{m}$ ” in chapter 4).

As discussed above, a step procedure was used during all the inversion. The inversion was allowed to run for 5 iterations at each step and restarted. This stepwise inversion (and relaxation of the prior model) was continued until the data fit could not be improved any more (4–7 steps).

3.4 The inversion

The inversion program was executed using a parallel processing version of the WSINV3DMT code using the Message Passing Interface (MPI) parallel computing environment (Siripurvaraporn, 2009). It was executed on a 32 core computer with 132 GB memory. The inversion is a very heavy computational task and each iteration with the 250 m grid spacing, took about 7–8 hours and the total computing time was more than 250 hours.

The data misfit is defined as the RMS (Root-Mean-Square) of the difference between the measured and calculated values, weighted by the variance of the measured values. In all cases the off diagonal tensor elements (real and imaginary parts) were used.

For the initial model compiled from the 1D model, the initial misfit was 5.32 and the lowest obtained misfit was 1.74. For the initial model based on 1D result above 3196 m b.sl. and $71 \Omega\text{m}$ homogeneous half-space beneath that, the initial RMS misfit was 17.3 and the final misfit was 1.94. For the $70 \Omega\text{m}$ homogeneous half-space initial model, the initial RMS misfit was 21.8 and the final misfit was 1.87. The final data fit are comparable for all these inversion results and the longer periods are generally more difficult to fit. A comparison of the (re-sampled) measured data for all the inverted soundings (presented as apparent resistivity and phase) and the calculated response of the final model from the inversion with the 1D initial model is shown in Appendix 4.

4 Comparison of different initial models

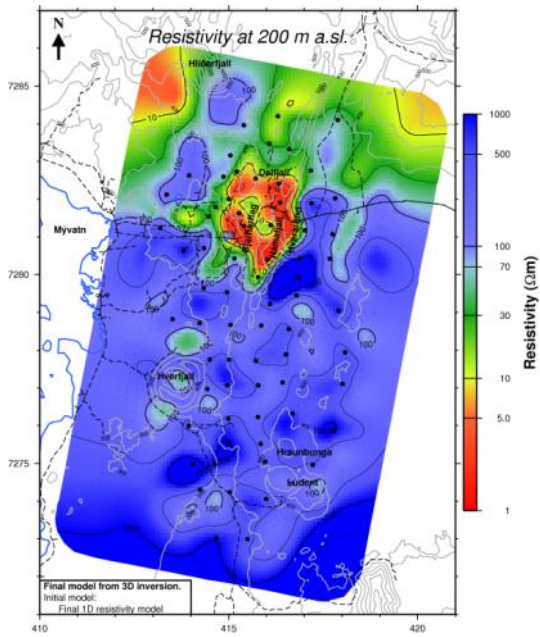
To test the robustness of the 3D resistivity models, it is important to inspect anomalies that are identical or similar in all of them. The initial model compiled from the final results of the 1D inversion includes high and low resistivity bodies. During the 3D inversion these bodies are altered as necessary to fit the data, possibly leaving high or low resistivity zones that are not resolved in the data. The 3D program assumes flat surface, so by correcting for static shift in the MT data prior to the inversion, the effect of the topography was largely removed. The resistivity models resulting from the inversion are elevation corrected, i.e. the depths below each model cell are converted to meters above sea level.

To lend more confidence in the resistivity anomalies, the inversion was run with homogeneous input model with resistivity of 70 Ωm . The inversion only introduces resistivity structures were needed, giving confidence in anomalies that differs considerably from 70 Ωm . The inversion had difficulties resolving the resistivity at greater depths than 3000 m b.sl. and the resulting model is almost homogeneous below 8 km b.sl. and hence the data fit for the longest periods are not as good as for the other periods. To further try to resolve the deep resistivity structure, a new input model was constructed. The uppermost 3196 m were identical to the resulting 3D model from the inversion with final 1D result as input model, underlain by homogeneous earth of 71 Ωm . A comparison between the

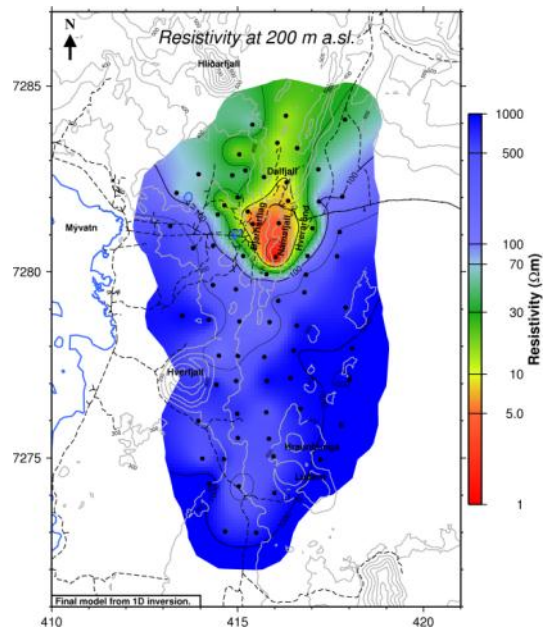
- 3D model based on the 1D inversion (RMS fit = 1,74)
- 1D model
- 3D model based on the 1D model in the uppermost 3196 m and a homogeneous initial resistivity of 71 Ωm below that (RMS fit = 1,94)
- 3D model based on a homogeneous model with initial resistivity of 70 Ωm (RMS fit = 1,87)

will be presented on the following pages for clarification. We look at the models at various depths from 200 m a.sl. to 8 km b.sl. (Figures 5–11). The location of TEM and MT soundings are shown in figure 12.

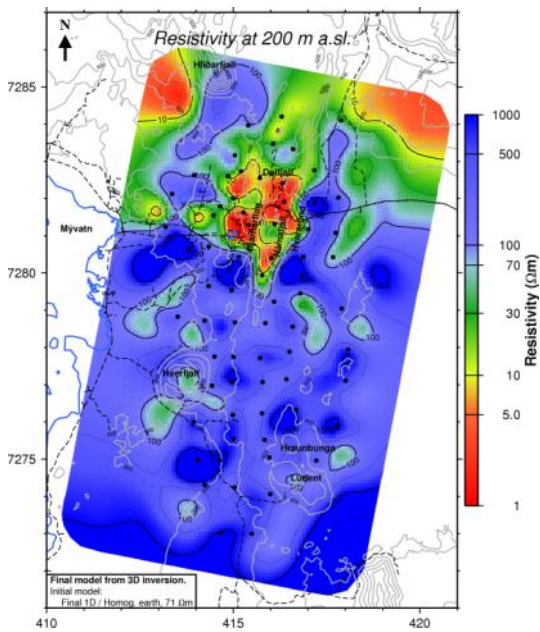
Figure 5 shows resistivity at 200 m a. sl. and displays the top of the low resistivity cap at 200–250 m below surface. The same character is seen in all four maps, the only difference is the smoothed appearance of the 1D model. This is to be expected as the 1D inversion gives result for each sounding and does not resolve the volume between the soundings. All models reveal a clear picture of the low resistivity cap but more constraints and more details are seen in the 3D models. Artefacts outside data coverage in the 3D models should be disregarded.



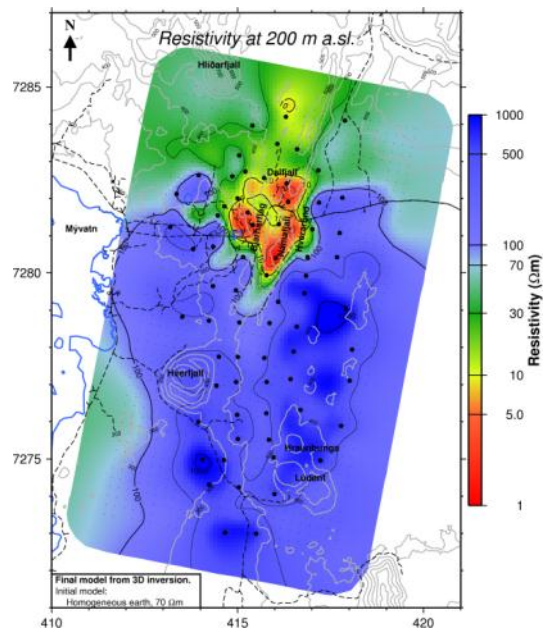
3D model with 1D input model



1D model



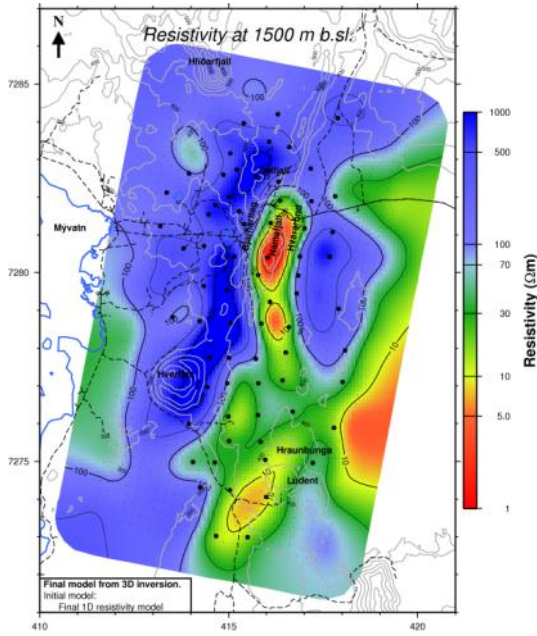
3D model with 1D/Homog 71Ωm



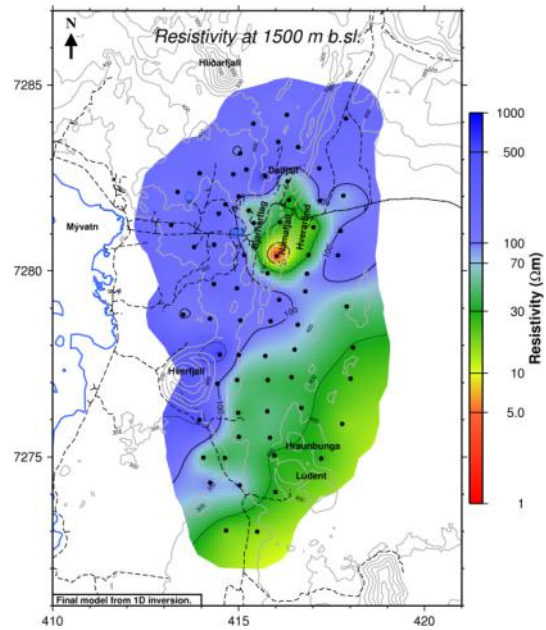
3D model with Homog. 70 Ωm

Figure 5. Comparison of models at 200 m a.s.l.

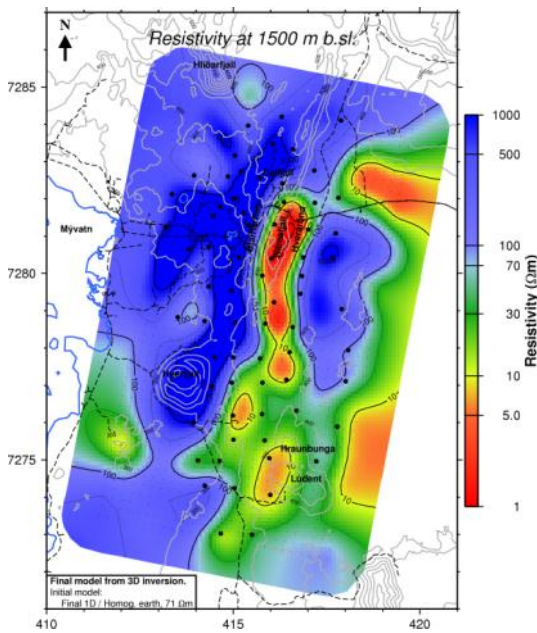
Figure 6 shows the resistivity at 1500 m b.sl. The 1D model reveals the top of the deep seated low resistivity under Námafjall. In the 3D models where 1D model has been used as input model, the top of the deep seated low resistivity appears under Námafjall. However in the 3D model where homogeneous input model was used, only a hint of lower resistivity is seen under Námafjall. The low resistivity anomalies in the southern part of the survey area are considered the lower boundary of the low resistivity cap tilting towards south.



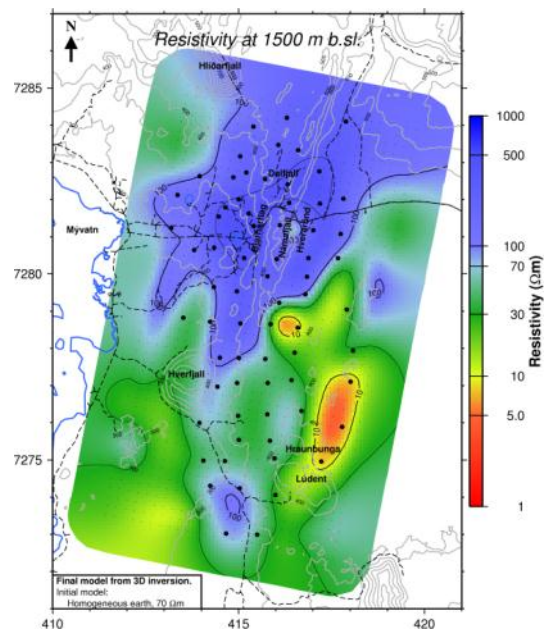
3D model with 1D input model



1D model



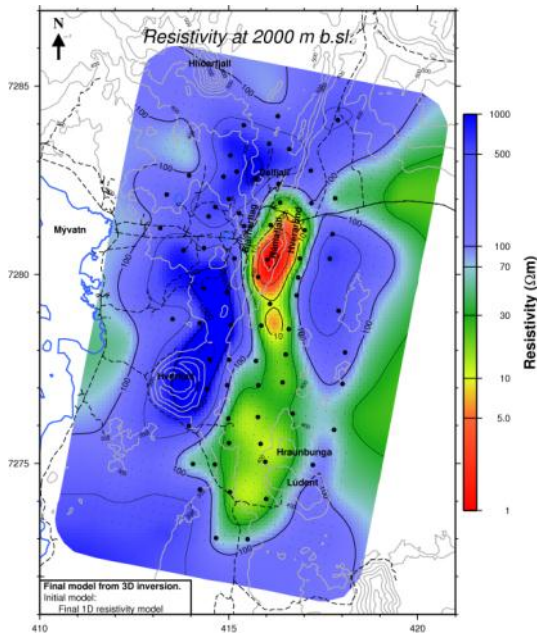
3D model with 1D/Homog 71Ωm



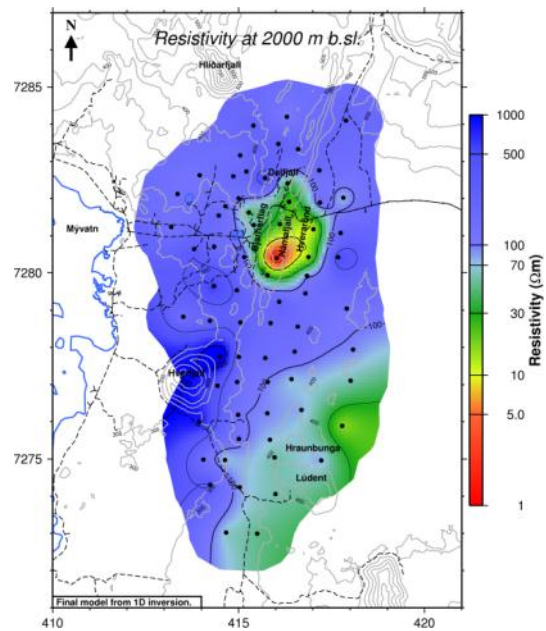
3D model with Homog. 70 Ωm

Figure 6. Comparison of models at 1500 m a.sl.

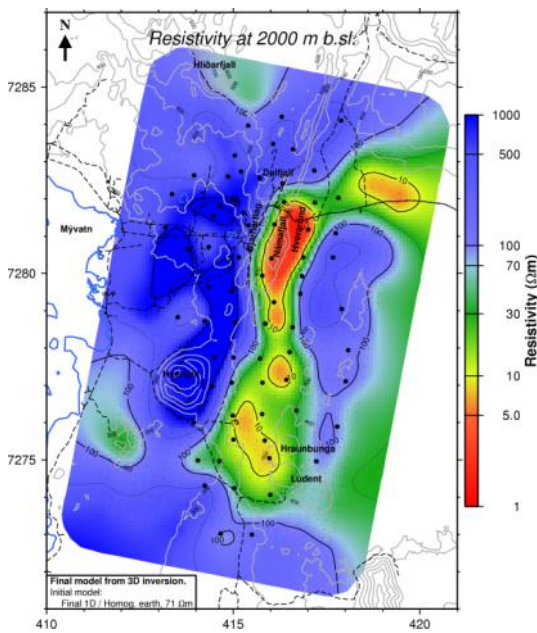
Figure 7 shows the resistivity at 2000 m b.sl. The 1D model and the 3D model based on the 1D show the top of the deep seated low resistivity layer under Námafjall mountain but the in the model based on homogeneous input model there is no sign of the low resistivity at Námafjall. The low resistivity east of Hverfjall seen in the 3D models based on the 1D are not the top of the deep seated low resistivity as seen in the resistivity cross sections discussed earlier.



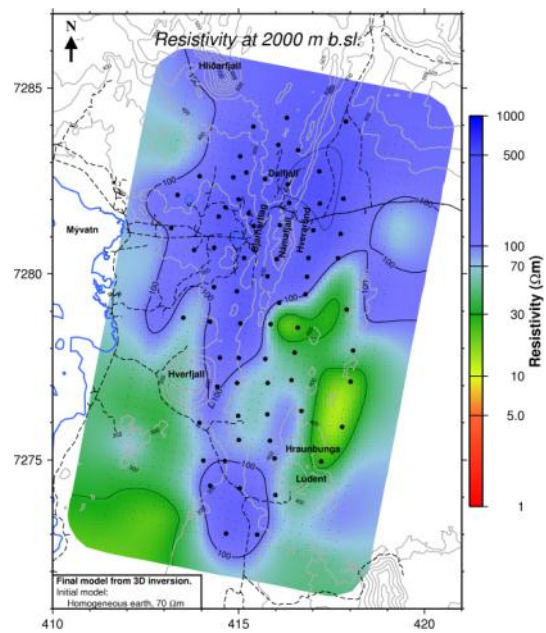
3D model with 1D input model



1D model



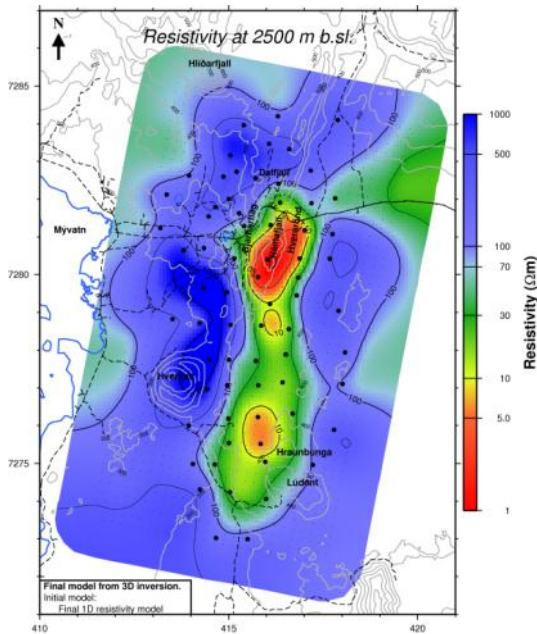
3D model with 1D/Homog 71Ωm



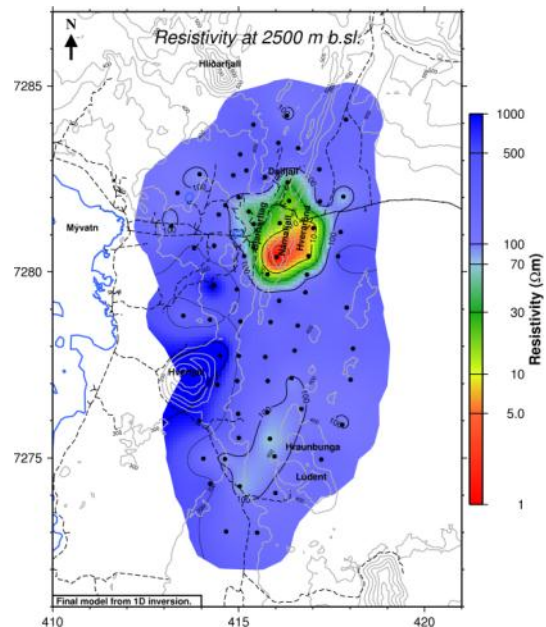
3D model with Homog. 70 Ωm

Figure 7. Comparison of models at 2000 m a.sl.

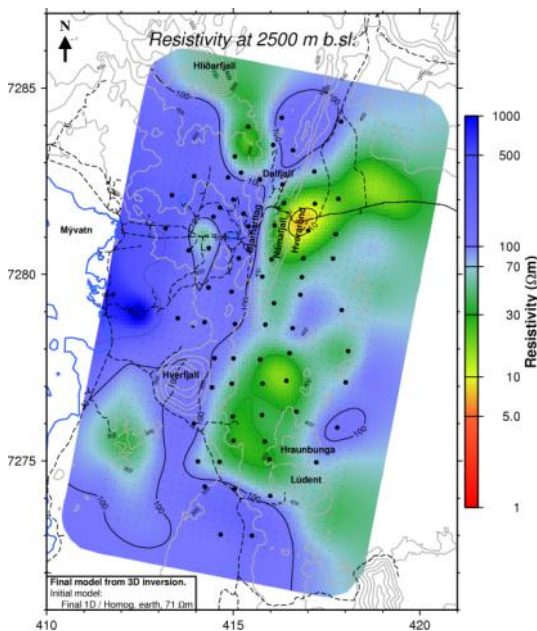
Figure 8 shows the resistivity at 2500 m b.sl. In the 1D model the anomaly under Námafjall mountain is expanding and there is a hint of low resistivity in the area east of Hverfjall. In the 3D model based on 1D same character are seen but less clearly in the one that starts with homogeneous input model (71 Ω m) below 3000 m.



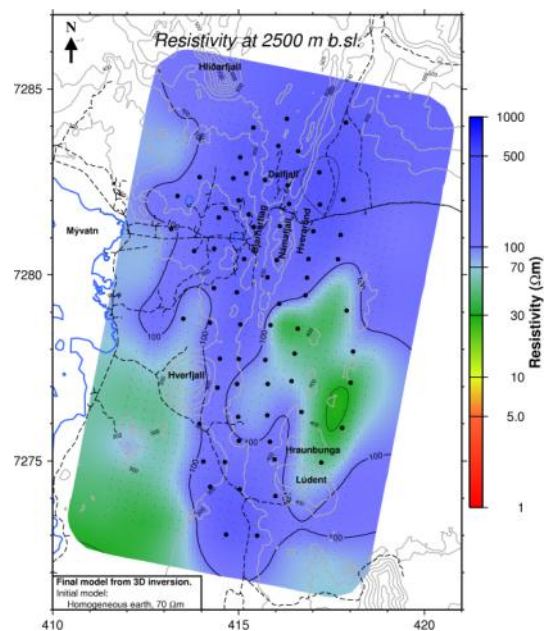
3D model with 1D input model



1D model



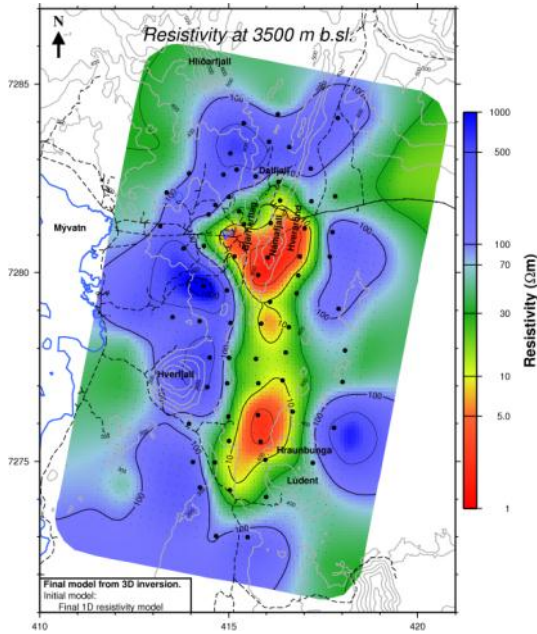
3D model with 1D/Homog 71 Ω m



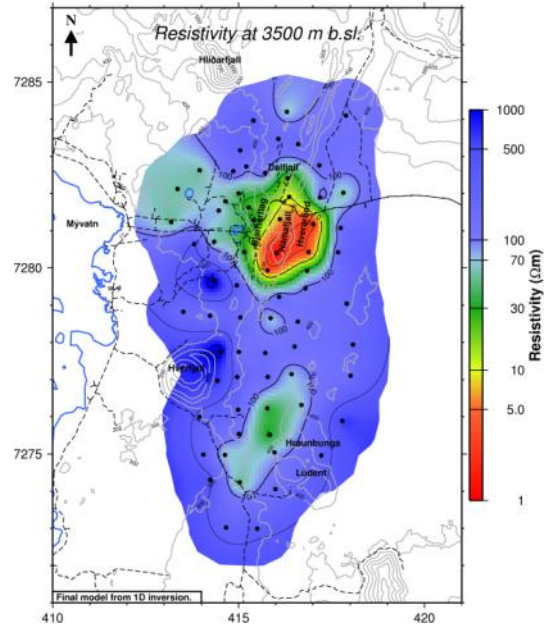
3D model with Homog. 70 Ω m

Figure 8. Comparison of models at 2500 m a.sl.

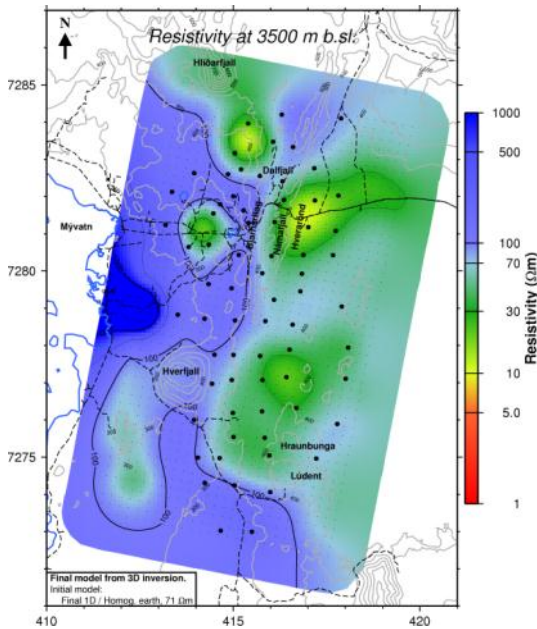
Figure 9 shows resistivity at 3500 m b.sl. Only the 3D model based on the 1D input model shows the deep seated low resistivity emerging under Námafjall mountain and east of Hverfjall.



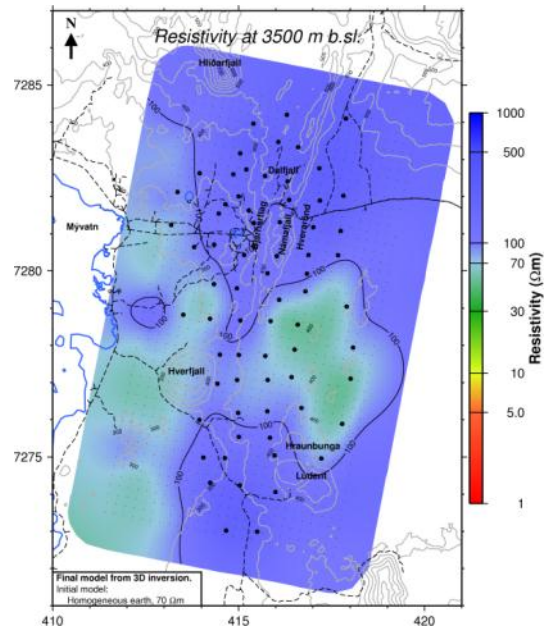
3D model with 1D input model



1D model



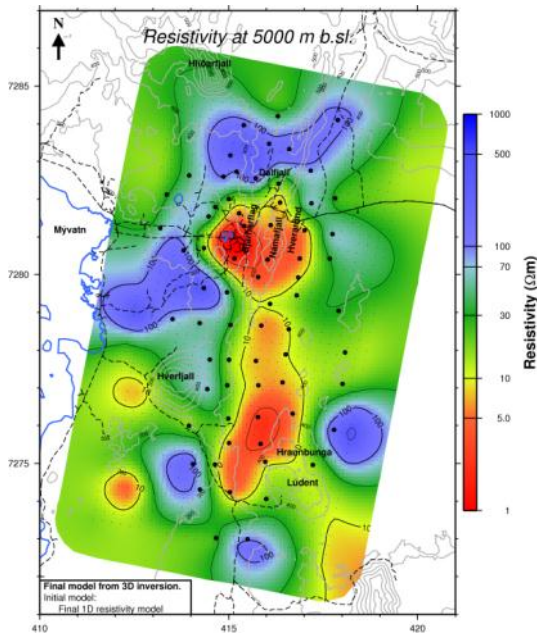
3D model with 1D/Homog 71Ωm



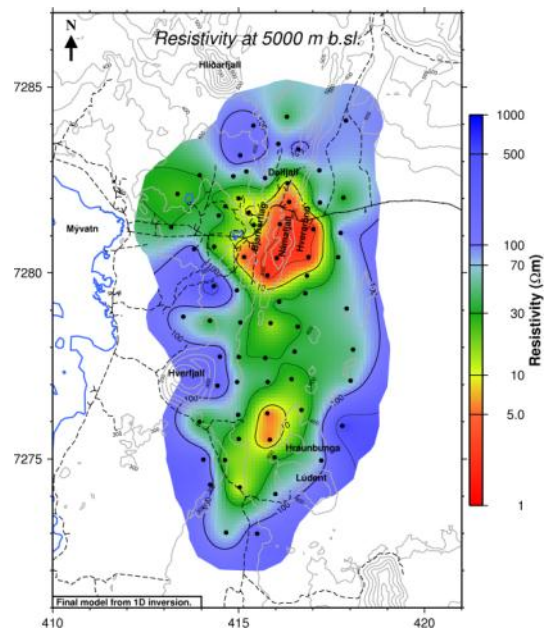
3D model with Homog. 70 Ωm

Figure 9. Comparison of models at 3500 m a.sl.

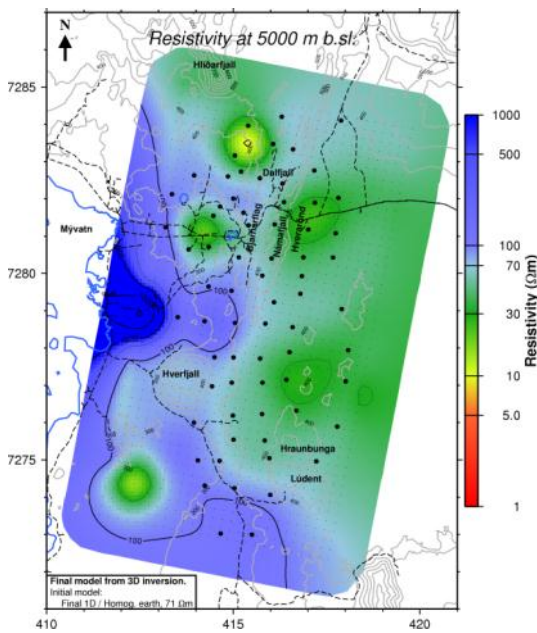
Figure 10 shows resistivity at 5000 m b.sl. Only the 3D model based on 1D shows low resistivity anomalies under Námafjall and near Hverfjall. At this depth the input homogeneous models have resistivity around 70 Ωm . The inversion however seems to require some variety in the resistivity in the resulting models with higher resistivity in the northern part and the southern part of the survey area and lower resistivity in middle.



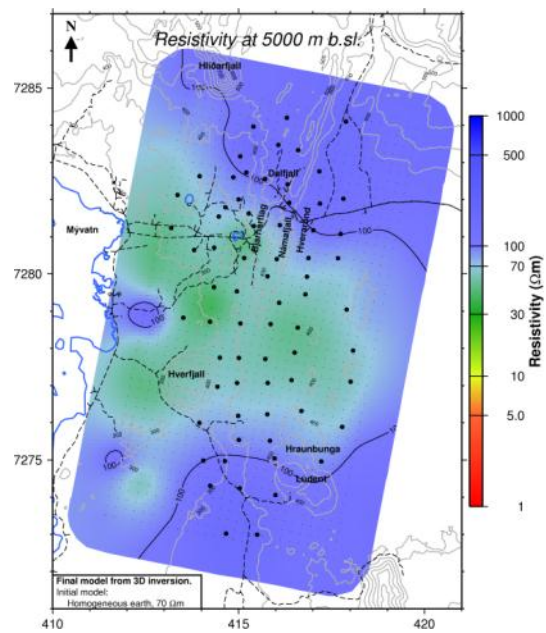
3D model with 1D input model



1D model



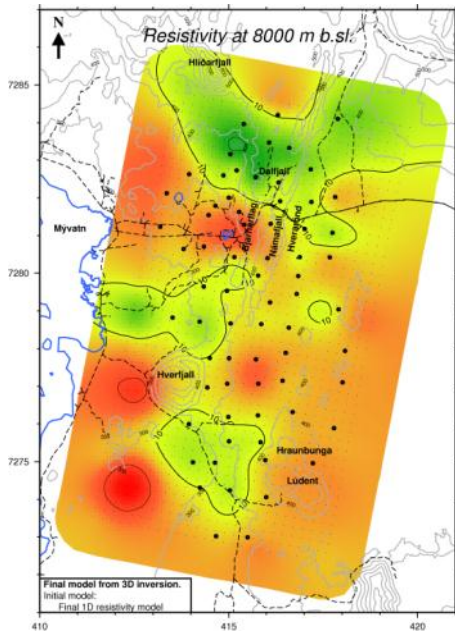
3D model with 1D/Homog 71 Ωm



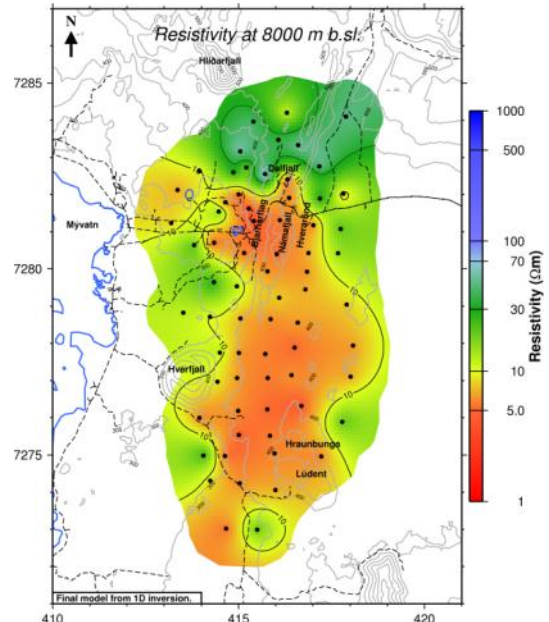
3D model with Homog. 70 Ωm

Figure 10. Comparison of models at 5000 m a.sl.

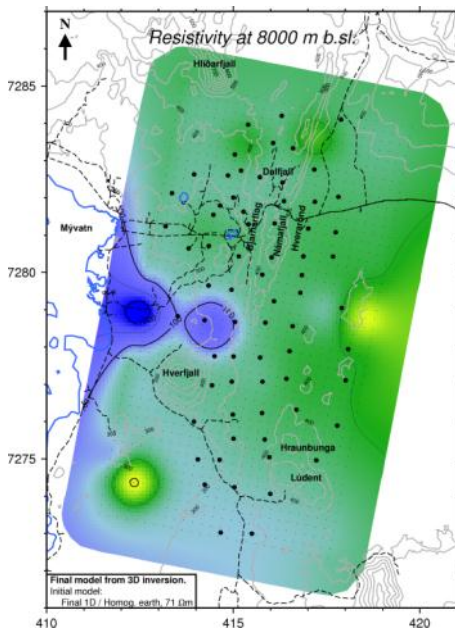
Figure 11 shows resistivity at 8000 m b.s.l. At this depth the deep low resistivity layer present beneath most of Iceland (Beblo and Björnsson, 1980; Eysteinnsson and Hermance, 1985; Vilhjálmsson et al., 2008) would be expected to be seen. However, only the 3D model, based on the 1D starting model, shows low resistivity at depth. The homogeneous initial models do not resolve any low resistivity contrast at this depth.



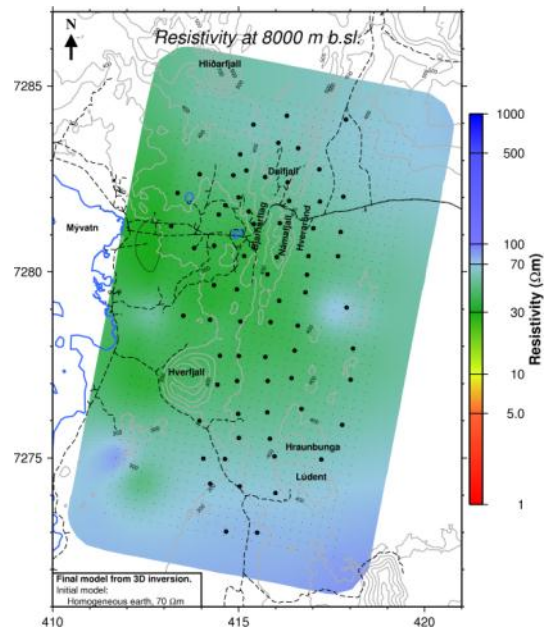
3D model with 1D input model



1D model



3D model with 1D/Homog 71Ωm



3D model with Homog. 70 Ωm

Figure 11. Comparison of models at 8000 m a.s.l.

5 Presentation of the 3D model

Visual presentation of 3D resistivity models is not straightforward. The final models are presented here in two different ways, i.e., as a resistivity map (contour plot) for different elevations (depths) and as resistivity cross sections. Figure 12 shows the TEM/MT survey area and soundings used in the 3D inversion.

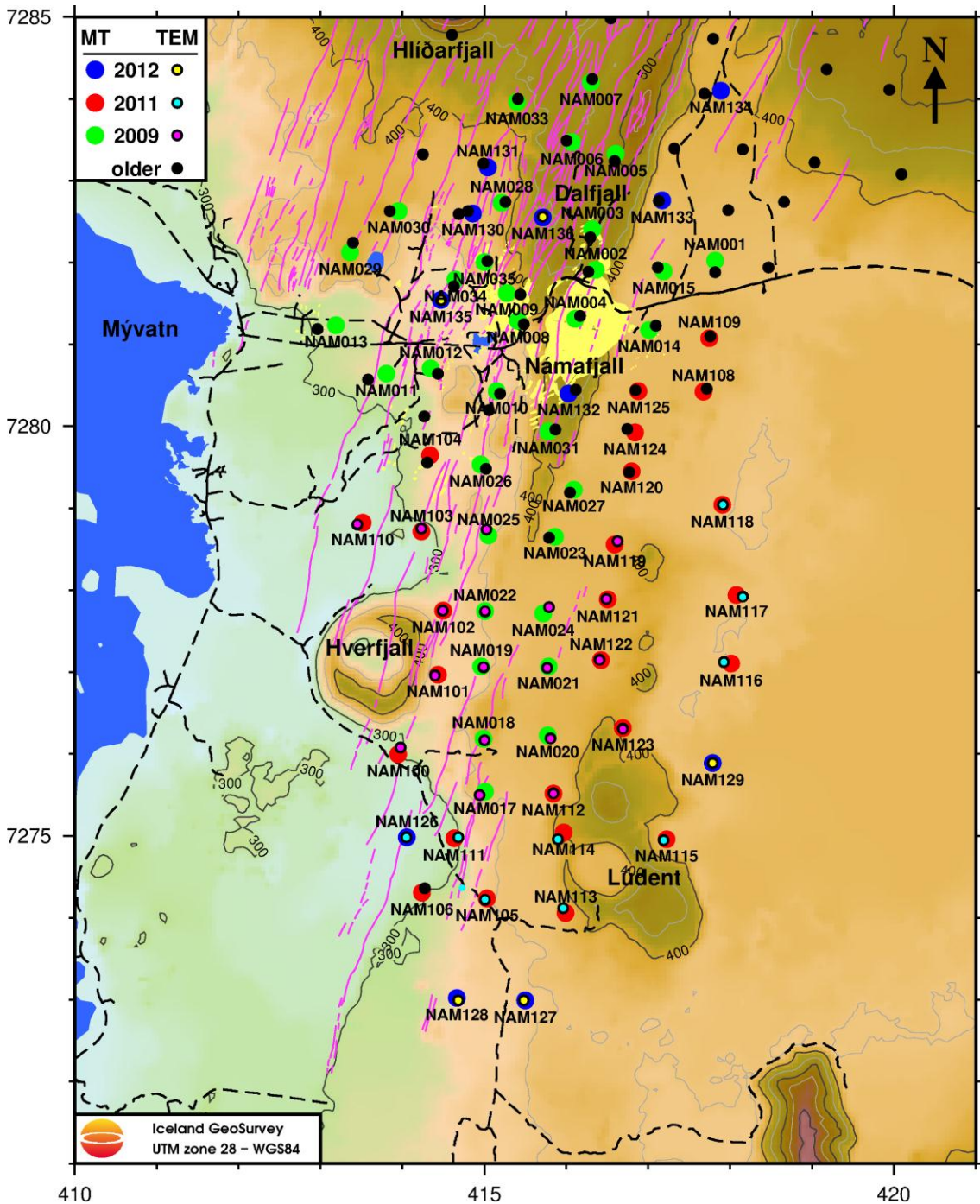


Figure 12. MT and TEM soundings at Námajfjall area. Colours of the dots indicate time when the soundings were performed (see legend).

As mentioned earlier the 3D inversion is run with different input models. A model based on the 1D inversion results is considered as the most reliable input model. Then homogeneous half-space initial models with different resistivity values are used to constrain the inversion, especially artefacts that may be created by the 3D inversion in areas outside the area of data coverage.

The outcome of the inversion for the initial model compiled from 1D inversion will be discussed as the final results of the 3D inversion.

Smoothed resistivity maps from the elevation corrected models, showing the outcome of the inversion for the 1D initial model are presented at 30 different elevations in Appendix 1. Smoothed elevation corrected N-S (SSW-NNE parallel to the x-axis) and E-W (WNW-ESE oriented parallel to the y-axis) cross-sections, through the dense part of the model grid, from the 1D initial model are presented in:

- Appendix 2 (E-W cross sections)
- Appendix 3 (N-S cross sections)

6 Discussion of the 3D model

The main features of the 3D inversion based on the 1D input model, are as follows: A low resistivity cap underlain by a high resistivity core and a deep seated low resistivity at depth. This will be discussed in more details. Resistivity maps are displayed in Appendix 1 and resistivity cross sections are displayed in Appendices 2 and 3.

6.1 Resistivity maps

Resistivity structure in Námafjall geothermal system reflects the characteristic alteration of a high temperature field. The low resistivity cap is underlain by a high resistivity core. Above the low resistivity cap, high resistivity reflects unaltered rocks on the surface.

The resistivity cap in Námafjall is however very unusual, showing features rarely seen in other high temperature areas. The low resistivity cap reaches surface in Námafjall/Námaskarð/Hverarönd where surface manifestations are abundant with prominent alteration, clay pits and steam vents. It tilts slightly towards all directions and at 200 m a.sl. it covers an area of approximately 4 km² (Figure 13). At sea level (Figure 14) the high resistivity core is clear under Námafjall mountain, surrounded by the low resistivity cap (< 10 Ωm) except towards the north under Dalfjall where the continuation of the low resistivity cap holds a little higher resistivity. This feature was first seen in a TEM survey that covered Námafjall area and viewed with TEM results from Krafla high temperature field. It revealed that the zone where the two high temperature fields meet the low resistivity layer that connects to the low resistivity caps in Námafjall and Krafla, has resistivity of 12–15 Ωm. This low resistivity layer is underlain by a little higher resistivity, 20–30 Ωm, not as high as in the high resistivity core of the high temperature fields (Karlsdóttir, 2002). This zone is to the immediate north of Dalfjall and west of Hlíðarfjall.

At 500 m b.sl. (Figure 15) the low resistivity cap covers the southern part of the survey area as it tilts towards south as well as towards east and west. The low resistivity cap is missing in the northern part as explained above. At 1000 m b.sl. (Figure 16) the low resistivity cap is seen in the outskirts of the survey area in the southern part and under Námafjall we see the first sign of the deep seated low resistivity.

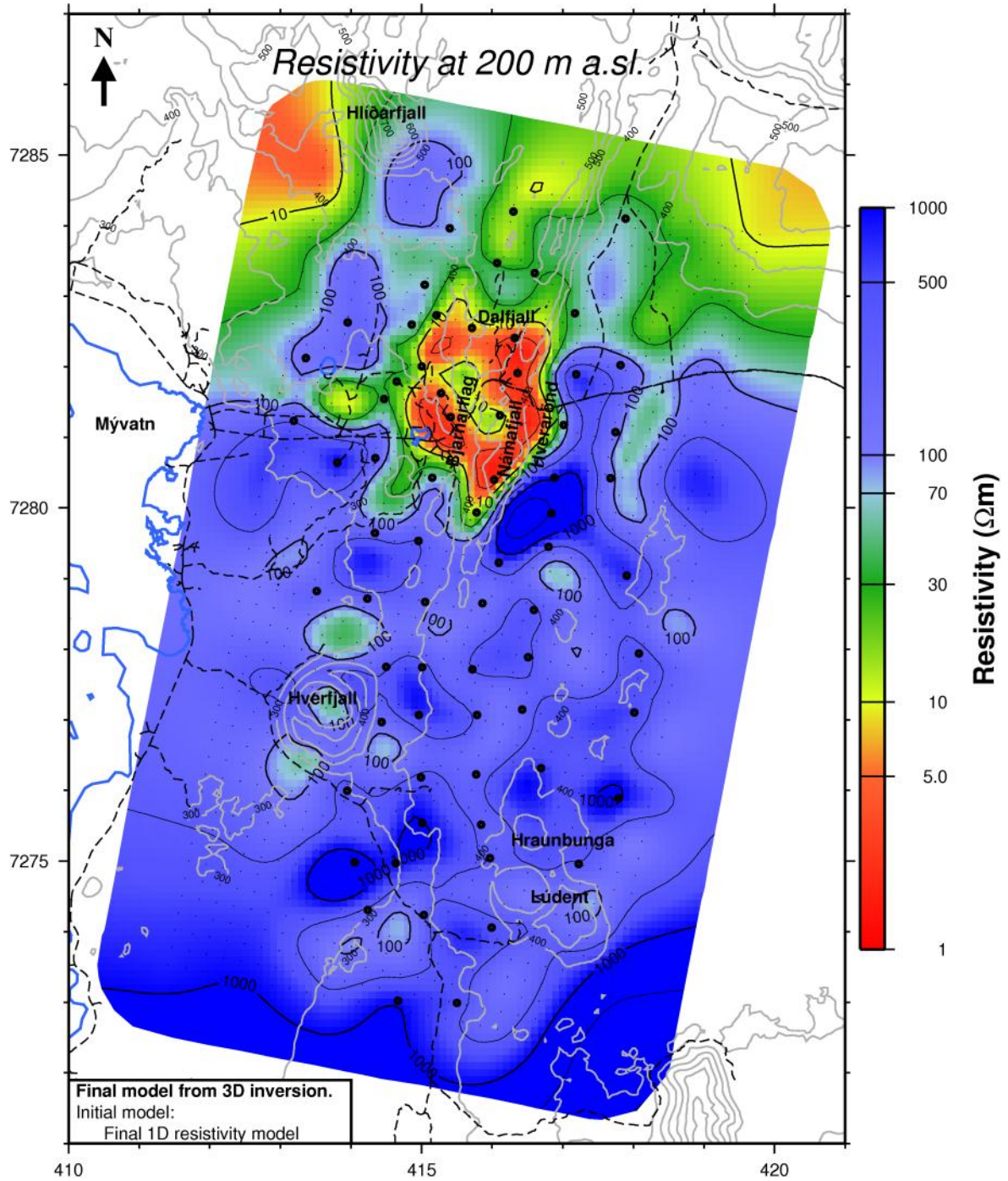


Figure 13. Resistivity at 200 m a.s.l.

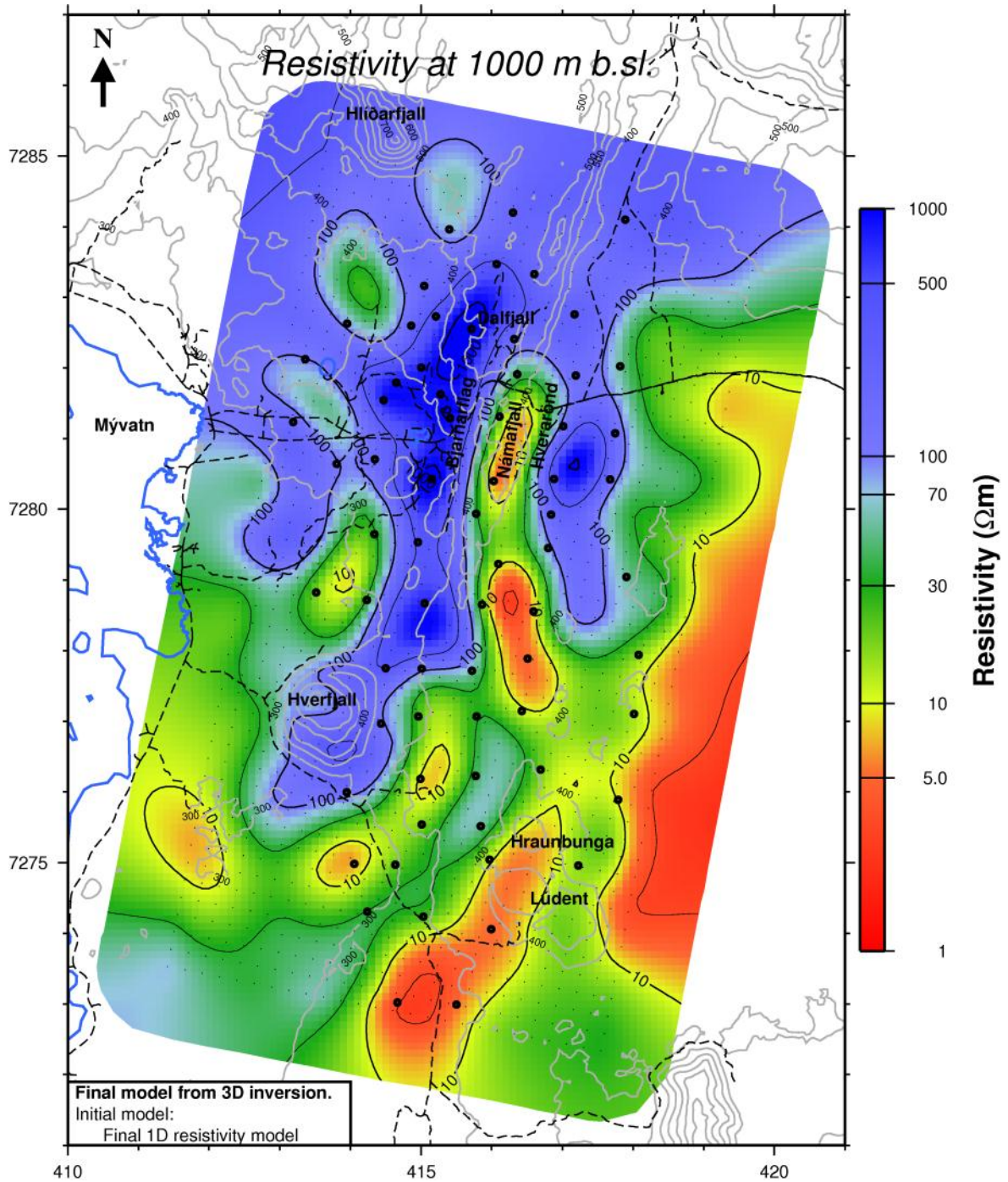


Figure 16. Resistivity at 1000 m b.s.l.

At 2000 m b.s.l. (Figure 17) the top of the deep seated low resistivity is prominent under Námafjall mountain and an area of resistivity less than 50 Ωm extends from Námafjall mountain to south surrounded by higher resistivity.

At 2500 m b.s.l. (Figure 18) the low resistivity under Námafjall has expanded and a top of low resistivity has emerged south east of Hverfjall. At the depth of 5000 m b.s.l. (Figure 19) the two low resistivity anomalies form an elongated low resistivity body from Námafjall to south east of Hverfjall.

The deep seated low resistivity may indicate a heat source and up flow zones into the geothermal system. The Námafjall anomaly reaches highest under Námafjall mountain, or up to 1000 m b.sl. Another top reaches up to 2300 m b.sl. south east of Hverfjall. Resistivity at 8000 m b.sl. (Figure 20) shows low resistivity in all southern part of the survey area. The northern part holds a little higher resistivity or 10–20 Ωm in the transition area between the high temperature areas in Námafjall and Krafla. At 10 km b.sl. (Figure 21) resistivity is low but it has to be considered that the resolution of the MT soundings is poor at that depths.

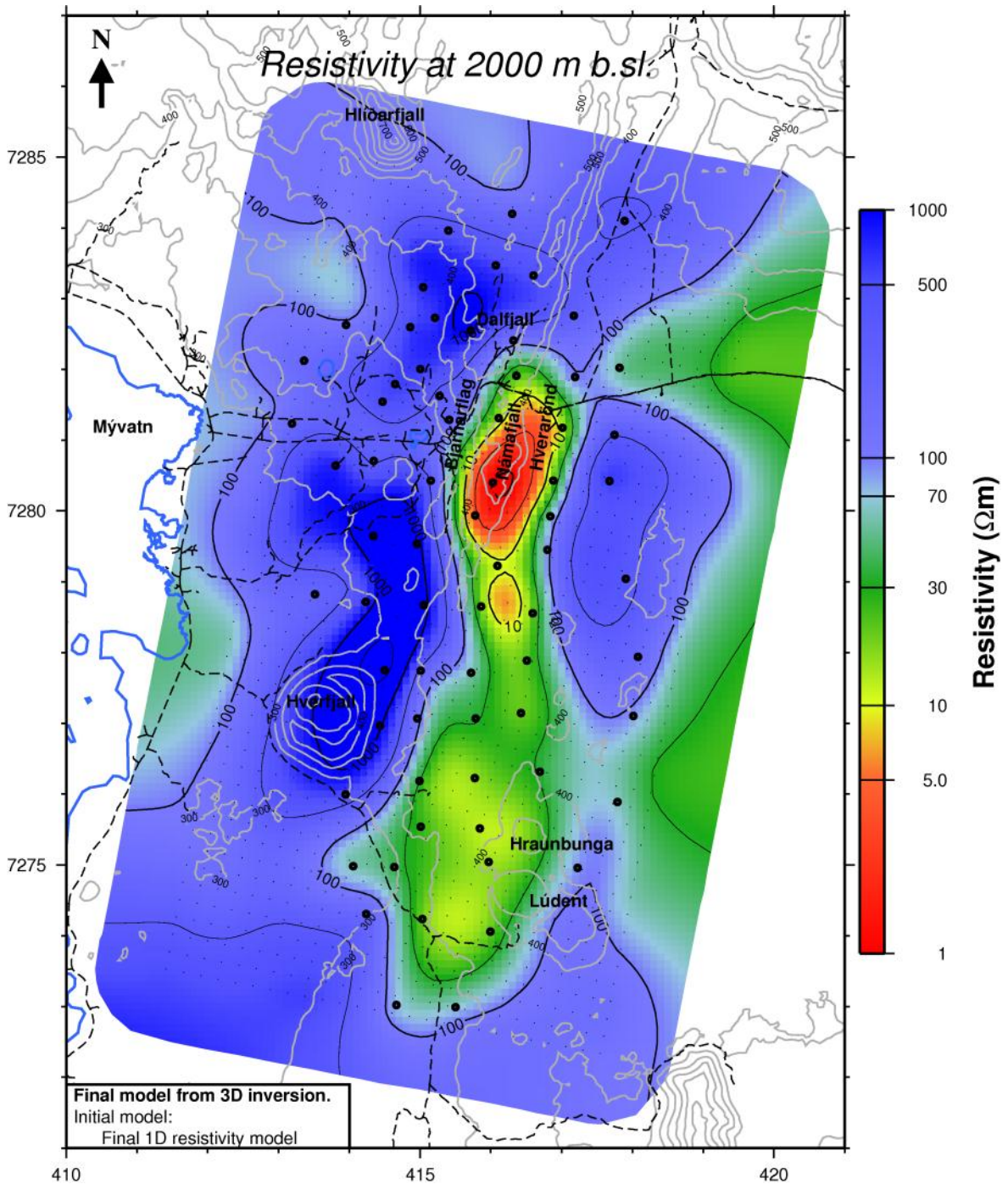


Figure 17. Resistivity at 1000 m b.sl.

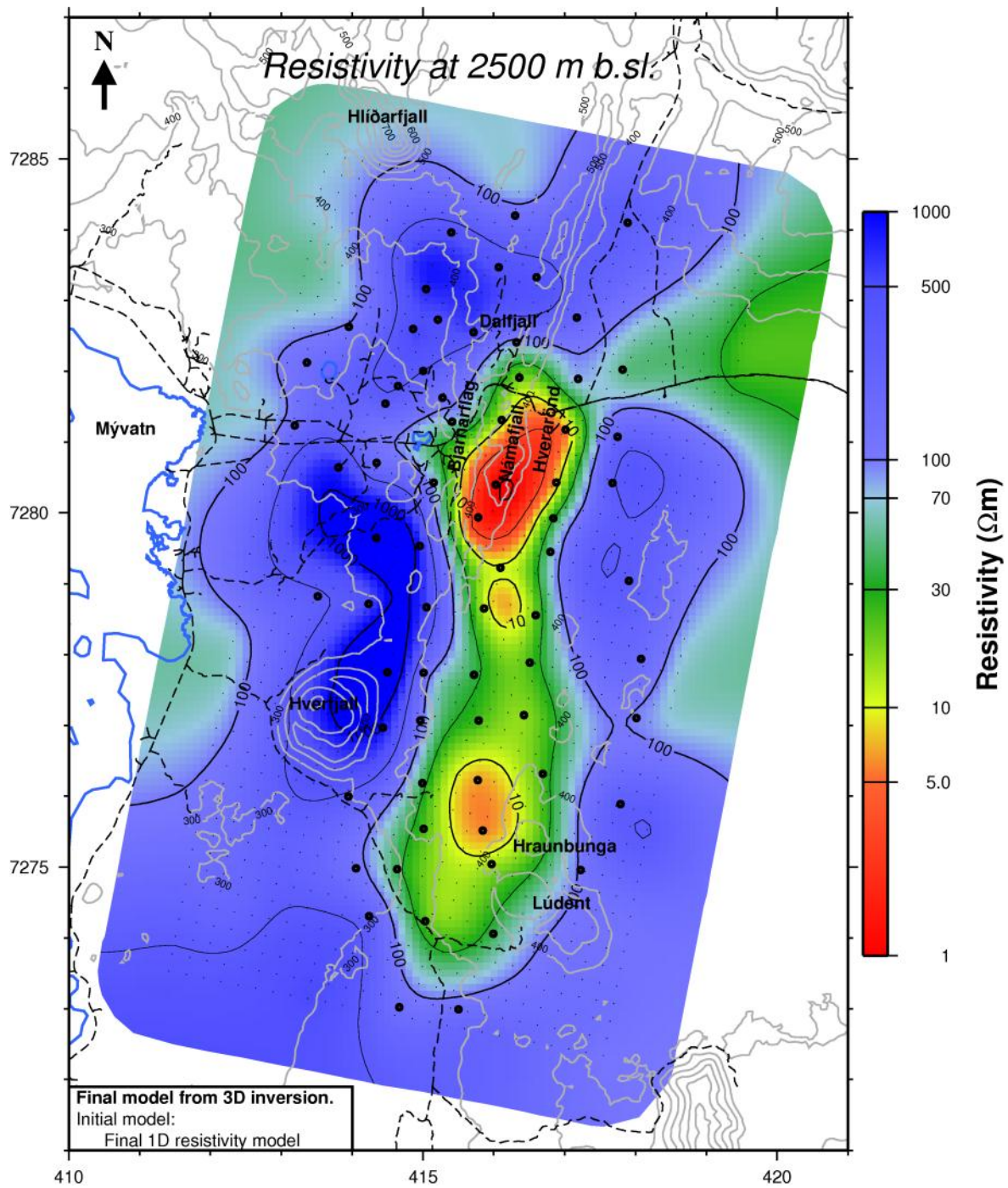


Figure 18. Resistivity at 2500 m b.s.l.

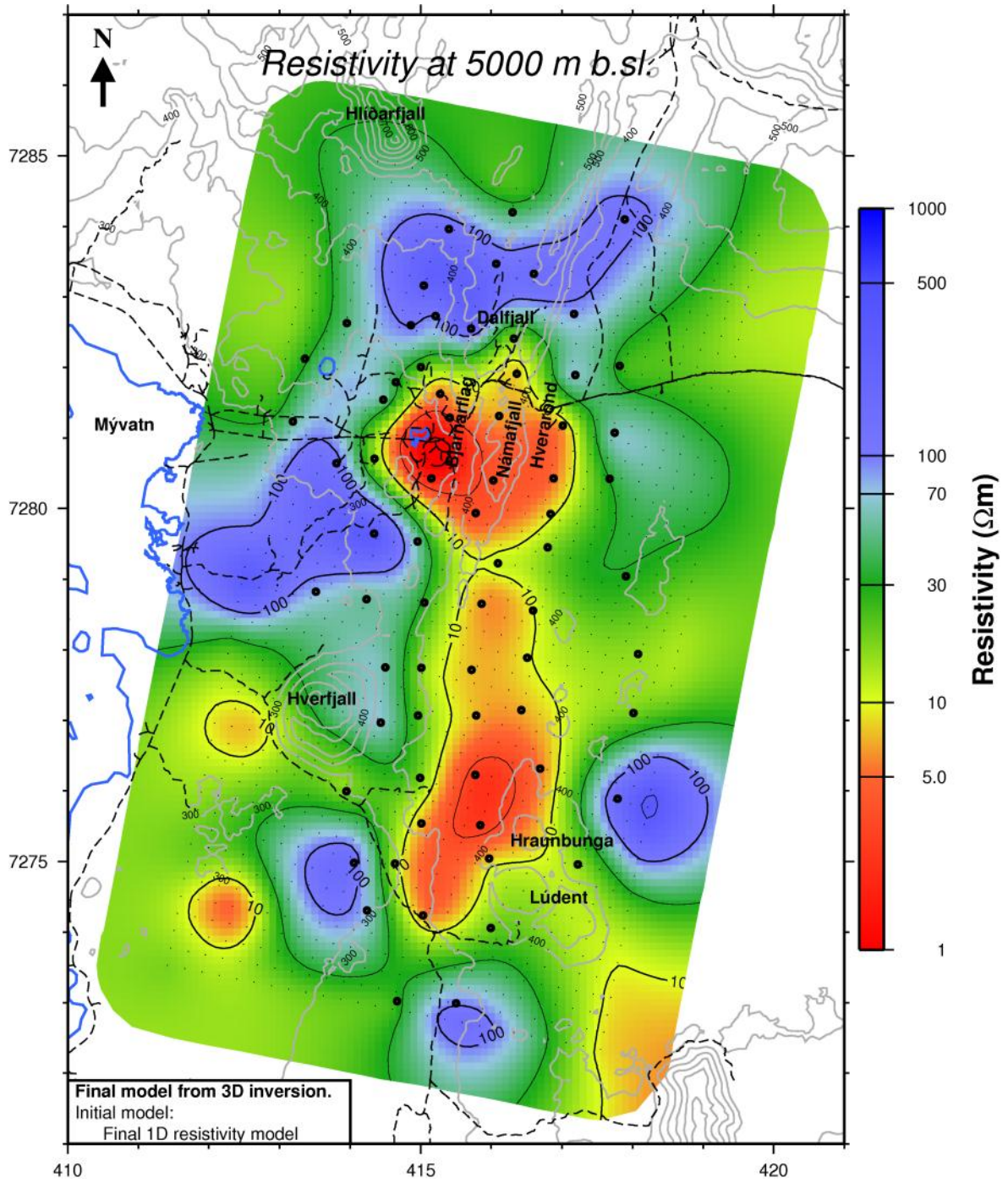


Figure 19. Resistivity at 5000 m b.s.l.

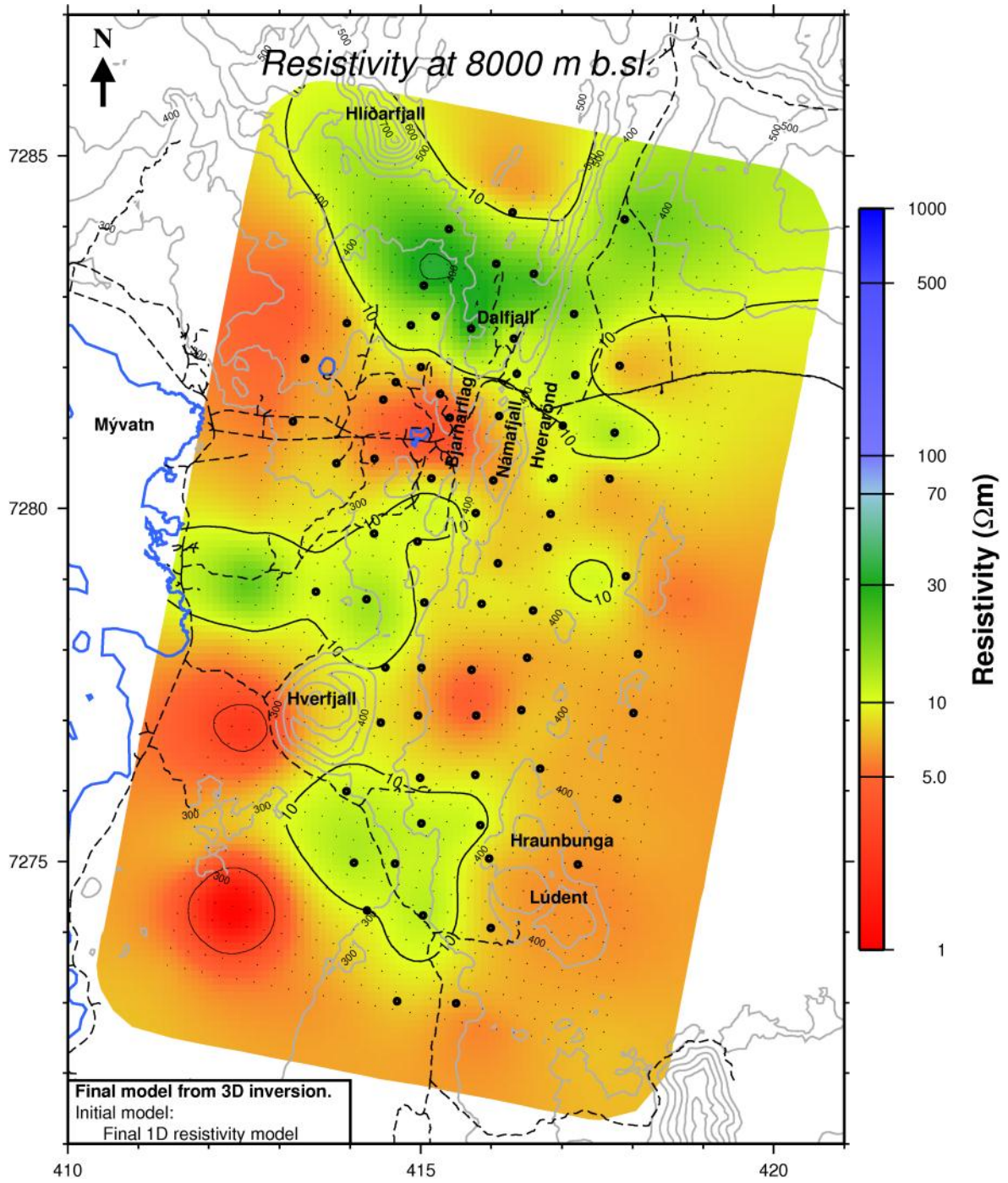


Figure 20. Resistivity at 8000 m b.s.l.

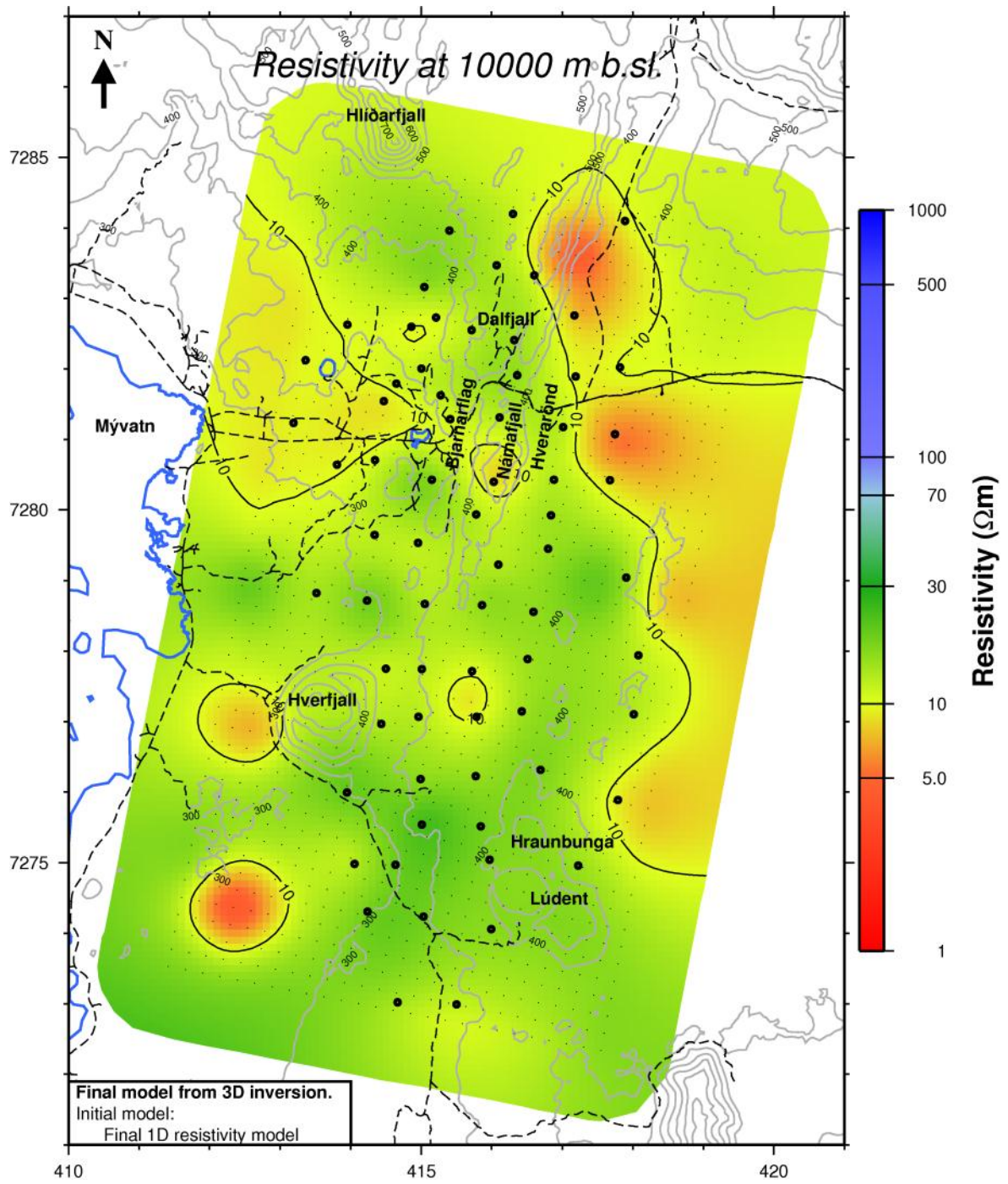


Figure 21. Resistivity at 10000 m b.s.l.

6.2 Resistivity cross sections

A few resistivity cross sections will be displayed in order to explain better the resistivity structure.

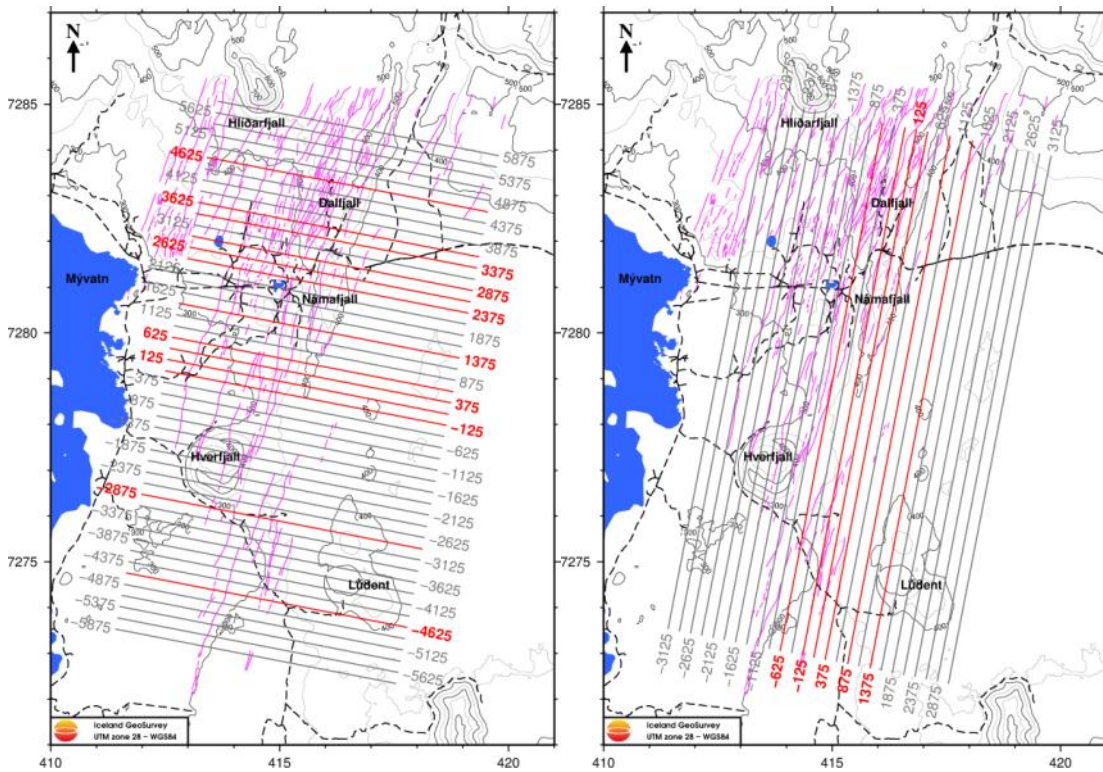


Figure 22. Resistivity cross sections. The resistivity cross sections discussed in the text are marked in red. The names of the cross sections refer to their distance from origin point of the grid, positive towards north and towards east (see Figure 3).

6.3 EW bound resistivity cross sections (Figure 15)

Connective zone between Námafjall and Krafla geothermal fields

Resistivity cross section EW_N4625 (Figure 23) crosses the northern part of Dal fjall. It shows that in this area a conventional low resistivity cap is not present but rather a layer at 500–1000 m b.s.l. with resistivity below 50 Ωm (yellow and green) underlain by a high resistivity core with resistivity above 100 Ωm . The low resistivity bodies at depth to both sides of the layer ($< 50 \Omega\text{m}$) have to be taken with caution as they are outside data coverage.

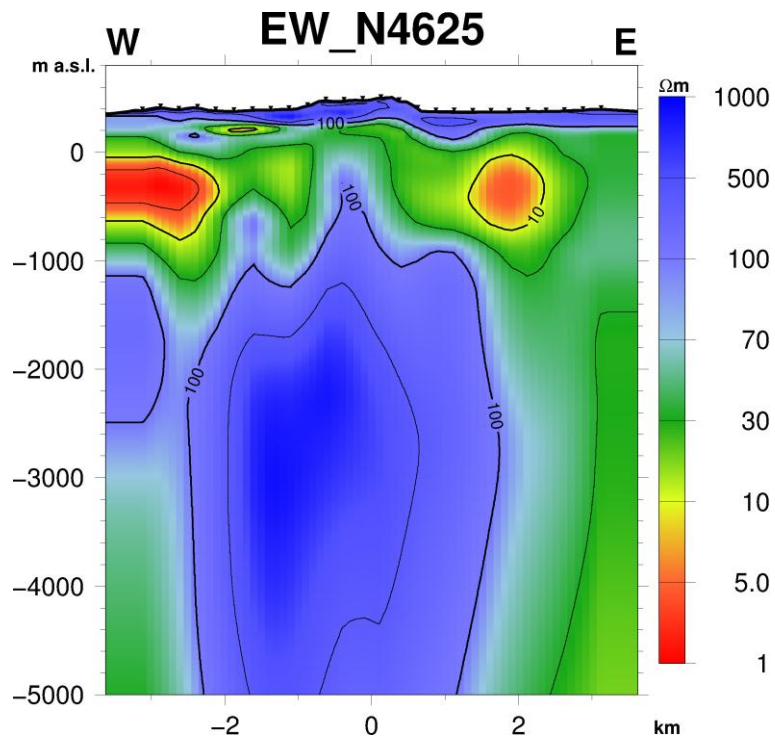


Figure 23. Resistivity cross section EW_N4625 down to 5 km b.s.l. beneath northern part of Dal fjall mountain.

Námafjall

Resistivity cross section EW_N3625 (Figure 24) crosses through Dal fjall. It shows the low resistivity cap with upper boundary 100 m below surface tilting down to west and east to a depth of 200–300 m b.s.l. The low resistivity cap is underlain by a high resistivity core with a hint of lowering resistivity at depth under Dal fjall. Cross section EW_N3375 (Figure 25) shows similar resistivity structure as in previous cross section but here a distinctive low resistivity appears 6–8 km b.s.l. In resistivity cross section EW_N2875 (Figure 26) the low resistivity cap reaches surface and a low resistivity body domes up under Námafjall mountain to a depth of 1,5 km b.s.l.

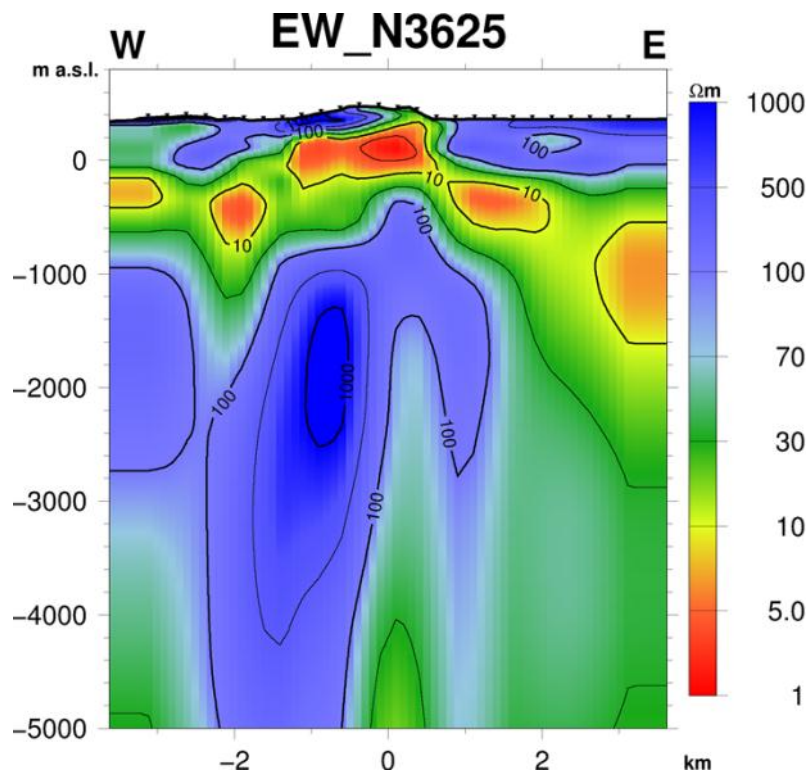


Figure 24. Resistivity cross section EW_N3625 down to 5 km b.s.l. beneath Dal fjall mountain.

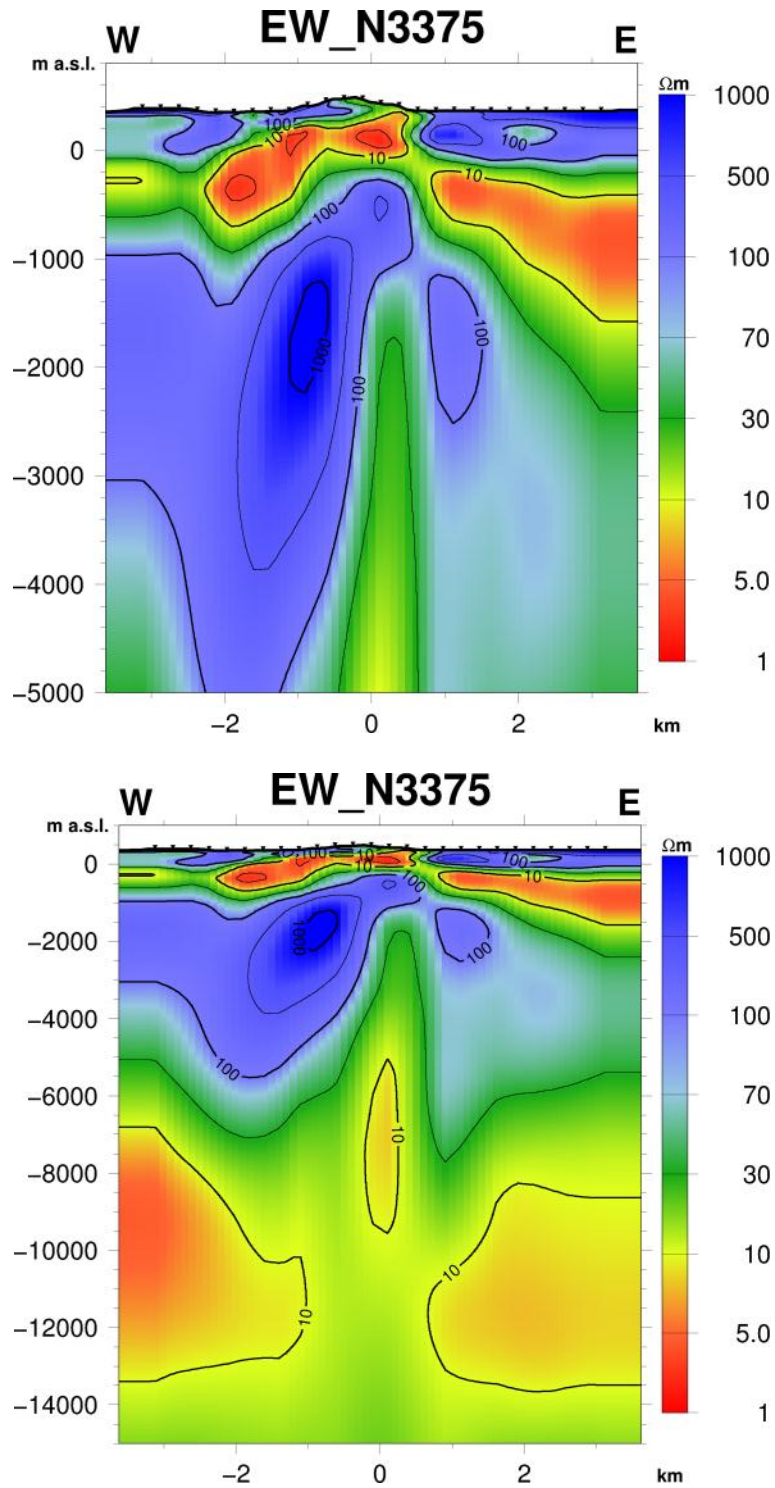


Figure 25. Resistivity cross section EW_N3375 down to 5 and 15 km b.s.l. between Námafjall and Dalafjall mountains.

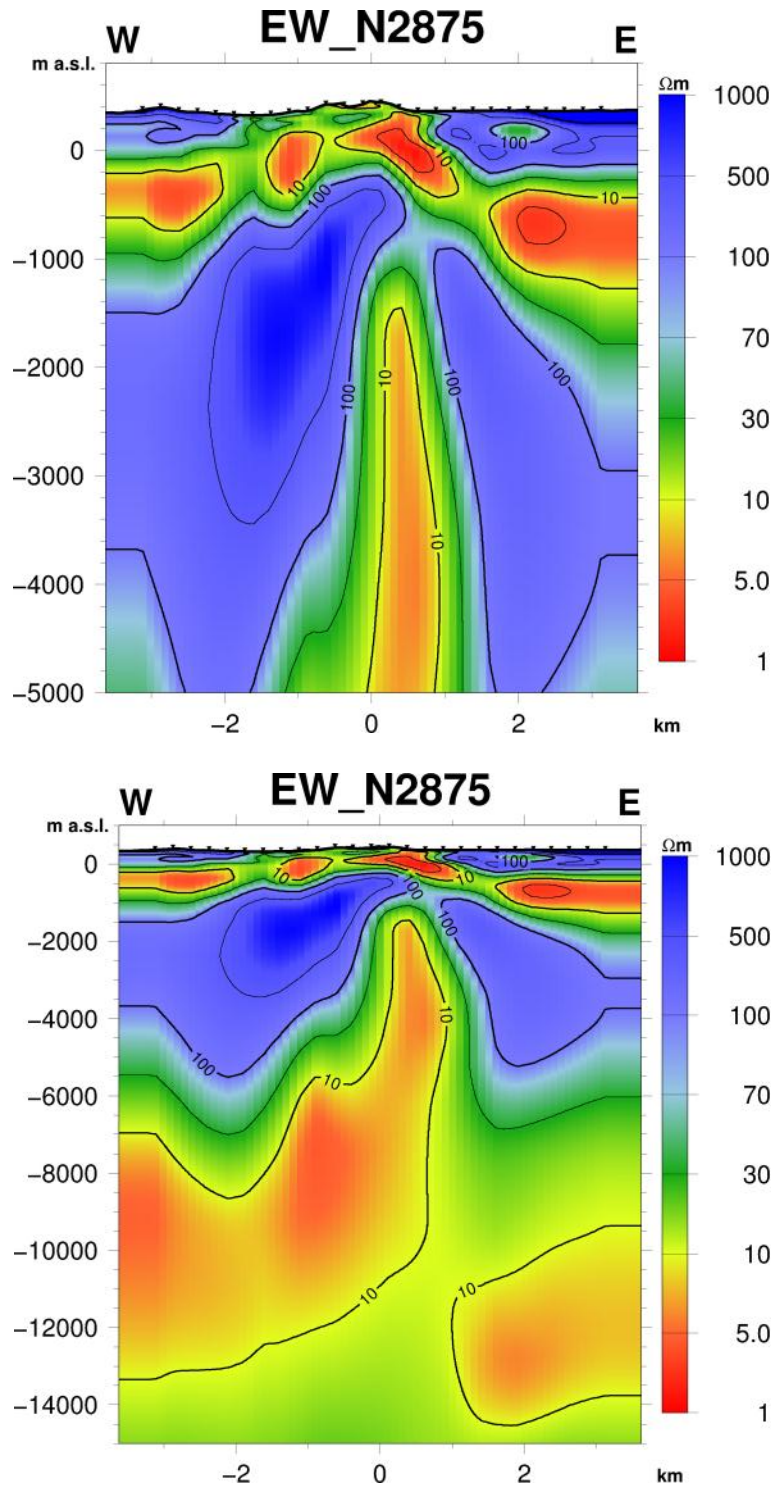


Figure 26. Resistivity cross section EW_N2875 down to 5 and 15 km b.s.l. under Námafjall mountain and Bjarnarflag (northern part).

The next two resistivity cross sections EW_N2625 (see Figure 27) and EW_N2375 (Figure 28) show similar structure as the previous cross section and here the low resistivity body takes shape of two bodies, one doming up to almost 1000 m b.s.l. below Námafjall mountain and another adjacent to the immediate west domes up to 5 km b.s.l. under Bjarnarflag. This structure extends towards south until cross section

EW_N1375 (Figure 29) that crosses the southern part of Námafjall mountain. Here the lower up doming top of the low resistivity body at depth has merged to the top below Námafjall mountain. The low resistivity cap has started to tilt towards south from the top of the geothermal system with its upper boundary at sea level. In cross section EW_N625 (Figure 30) that crosses just south of Námafjall mountain, the low resistivity cap has its upper boundary at 500 m b.s.l. and the deep seated low resistivity body is seen at 7–9 km b.s.l.

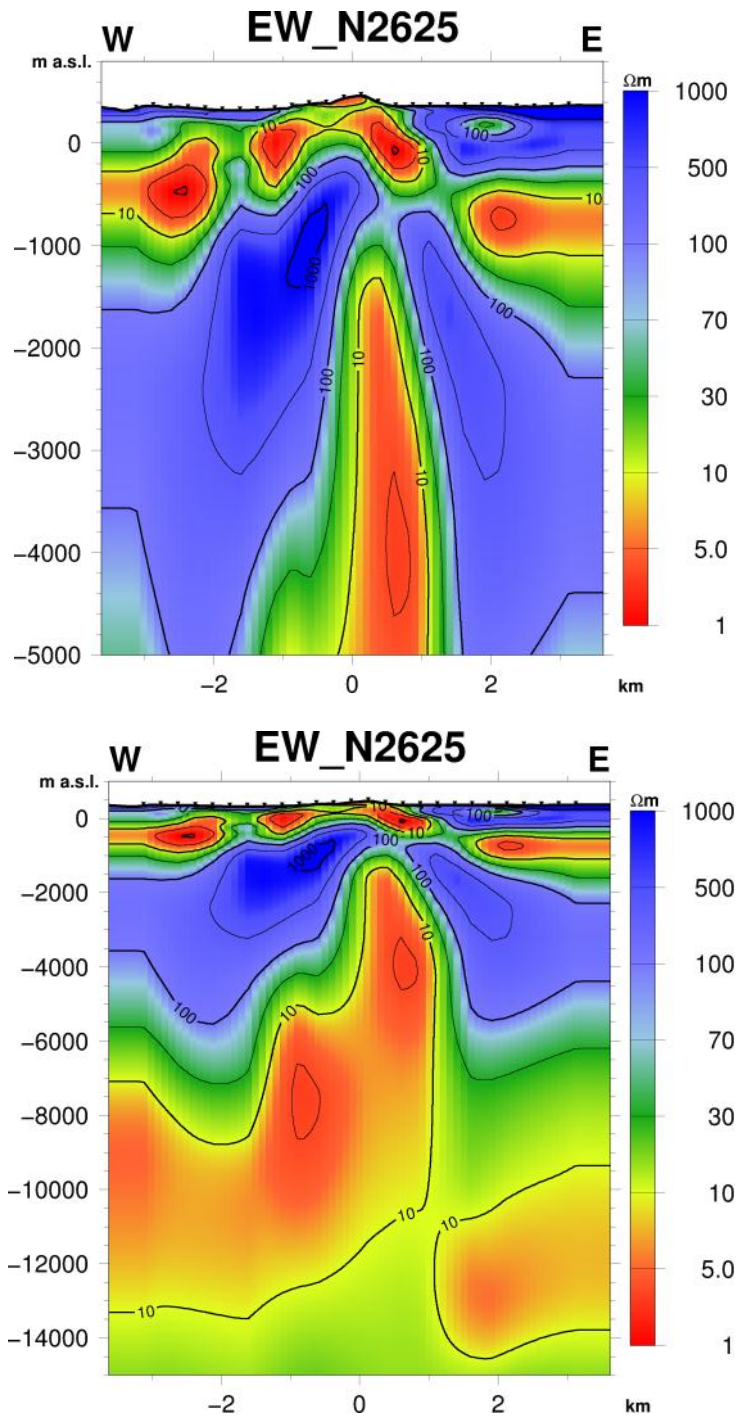


Figure 27. Resistivity cross section EW_N2625 down to 5 and 15 km b.s.l. under Námafjall mountain and Bjarnarflag.

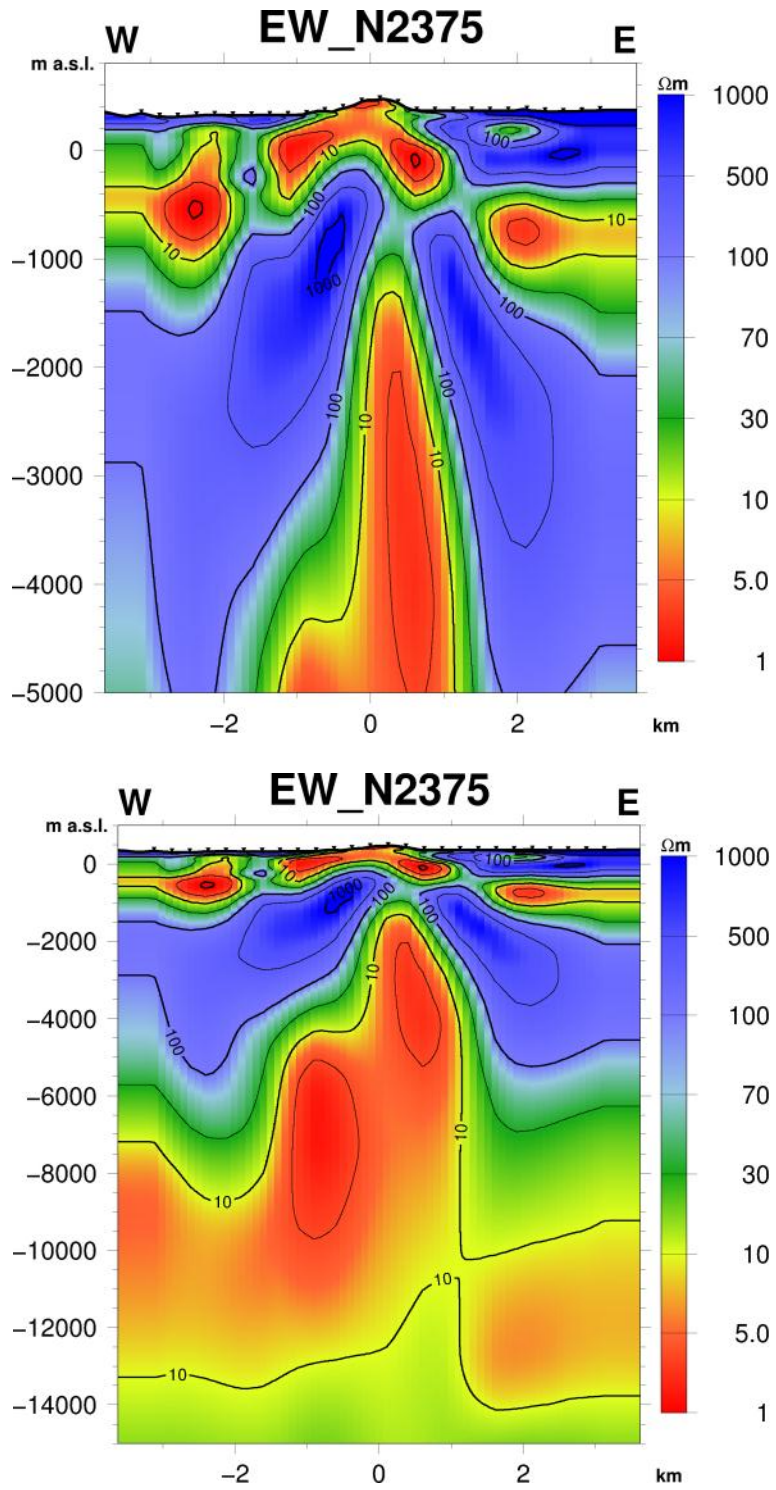


Figure 28. Resistivity cross section EW_N2375 down to 5 and 15 km b.s.l. under Námafjall mountain and Bjarnarflag.

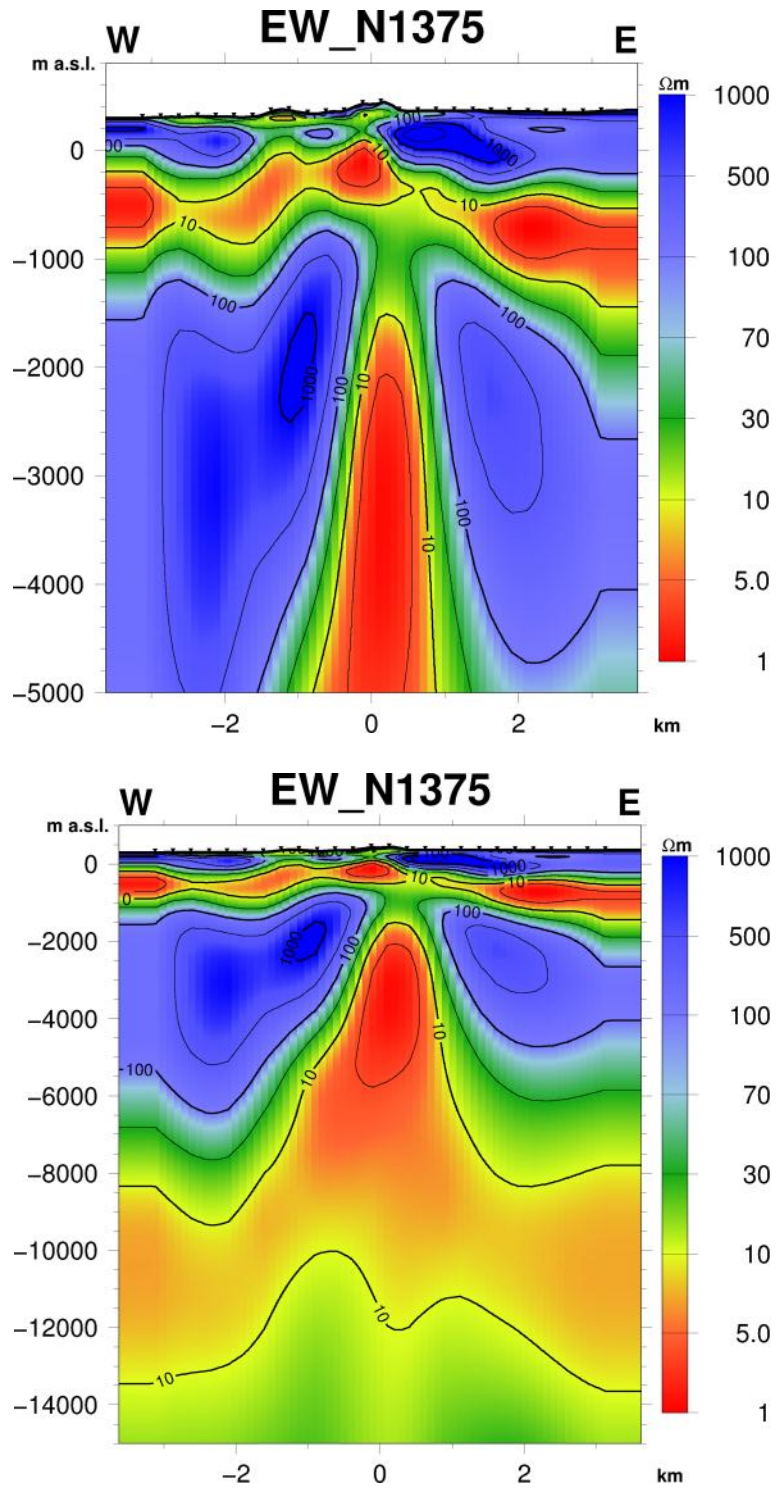


Figure 29. Resistivity cross section EW_N1375 down to 5 and 15 km b.s.l. under Námafjall mountain.

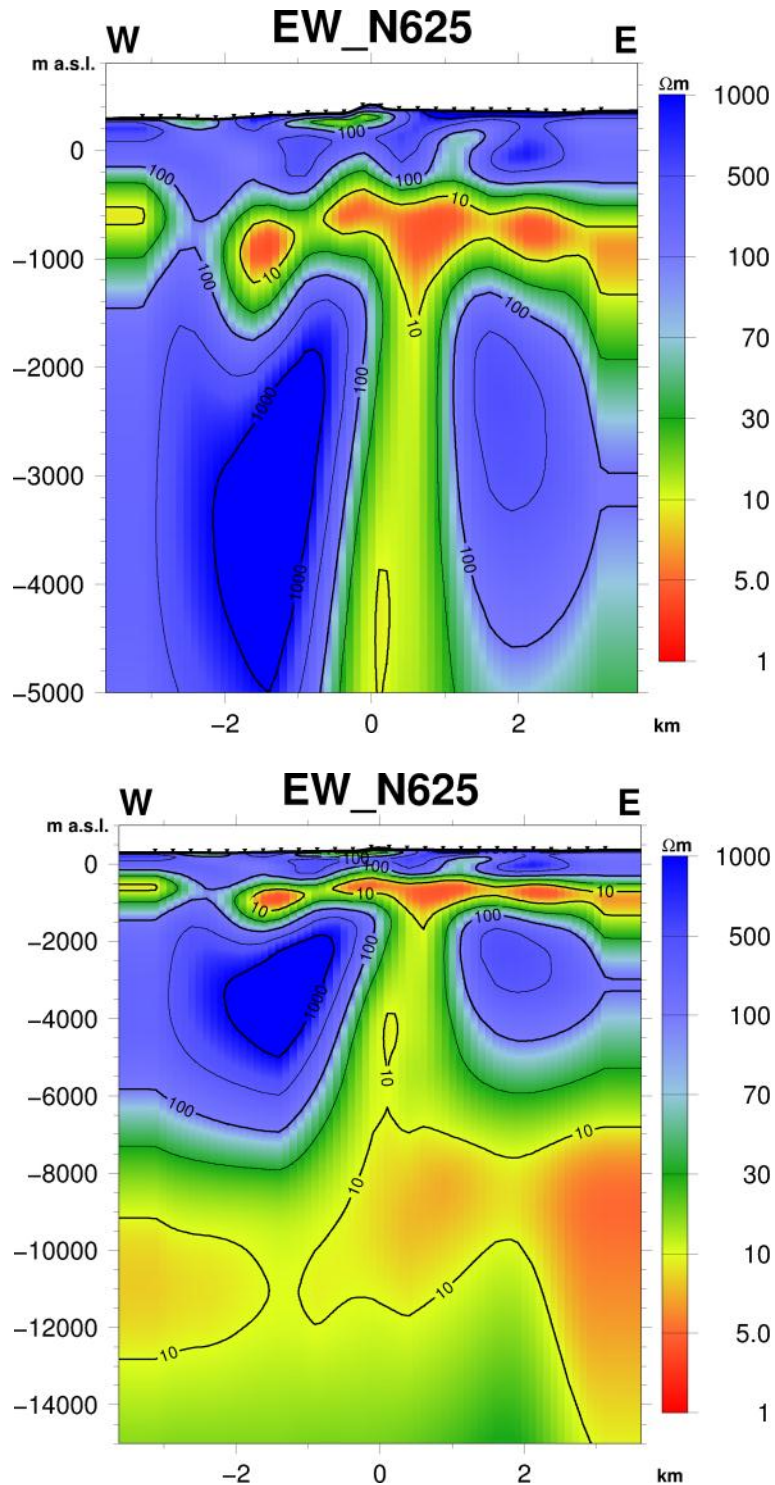


Figure 30. Resistivity cross section EW_N625 down to 5 and 15 km b.s.l. under southern tip of Námafjall mountain.

In three cross sections EW_N375 (Figure 31) and EW_N125 (Figure 32) and EW_N-125 (Figure 33) an interesting feature is encountered. A low resistivity column from the deep seated low resistivity connects to the low resistivity cap. If this is indeed a separate up flow column is hard to say. This is more likely a part of the Námafjall up flow zone.

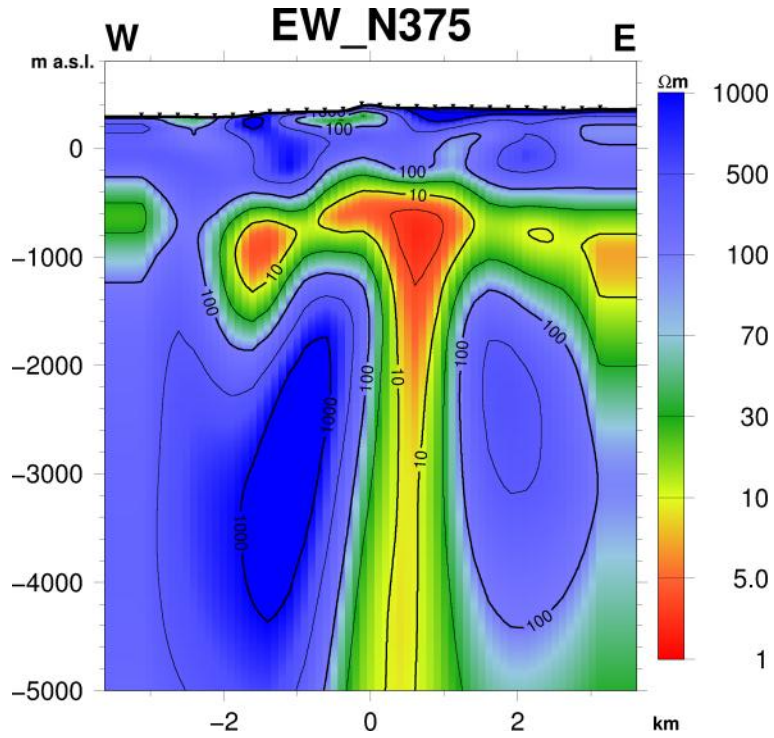


Figure 31. Resistivity cross section EW_N375 down to 5 km b.s.l. south of Námafjall mountain.

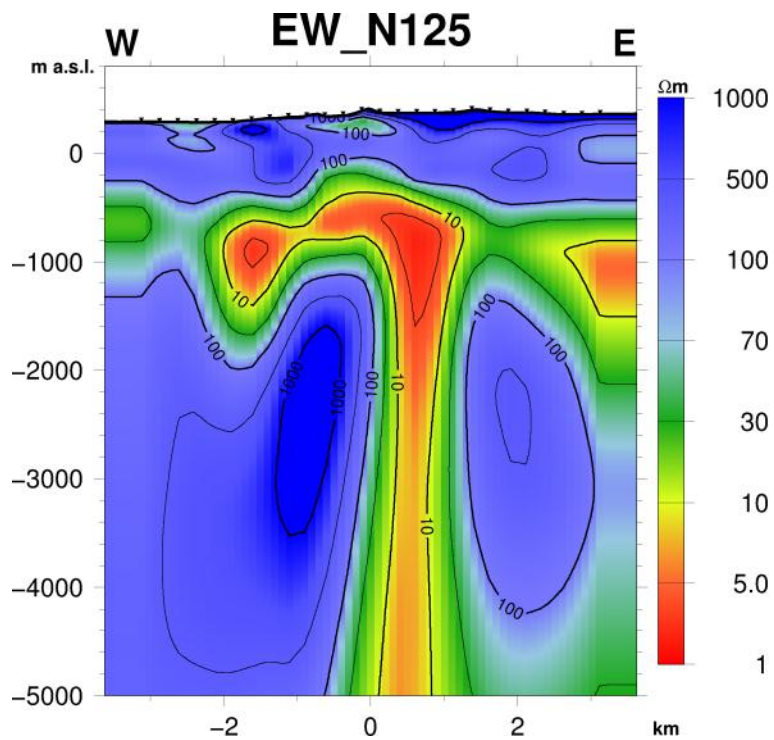


Figure 32. Resistivity cross section EW_N125 down to 5 km b.s.l. south of Námafjall mountain.

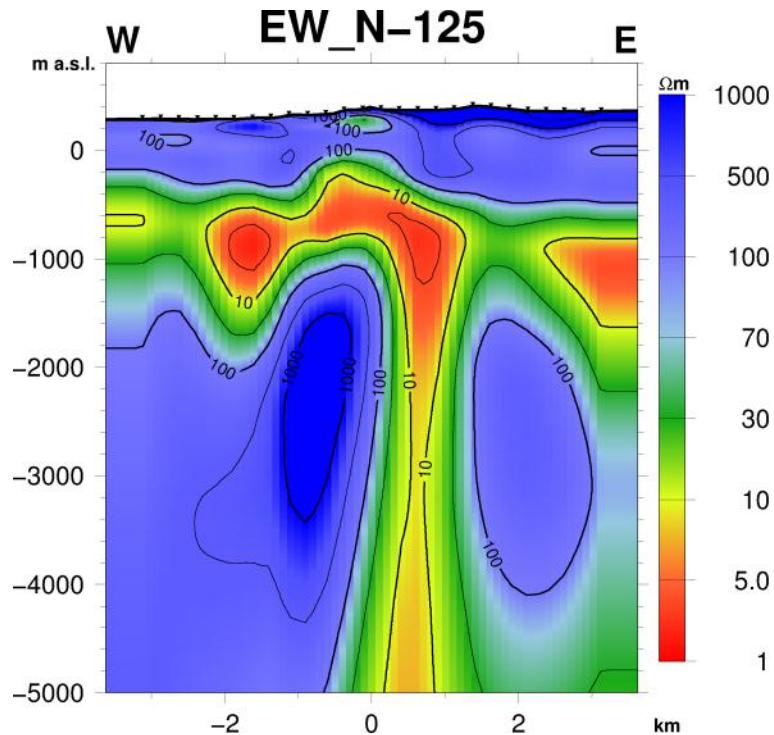


Figure 33. Resistivity cross section EW_N-125 down to 5 15 km b.s.l. south of Námafjall mountain.

Hverfjall

Southwards from the above mentioned low resistivity zone in Námafjall to Hverfjall the low resistivity cap has upper boundary at 500 m b.sl. with underlying high resistivity core. The deep seated low resistivity body forms a ridge up to 5 km b.s.l. from Námafjall towards SSE and east of Hverfjall it starts doming up and peaks in the area between Hverfjall and Hraunbunga.

Resistivity cross section EW_N-2875 (Figure 34) crosses through Hraunbunga and south of Hverfjall. It reveals a low resistivity cap at approximately 1000 m b.sl. underlain by a high resistivity core. Low resistivity body domes up to a depth of 3000 m b.sl. in the area south east of Hverfjall, in the area between Hverfjall and Hraunbunga. Cross section EW_N-4625 (Figure 35) shows the resistivity structure outside the geothermal field except a little up doming of the deep seated low resistivity layer with a hint of low resistivity above that.

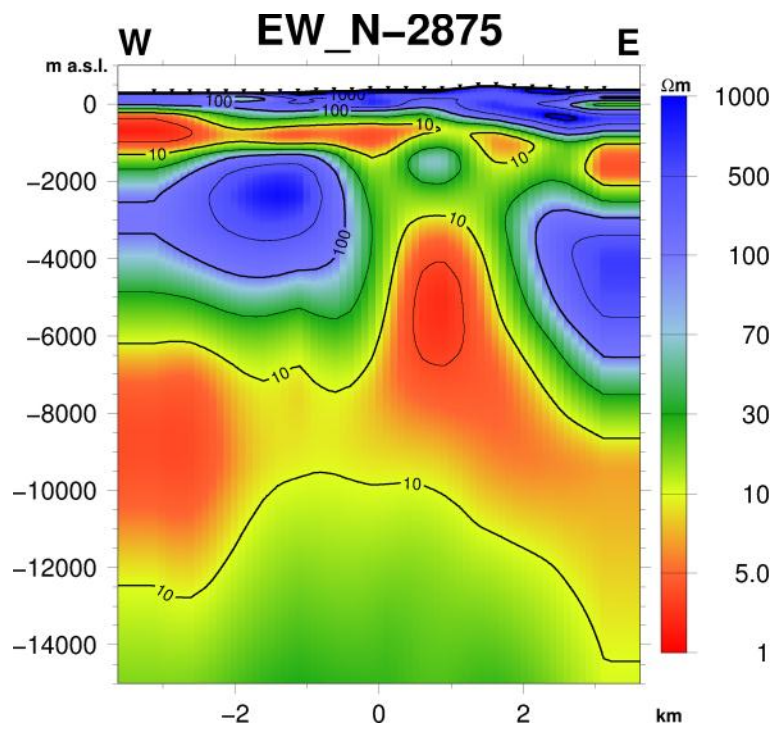
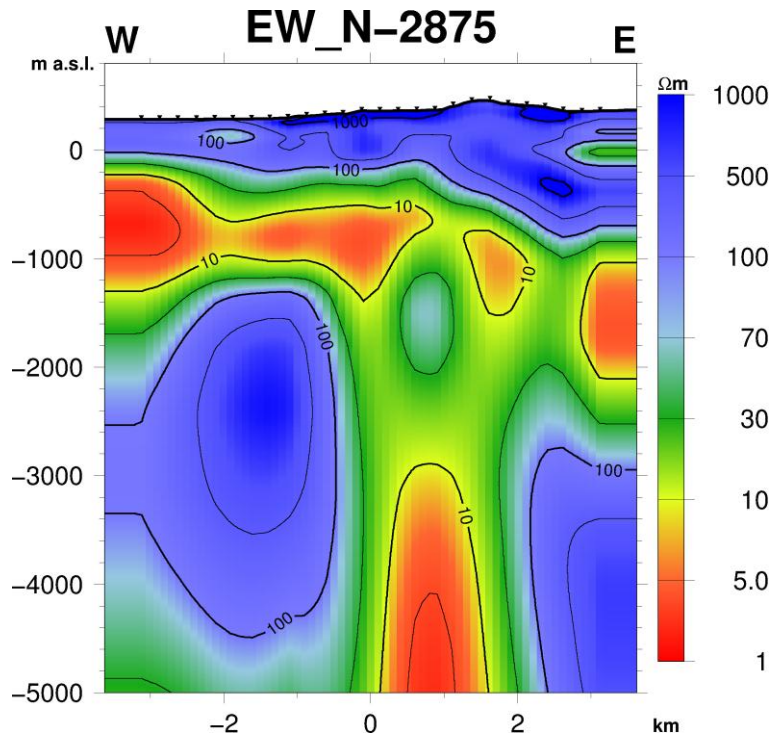


Figure 34. Resistivity cross section EW_N-2875 down to 5 and 15 km b.s.l. to the south of Hverfall and under Hraunbunga.

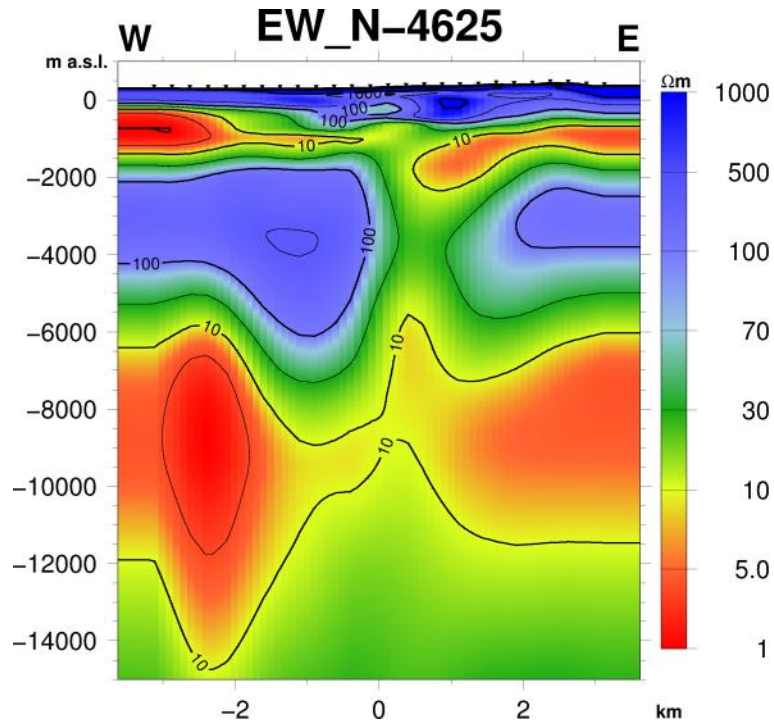


Figure 35. Resistivity cross section EW_N-4625 down to 5 km b.s.l. south of Lúdent at the southern boundary of the survey area.

6.4 NS bound resistivity cross sections (Figure 15)

Resistivity cross section NS_E-625 (Figure 36) crosses north-south through the outskirts of Bjarnarflag. It displays how the low resistivity cap reaches almost to surface and tilts down towards south and connects towards north with a layer with higher resistivity than in a conventional low resistivity cap. The deep low resistivity body domes up to a depth of 3500 m b.s.l. In cross section NS_E-125 (Figure 37) that crosses through the western slopes of Námafjall the low resistivity cap reaches surface and the top of the deep seated low resistivity body reaches the depth of 2000 m b.s.l.

Resistivity cross section NS_E125 (Figure 38) crosses the top of Námafjall mountain. The low resistivity cap reaches surface in Námafjall mountain and tilts towards south and has the same characteristics as discussed earlier towards north. Here, the deep low resistivity body reaches the depth of approximately 1500 m b.s.l. to its highest point in the area. From the Námafjall anomaly the deep seated low resistivity body extends towards south and starts doming up near Hverfjall as the cross section cuts through the western part of the Hverfjall anomaly.

As the up doming of the low resistivity is considered to indicate the up flow of heat into the geothermal system the main up flow into the geothermal system in Námafjall is under Námafjall mountain.

Resistivity cross section NS_E375 (Figure 39) cuts through both anomalies in the deep seated low resistivity as well as it displays the low resistivity column that connects to the low resistivity cap close to the Námafjall anomaly and discussed above.

Resistivity cross section NS_E875 (Figure 40) cuts through the highest point of the Hverfjall anomaly at 3000 m b.s.l. and the eastern part of the Námafjall anomaly. The last cross section NS_E1375 (Figure 41) cuts through the Hverfjall anomaly but here there is no sign of the Námafjall anomaly.

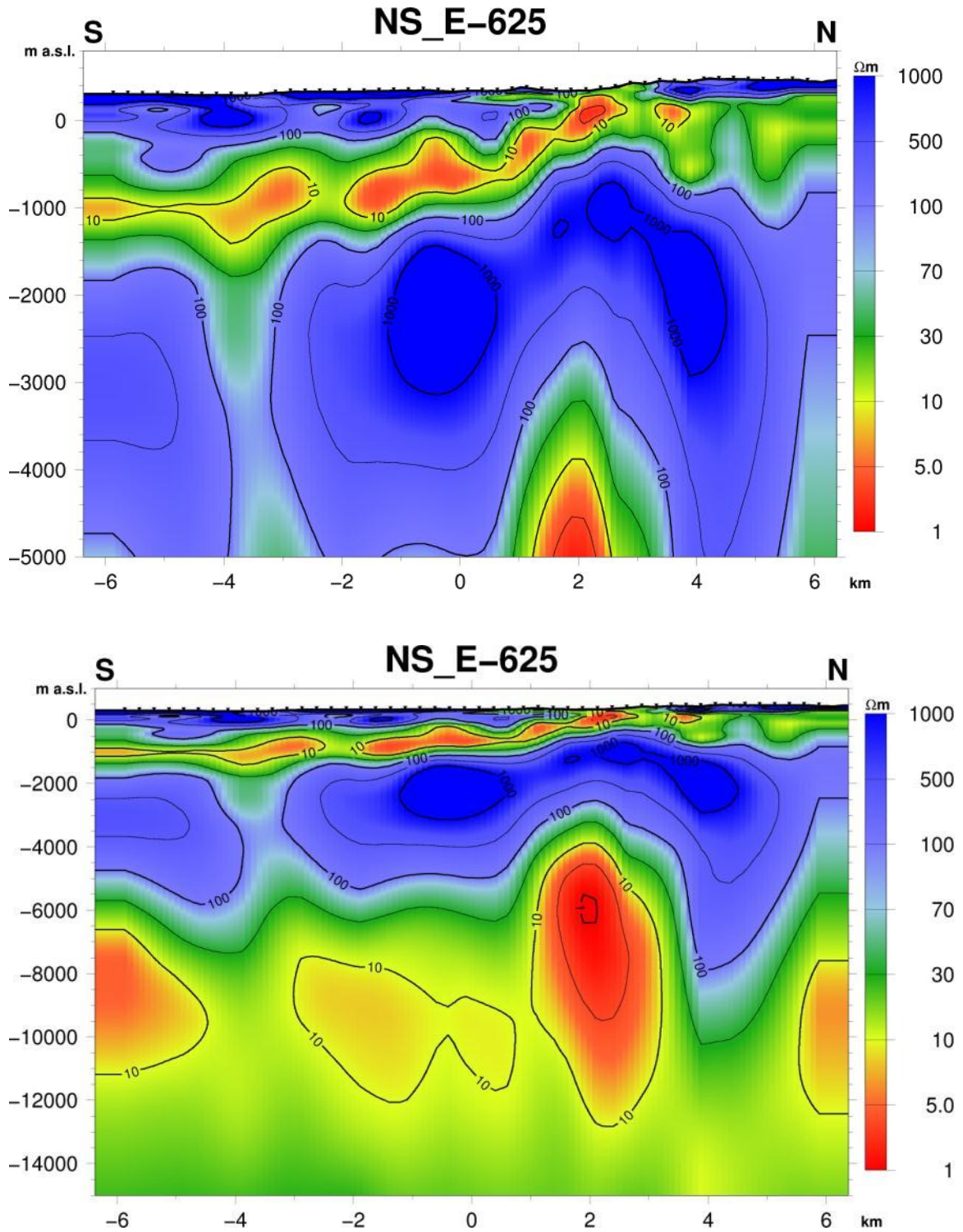


Figure 36. Resistivity cross section NS_E-625 down to 5 and 15 km b.s.l. under Bjarnarflag.

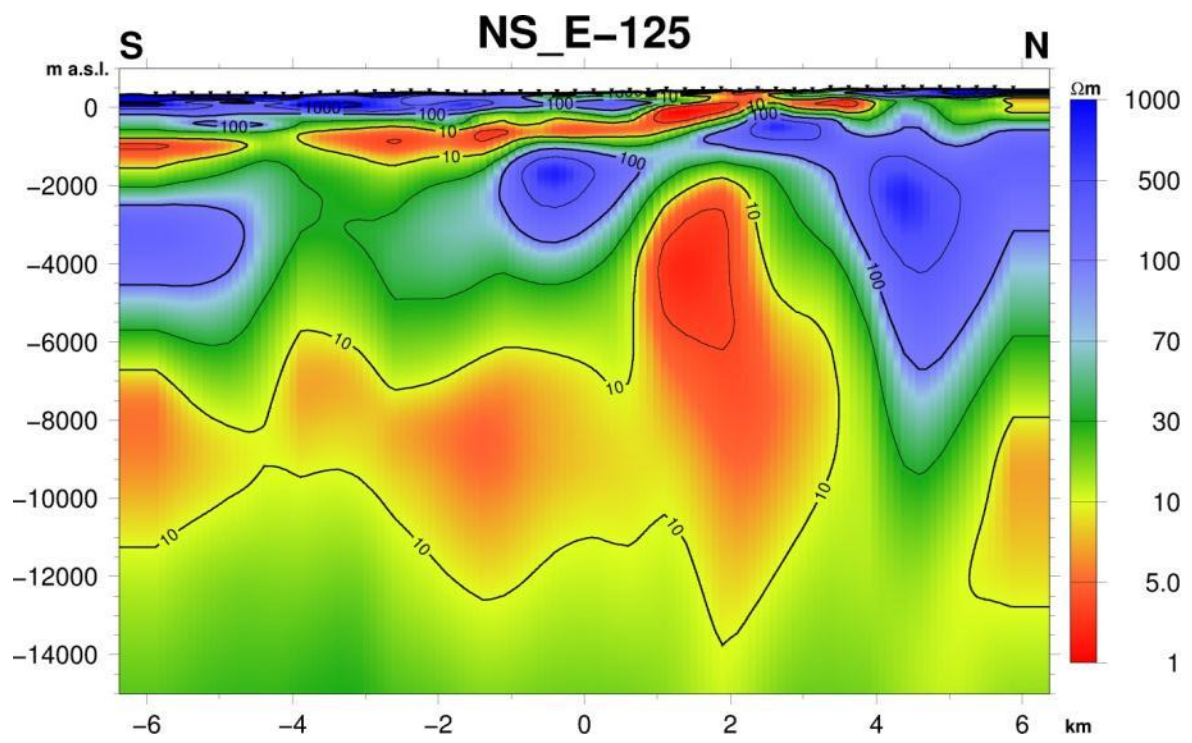
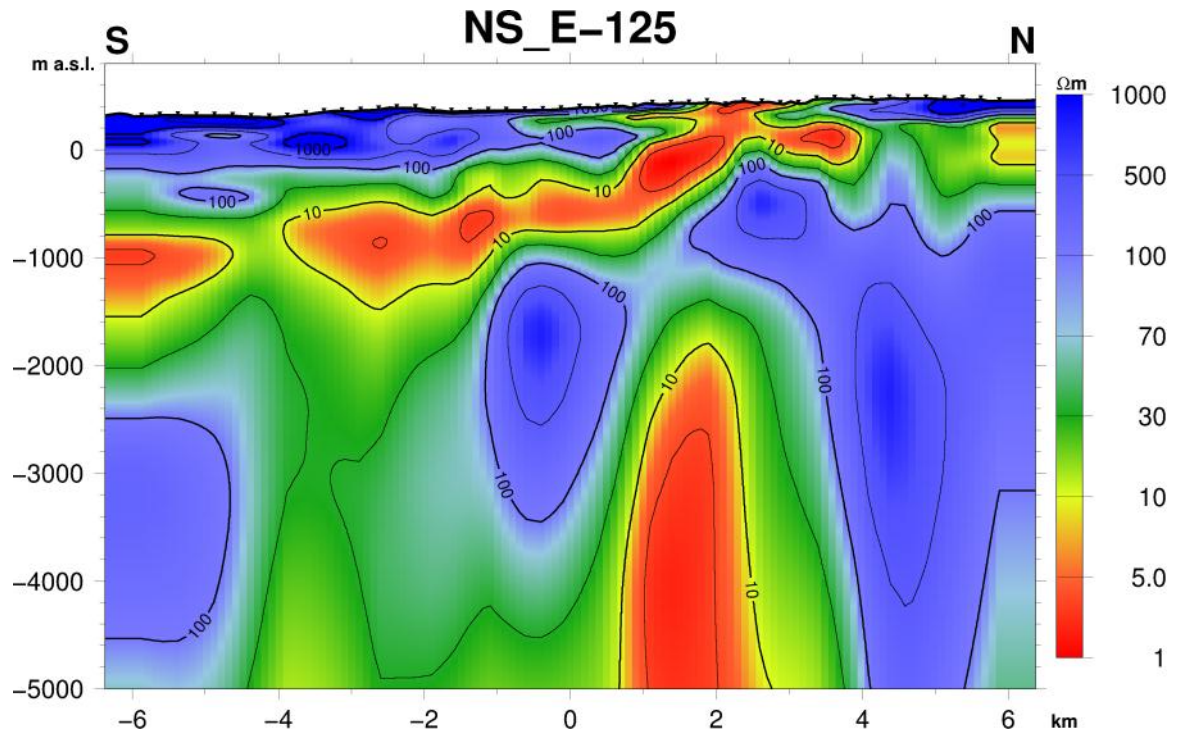


Figure 37. Resistivity cross section NS_E-125 down to 5 and 15 km b.s.l. under the western slopes of Námafjall mountain and Dal fjall mountain.

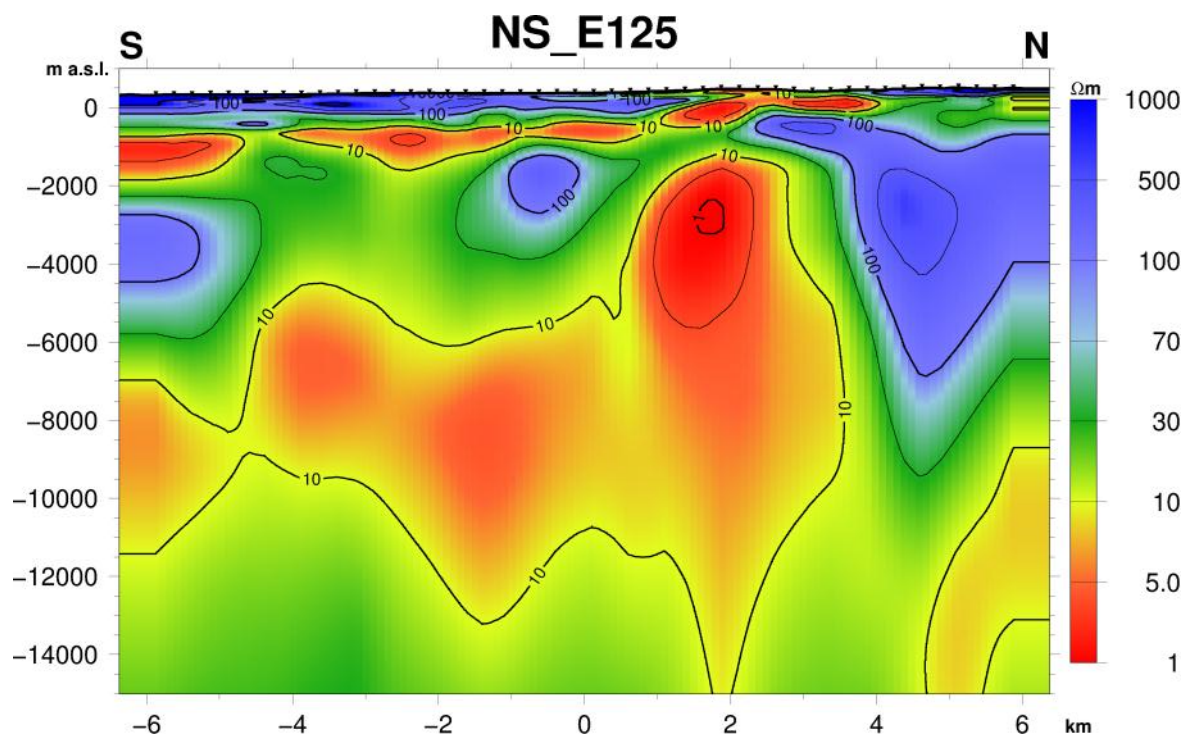
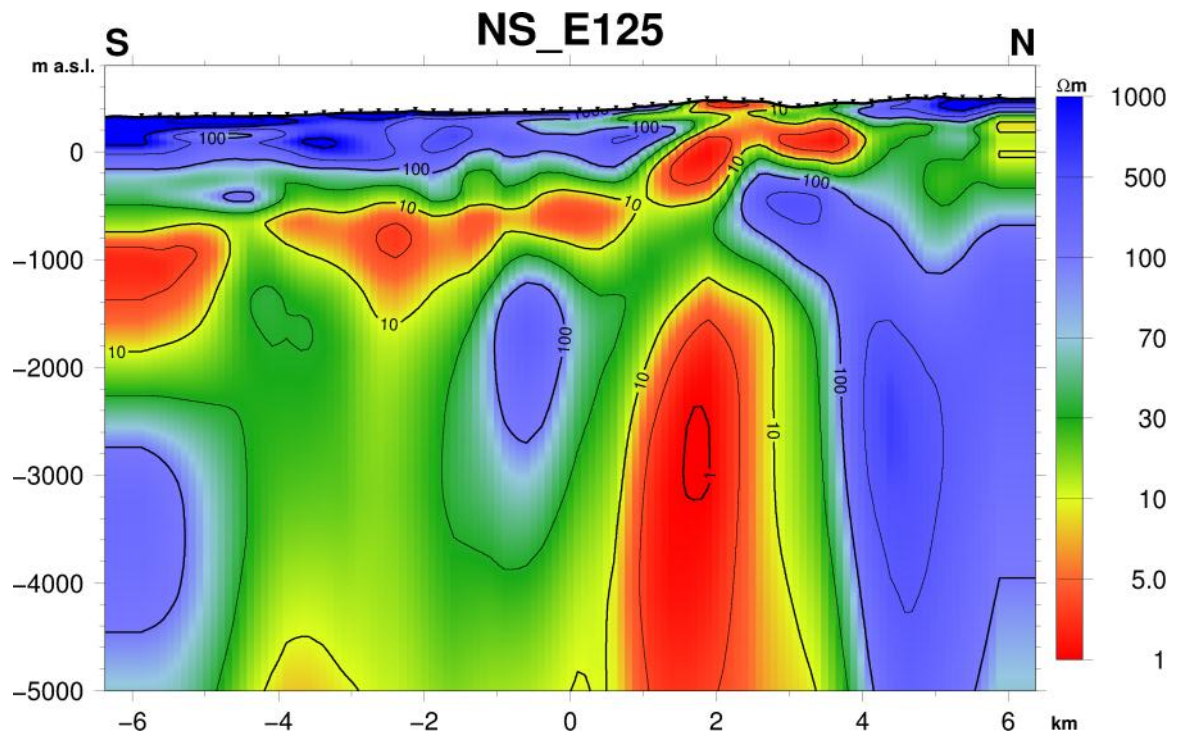


Figure 38. Resistivity cross section NS_E125 down to 5 and 15 km b.s.l. under Námajfall mountain. It shows the Námajfall anomaly and the Hverfjall anomaly in the south.

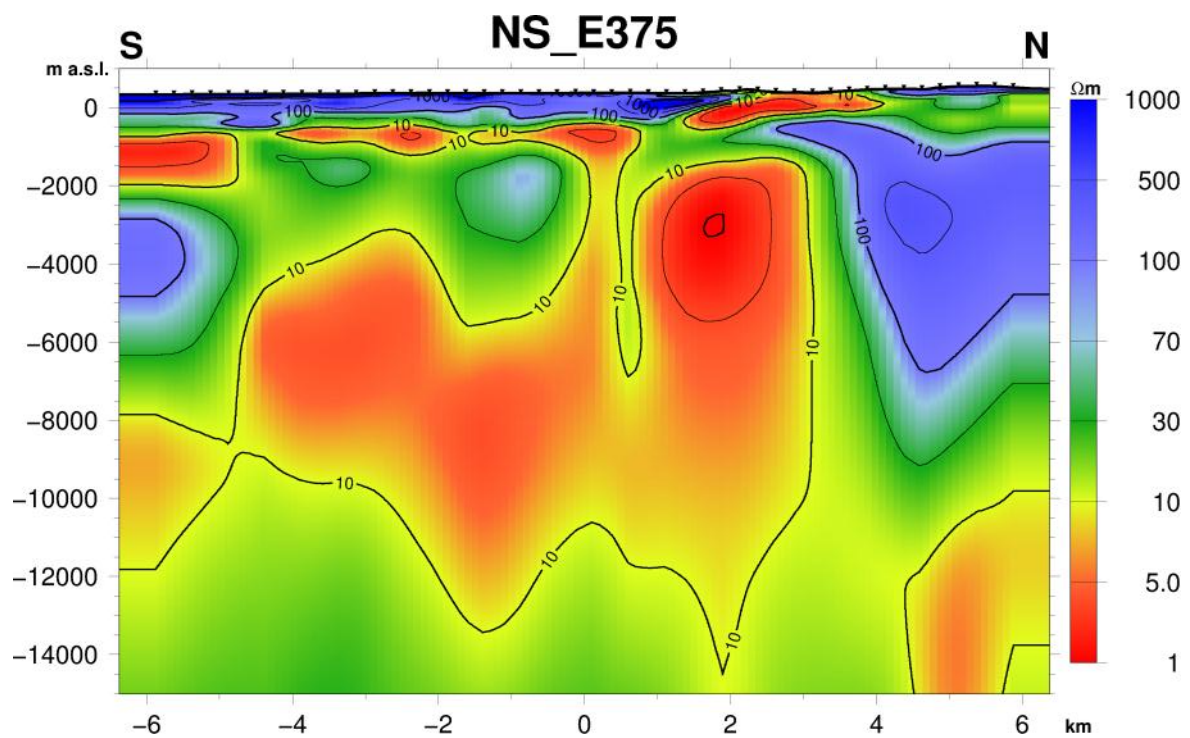
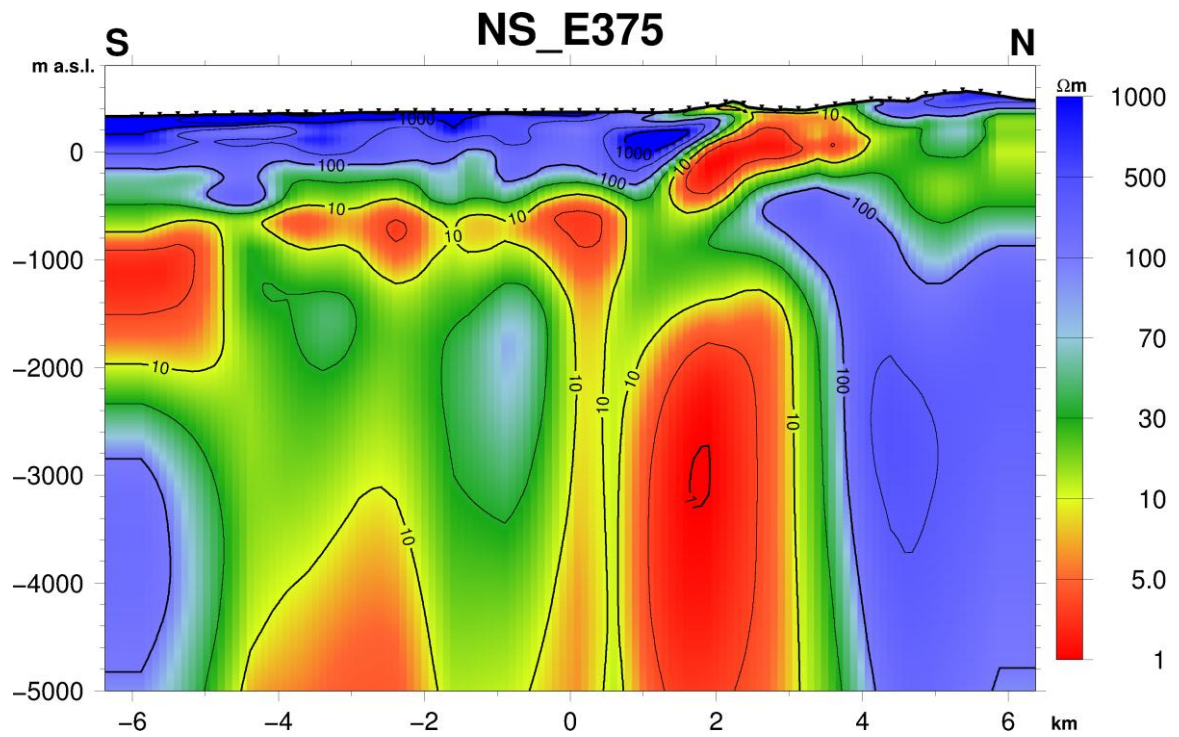


Figure 39. Resistivity cross section NS_E375 down to 5 and 15 km b.s.l. through the Hverfjall anomaly and the eastern part of the Námafjall anomaly. It also displays the low resistivity column just south of Námafjall mountain.

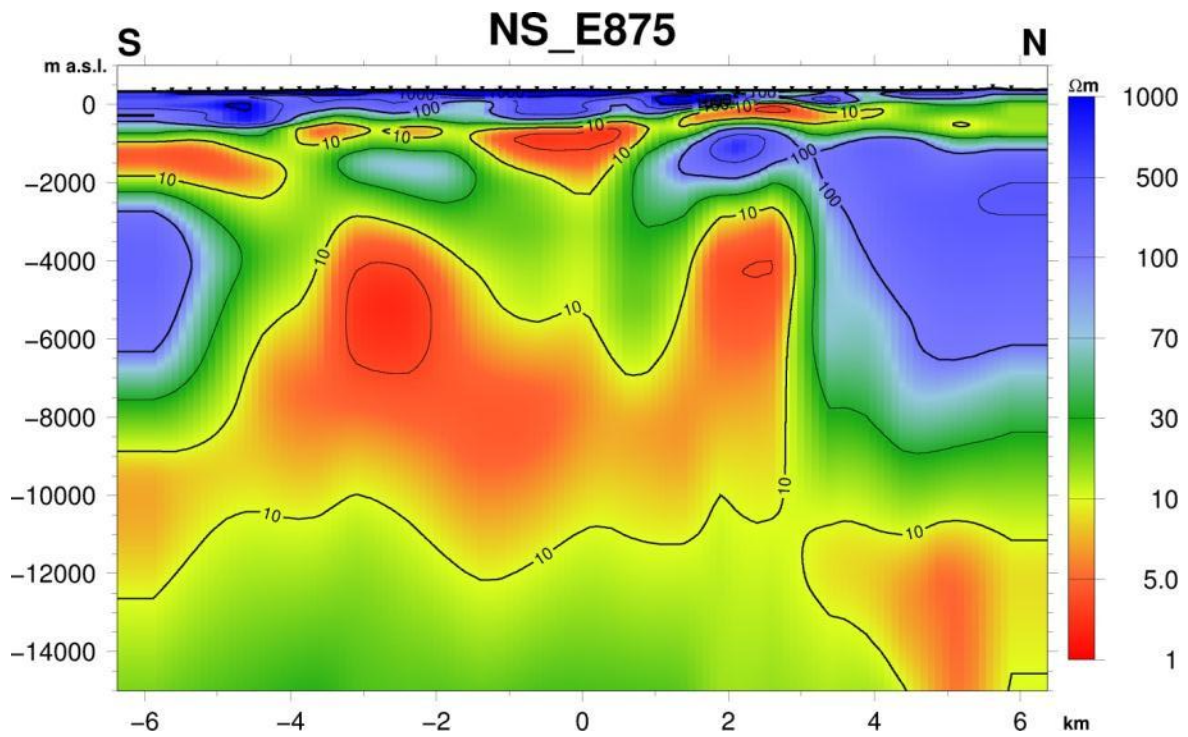
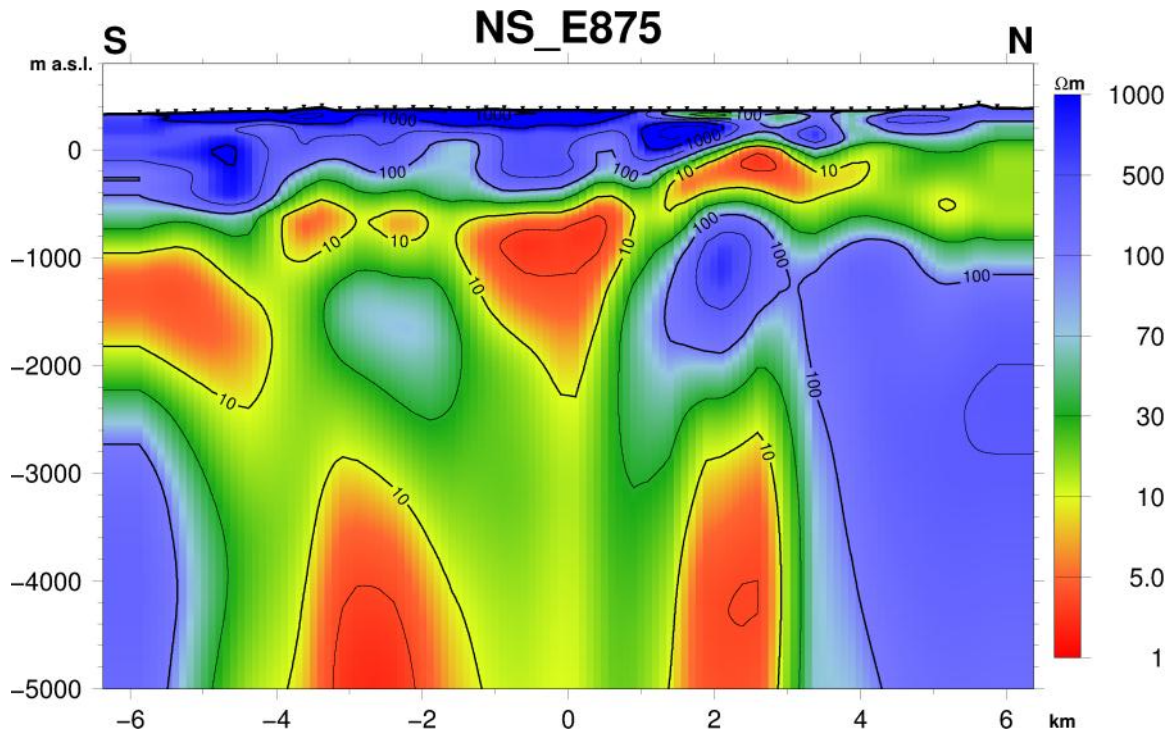


Figure 40. Resistivity cross section NS_E875 down to 5 and 15 km b.s.l. under Hverarönd and Hraunbunga.

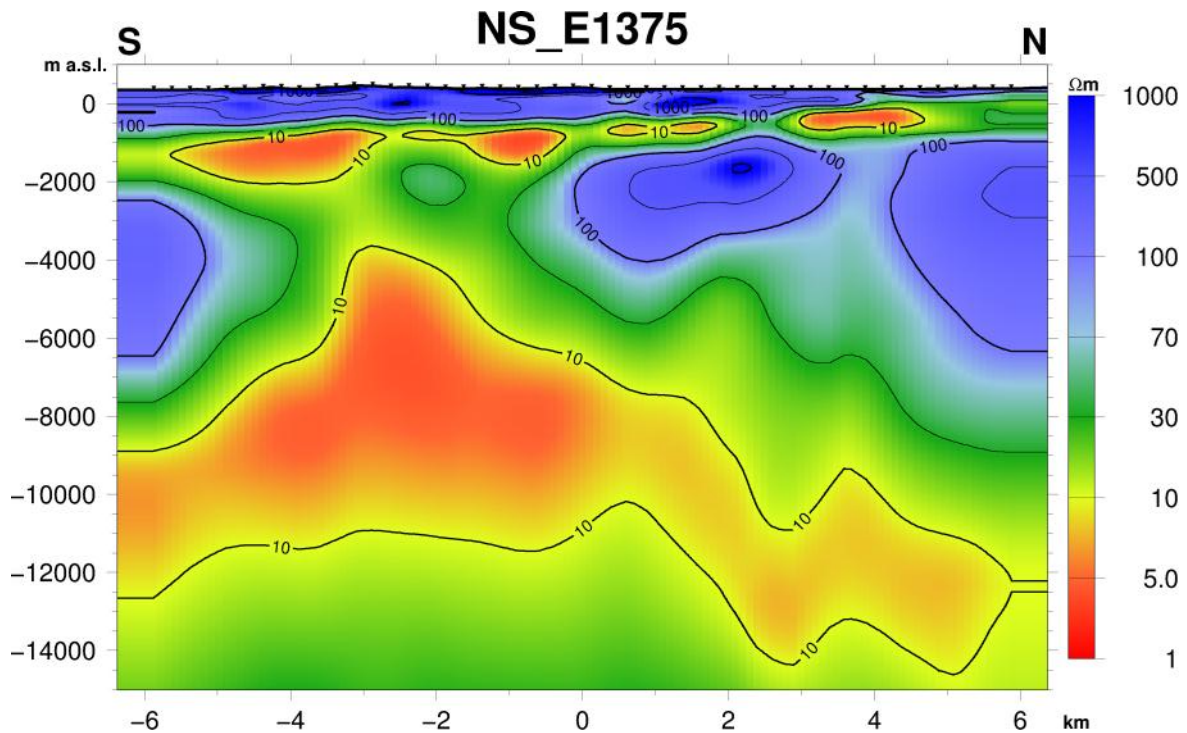


Figure 41. Resistivity cross section NS_E1375 down to 15 km b.s.l. east of Námafjall mountain, showing sign of the Hverfjall anomaly, but there is no sign of the Námafjall anomaly.

7 Conclusion

The TEM/MT survey in Námafjall reveals a conventional resistivity structure of a high temperature field i.e. a low resistivity cap underlain by a high resistivity core and a deep seated low resistivity body at depth indicating the heat source.

- A low resistivity cap that reflects the zeolite/smectite zone covers the whole area. It reaches surface in Námafjall, Bjarnarflag and Hverarönd. It tilts down towards all directions except to the north. Its upper boundary levels at approximately 500 m b.sl. To the south, where the data coverage is best, the cap levels at 500 m b.sl. between Námafjall and Hverfjall south of which it tilts further down to approximately 1000 m b.sl.
- To the north, the low resistivity cap connects to a layer with low resistivity (12–20 Ωm) in the area where Námafjall and Krafla Geothermal fields meet. This low resistivity layer has a character of a low resistivity cap with an underlying higher resistivity.
- A high resistivity core reflecting the chlorite/epidote zone underlies the low resistivity cap. The margin between the two reflect the 230–240°C temperature boundary provided there is a thermal equilibrium between thermal alteration and temperature at present within the geothermal system. The high resistivity core rises highest to 150–200 m a.sl. below Námafjall mountain.

- In all MT surveys conducted in Iceland, a deep seated low resistivity layer has been encountered at 8–15 km depth b.sl., except in Reykjanes peninsula and close to the coast line. Most MT surveys have been conducted in geothermal fields and within the volcanic zone. The deep seated low resistivity layer domes up to a shallower depth beneath high temperature fields. At Námafjall it can be seen at 1500 m b.sl. or at approximately 2 km depth below surface. The up doming of the deep low resistivity layer is considered to indicate the up flow of heat into the geothermal system.
- An up flow of heat into the system is indicated by two anomalies, one under Námafjall and another south east of Hverfjall.

The **Námafjall** low resistivity anomaly domes up to 1500 m b.sl. under Námafjall mountain and seems to indicate the main up flow zone into the geothermal system

The **Hverfjall** low resistivity anomaly domes up to 3000 m b.sl. just south east of Hverfjall and may indicate a second up flow zone into the geothermal system.

- The 3D model run with the 1D input model had the best fit of the data (RMS fit 1.76). Running input models with different initial resistivity did not give resolution at depth below 3 km b.sl. and did not get as good RMS data fit.
- It is clear that the result of the 3D inversion is dependent on the input model. As the best fit of the data was acquired with the 1D input model and that model is used as output model here. Better fit in the longer periods would be preferable, even in the output model used. Better fit at the longer periods would most likely require low resistivity at depth i.e. the low resistivity at depth is present in the data even though it seems so difficult to fit by the 3D inversion run with different initial models.
- The available resistivity well logs have been presented along with the 3D resistivity model in PETREL visualization software. Other data now being incorporated into Petrel are: Data on petrology from the cuttings, data on alteration minerals/zones from X-ray diffraction, temperature distribution from temperature logs as well as inferred data from the inspection of the wells, such as location of feed zones, fractures and faults.
- A DVD disc presenting the 3D resistivity model in the visualizing software PETREL along with available other data from wells will be submitted with this report. It will not do the visualization in the PETREL software any justice to even try to describe in words how the data compare to each other. One picture says more than hundred words.
- It is recommended that a further and more detailed comparison of all data available for the Námafjall field be done utilizing Petrel. Visualizing the data in 3D gives opportunity to compare one data set to another from various angles and adding data gradually (“layer by layer”) to the picture in an attempt to understand the inner structure and physical conditions within a geothermal system.

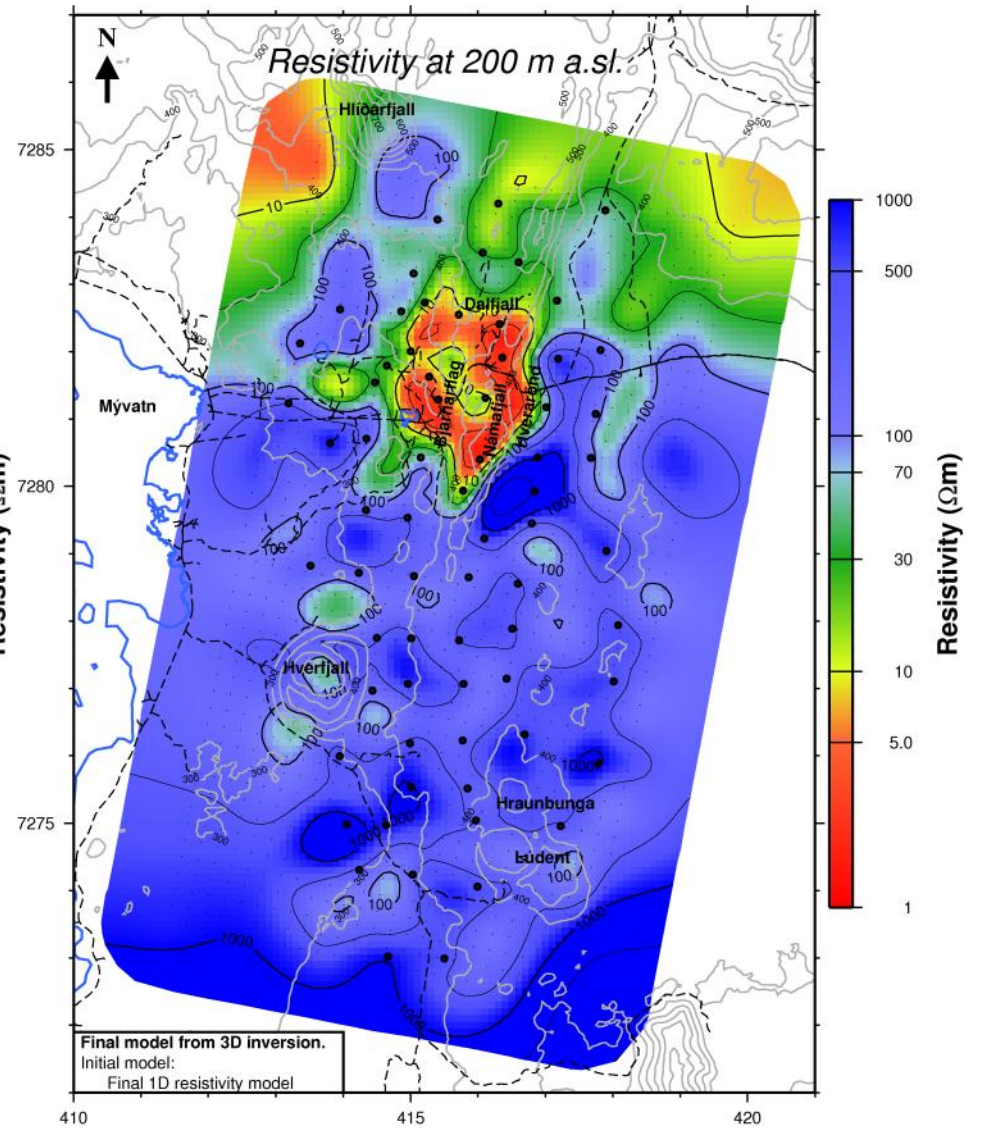
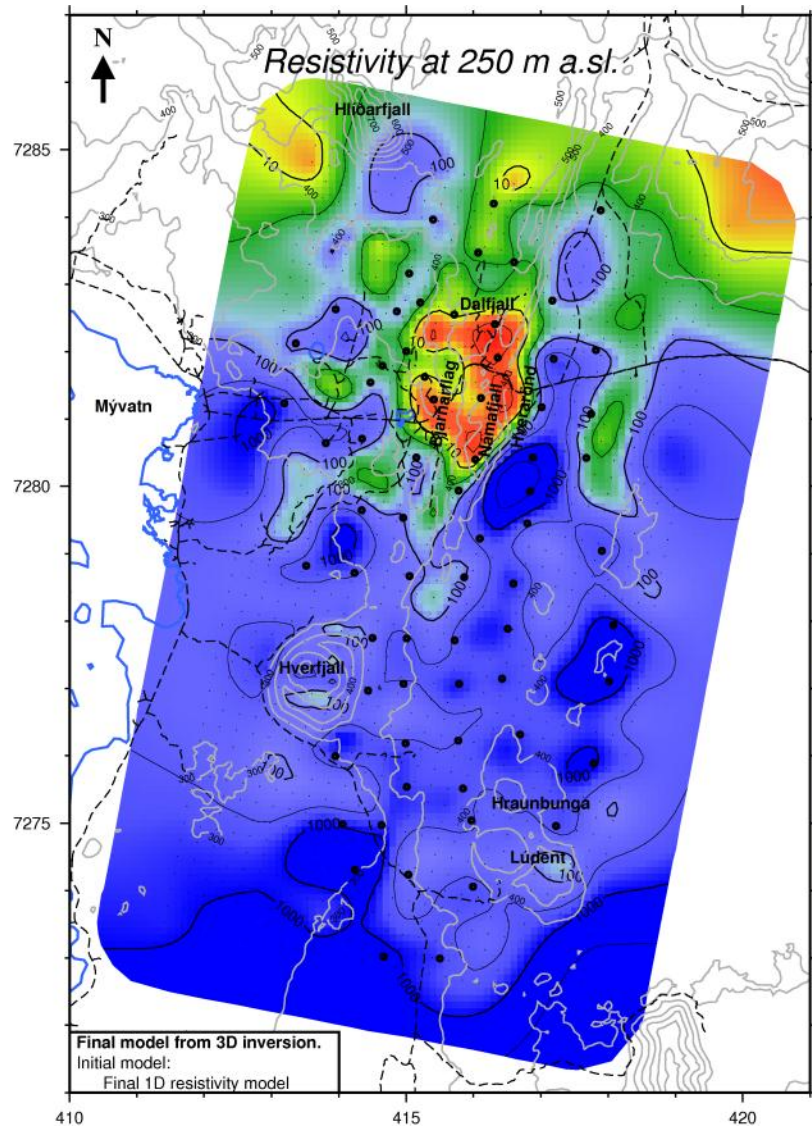
8 References

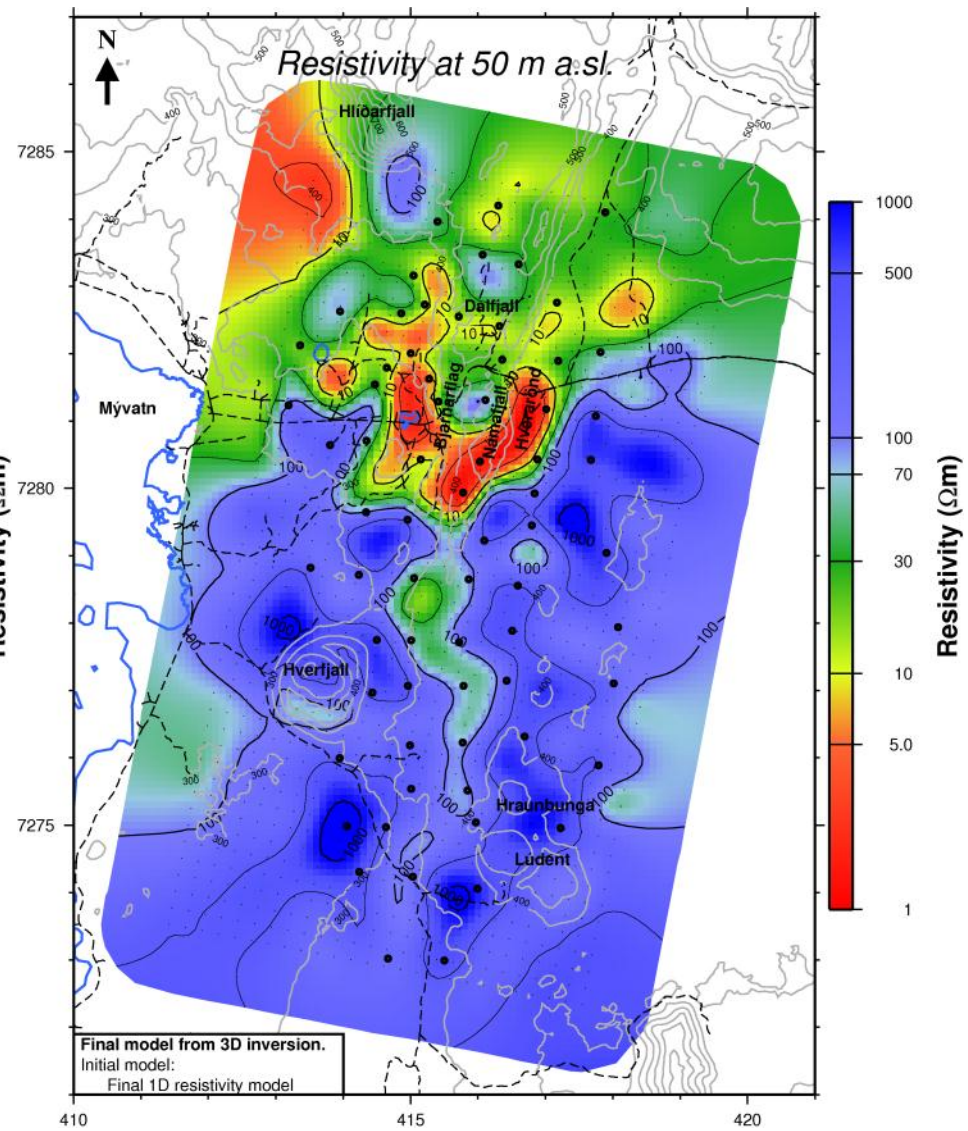
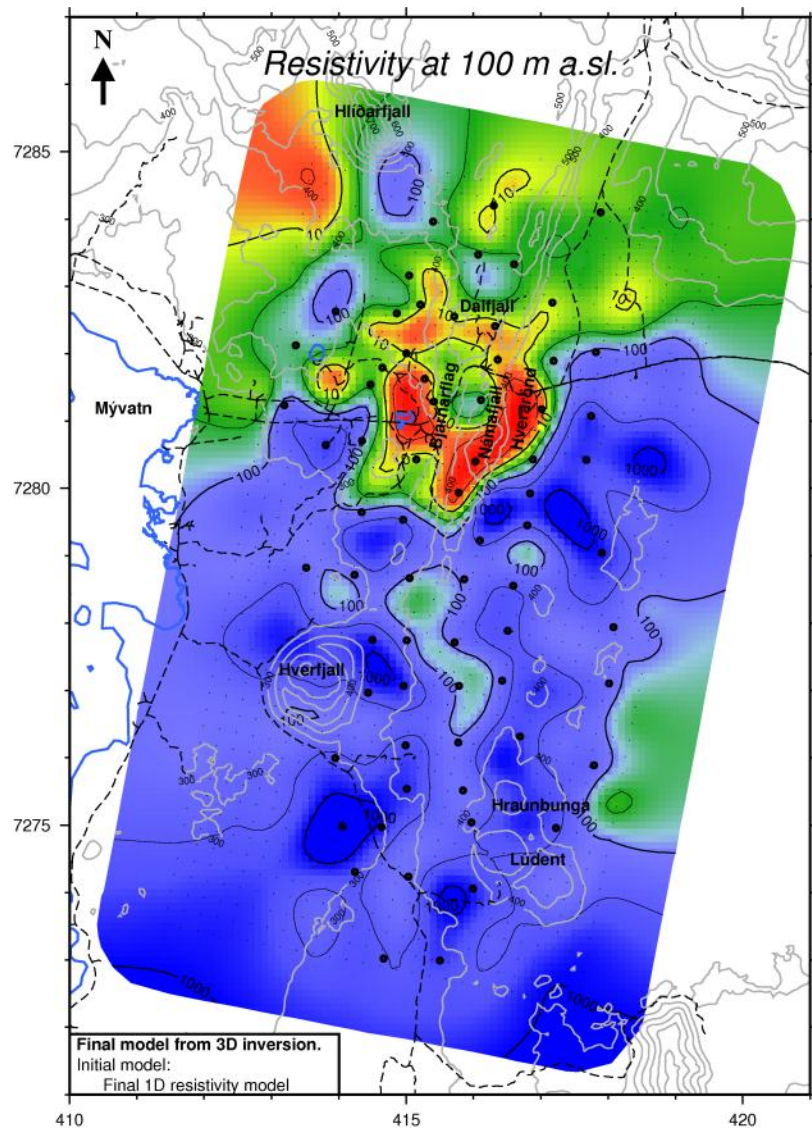
- Árnason, K. (2008). *The Magnetotelluric static shift problem*. Iceland GeoSurvey, short report, ÍSOR-08088, 16 pp.
- Árnason, K., Eysteinnsson, H. and Hersir, G. P. (2010). Joint 1D inversion of TEM and MT data and 3D inversion of MT data in the Hengill area, SW Iceland. *Geothermics* 39, 13–34.
- Árnason, K., Karlsdóttir, R., Eysteinnsson, H., Flóvenz, Ó. G., and Gudlaugsson, S. Th., (2000). The resistivity structure of high-temperature geothermal systems in Iceland. *Proceedings of the World Geothermal Congress 2000, Kyushu-Tohoku, Japan*, 923–928.
- Beblo, M. and Björnsson, A. (1980). A model of electrical resistivity beneath NE-Iceland, correlation with temperature. *J. Geophys.*, 47, 184–190.
- Constable, C. S., Parker, R. L. and Constable, C. G. (1987). Occam's inversion: a practical algorithm for generating smooth models from electromagnetic sounding data. *Geophysics* 52, 289–300.
- Egbert, G. D. and Booker, J. R. (1986). Robust estimation of geomagnetic transfer functions. *Geophys. J. R. Astr. Soc.* 87, 173–194.
- Eysteinnsson, H. and Hermance, J. F. (1985). Magnetotelluric measurements across the eastern neovolcanic zone in South Iceland. *J. geophys. Res.*, 90, 10093–10103.
- Flóvenz, Ó. G., Spangenberg, E., Kulenkampff, J., Árnason, K., Karlsdóttir, R. and Huenges, E. (2005). The role of electrical interface conduction in geothermal exploration. Oral presentation at IGA, *World Geothermal Congress, in Turkey 2005*. Published in conference proceedings.
- Karlsdóttir, R. (2002). *Námafjall. TEM viðnámsmælingar 2001*. Report in Icelandic. National Energy Authority, OS-2002/057 68 p.
- Karlsdóttir, R. (2011). TEM-MT survey at Námafjall high temperature field 2009. 1D interpretation. Iceland GeoSurvey, ÍSOR-2011/029. LV-2011/068. 50 p.
- Mortensen, A. K., Guðmundsson, Á., Steingrímsson, B., Sigmundsson, F., Axelsson, G., Ármannsson, H., Björnsson, H., Ágústsson, K., Sæmundsson, K., Ólafsson, M., Karlsdóttir, R., Halldórsdóttir, S. and Hauksson, T. (2009). *Krafla Geothermal System. Conceptual Model*. Iceland GeoSurvey, ÍSOR-2009/057, LV-2009/111. In Icelandic. 206 p.
- Phoenix Geophysics (2005). *Data Processing User Guide*. Phoenix Geophysics. 201 p.
- Phoenix Geophysics (2009). *V5 System 2000 MTU/MTU-A User Guide*. Phoenix Geophysics. 178 p.
- SEG (1991). *MT/EMAP data interchange standard*. Society of Exploration Geophysicists, 112 p.
- Siripunvaraporn, W., Egbert, G., Lenbury, Y. and Uyeshima, M. (2005). Three-dimensional magnetotelluric inversion: data-space method. *Phys. Earth Planet. Int.* 150, 3–14.

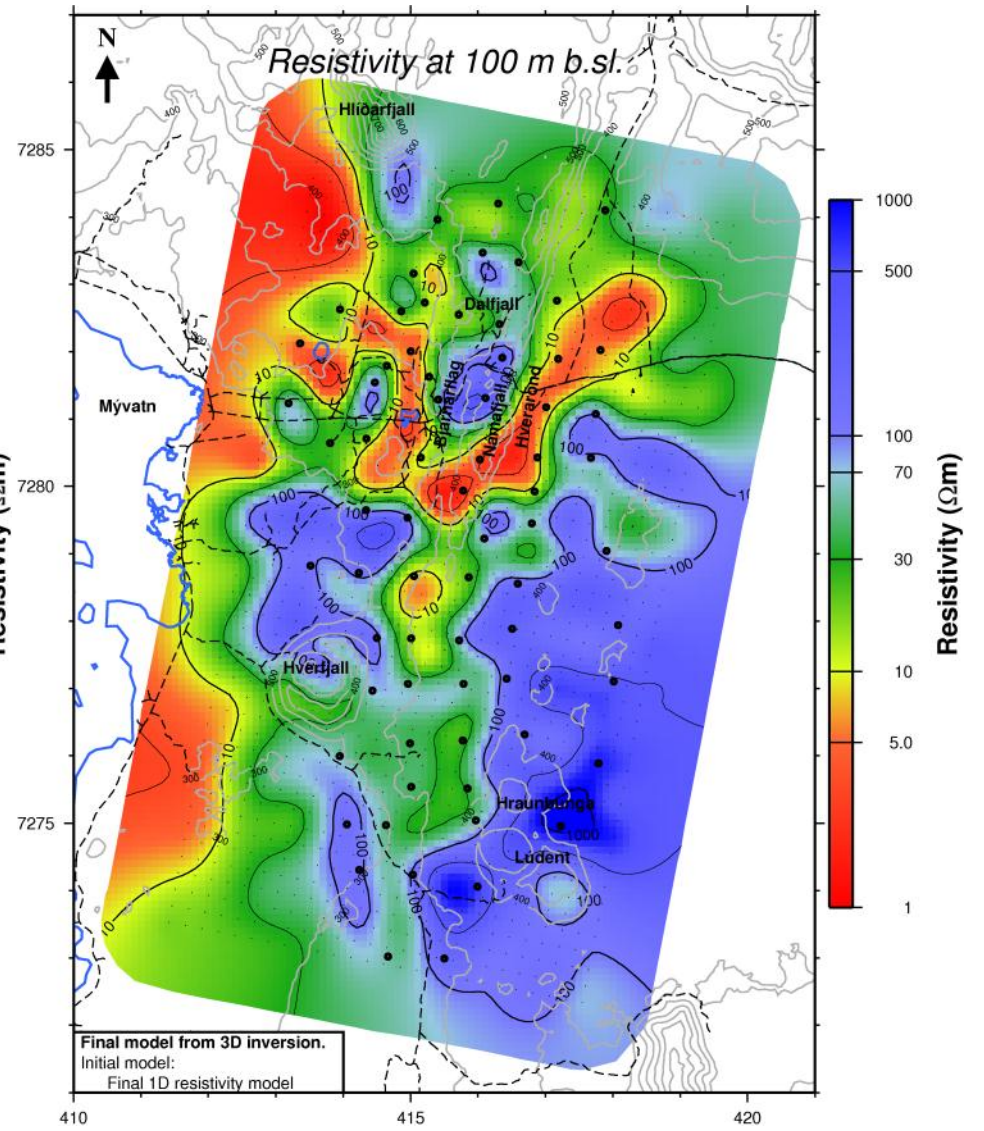
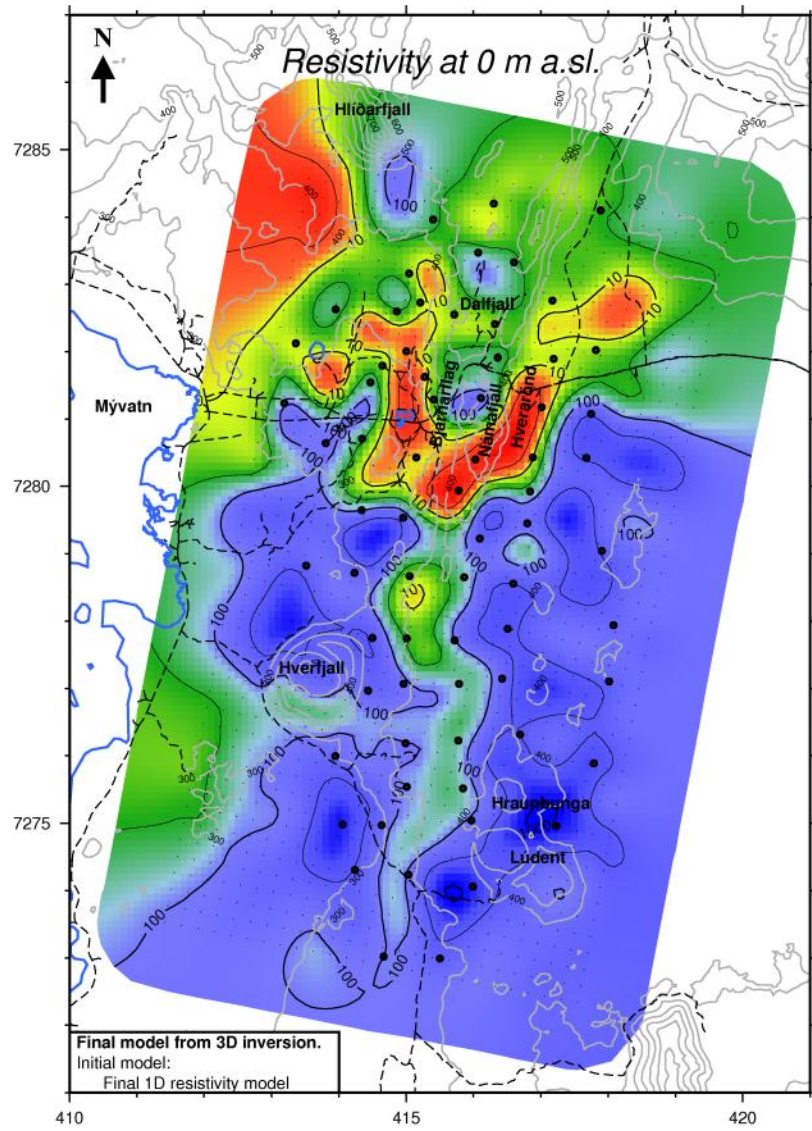
- Siripunvaraporn, W. and Egbert, G. (2009). WSINV3DMT: Vertical magnetic field transfer function inversion and parallel implementation. *Phys. Earth Planet. Int.* 173, 317–329.
- Vilhjálmsón, A. M., Flóvenz, Ó. G., Karlsdóttir, R., Árnason, K., Eysteinnsson, H. and Sæmundsson, K. (2008). Geophysical evidence for magmatic Transport in the Lower Crust in Iceland. *Poster at AGU conference 2008*. Paper number MR43A-1803
- Violay, M., Gibert, B., Azais, P., Lods, G. and Pezard, P. (2010). *A new cell for electrical conductivity measurement on saturated samples at upper crust conditions*. Submitted to *Transport in porous media*.
- Weidelt, P. (1972). The inverse problem of geomagnetic induction. *J. Geophys.*, 38, 257–289.

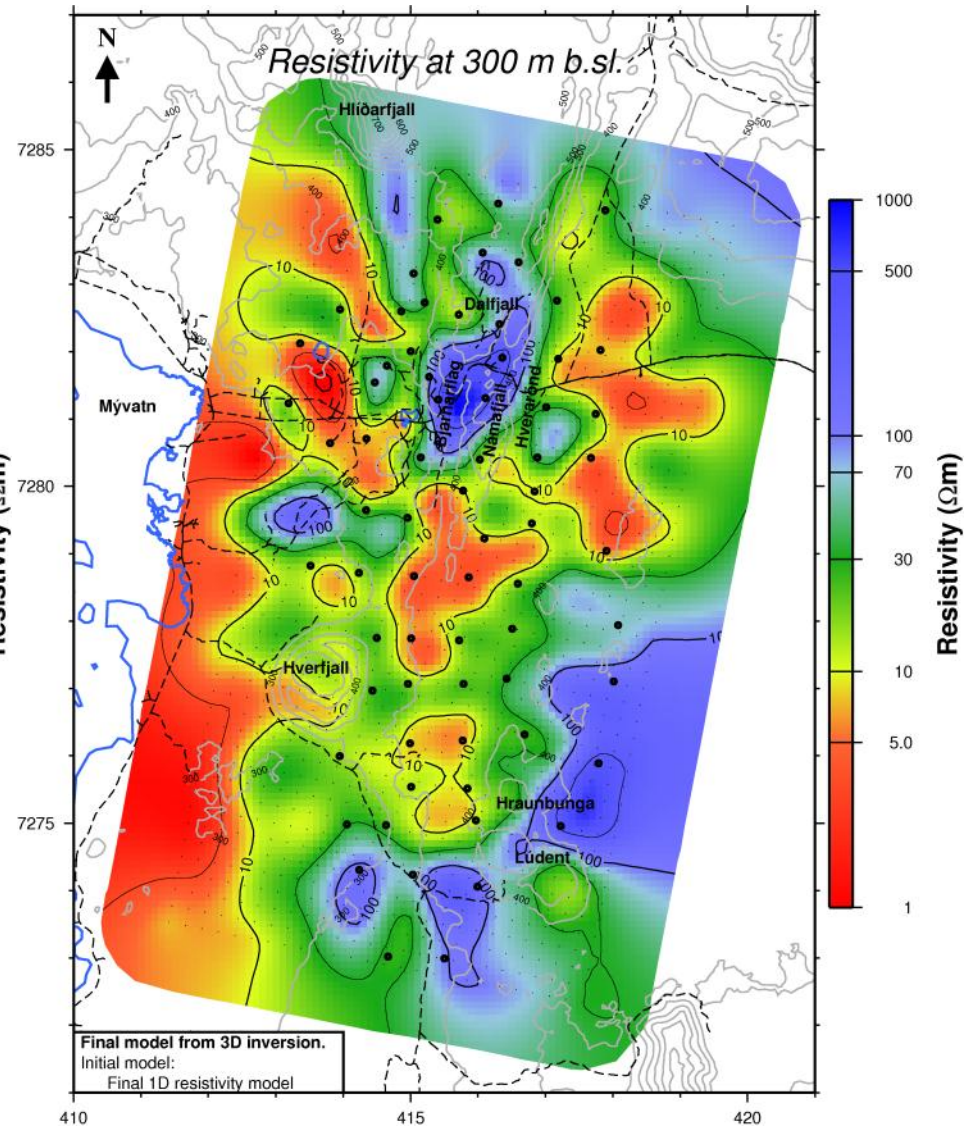
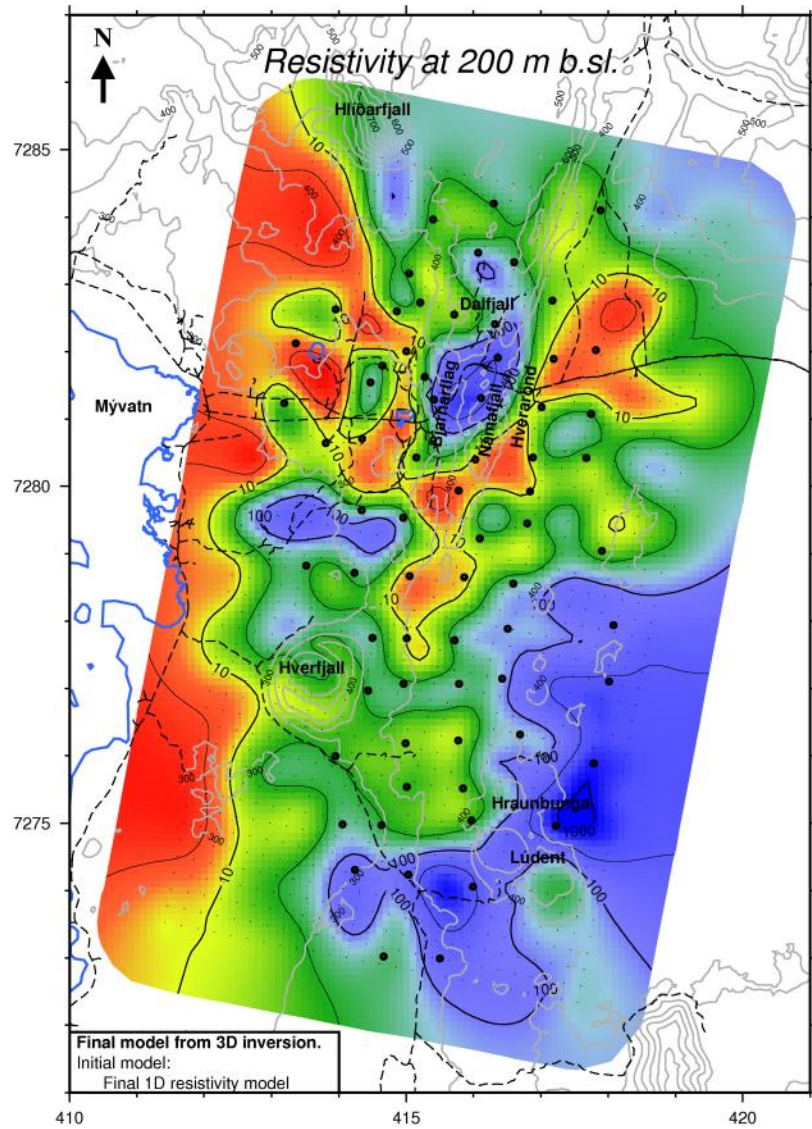
Appendix 1:

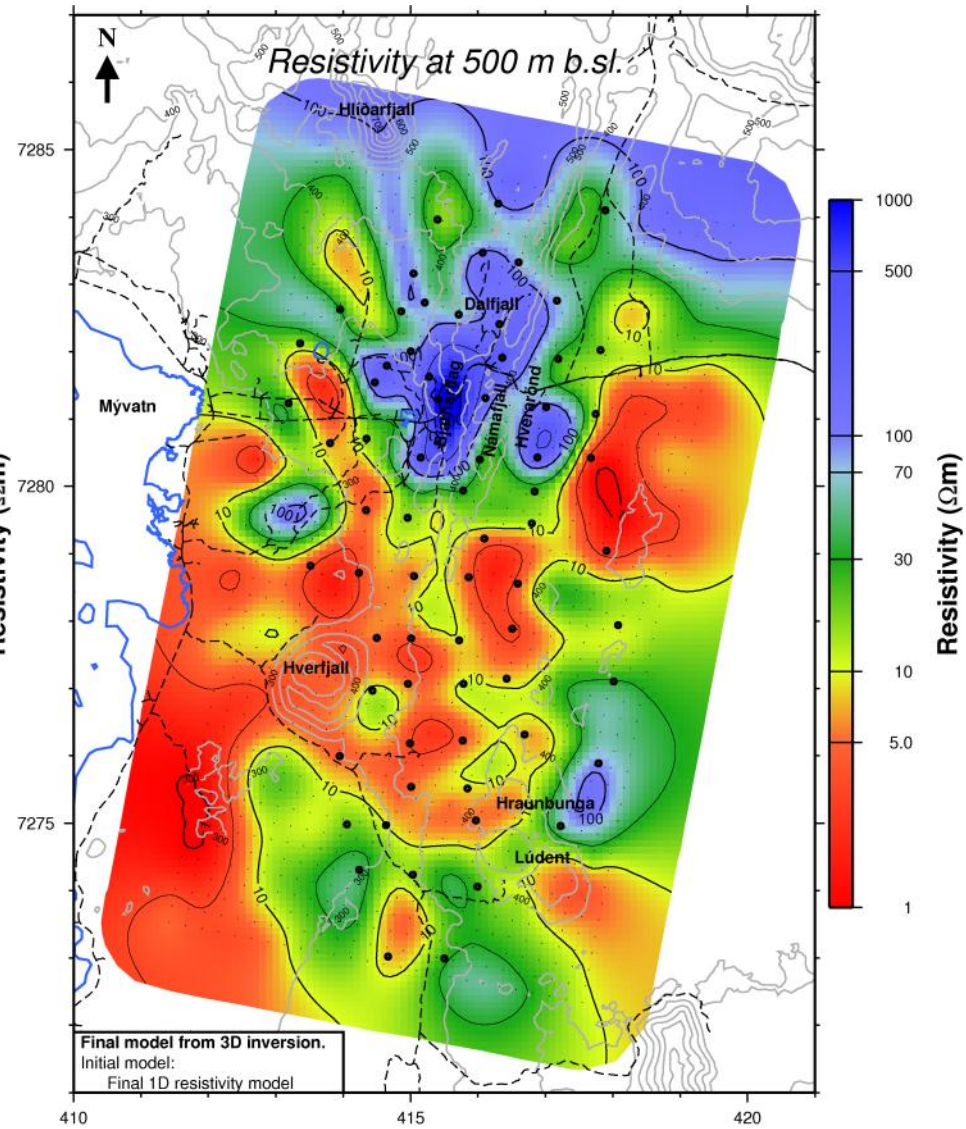
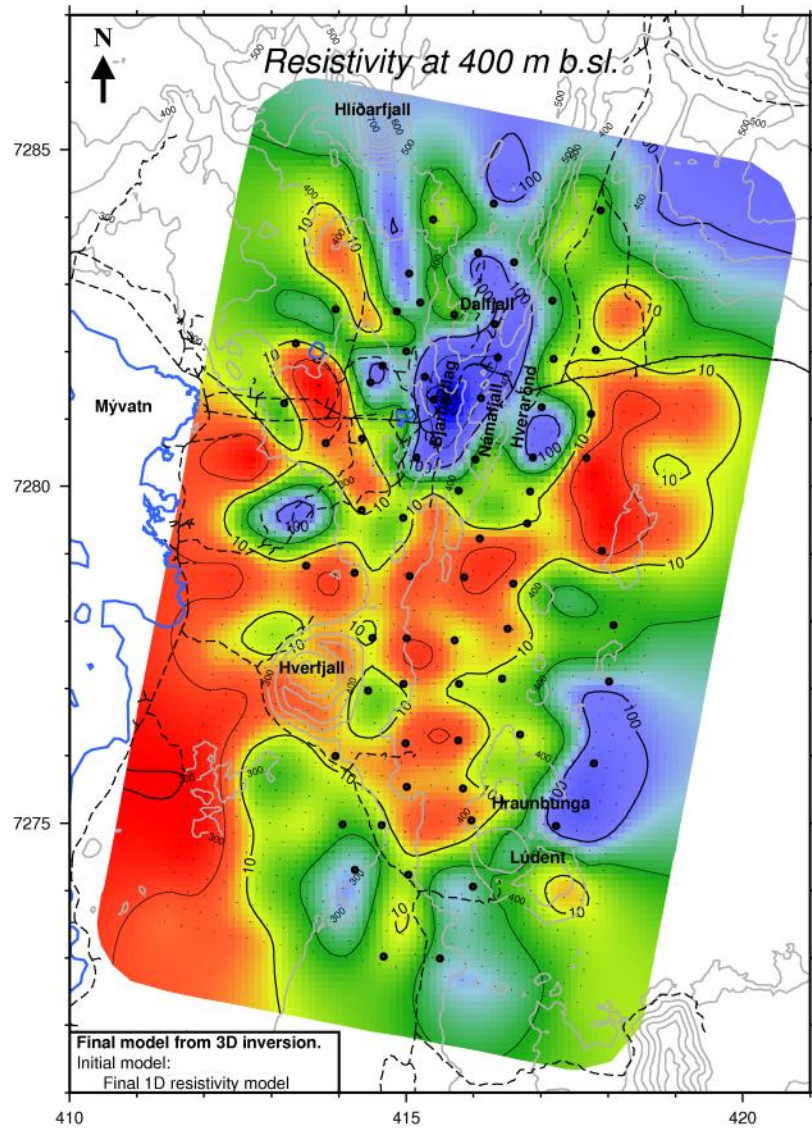
Resistivity maps

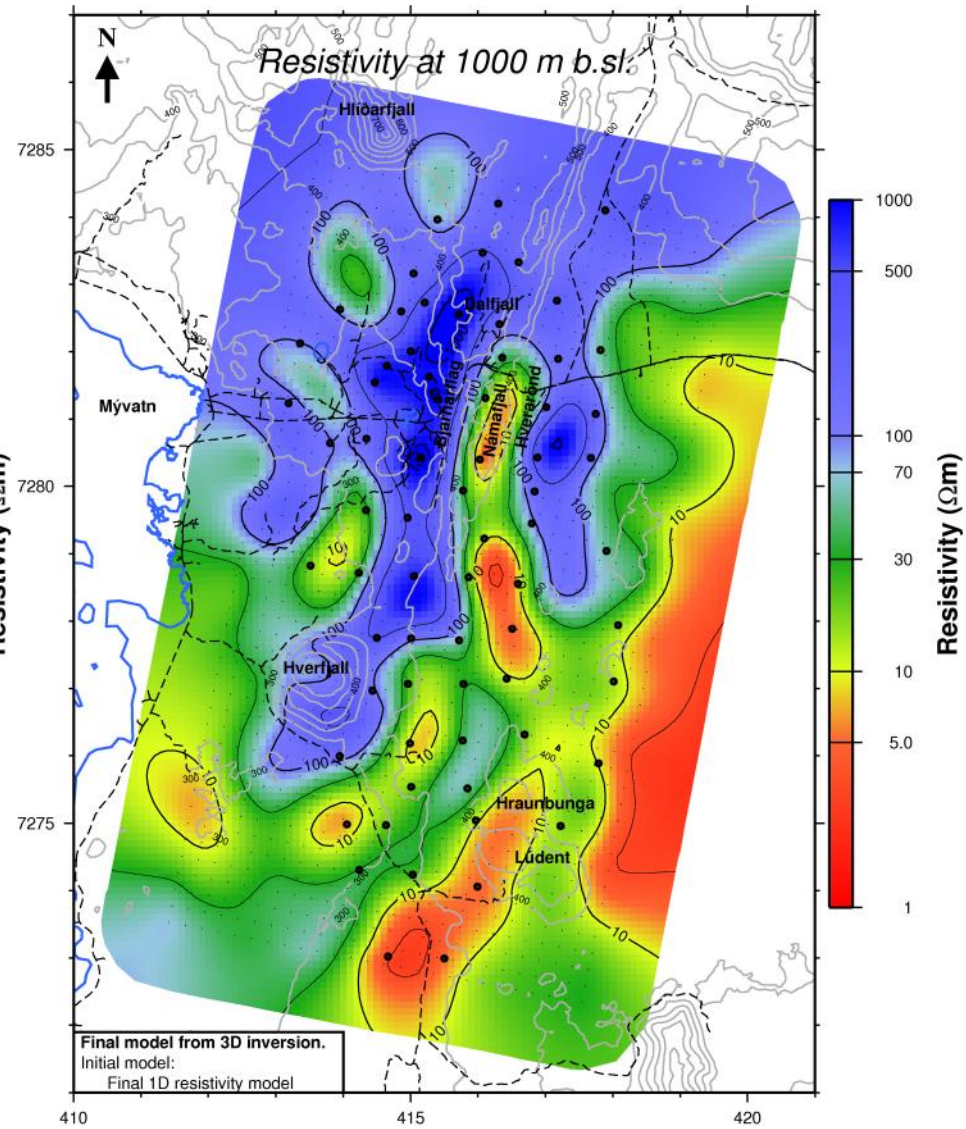
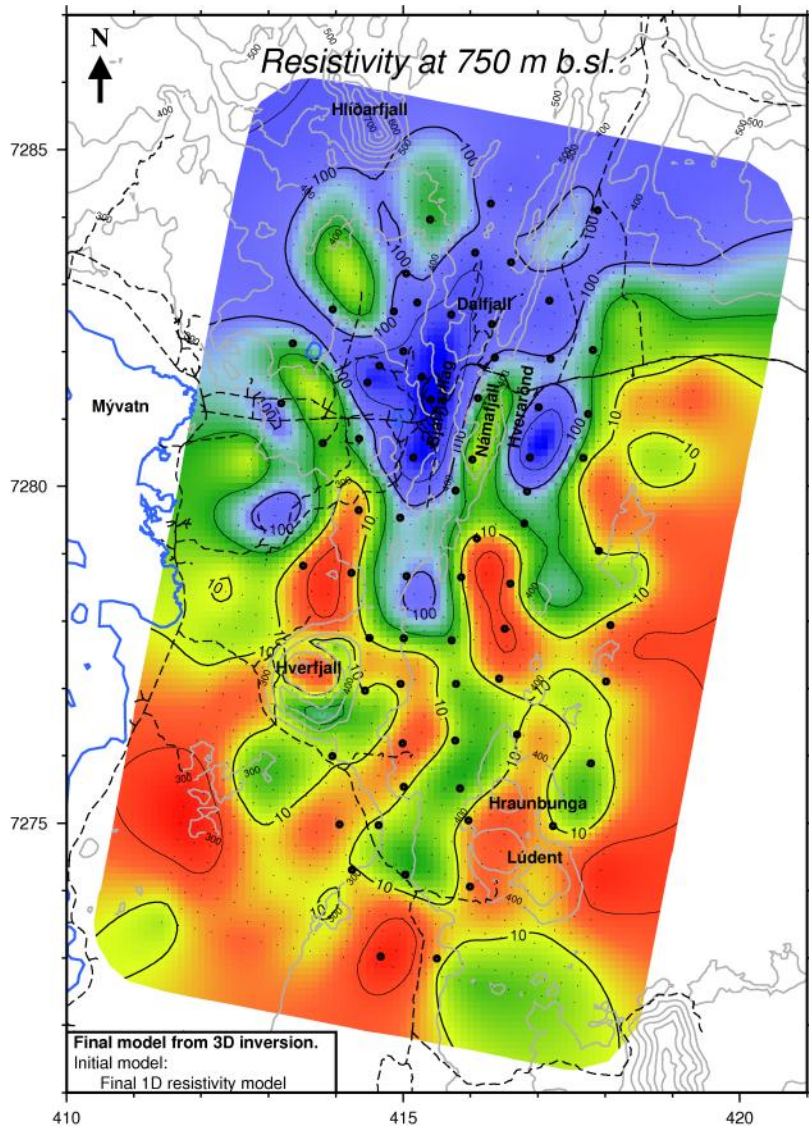


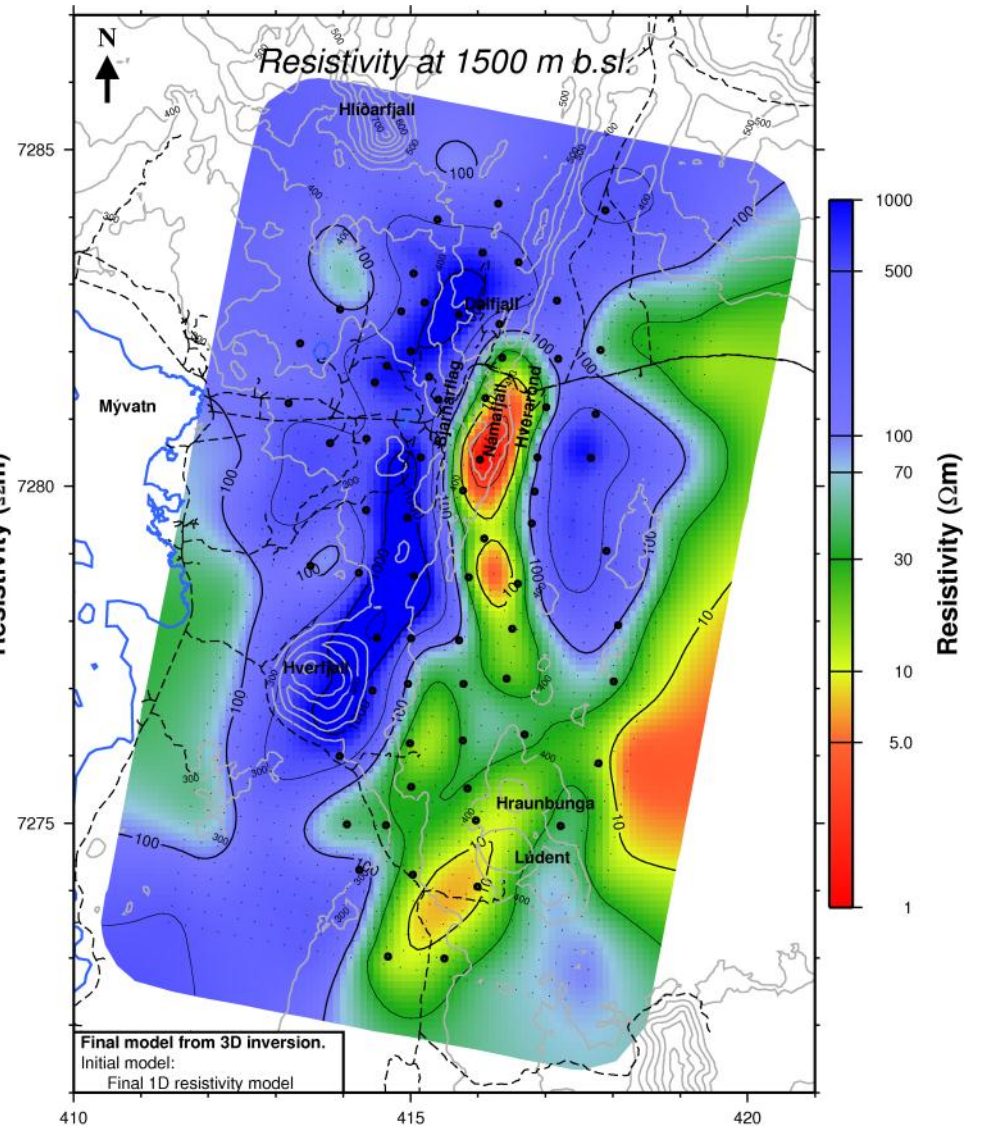
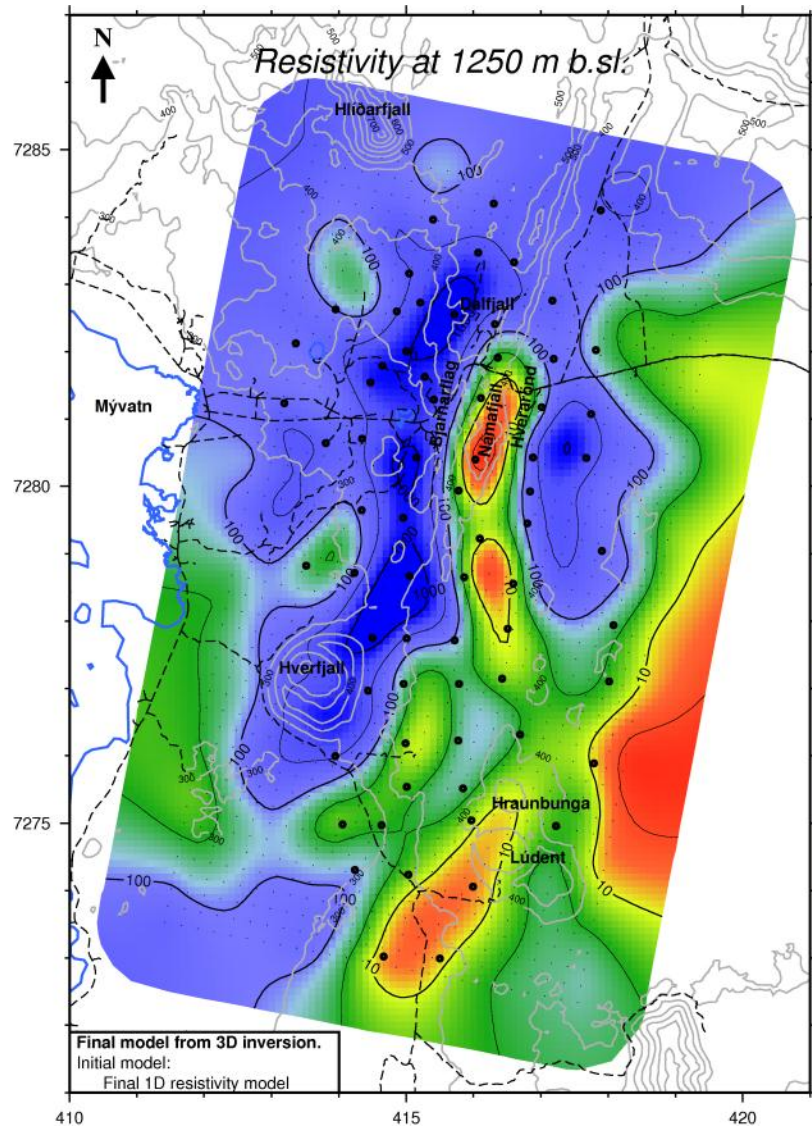


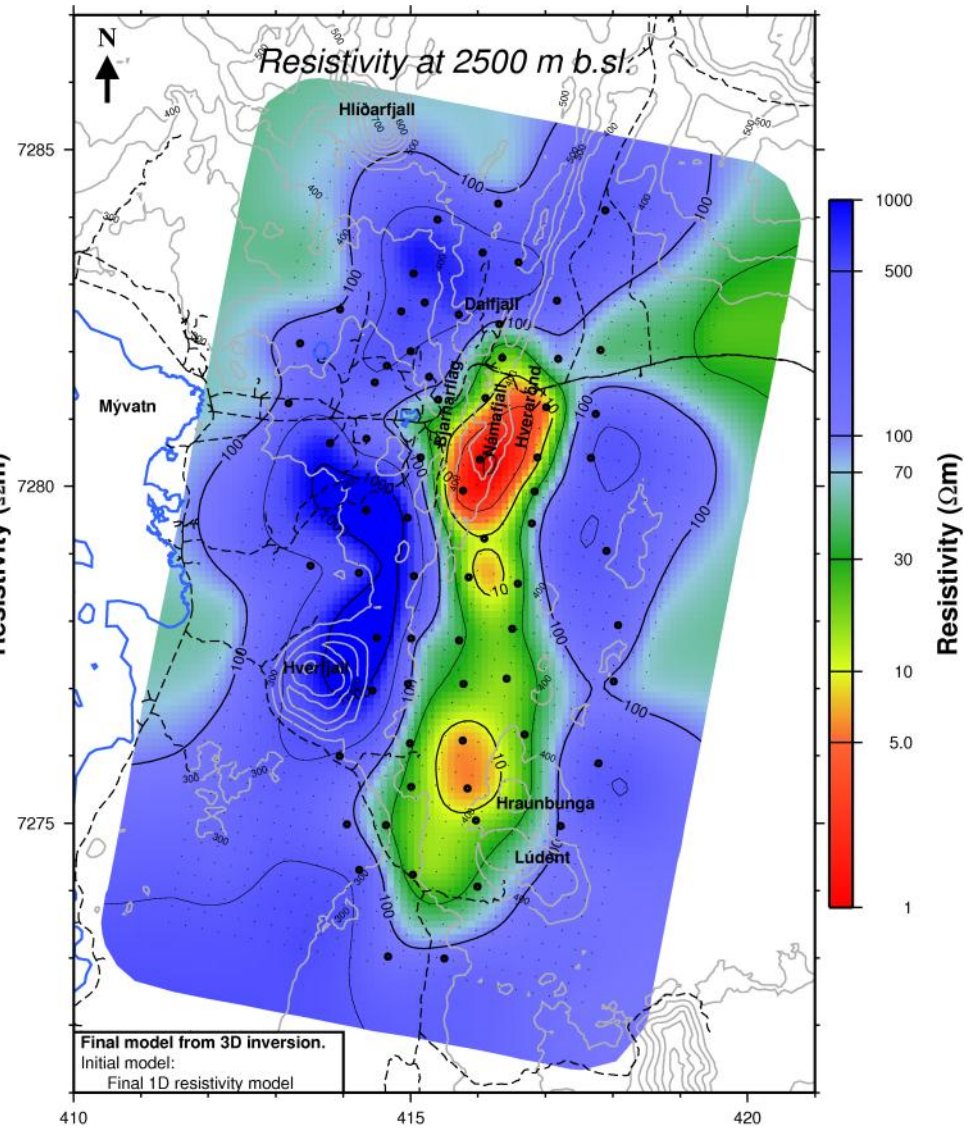
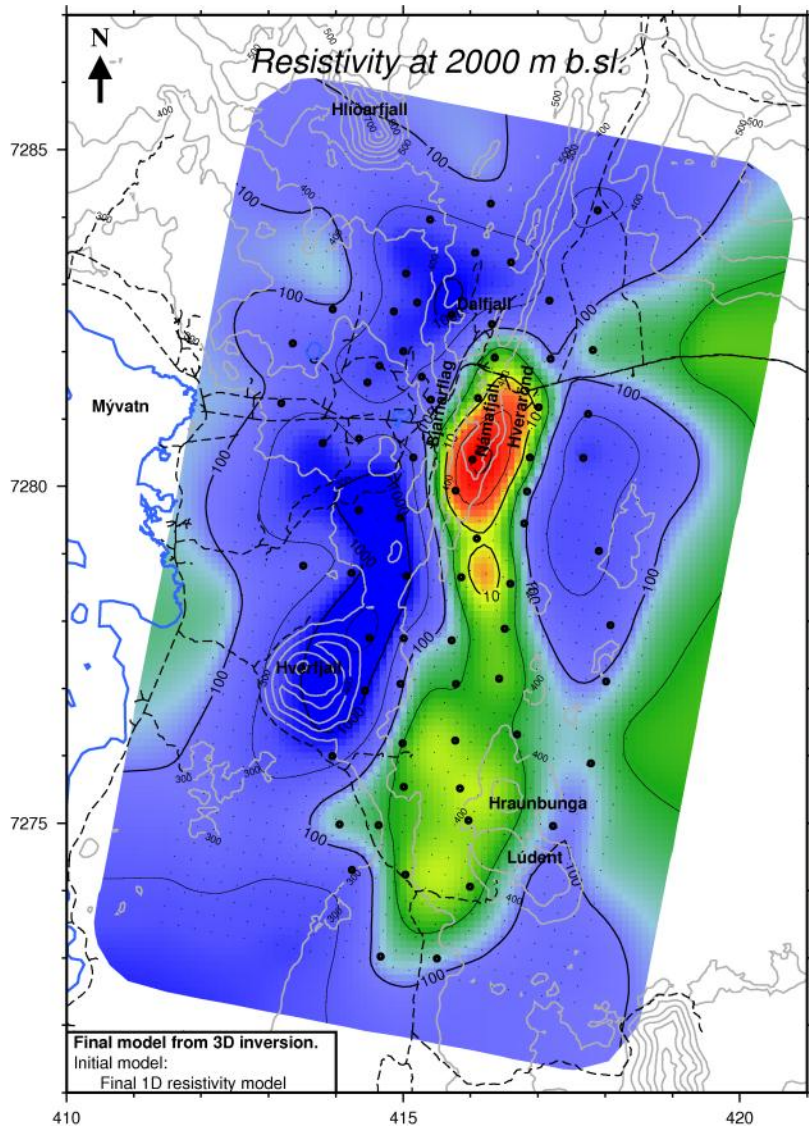


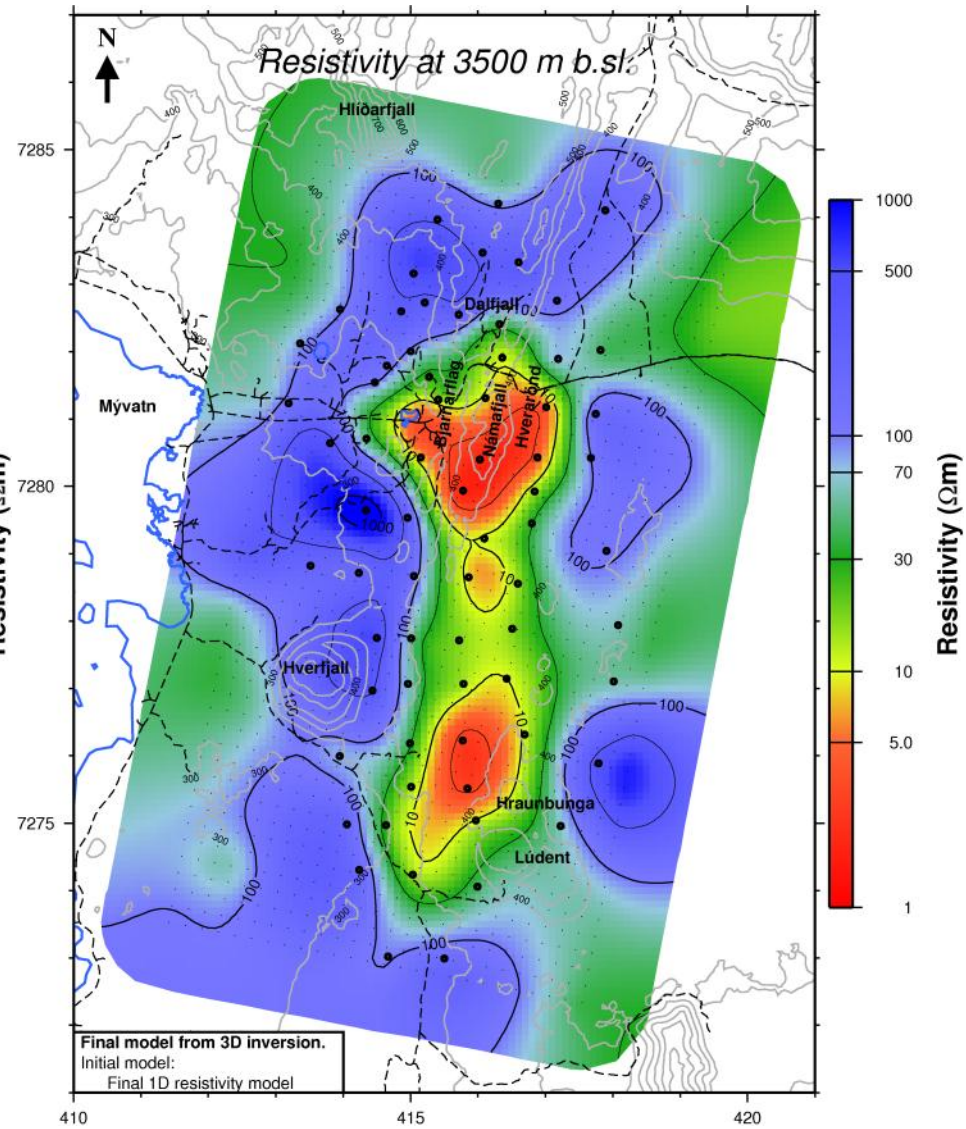
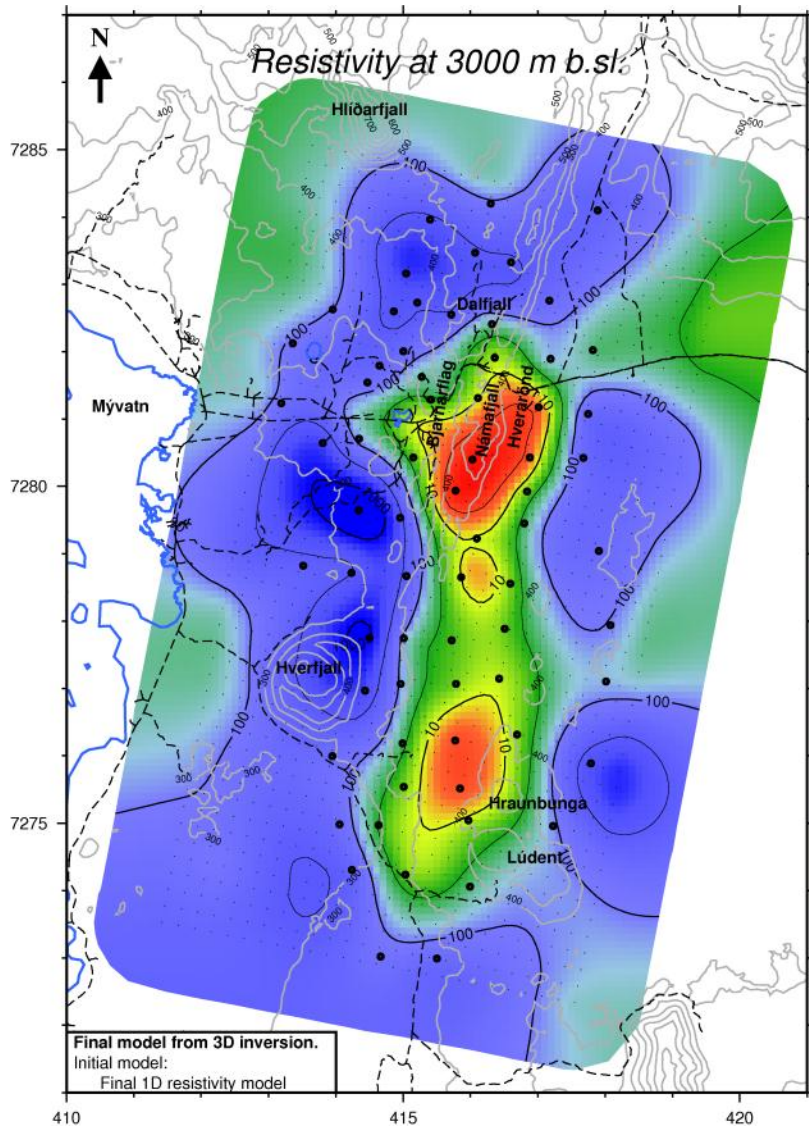


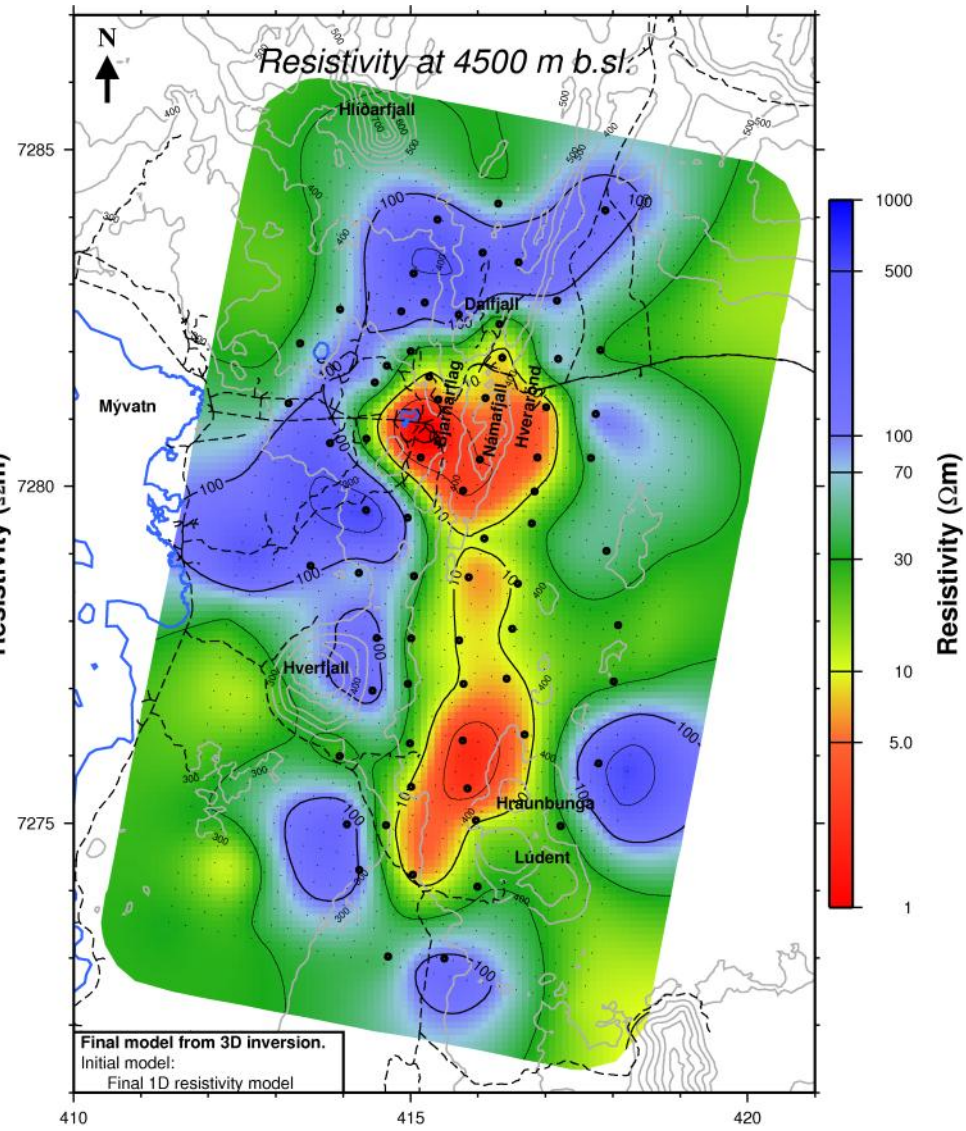
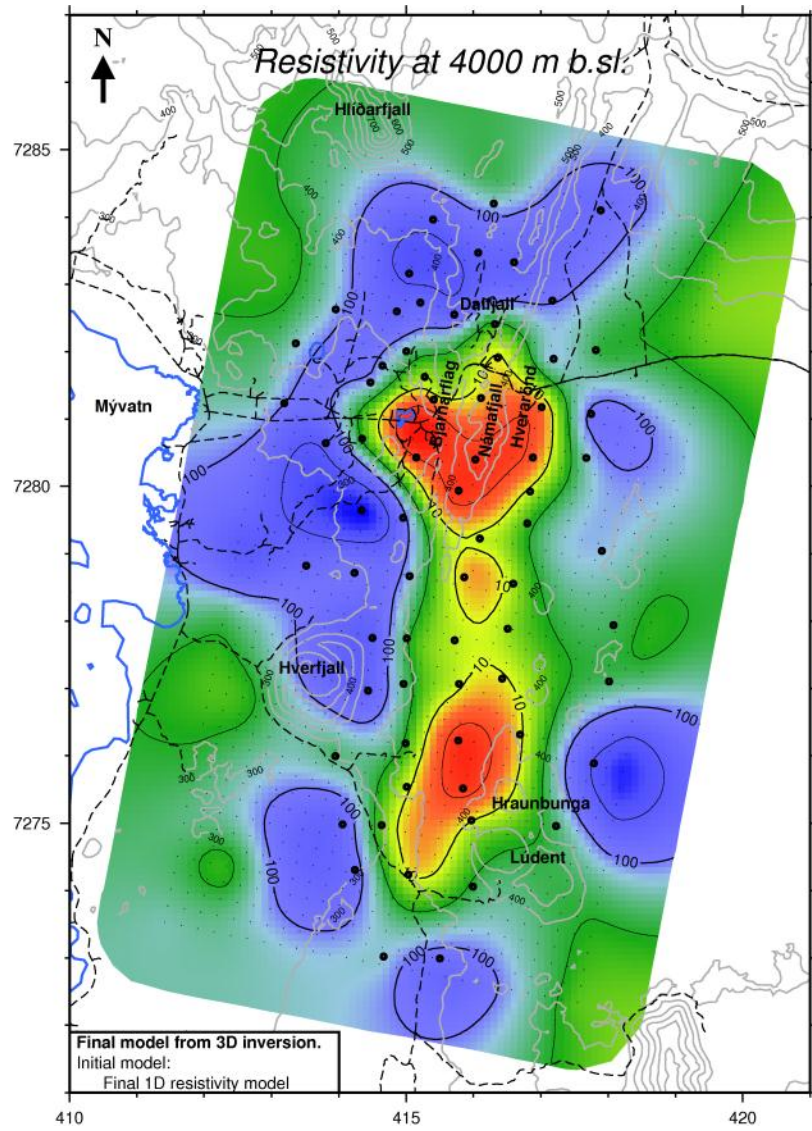


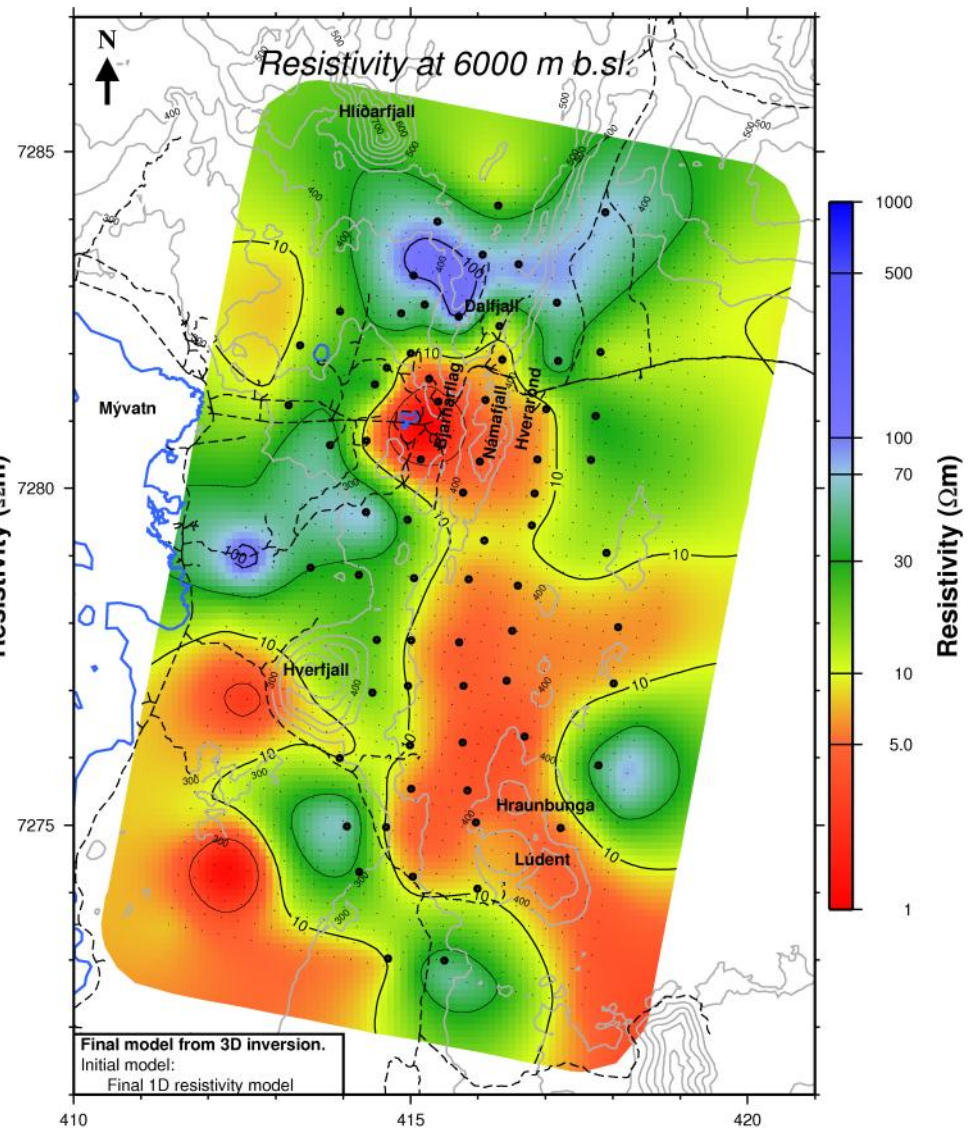
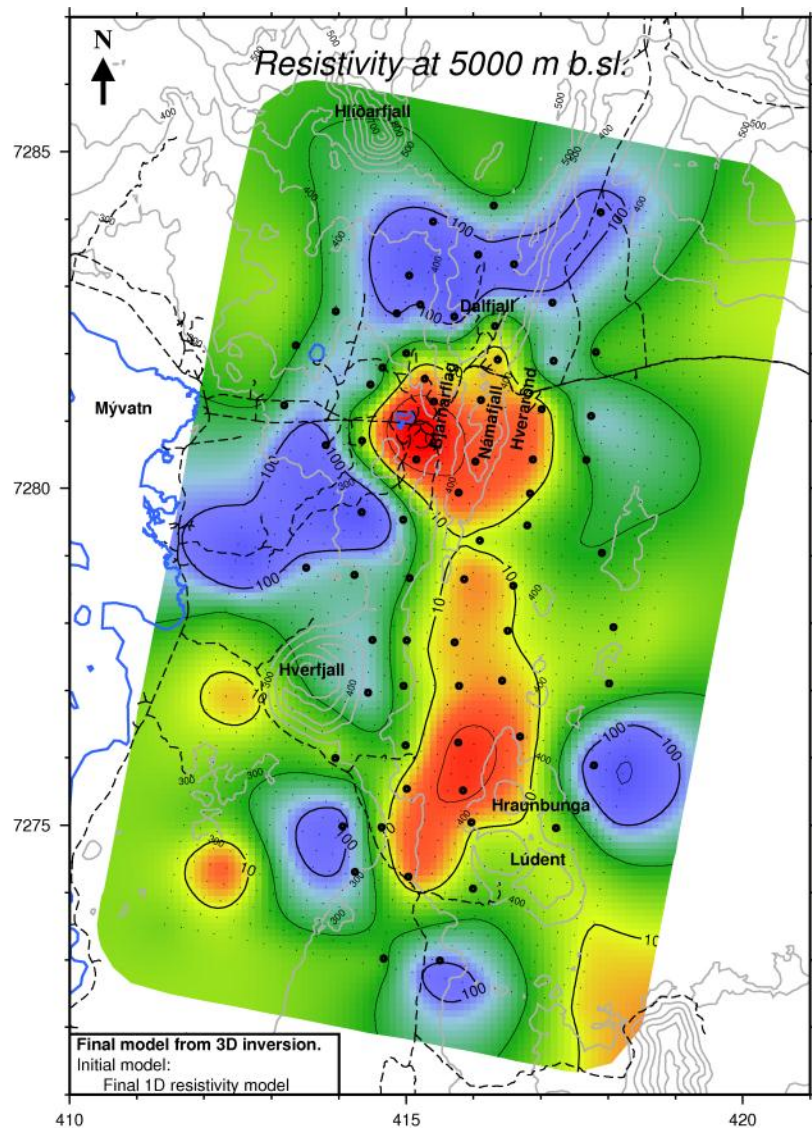


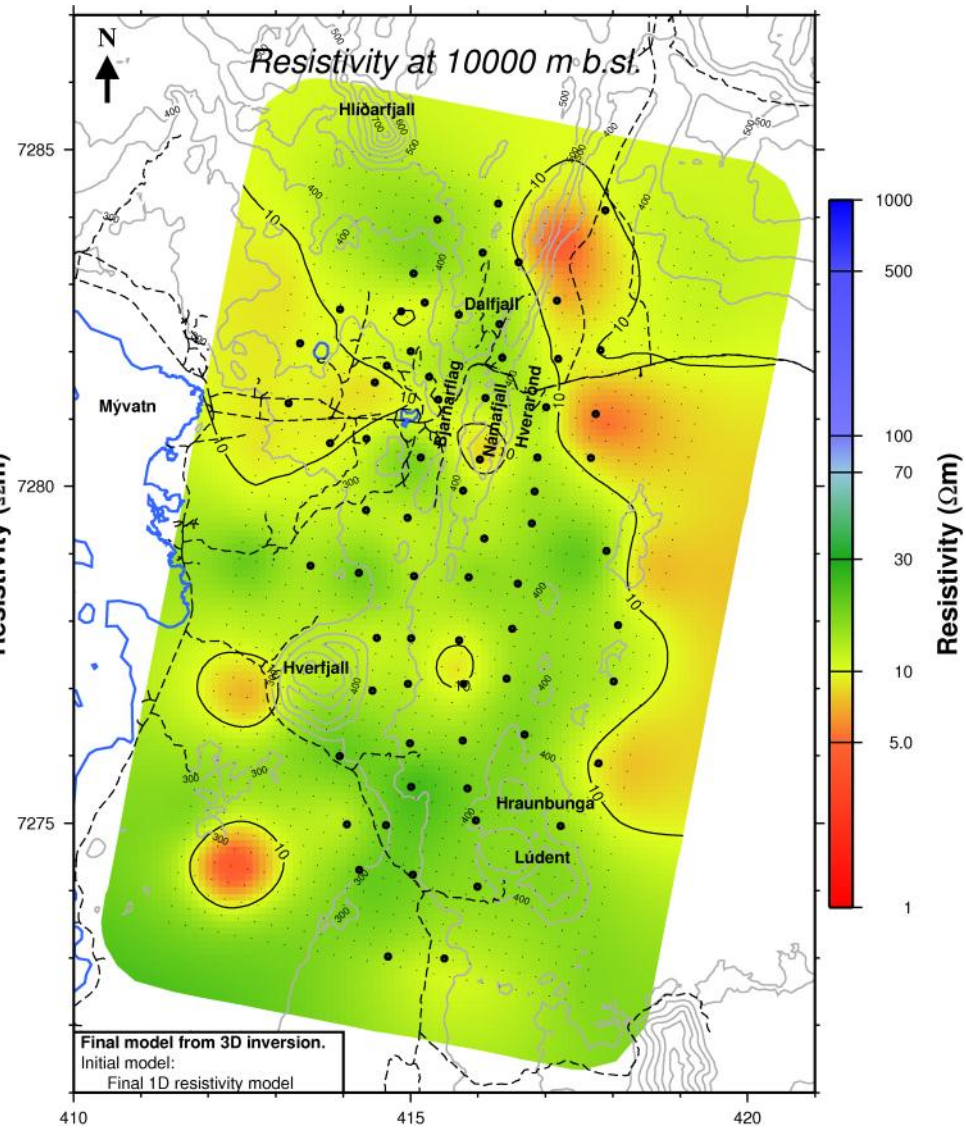
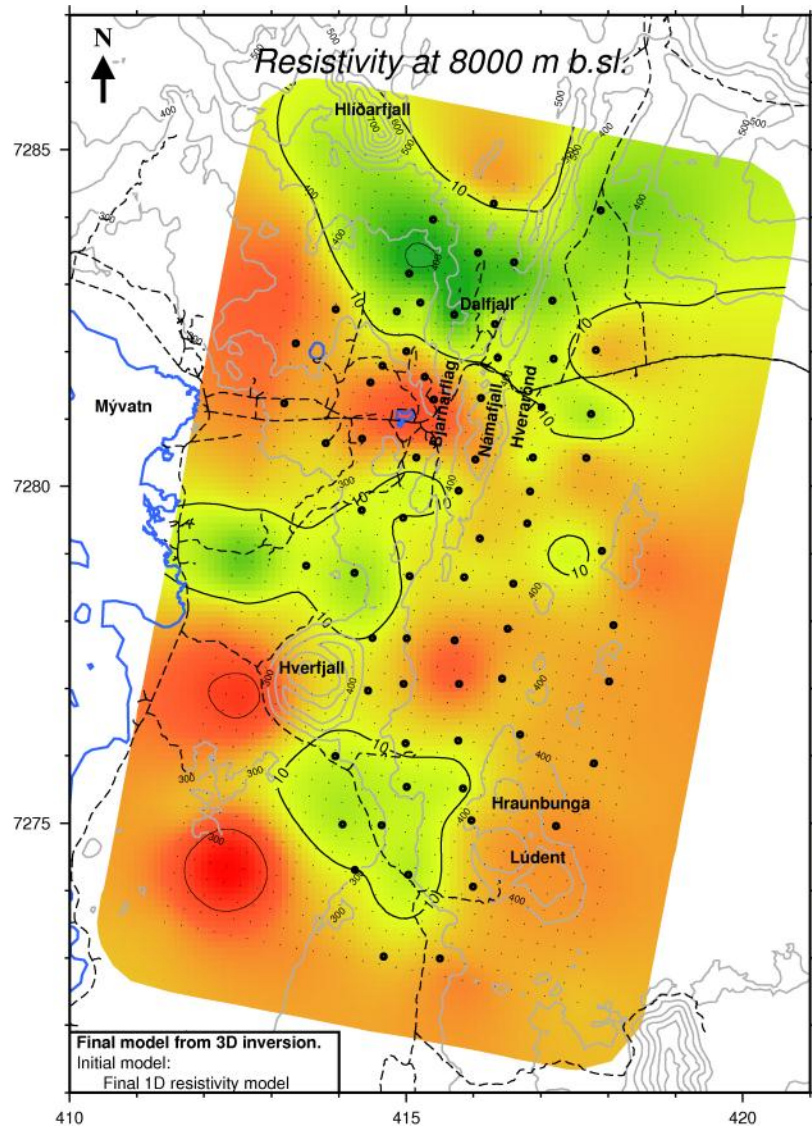


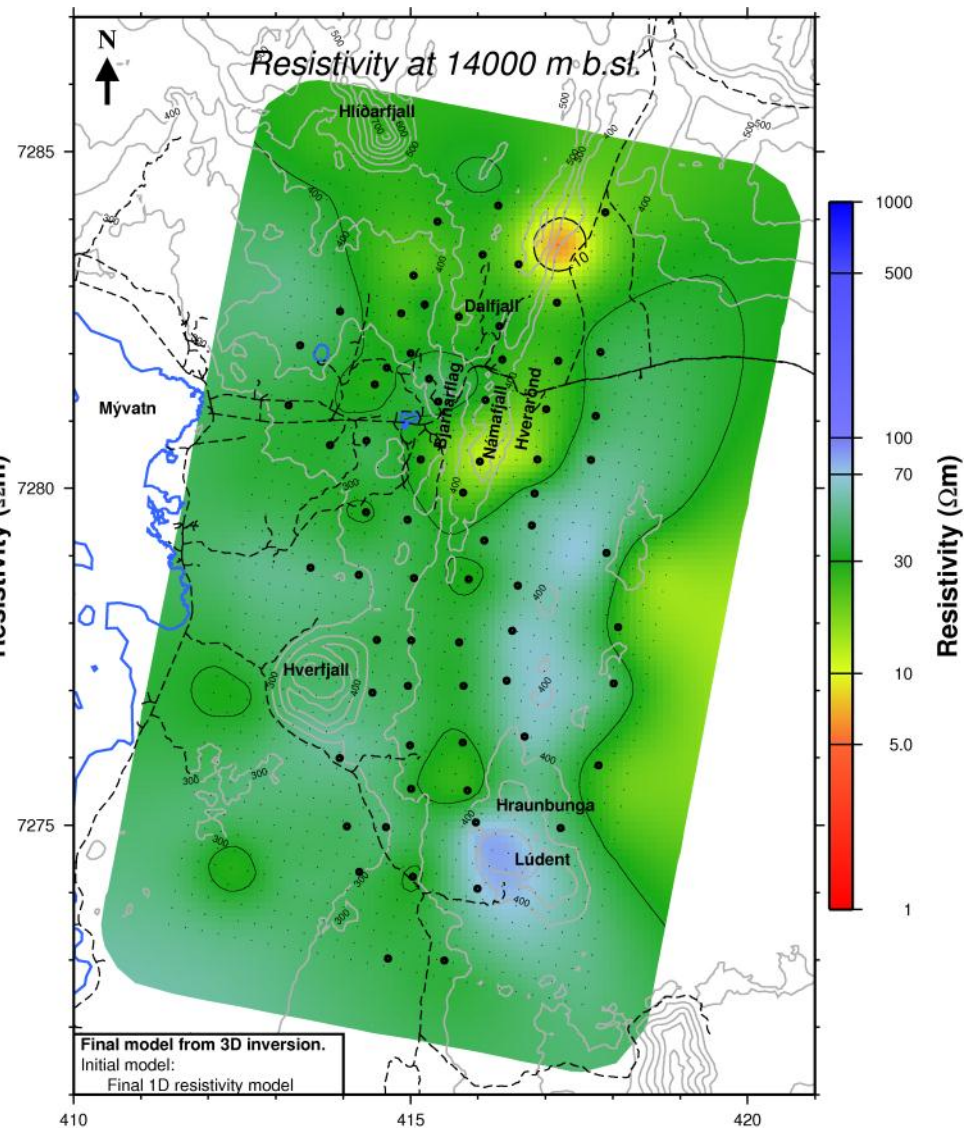
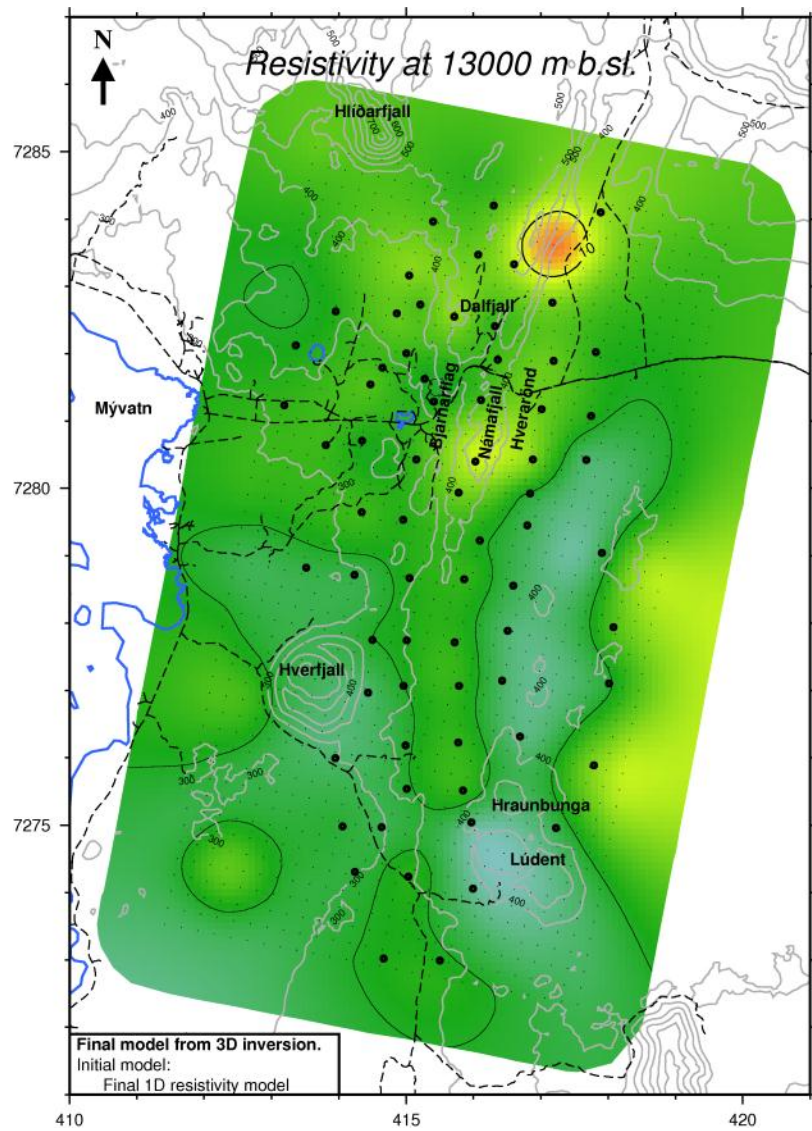


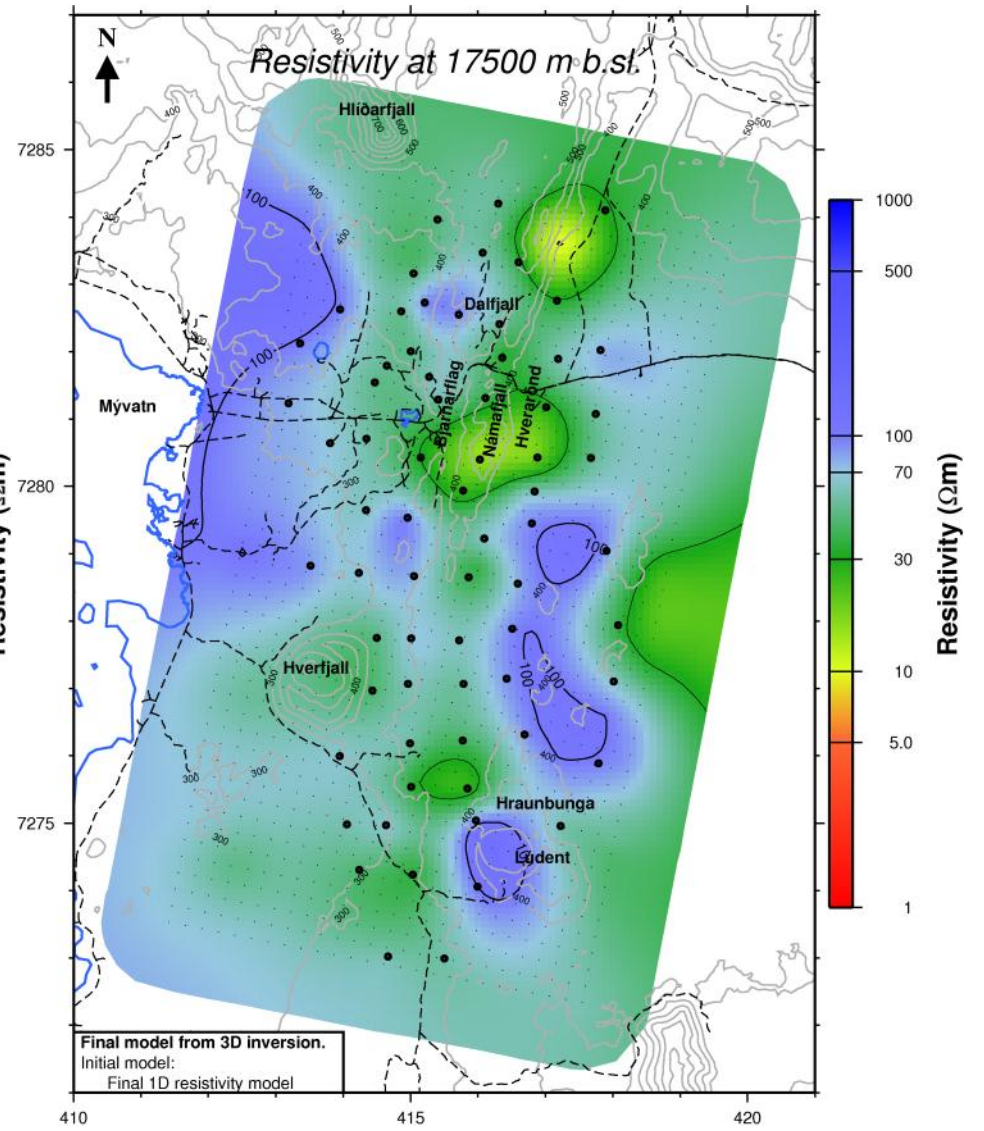
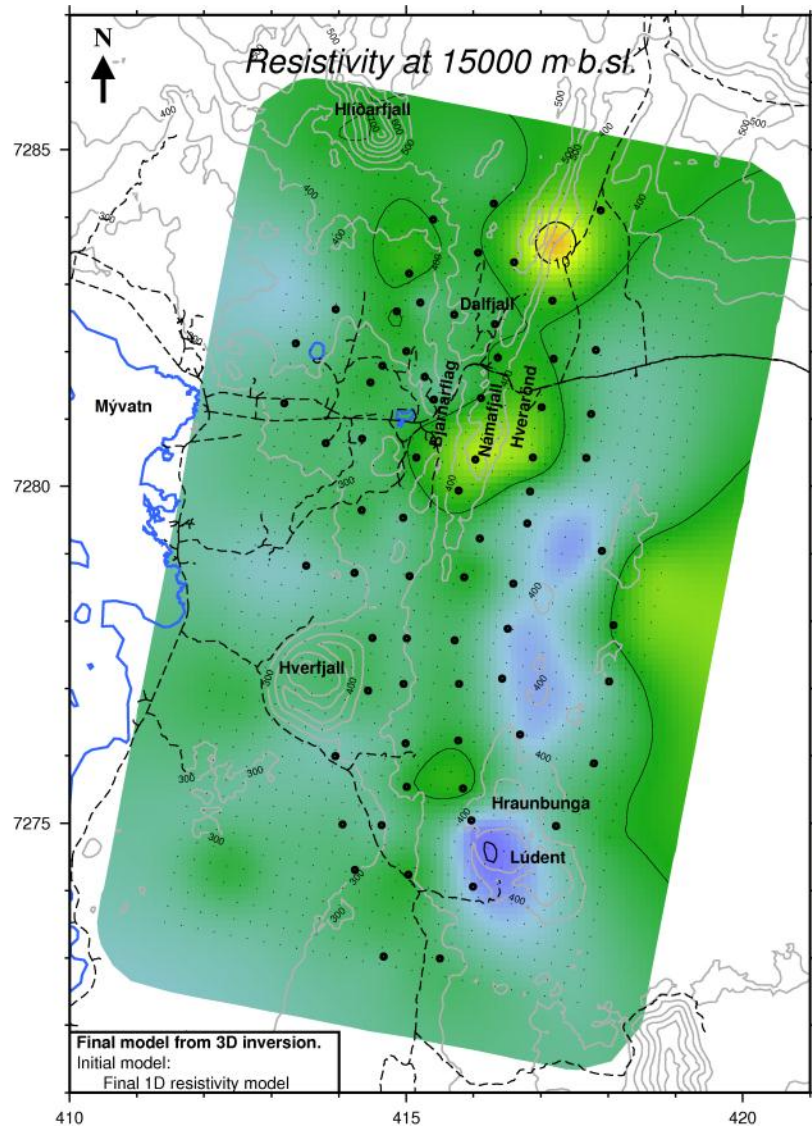


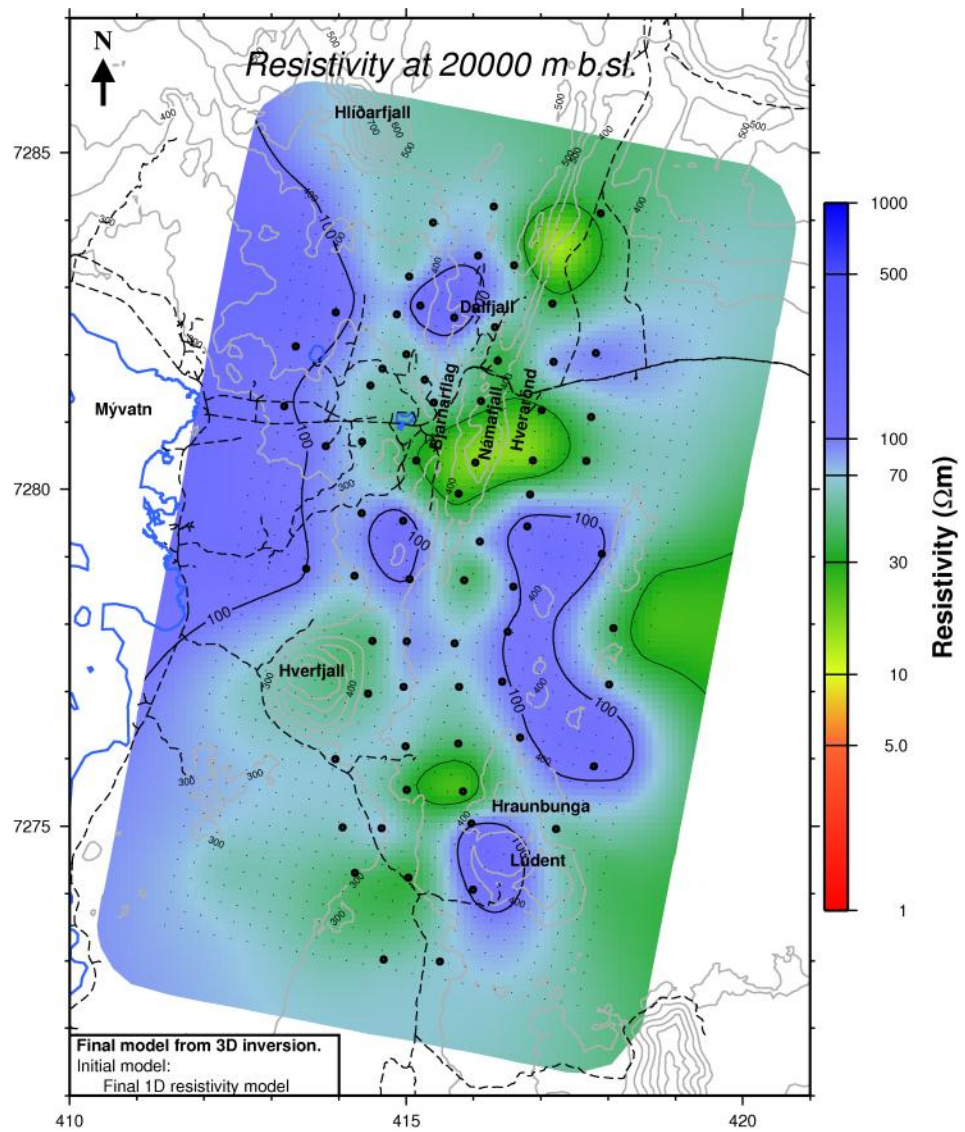




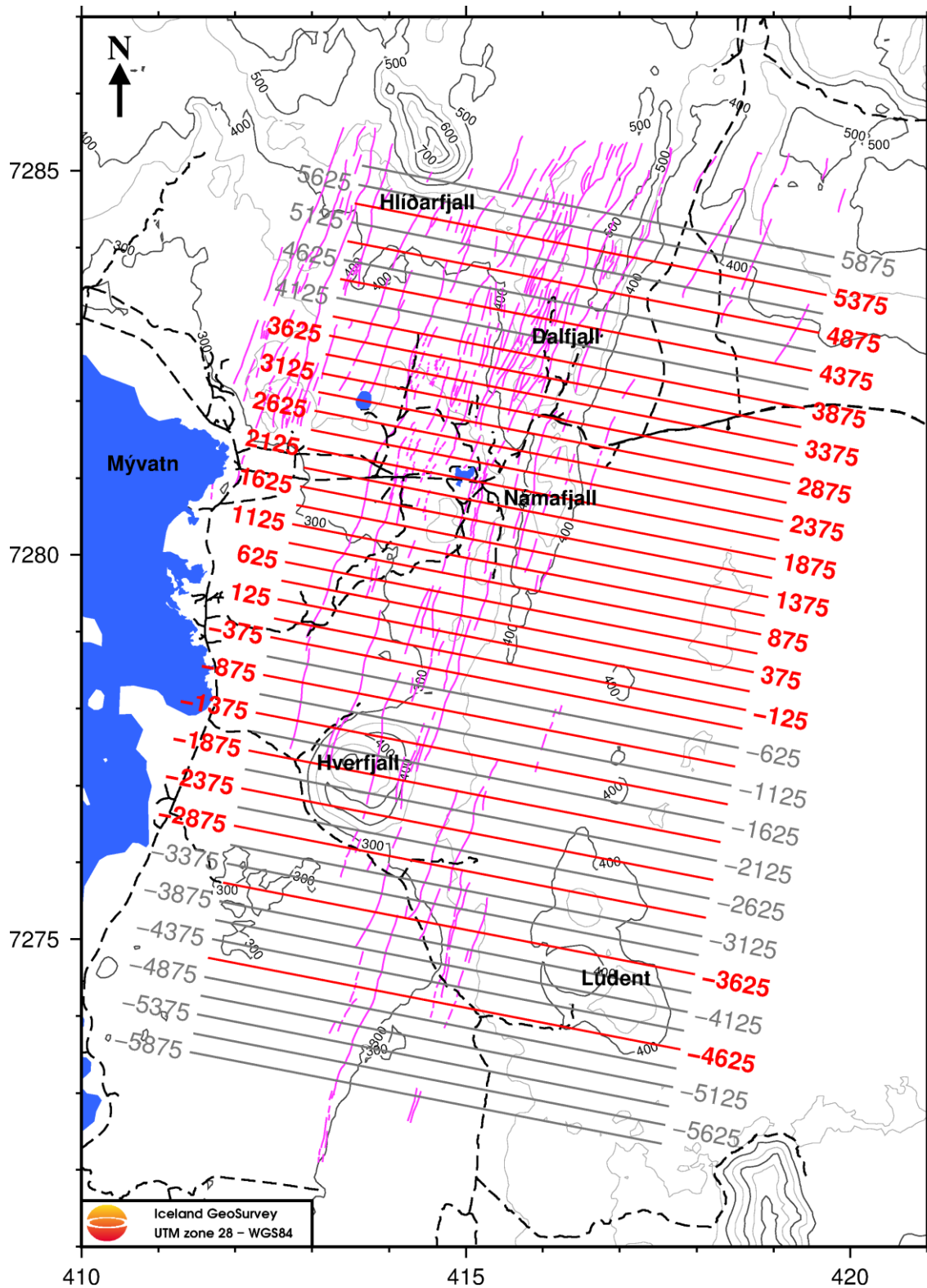


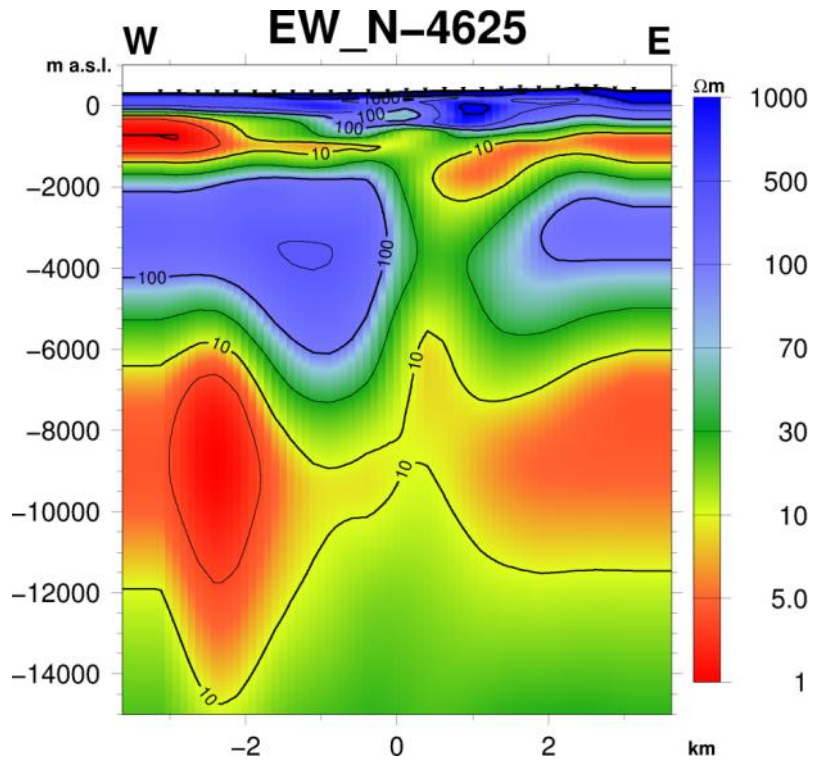
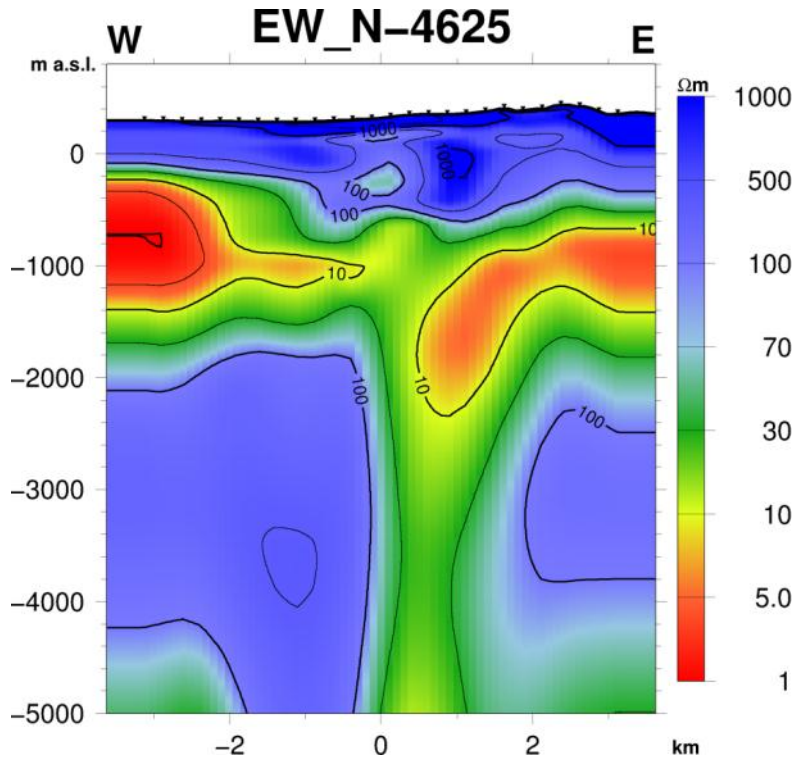


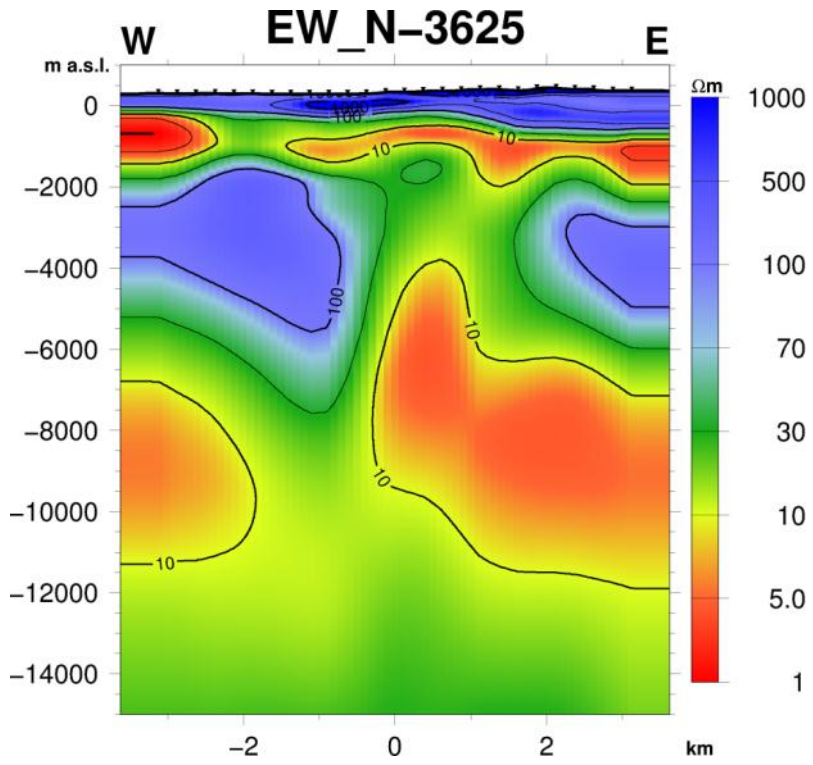
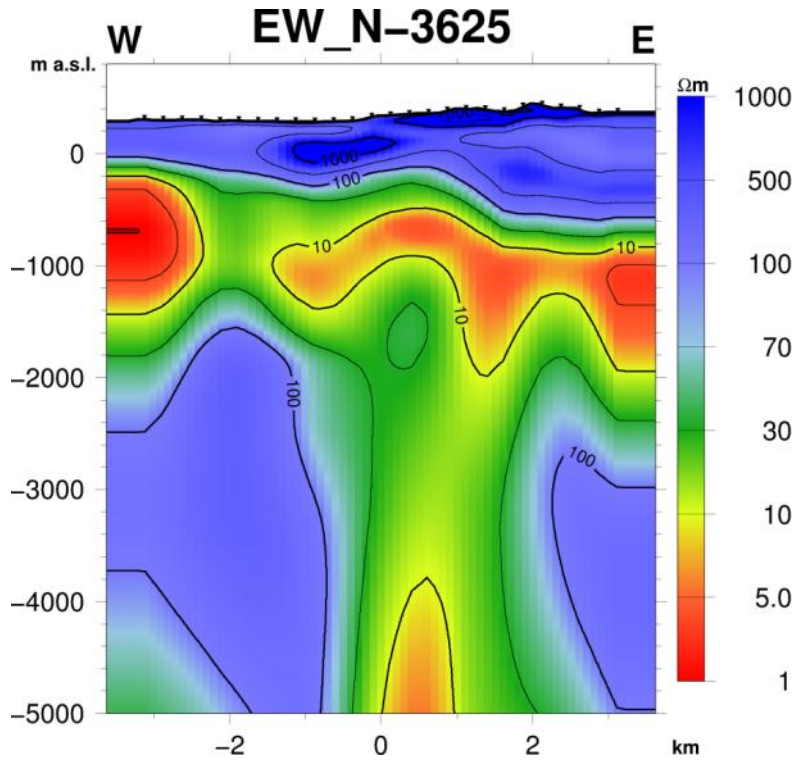


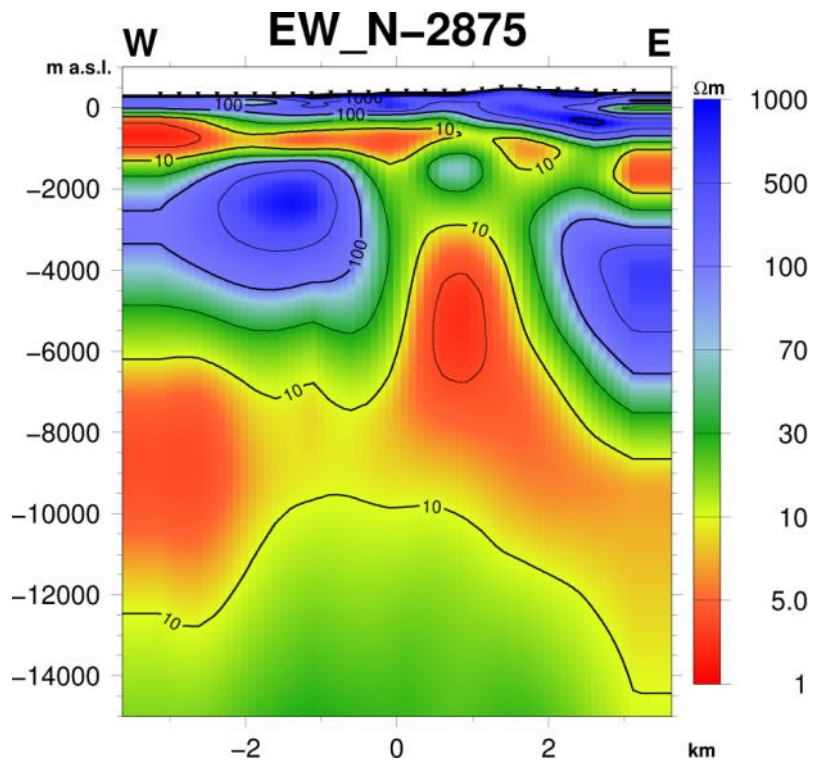
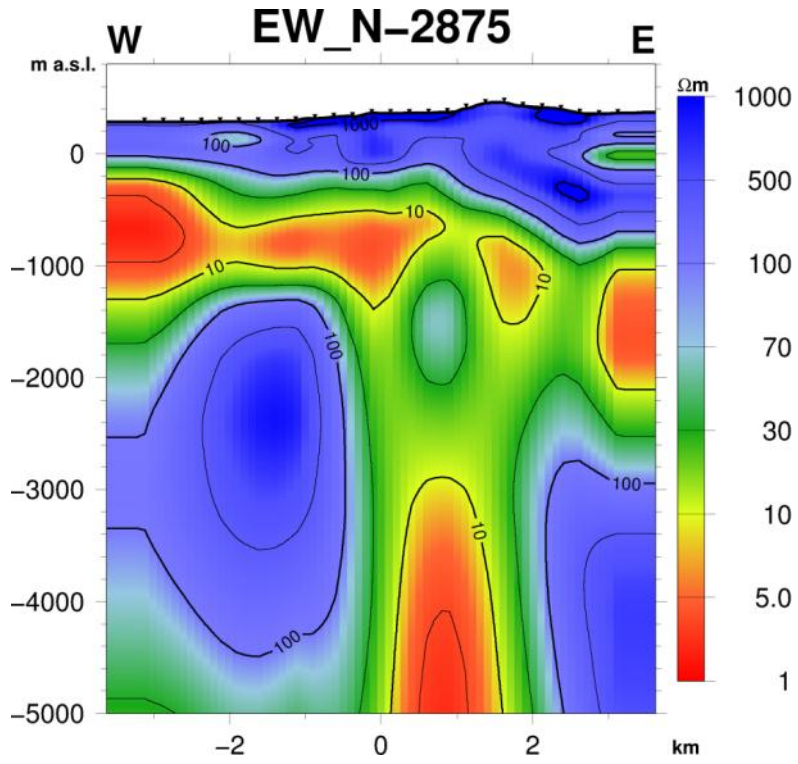


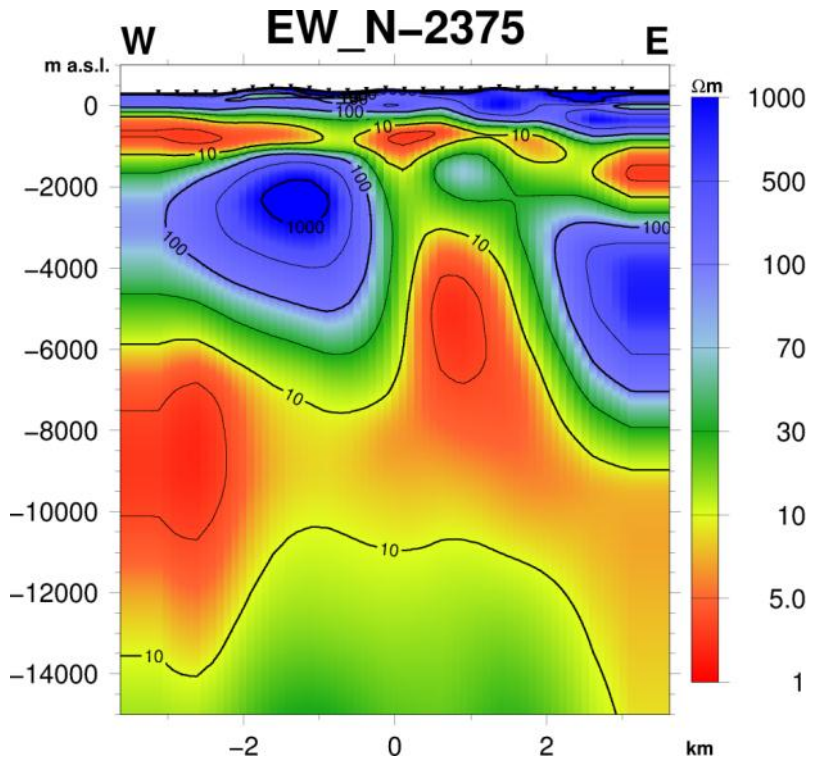
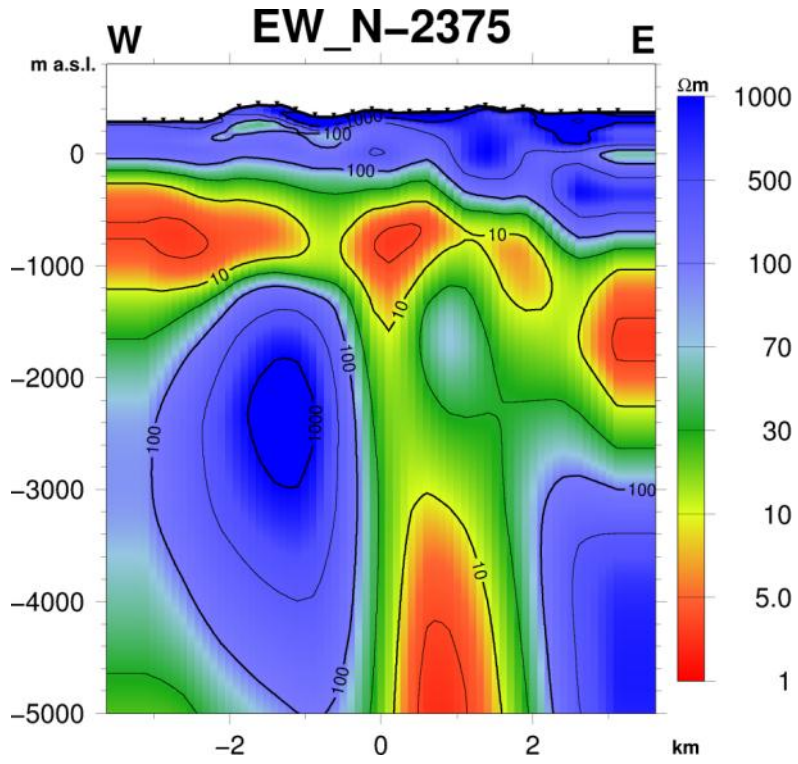
Appendix 2:
East – West
Resistivity cross sections

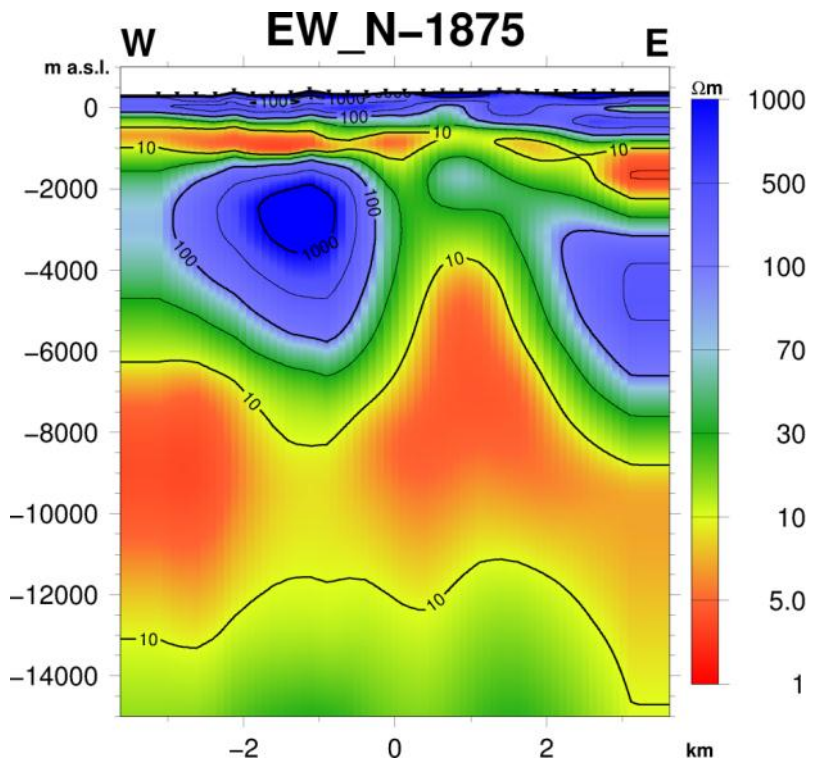
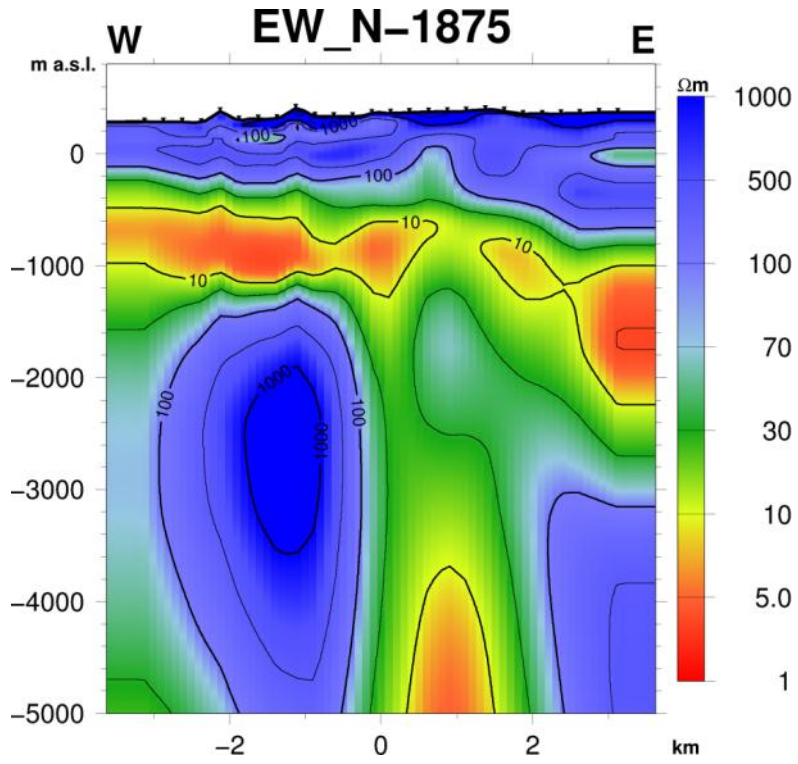


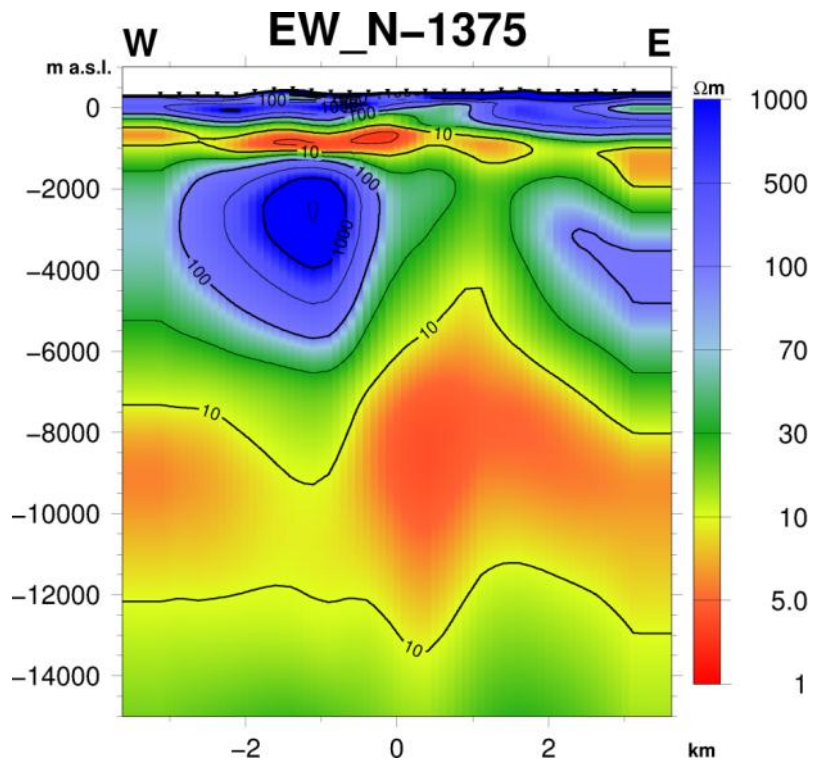
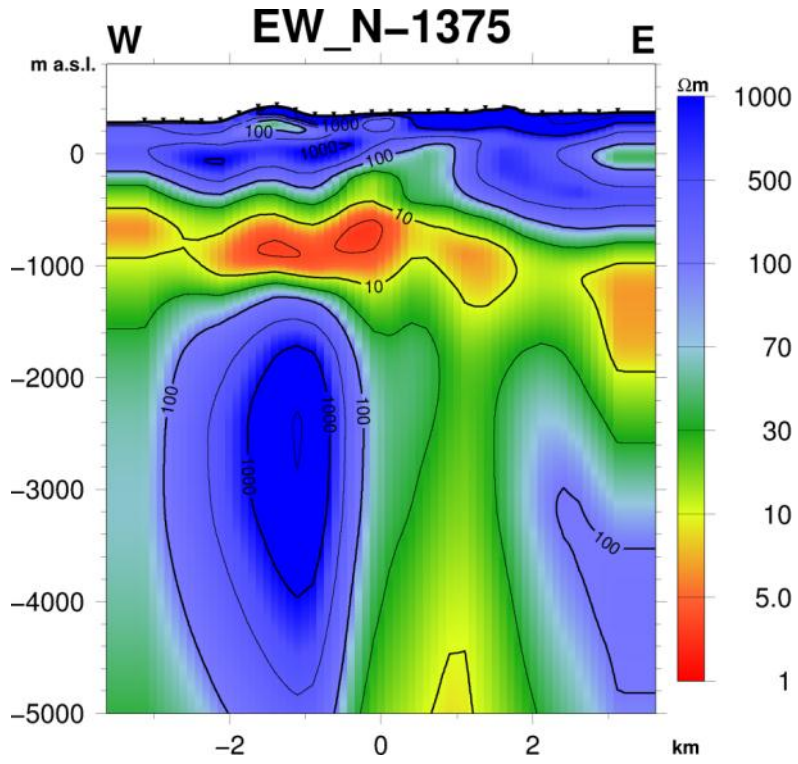


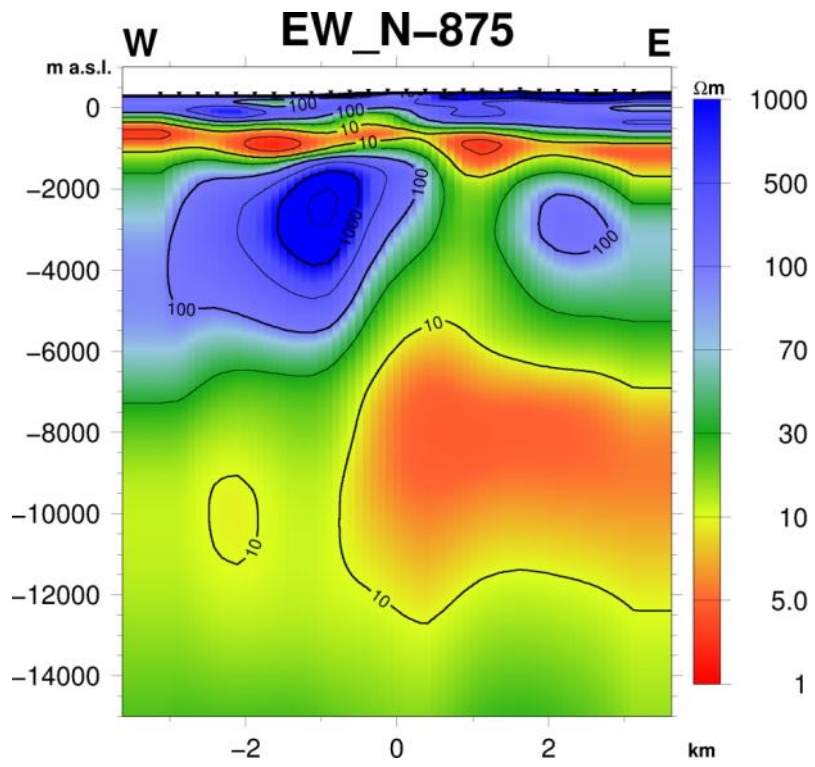
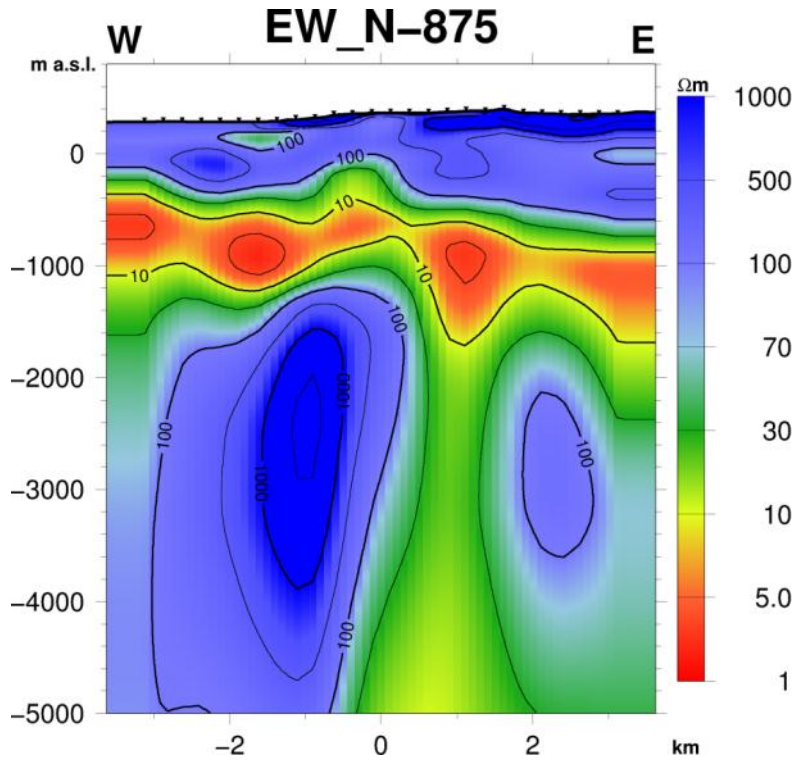


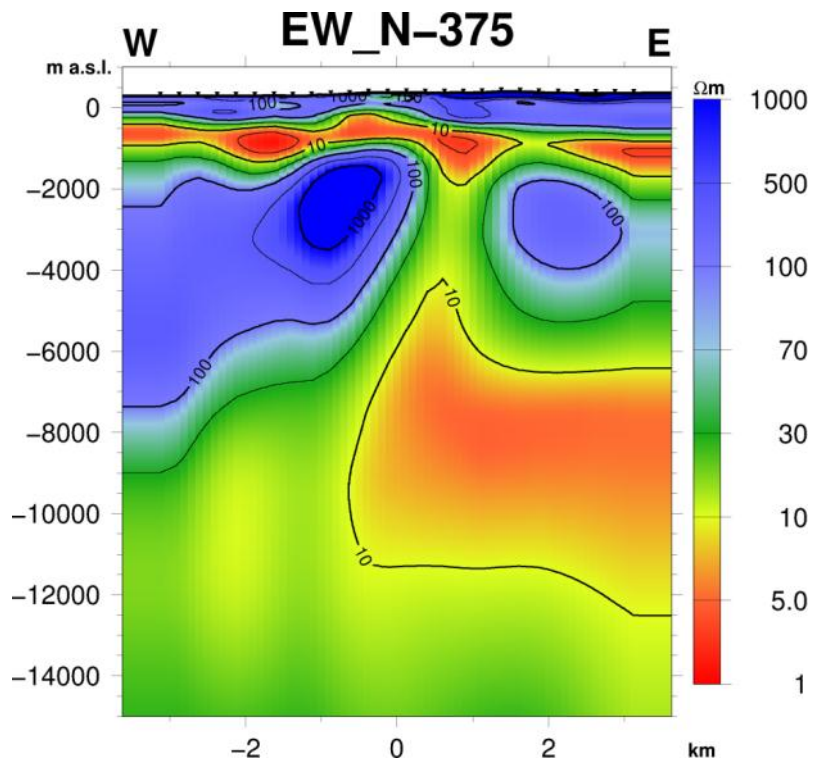
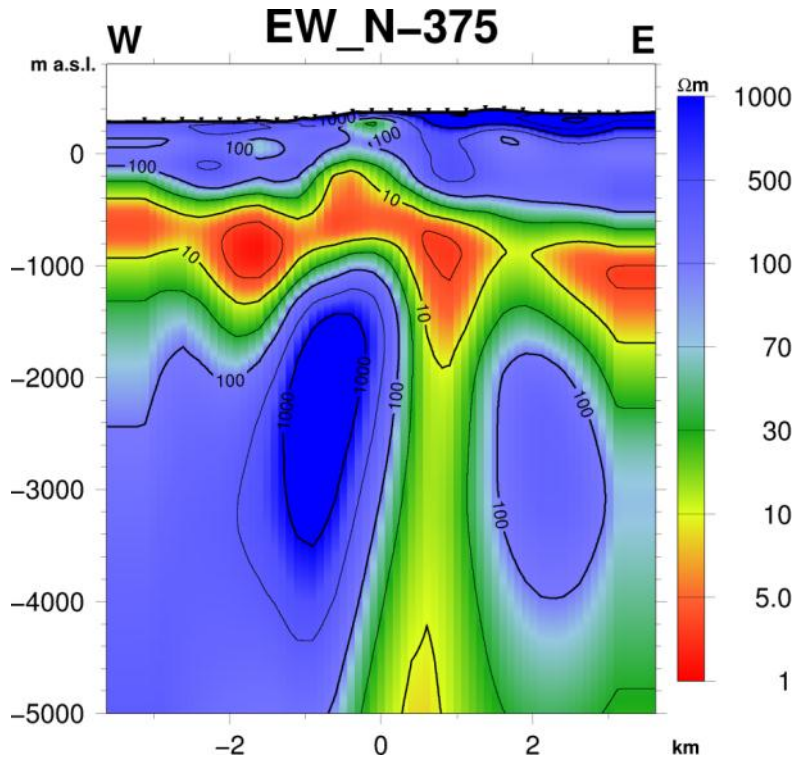


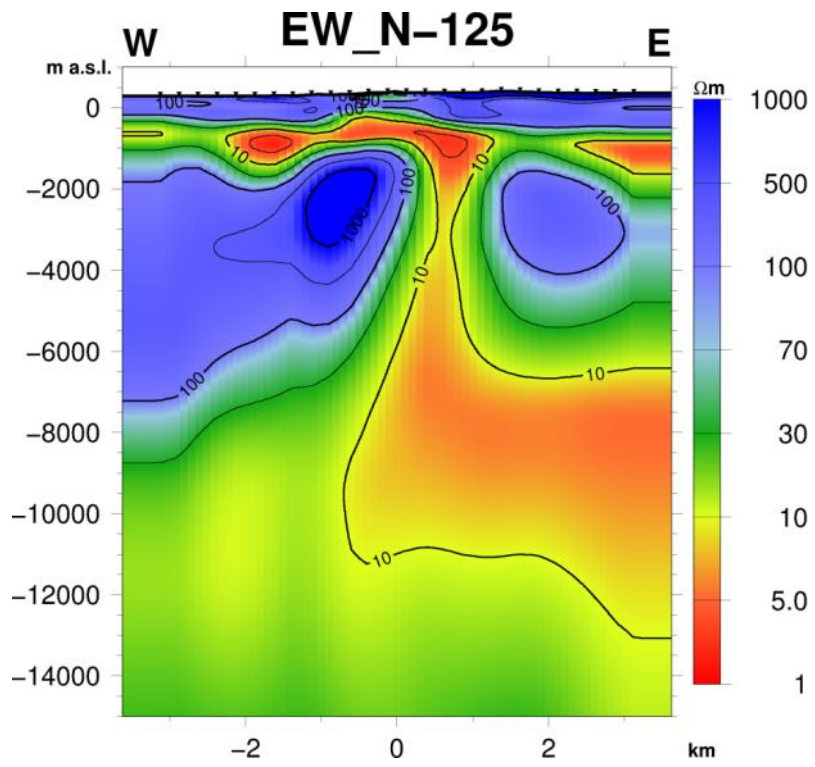
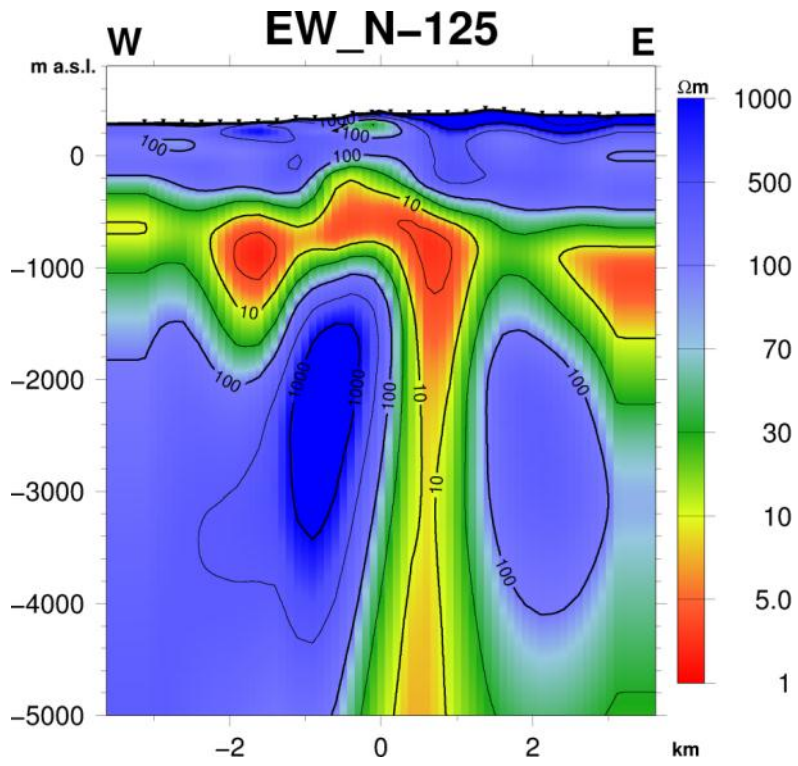


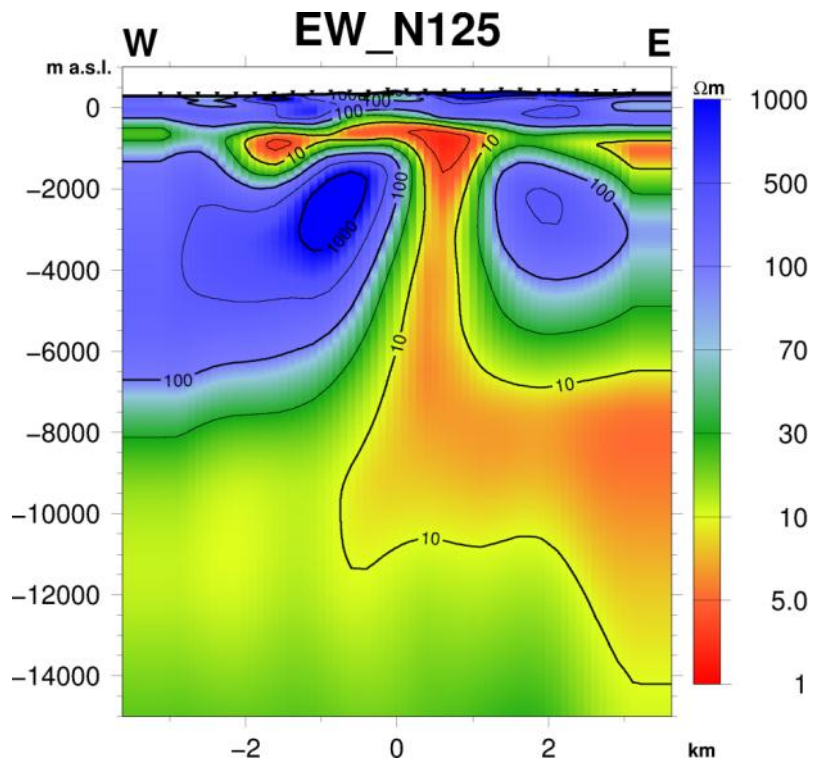
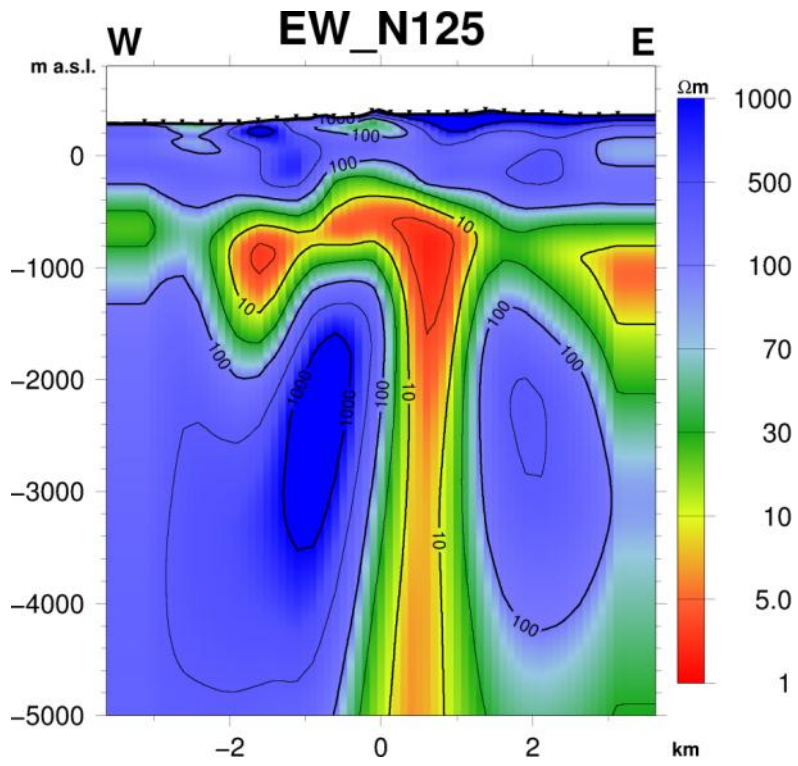


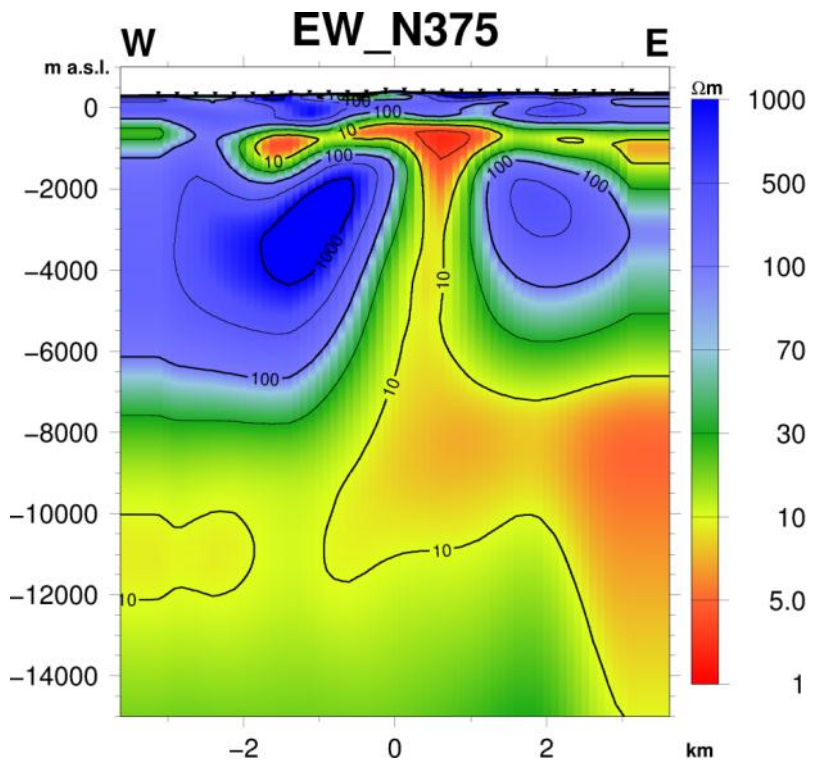
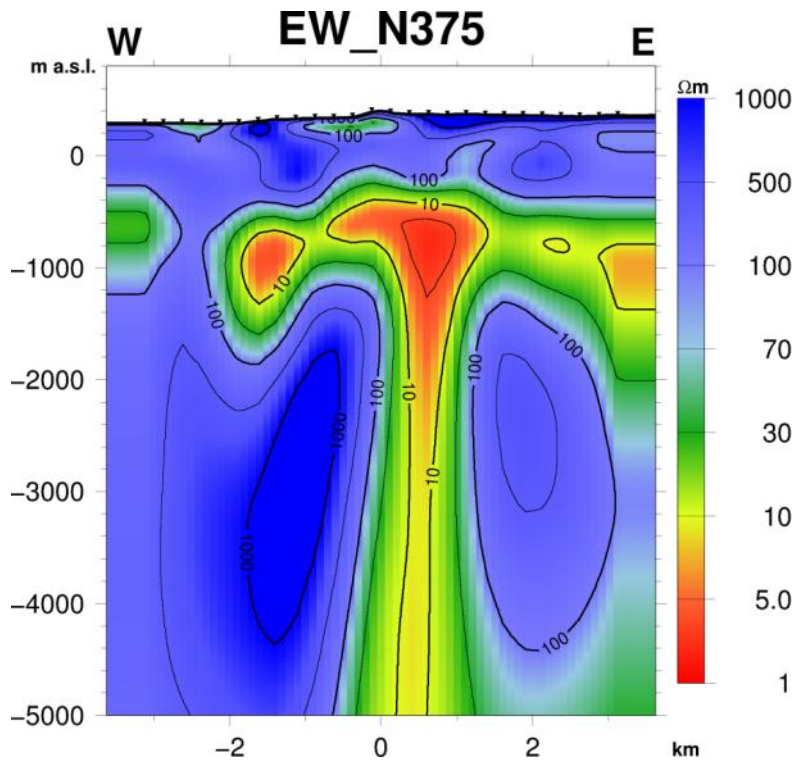


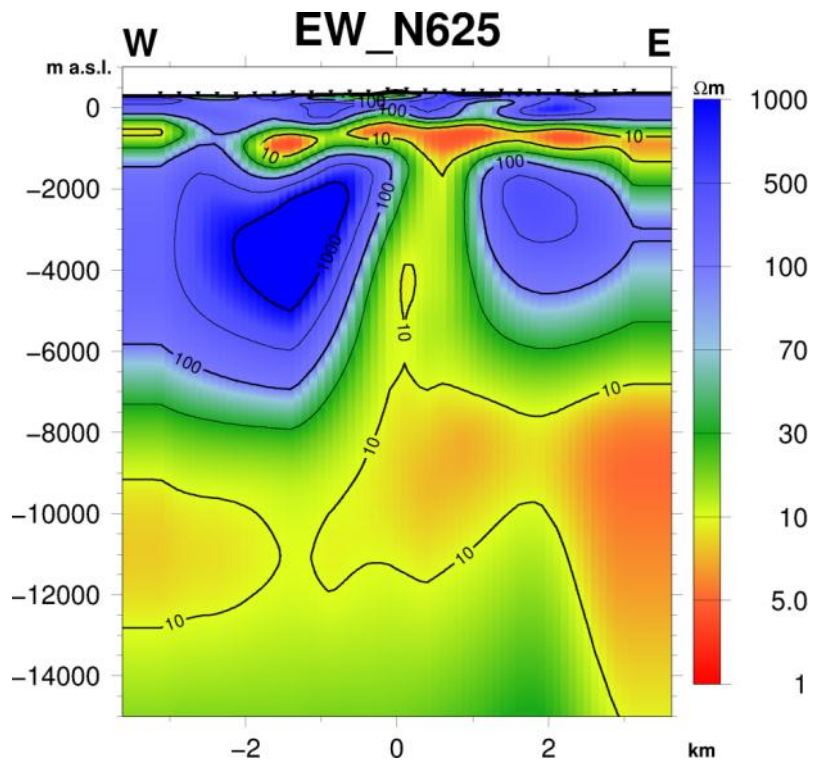
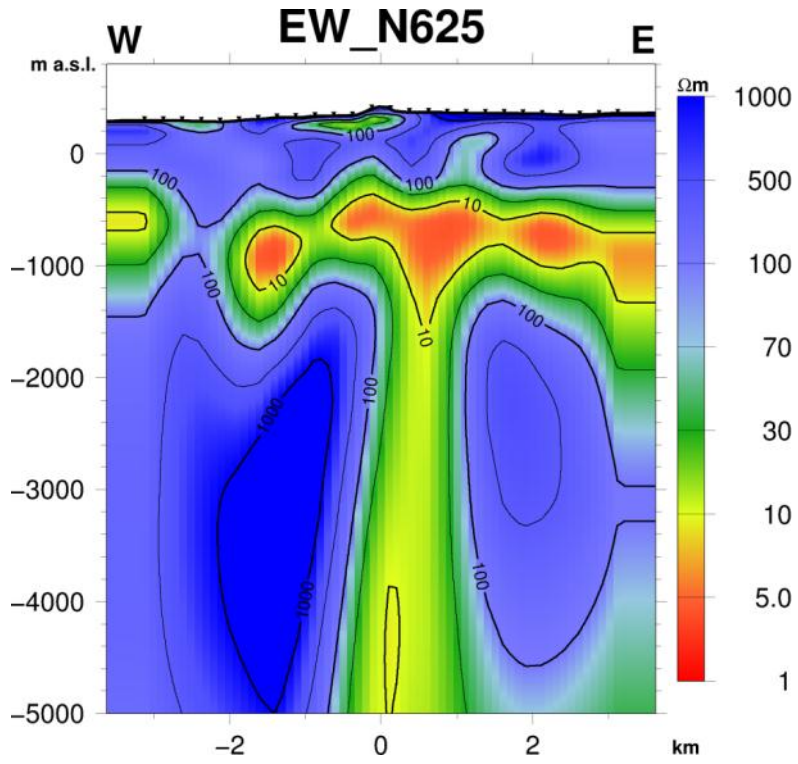


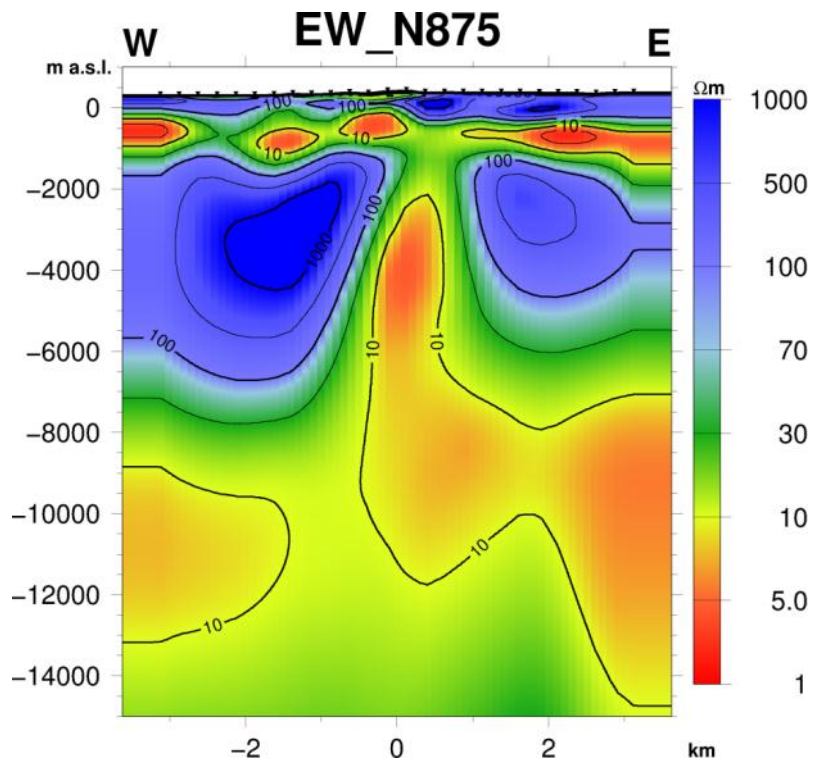
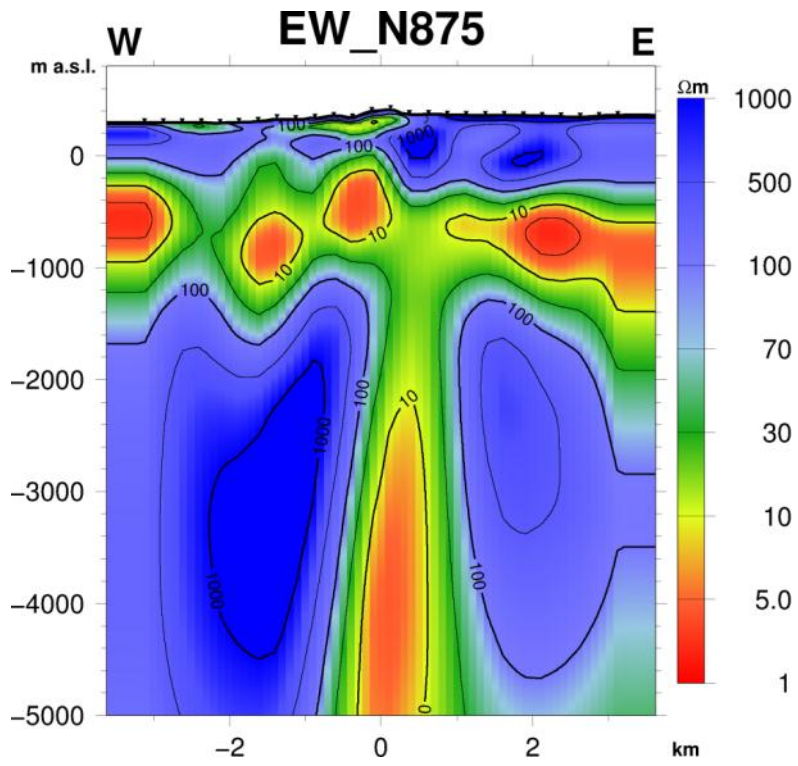


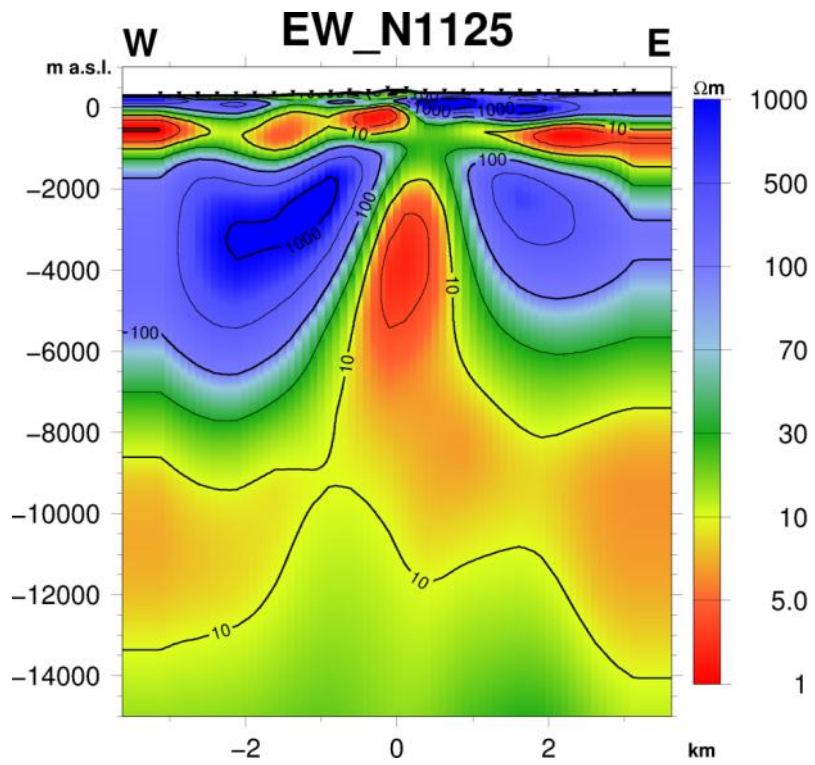
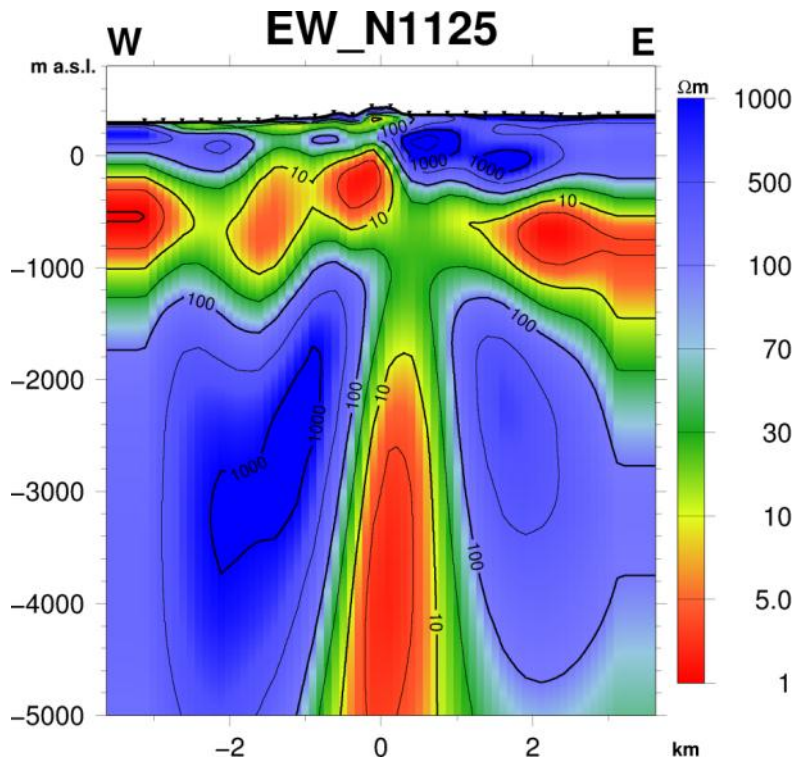


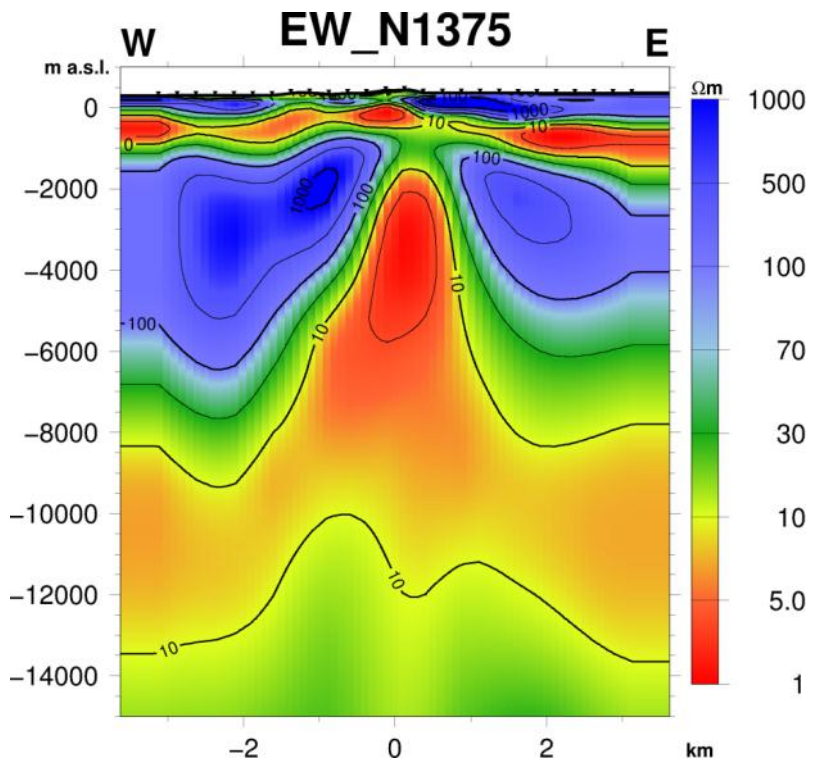
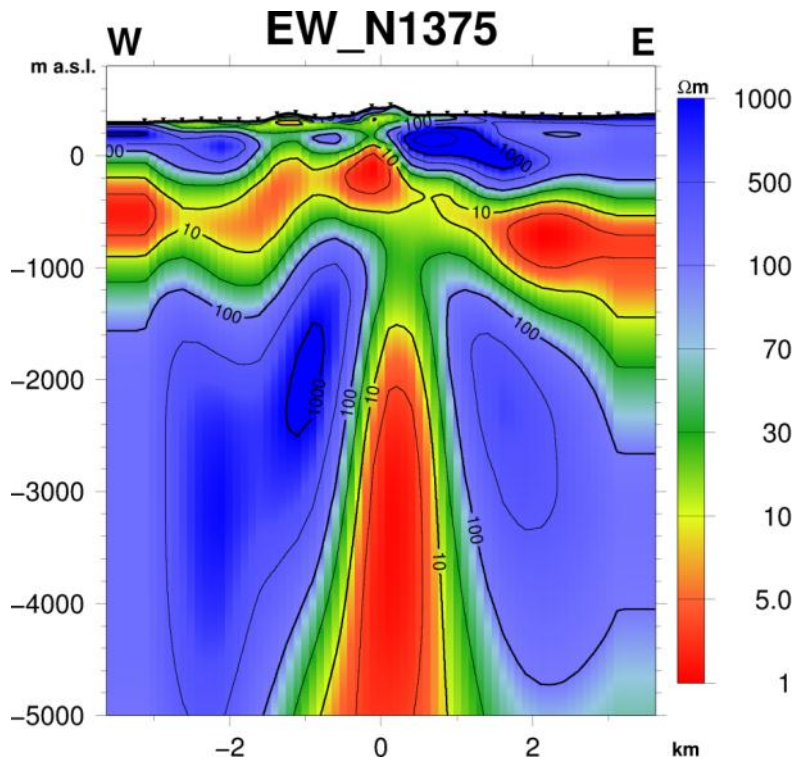


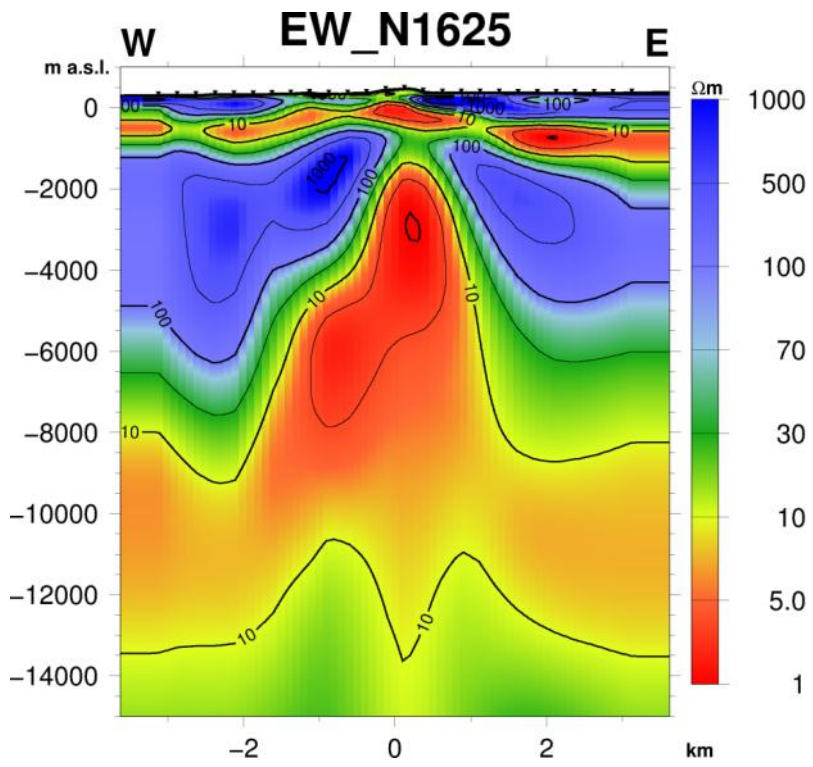
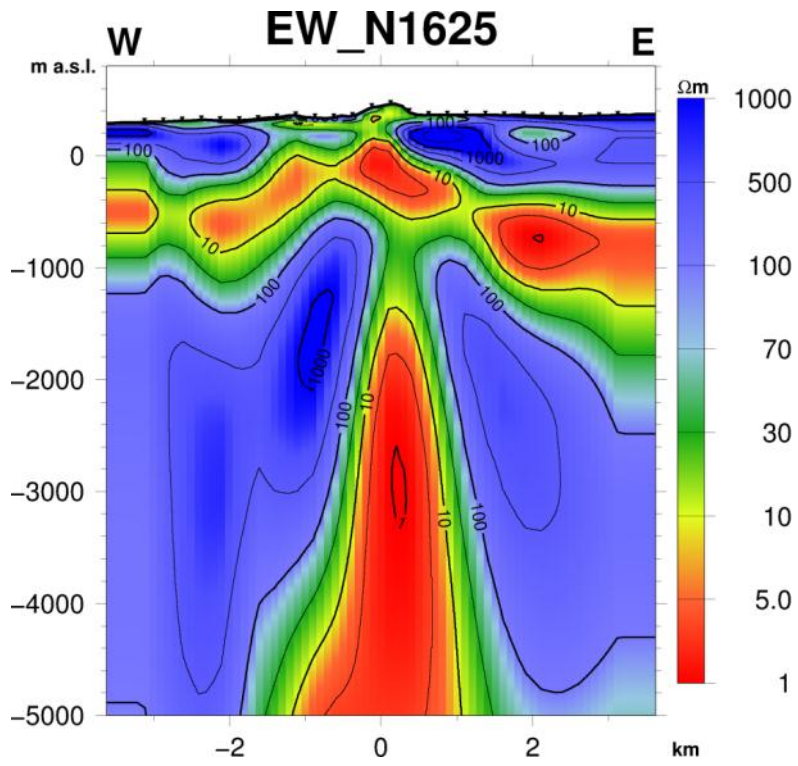


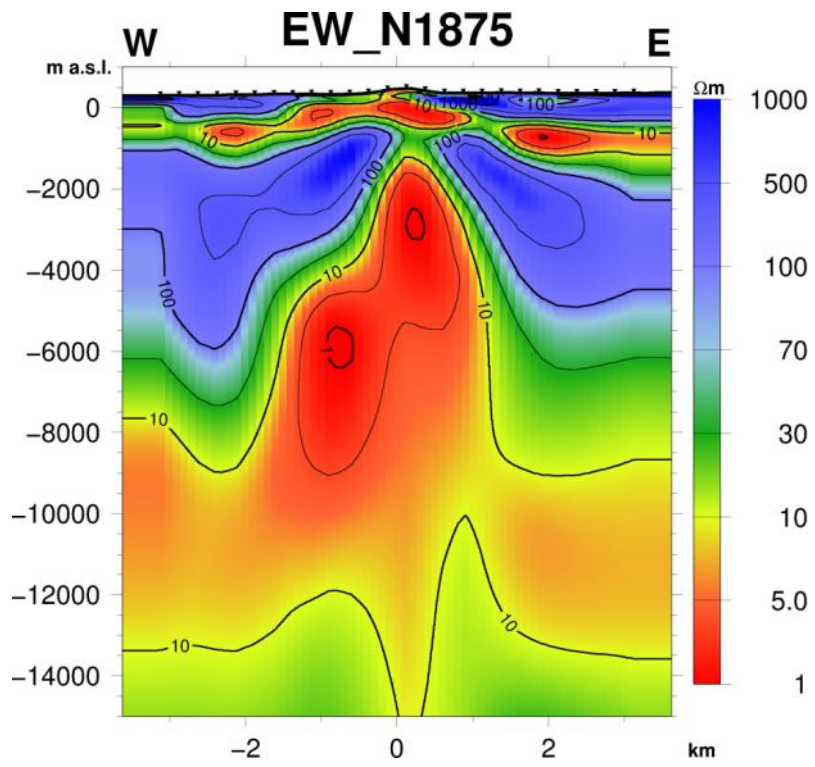
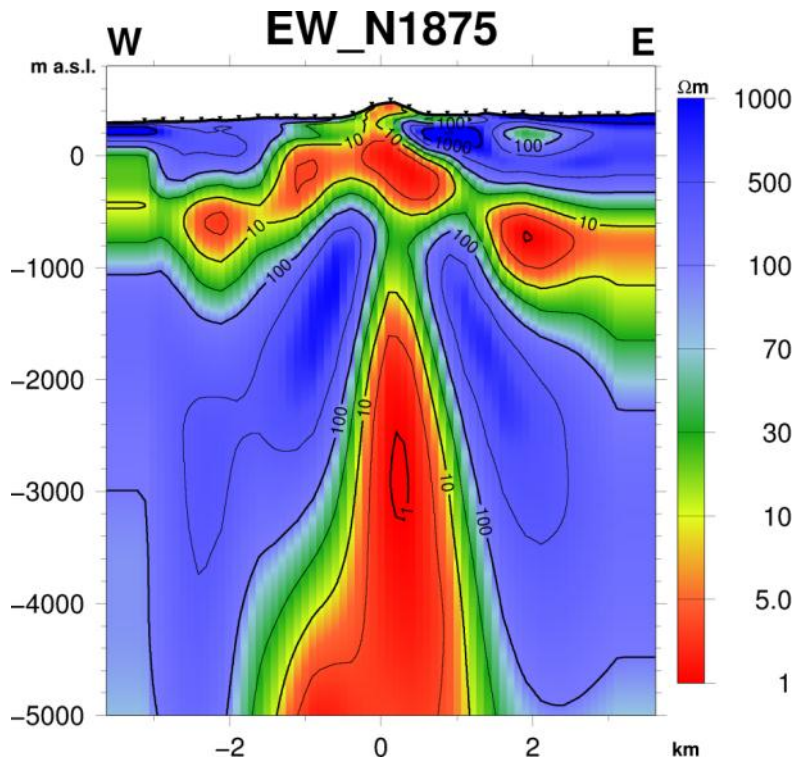


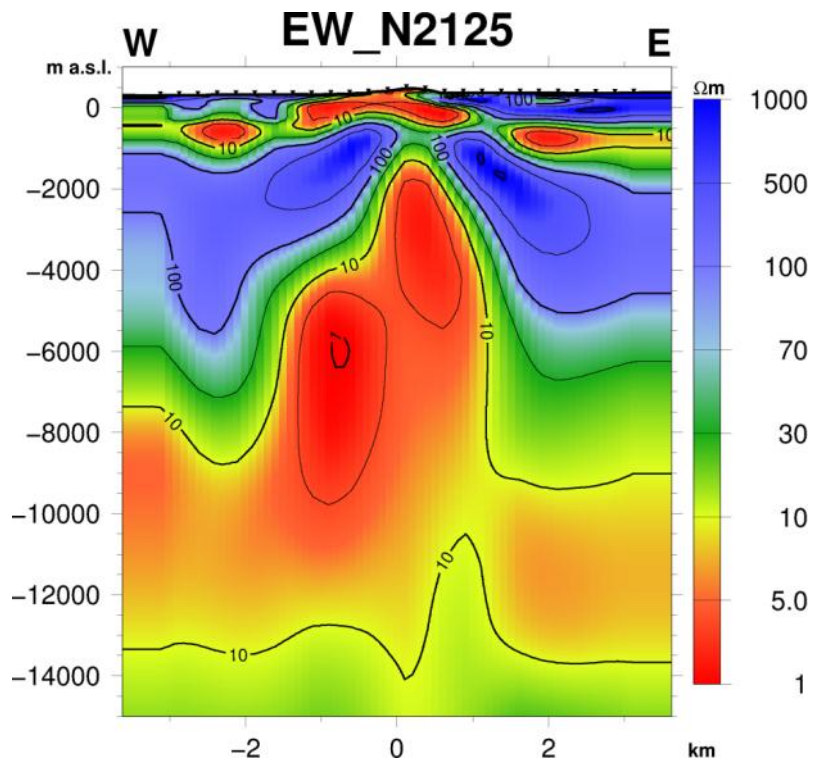
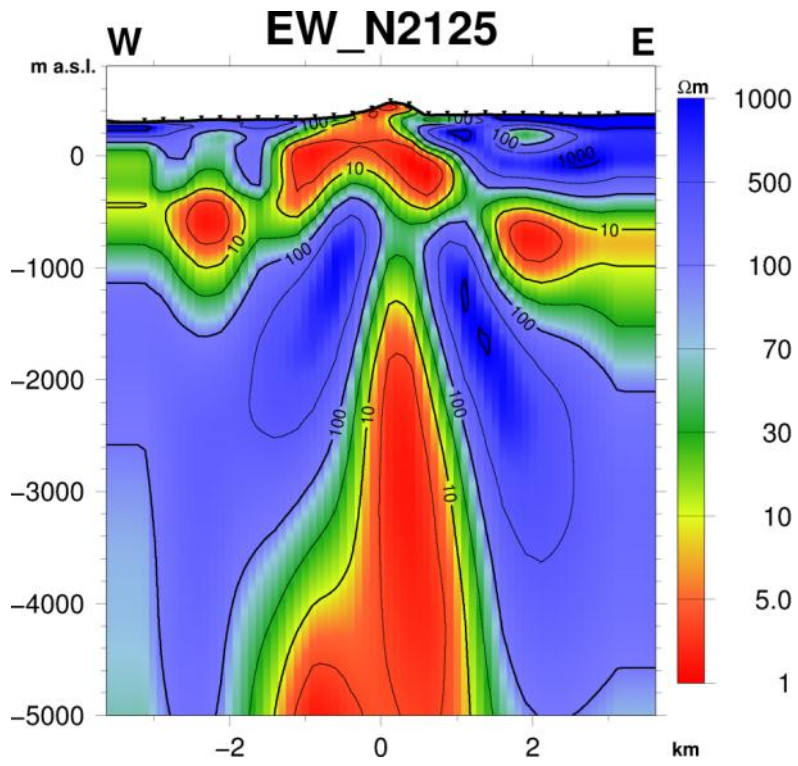


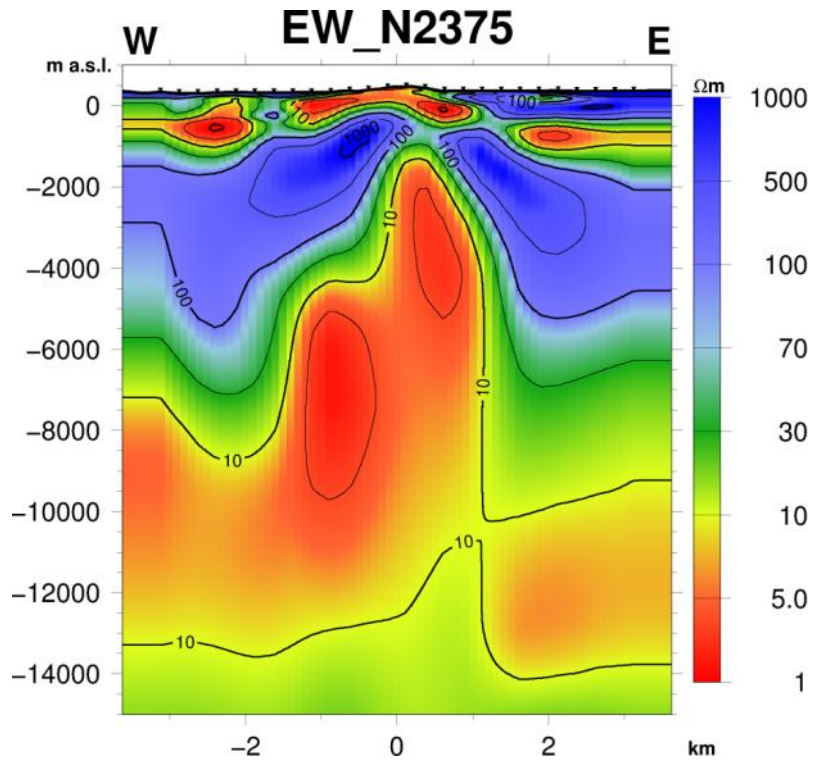
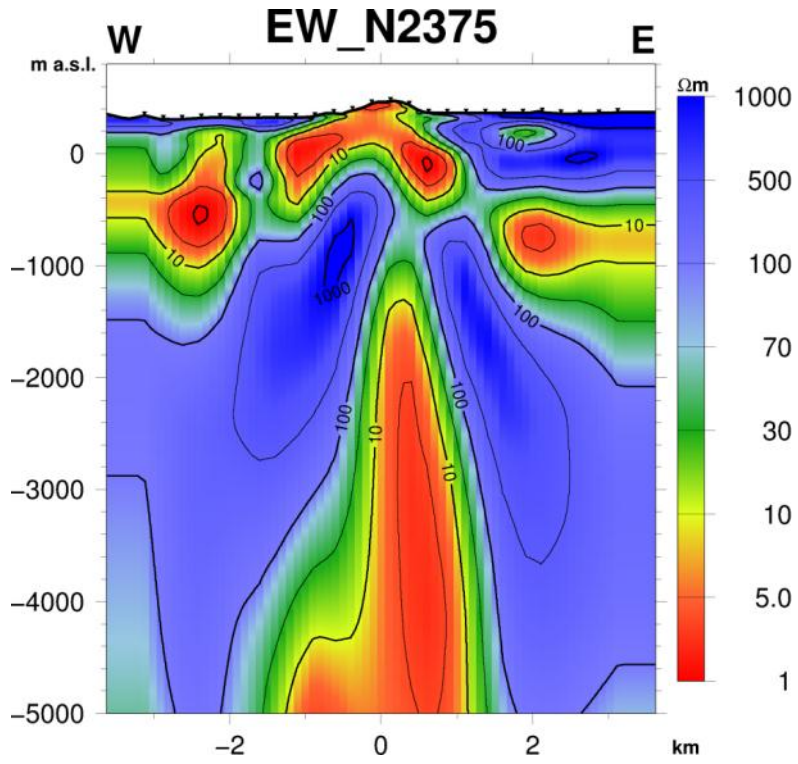


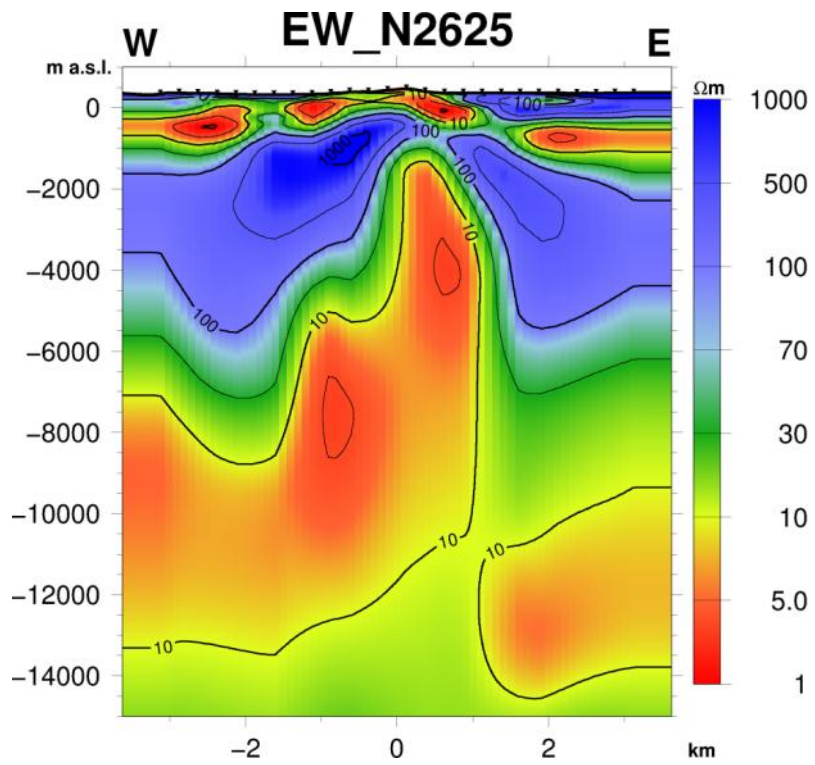
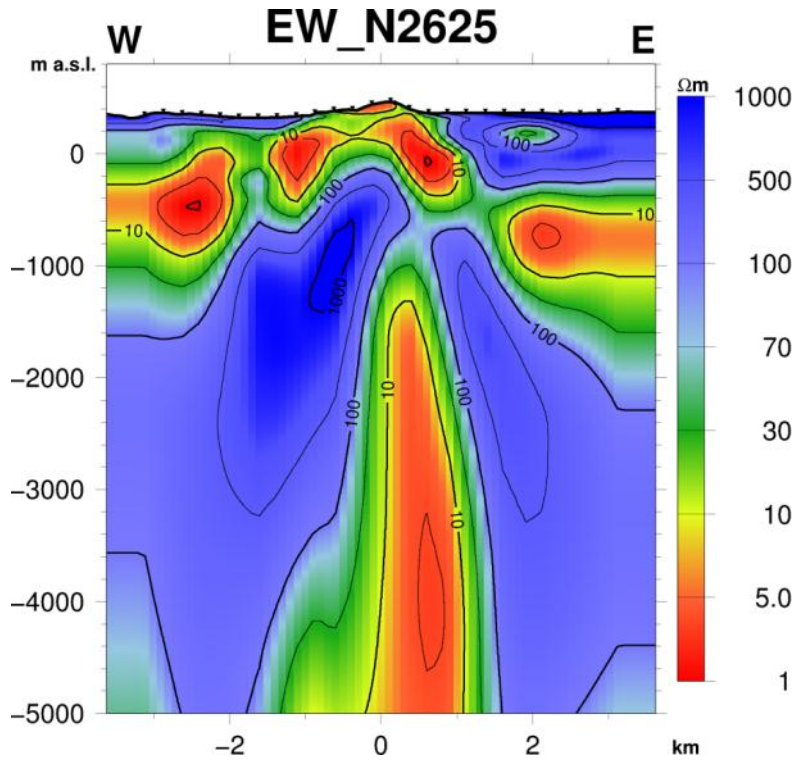


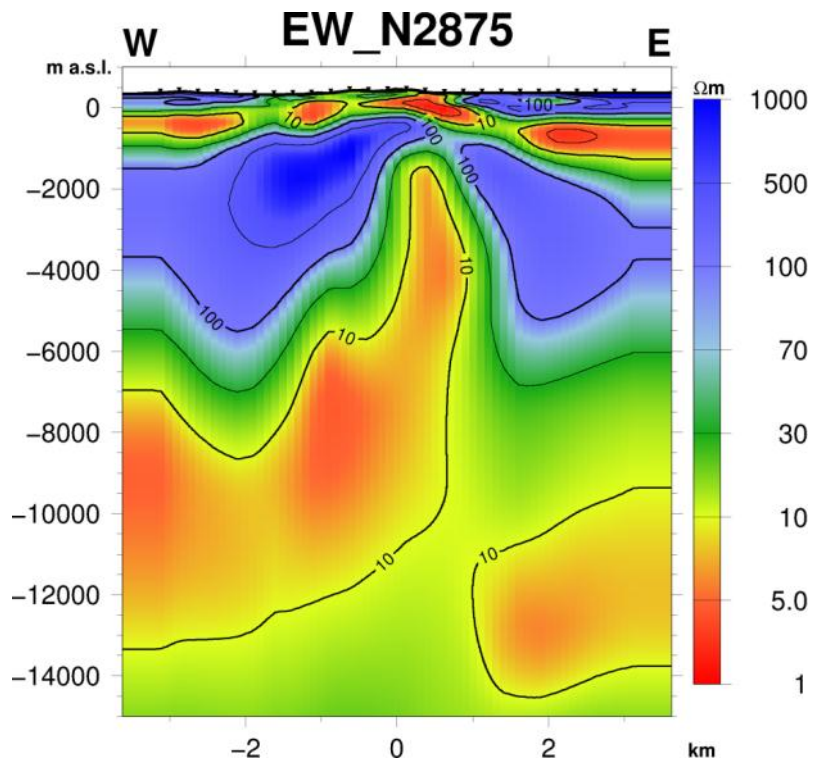
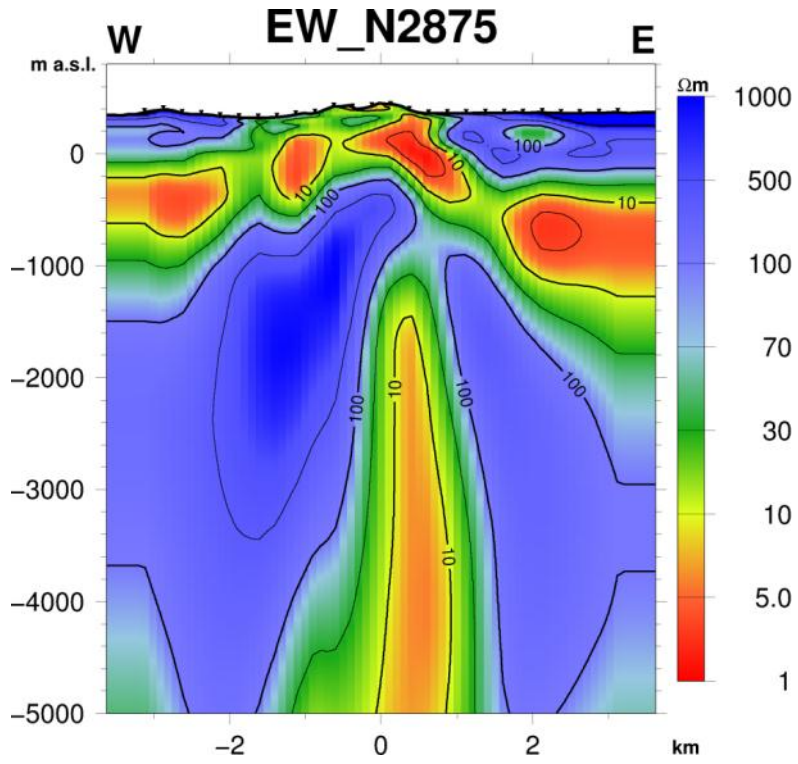


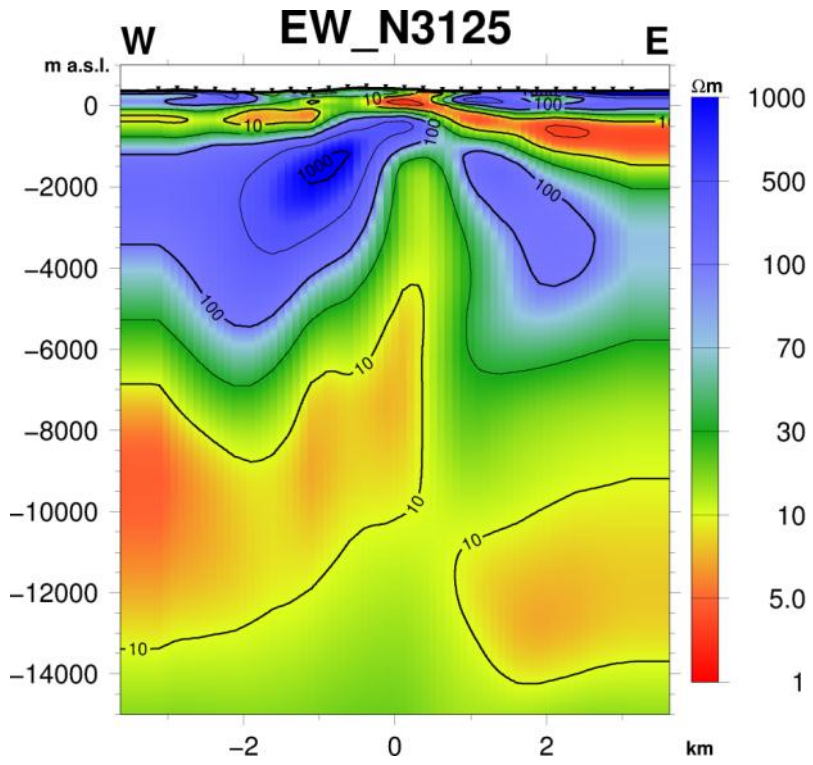
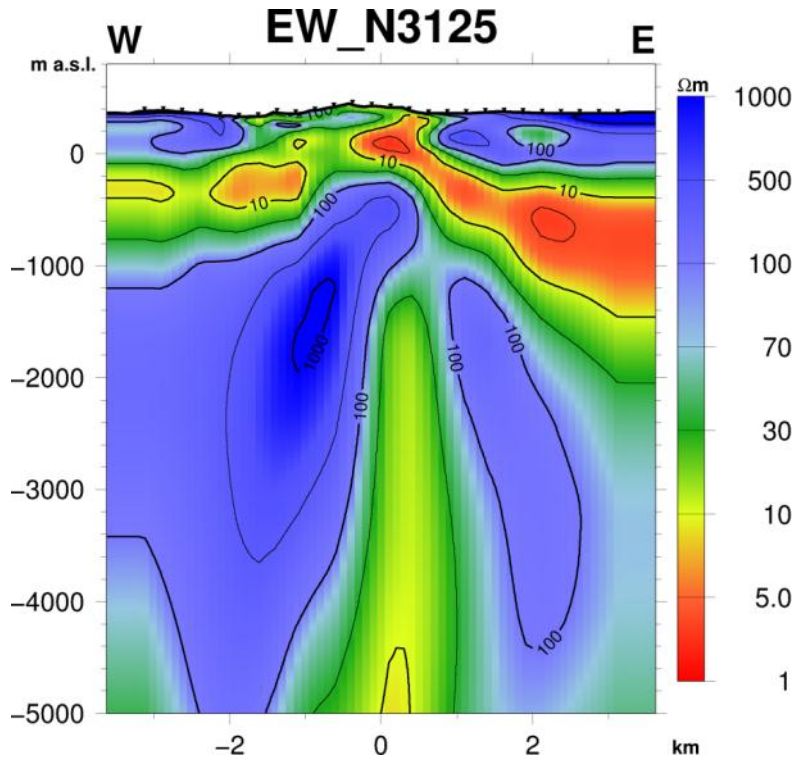


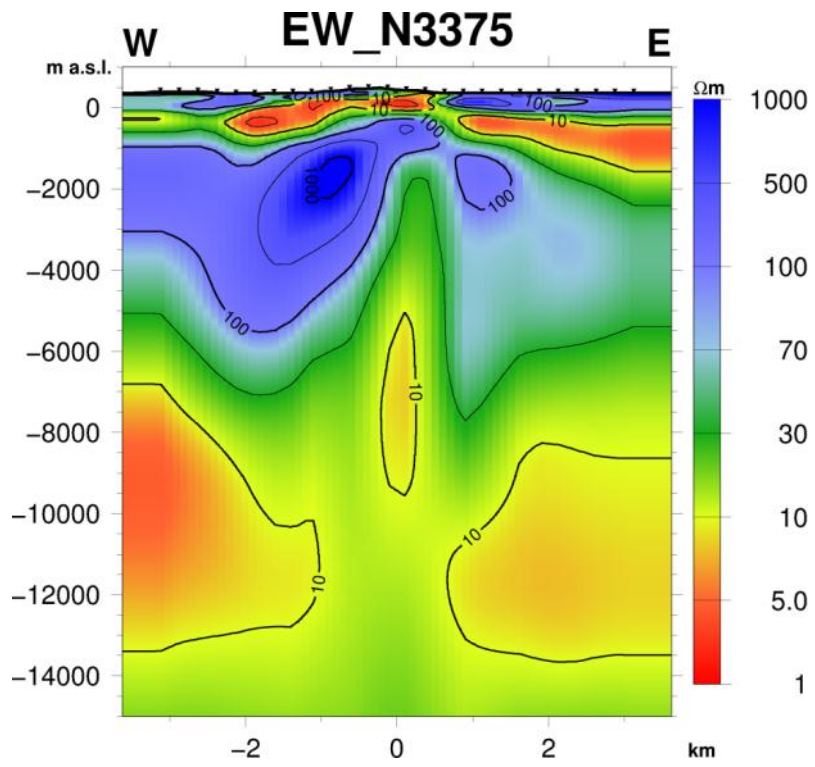
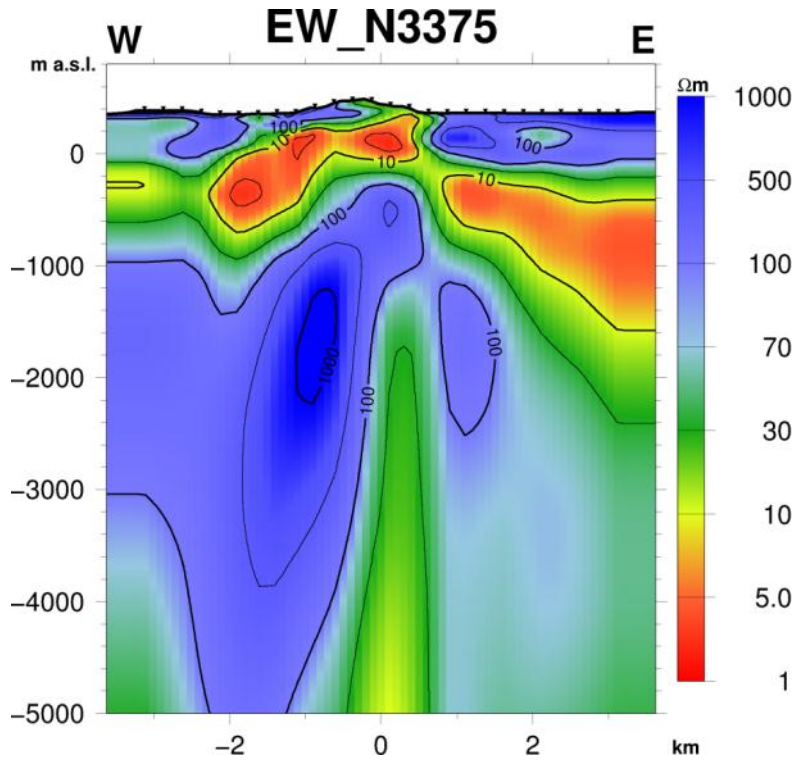


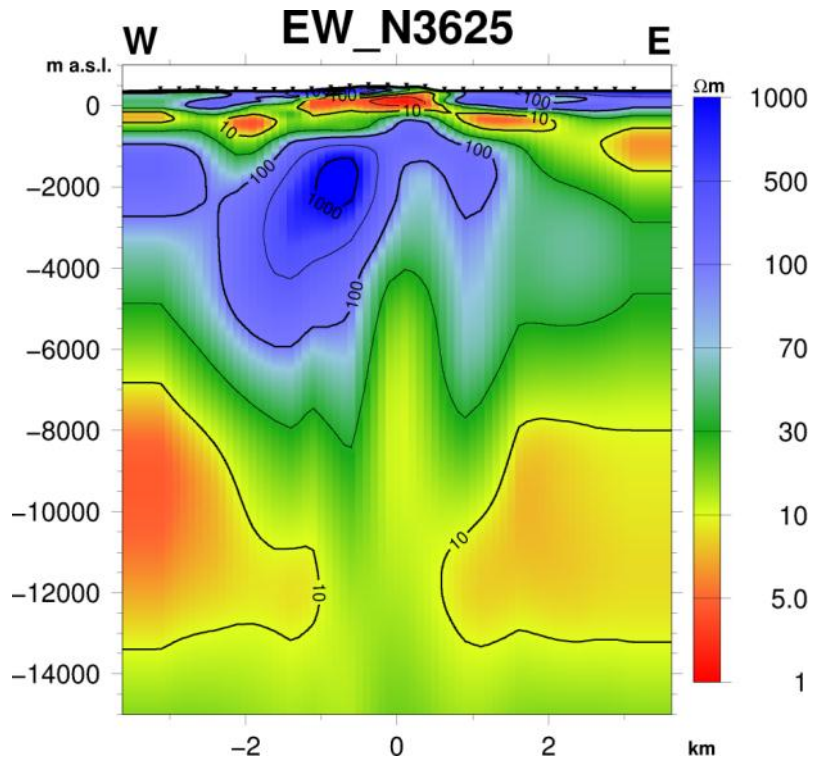
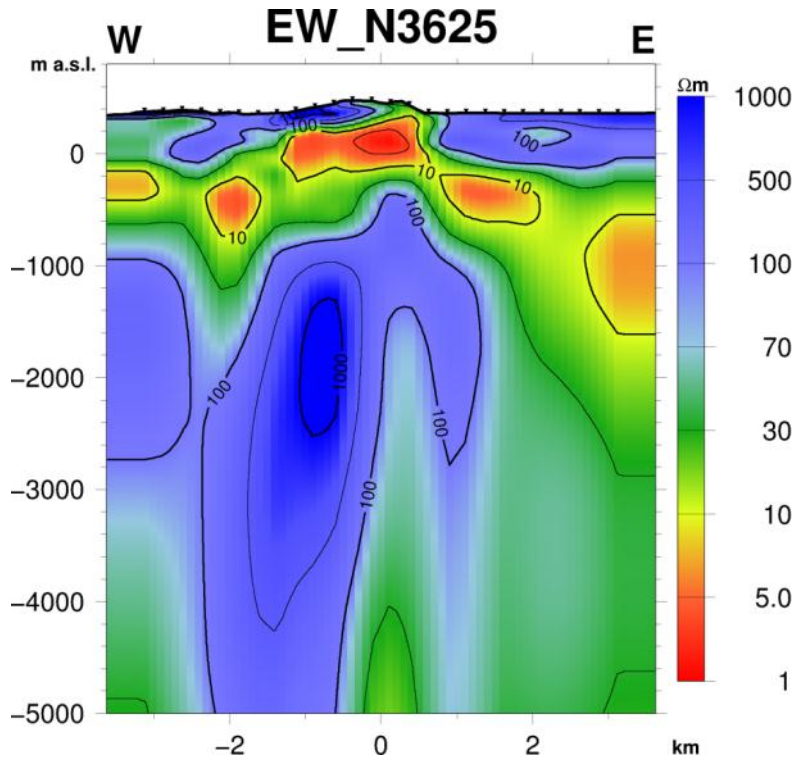


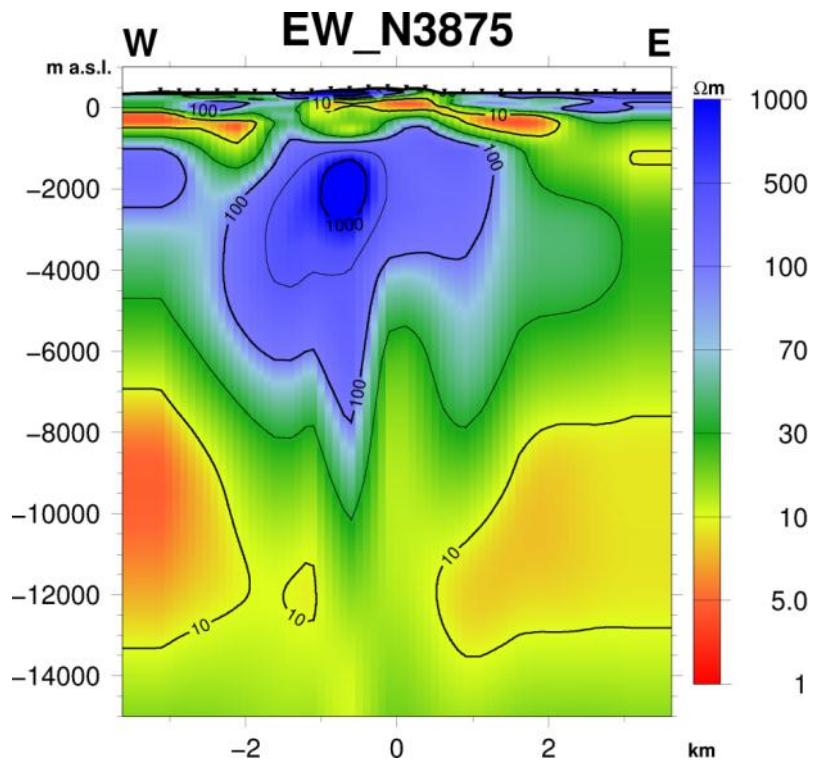
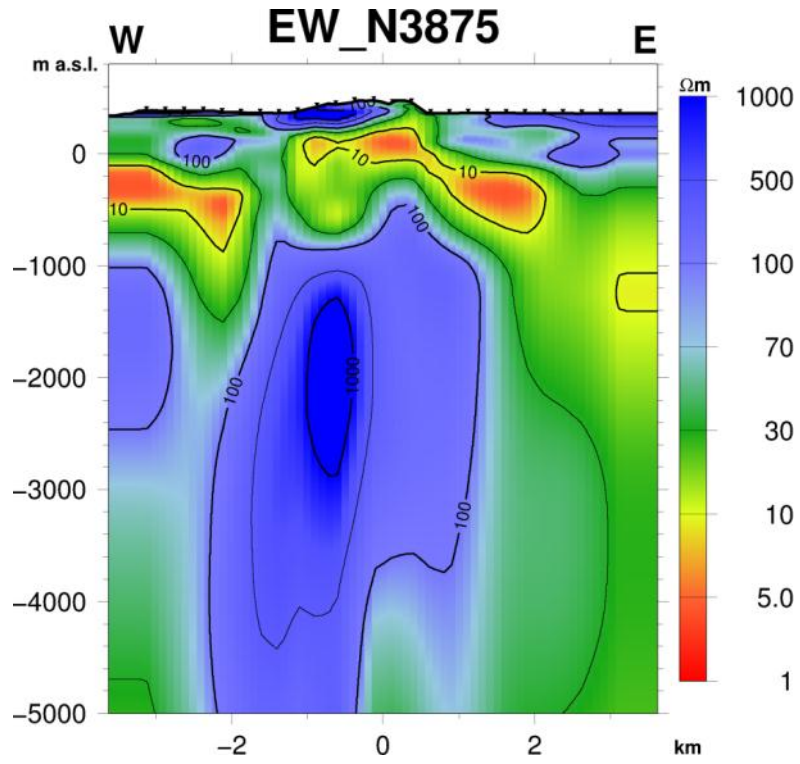


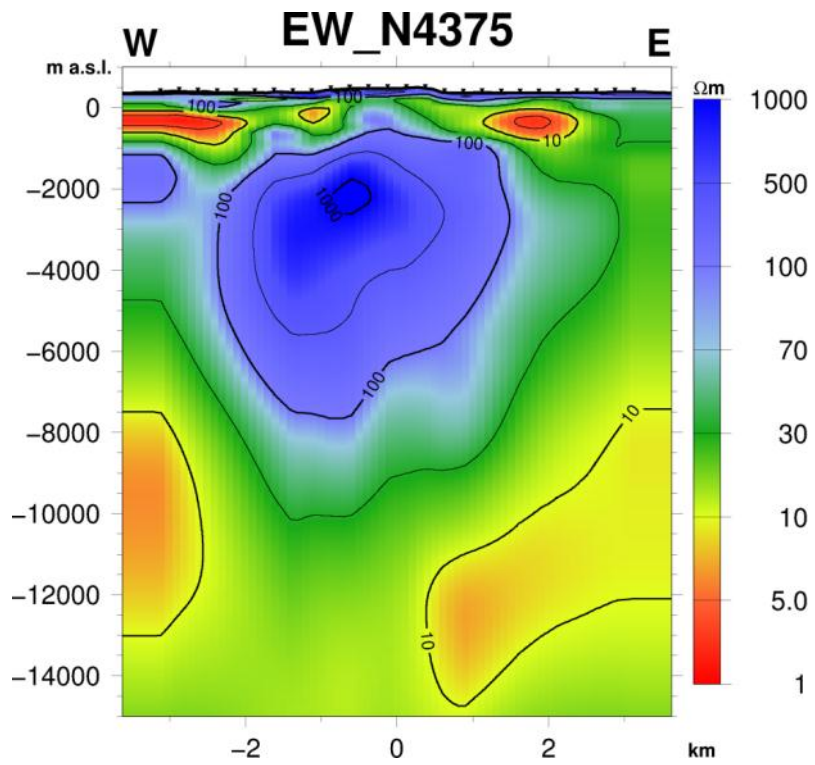
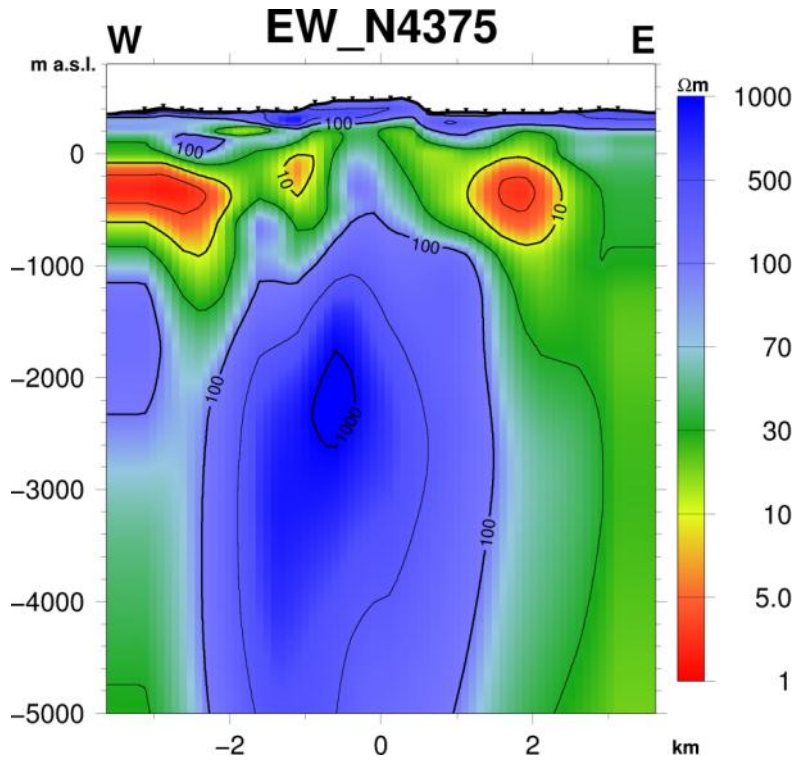


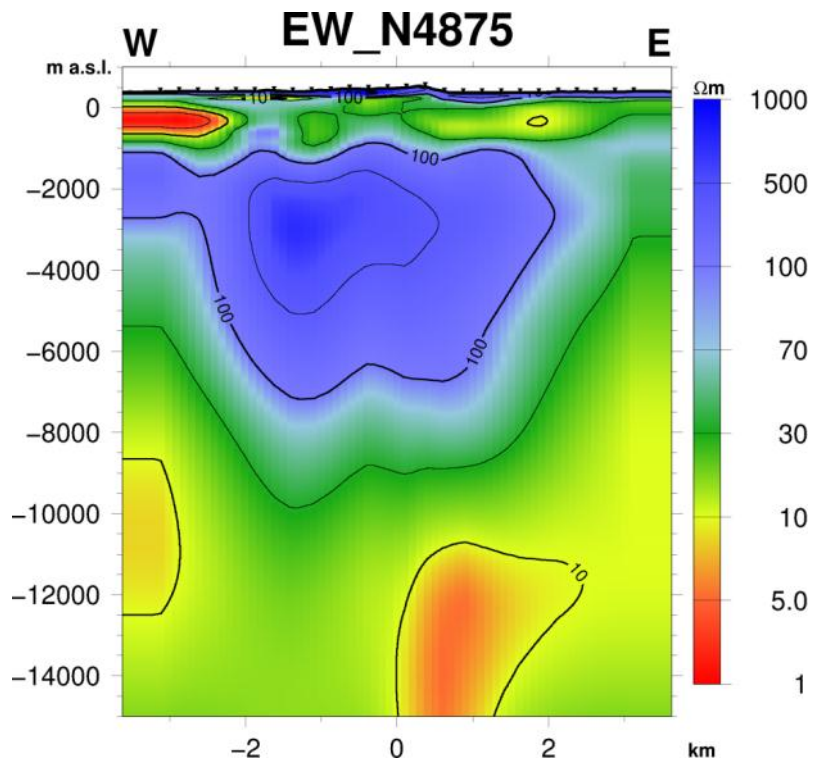
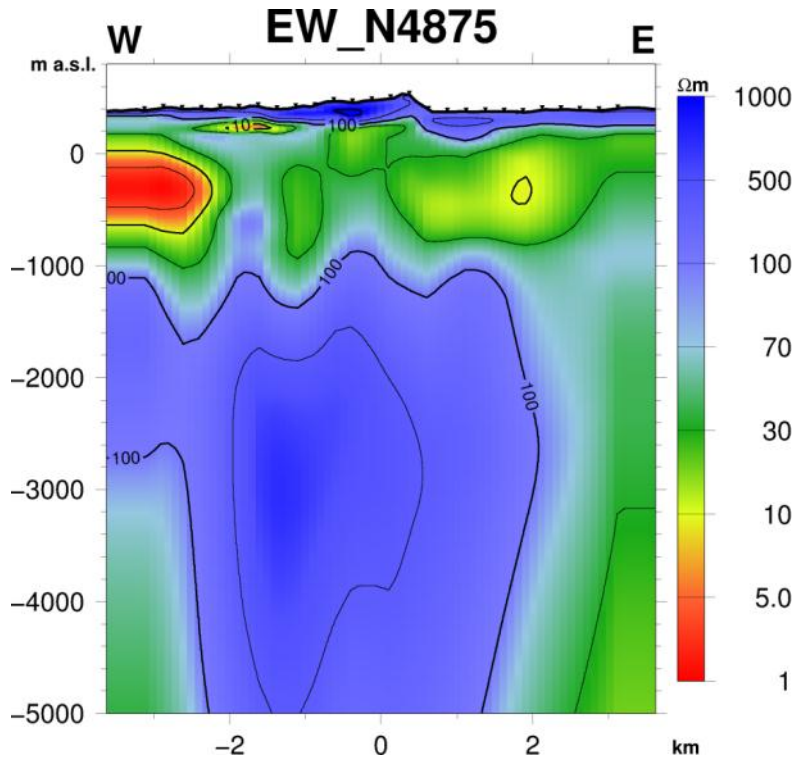


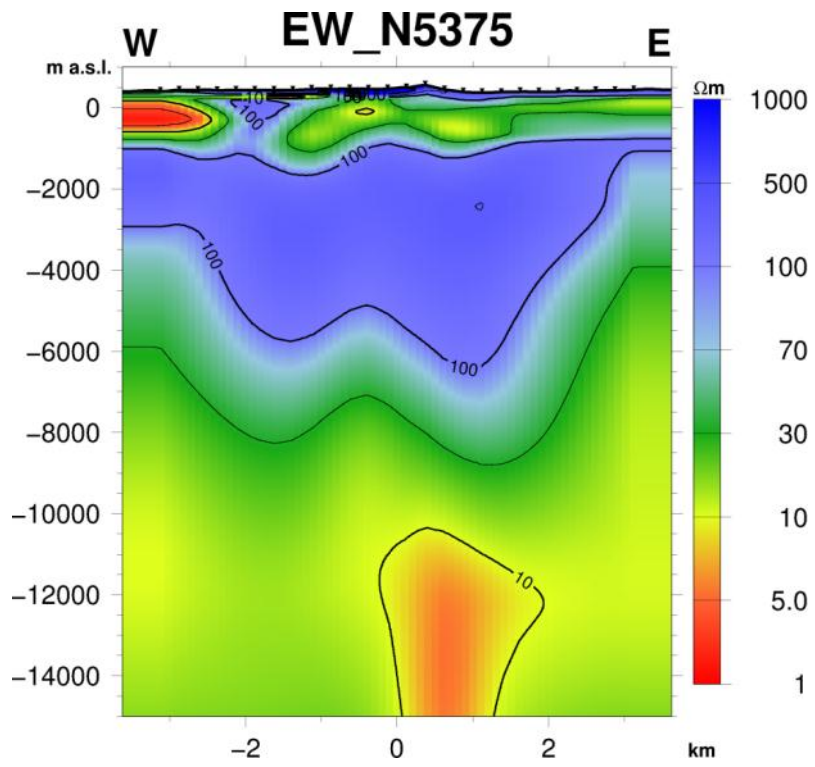
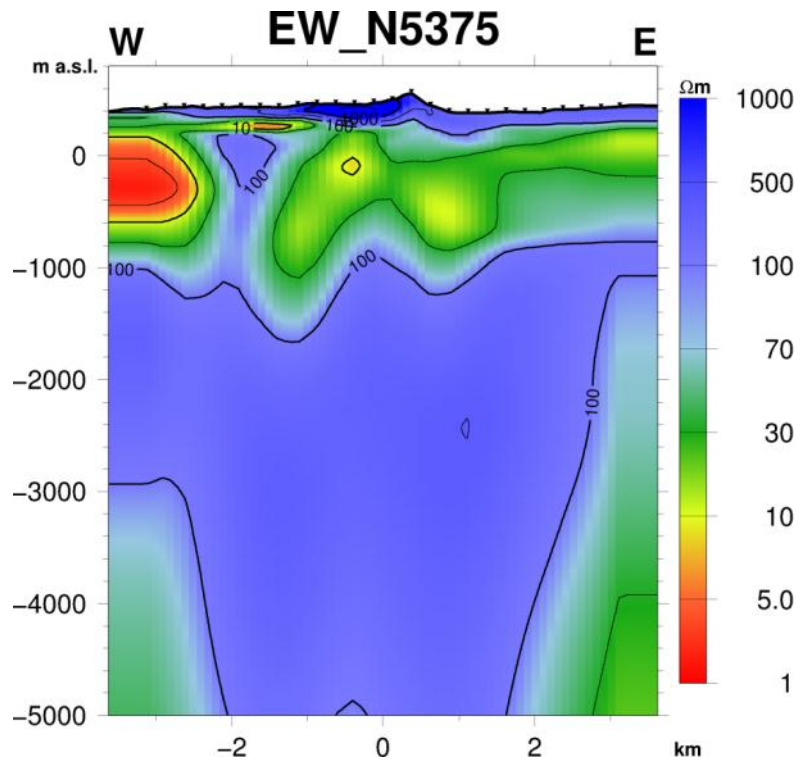




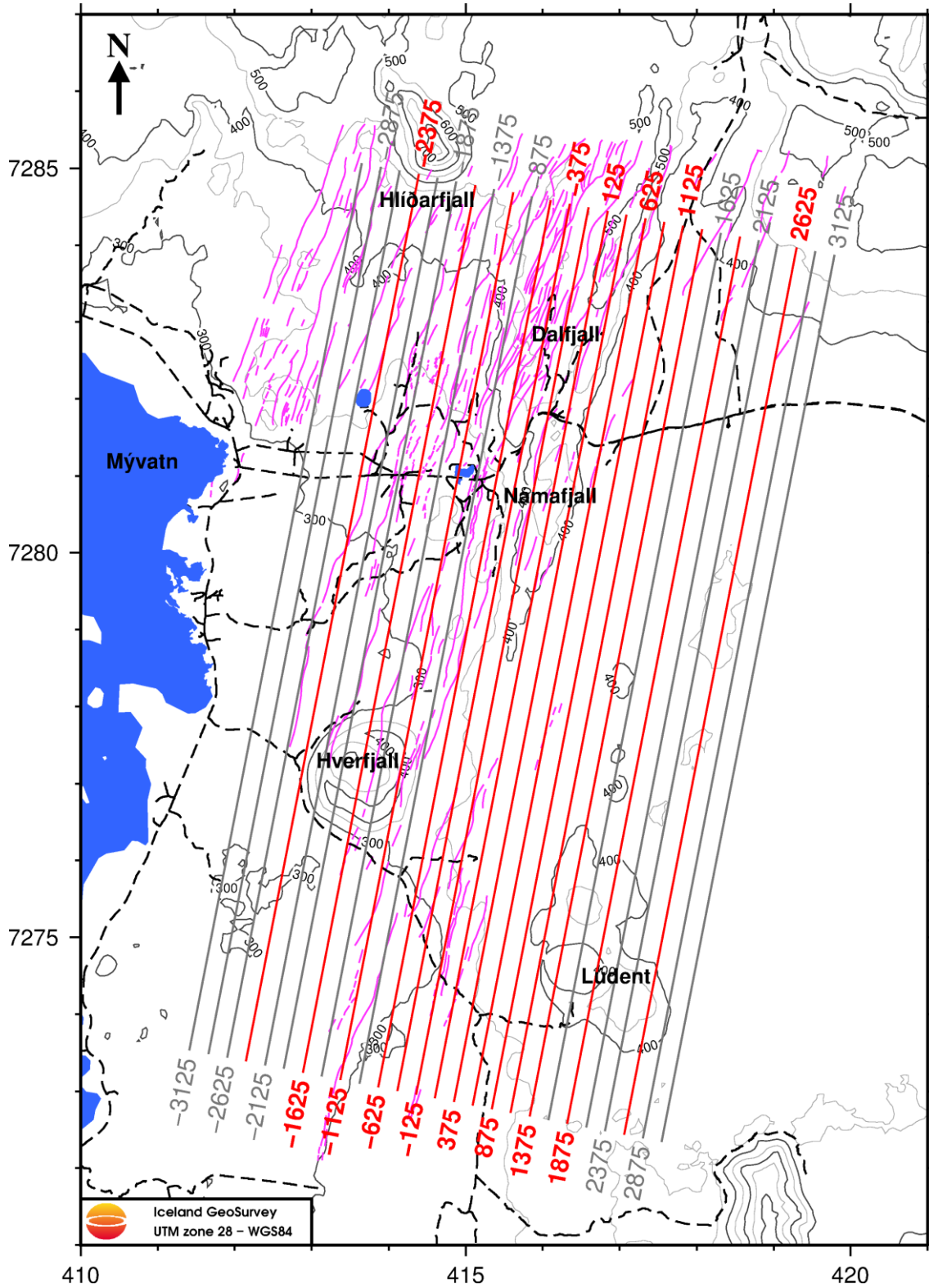


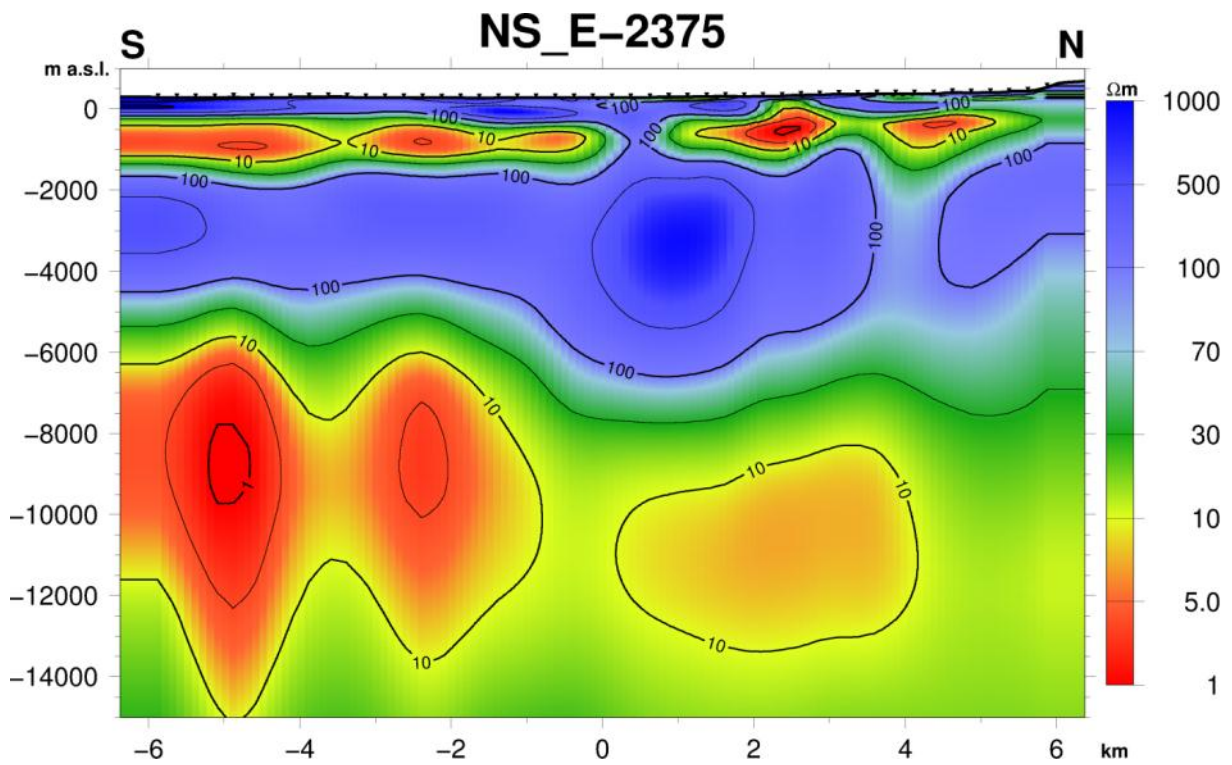
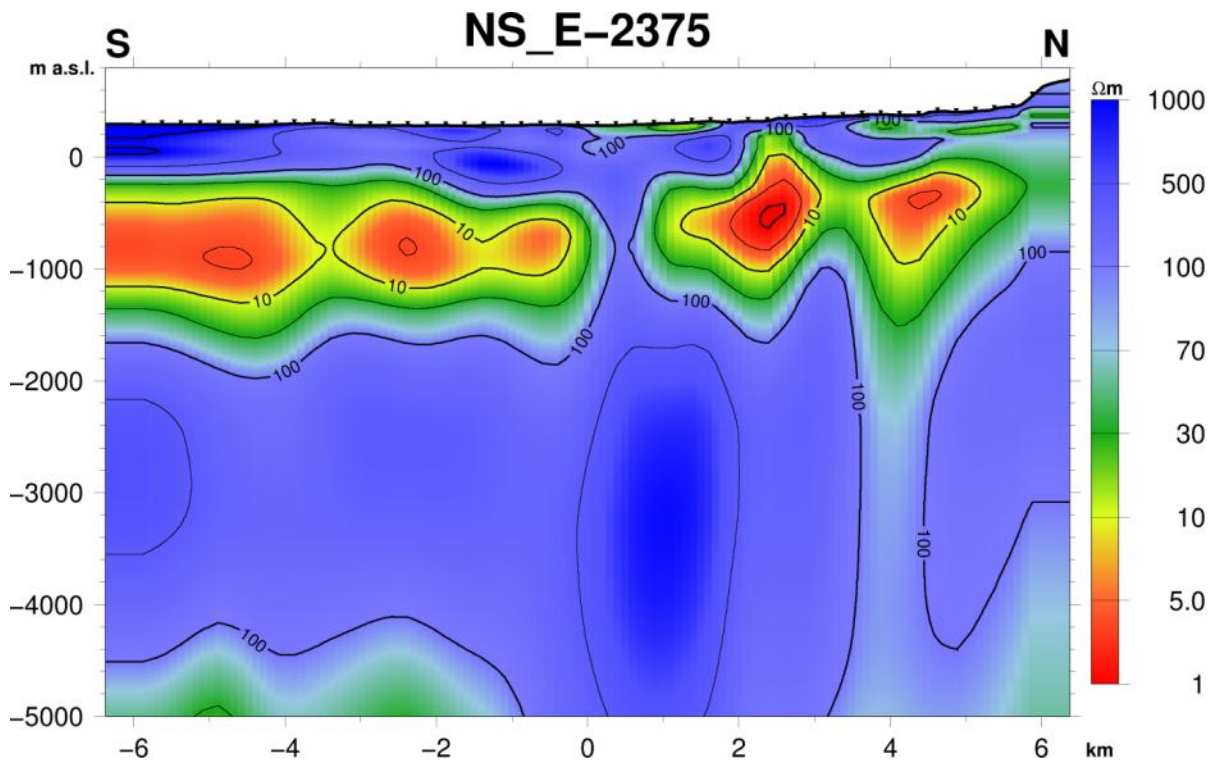


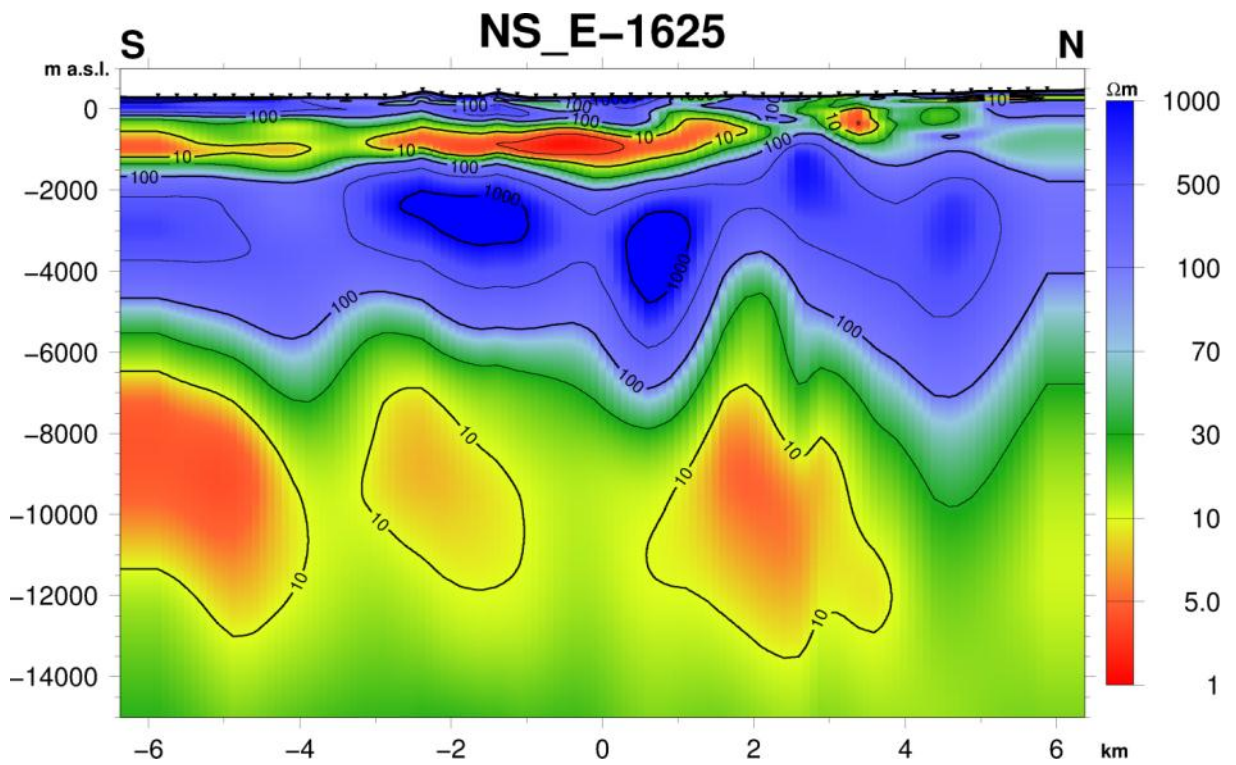
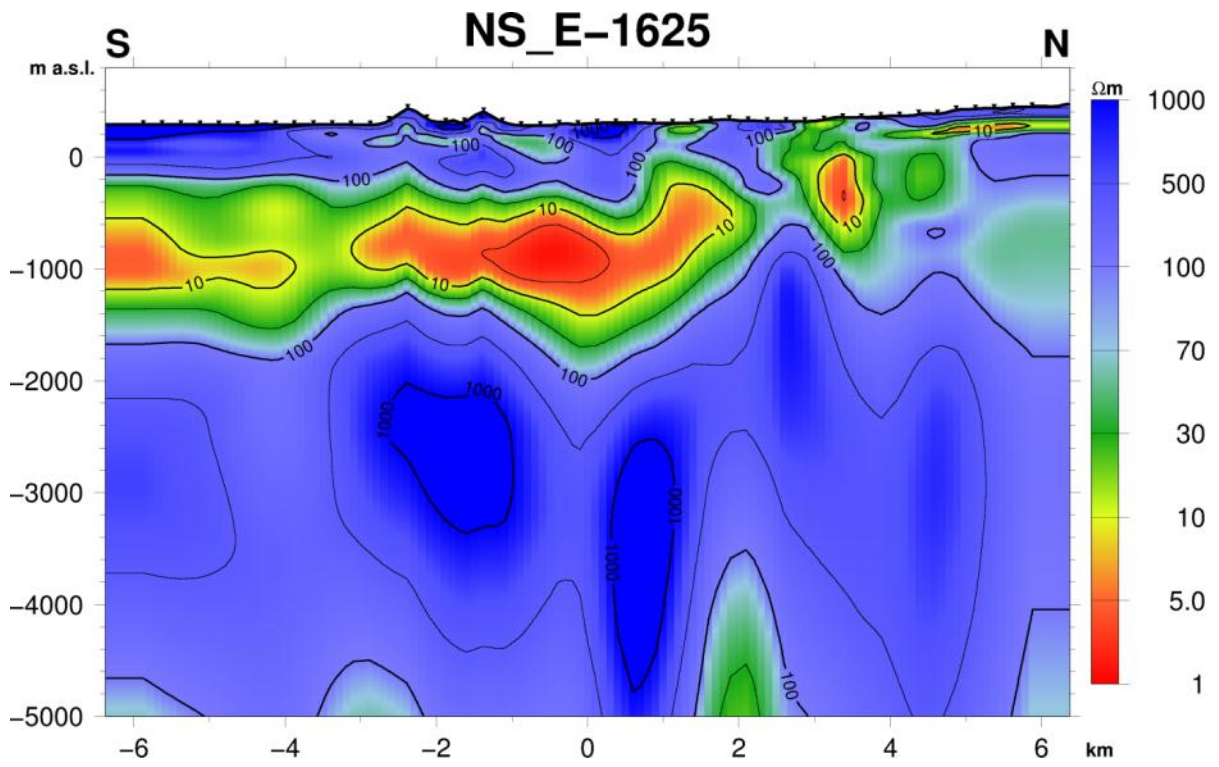


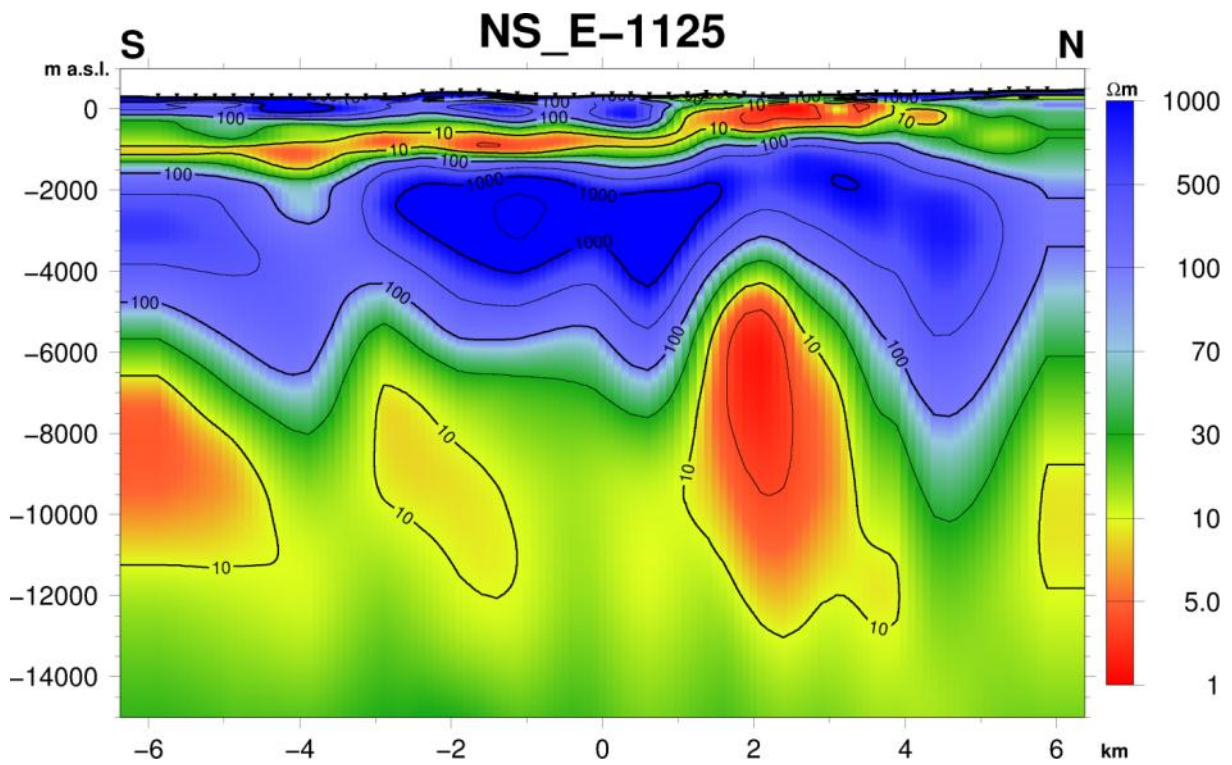
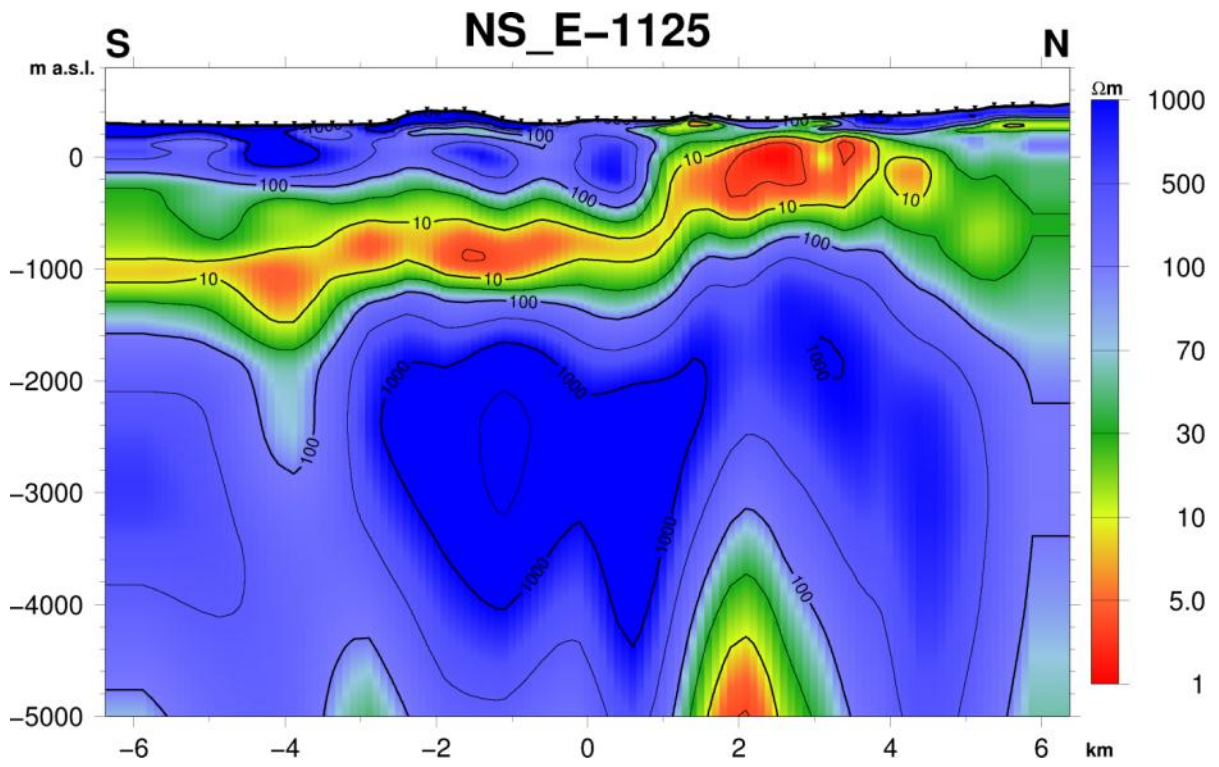


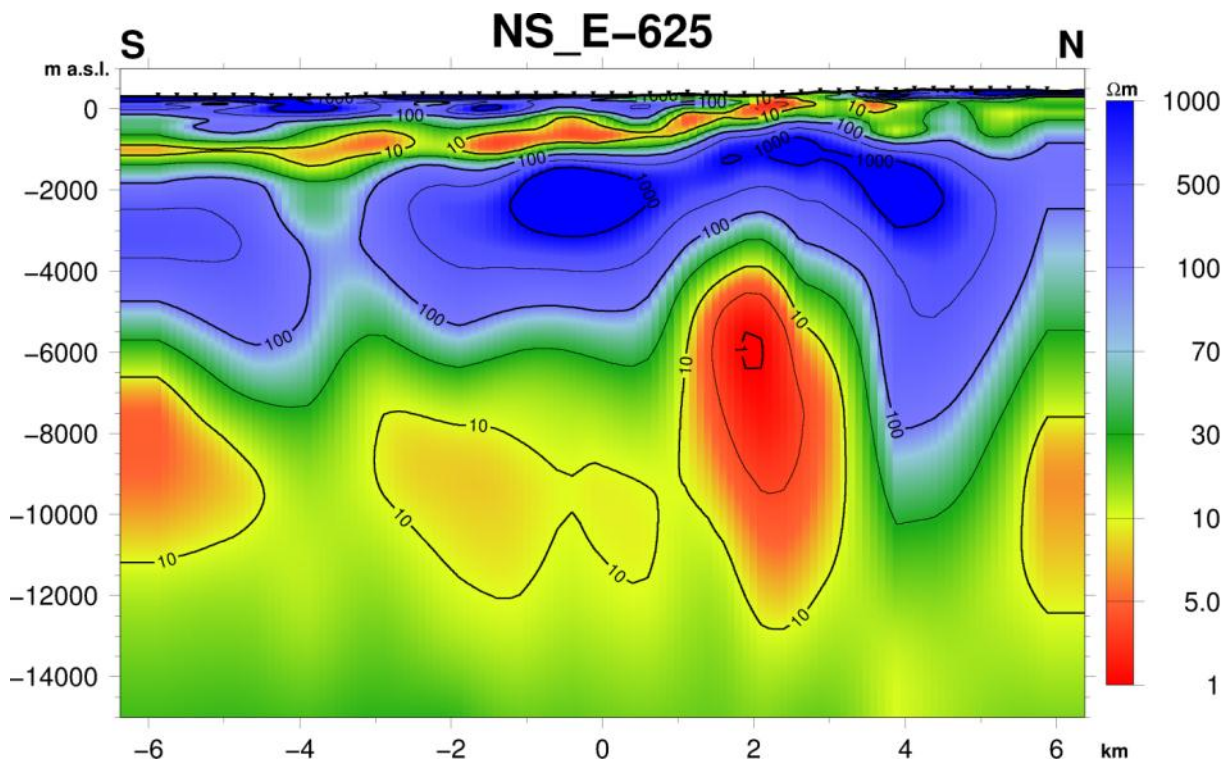
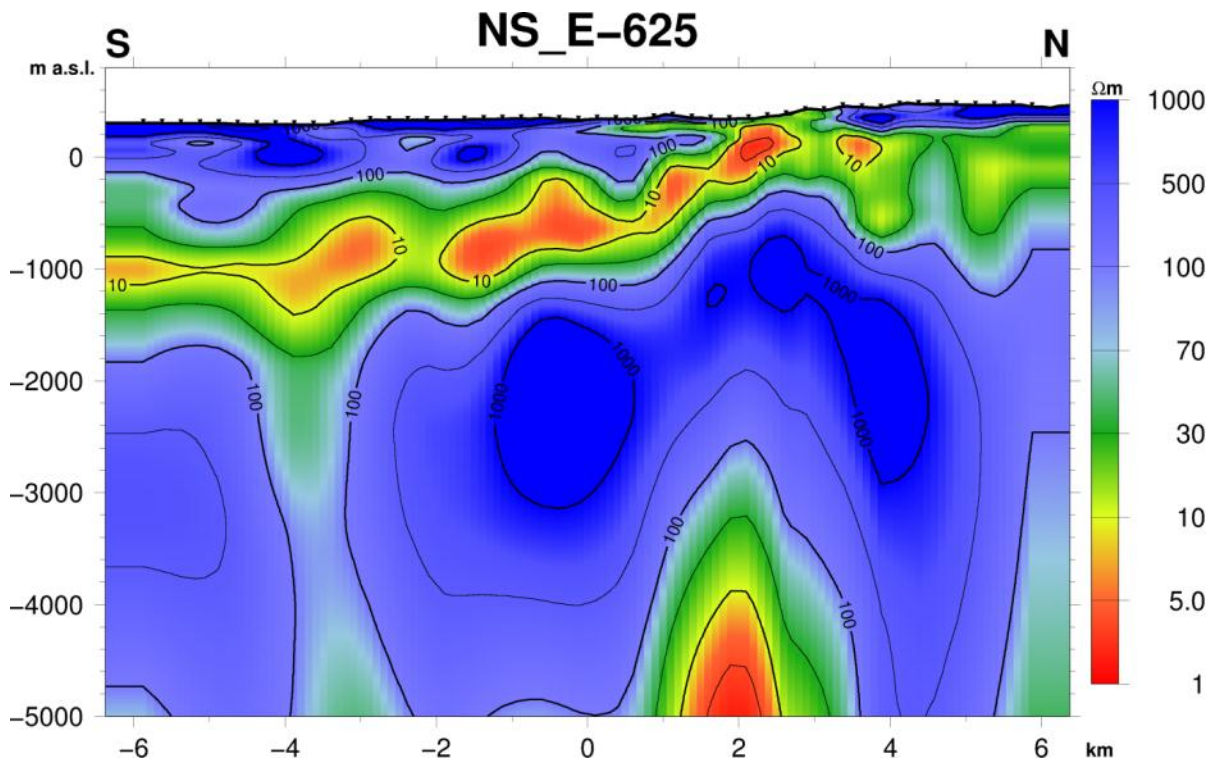
Appendix 3:
North – South
Resistivity cross sections

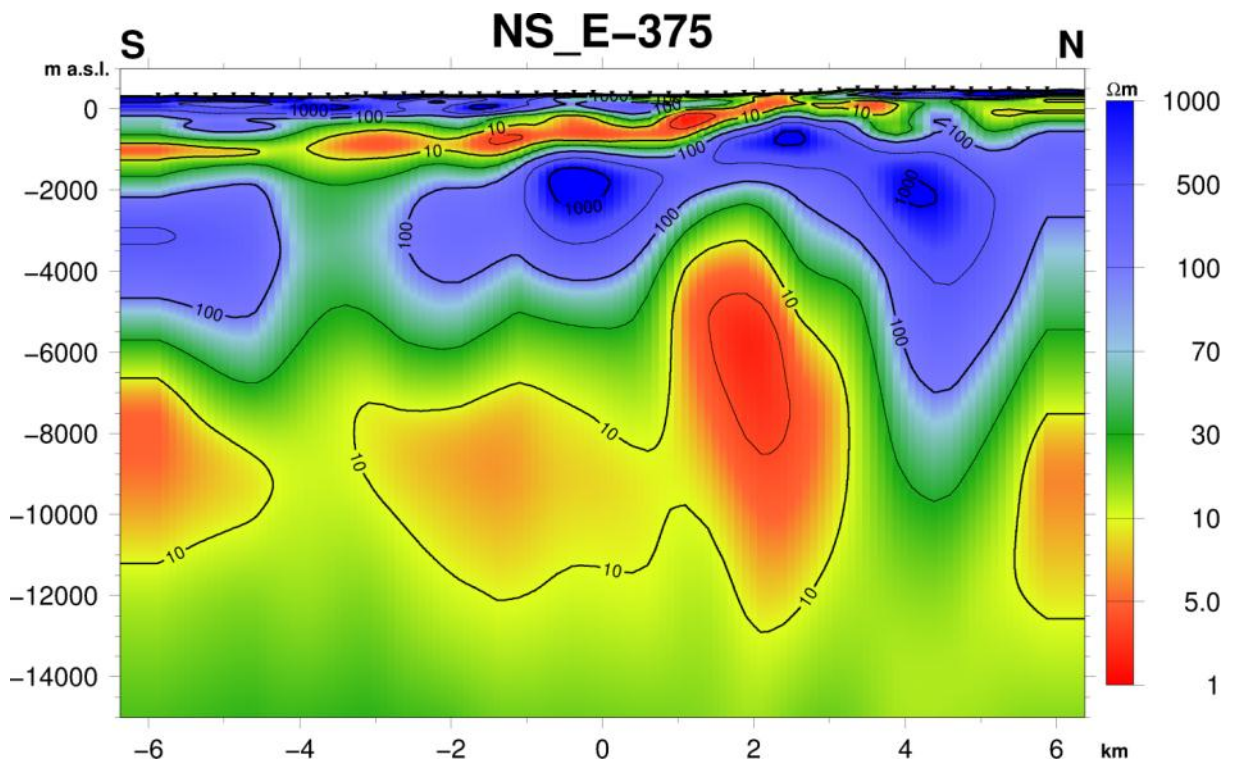
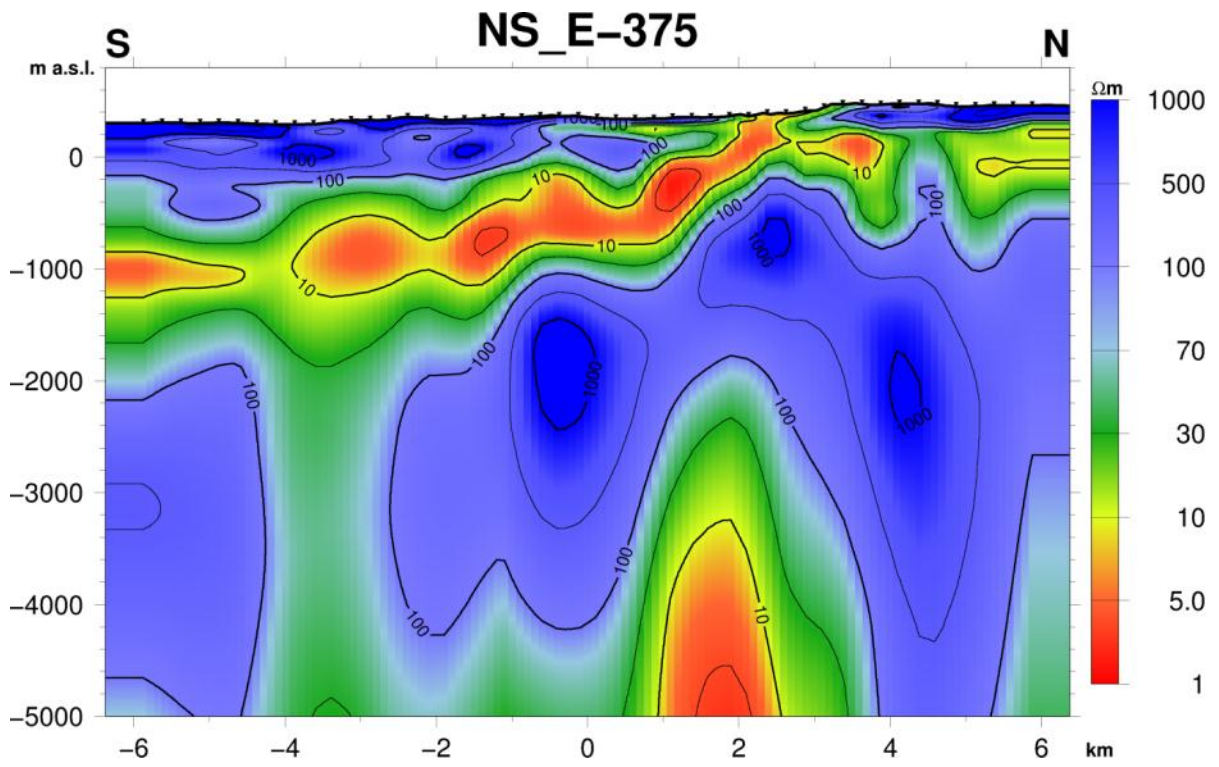


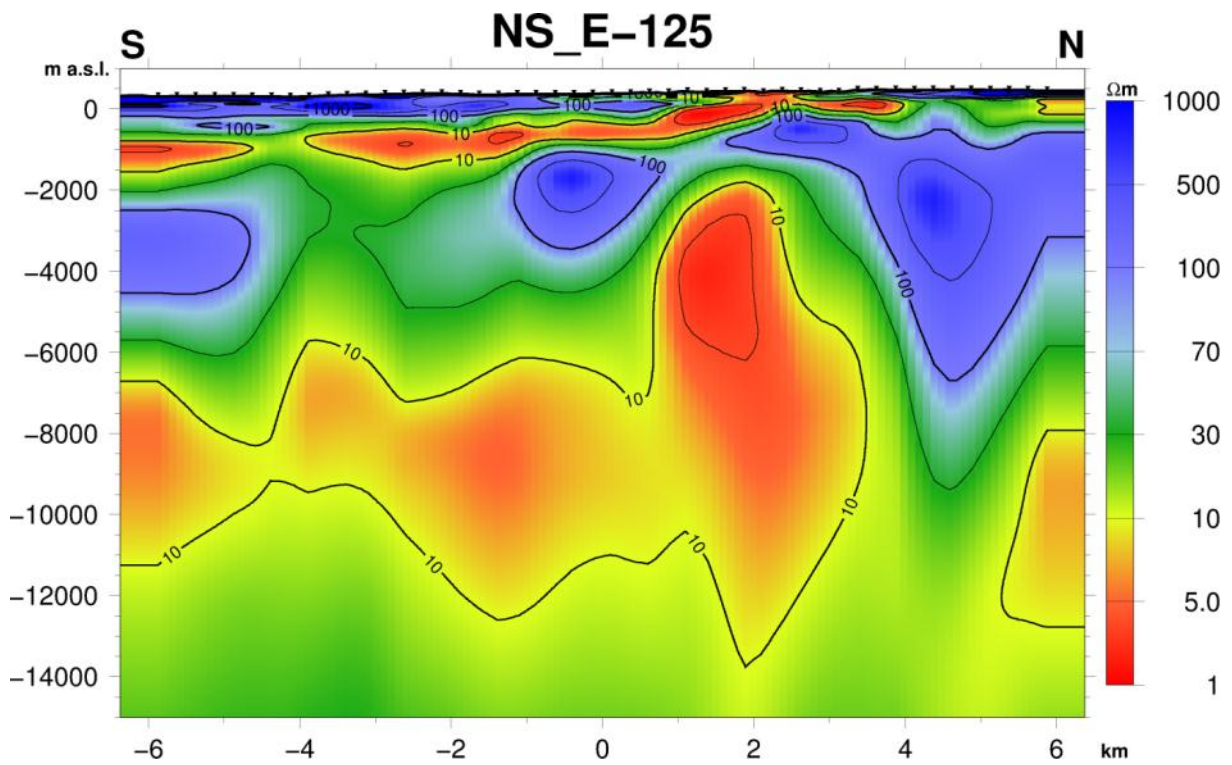
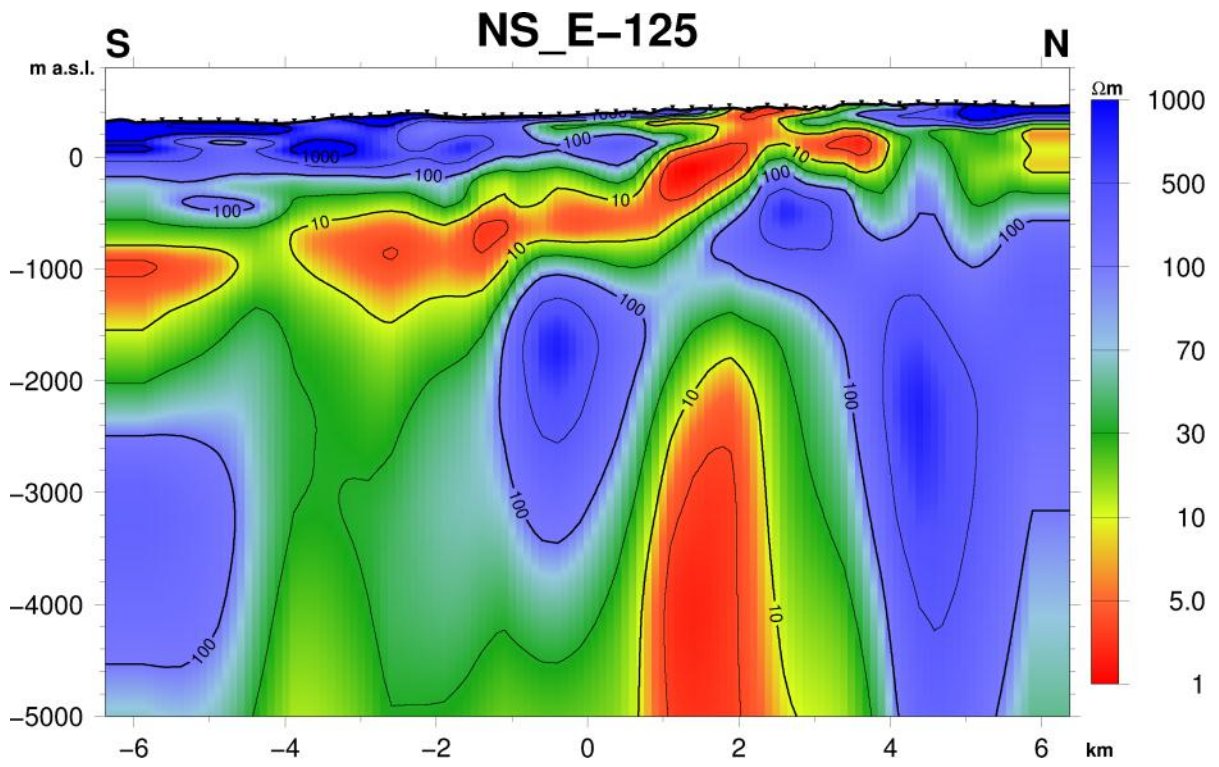


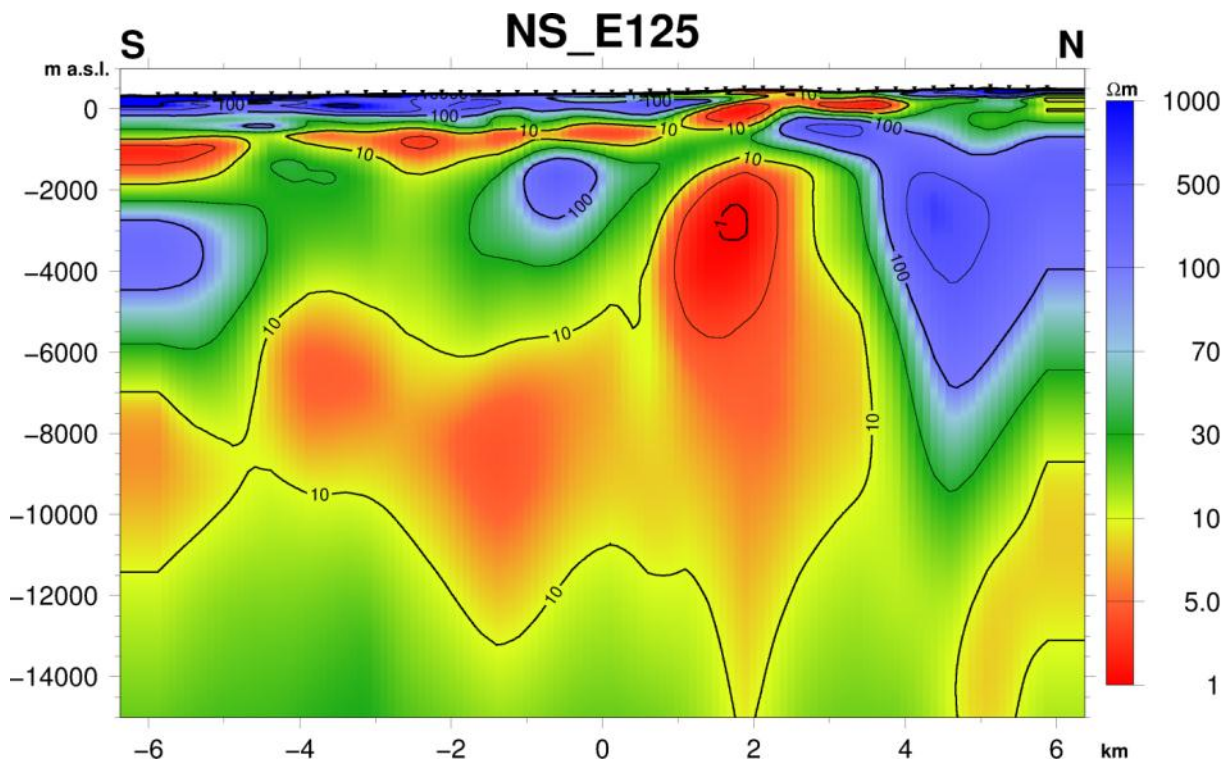
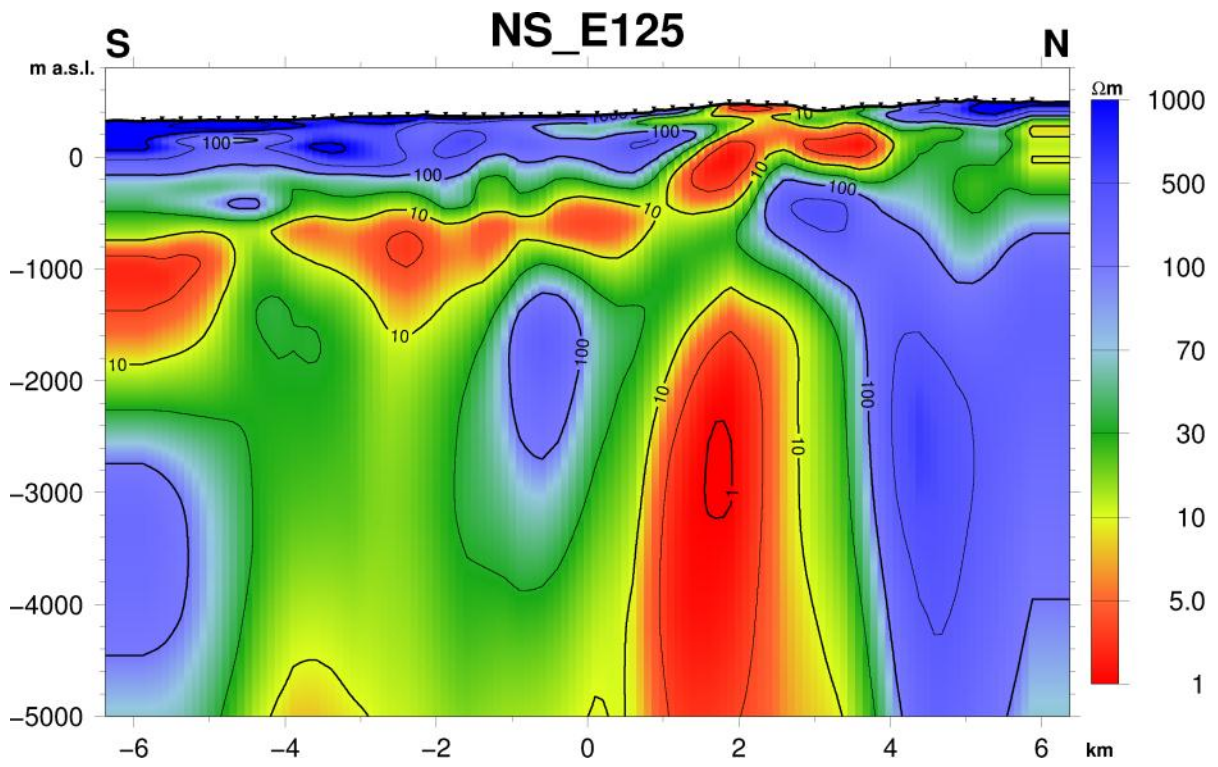


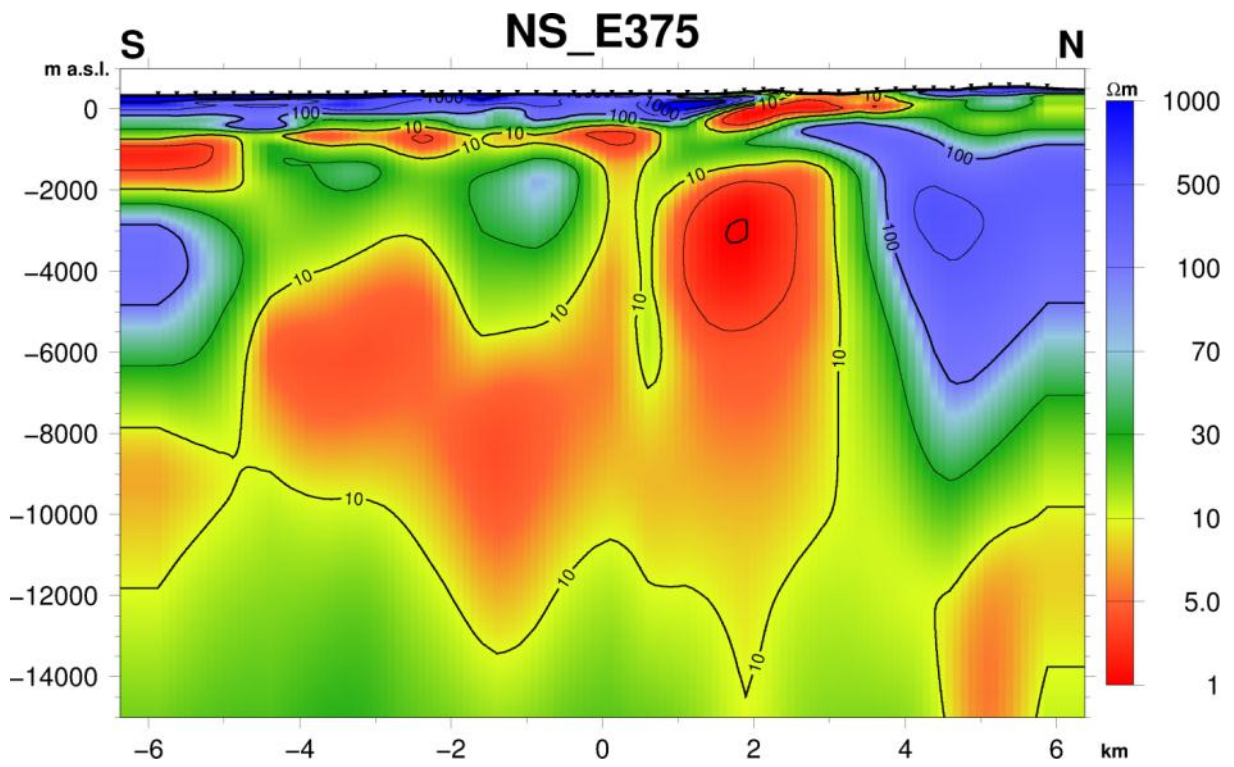
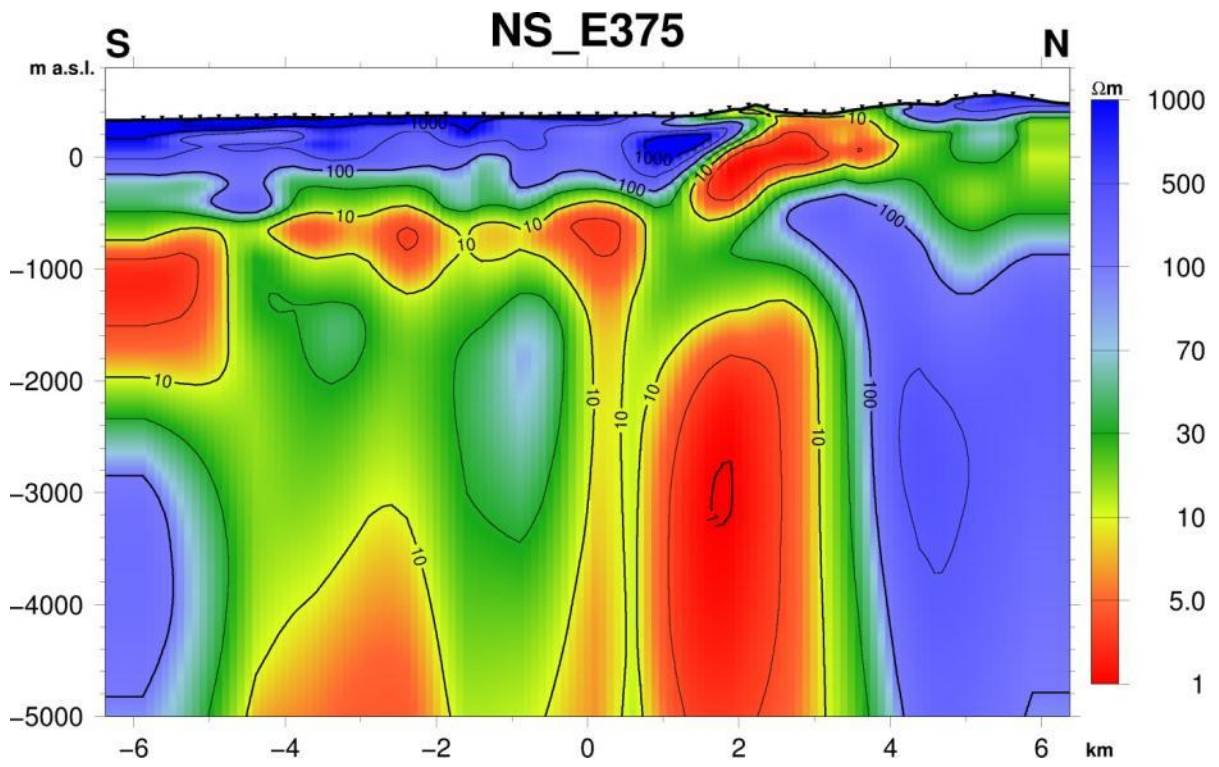


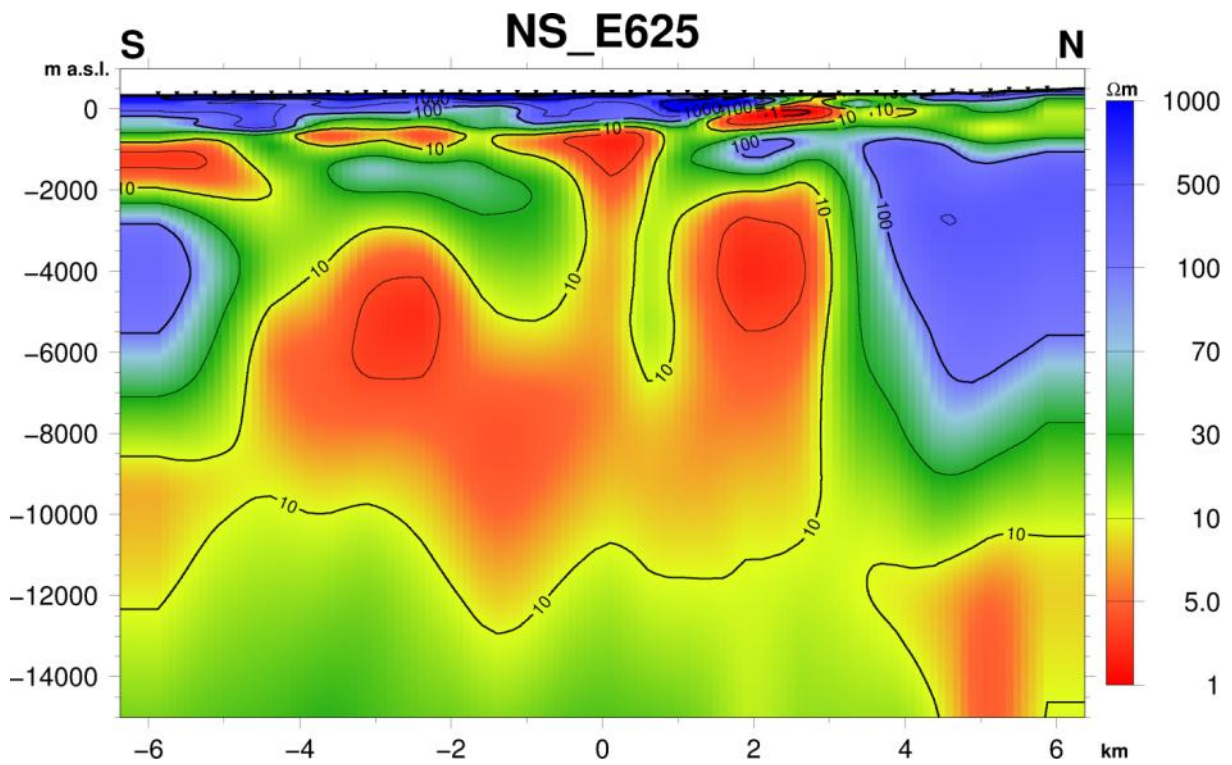
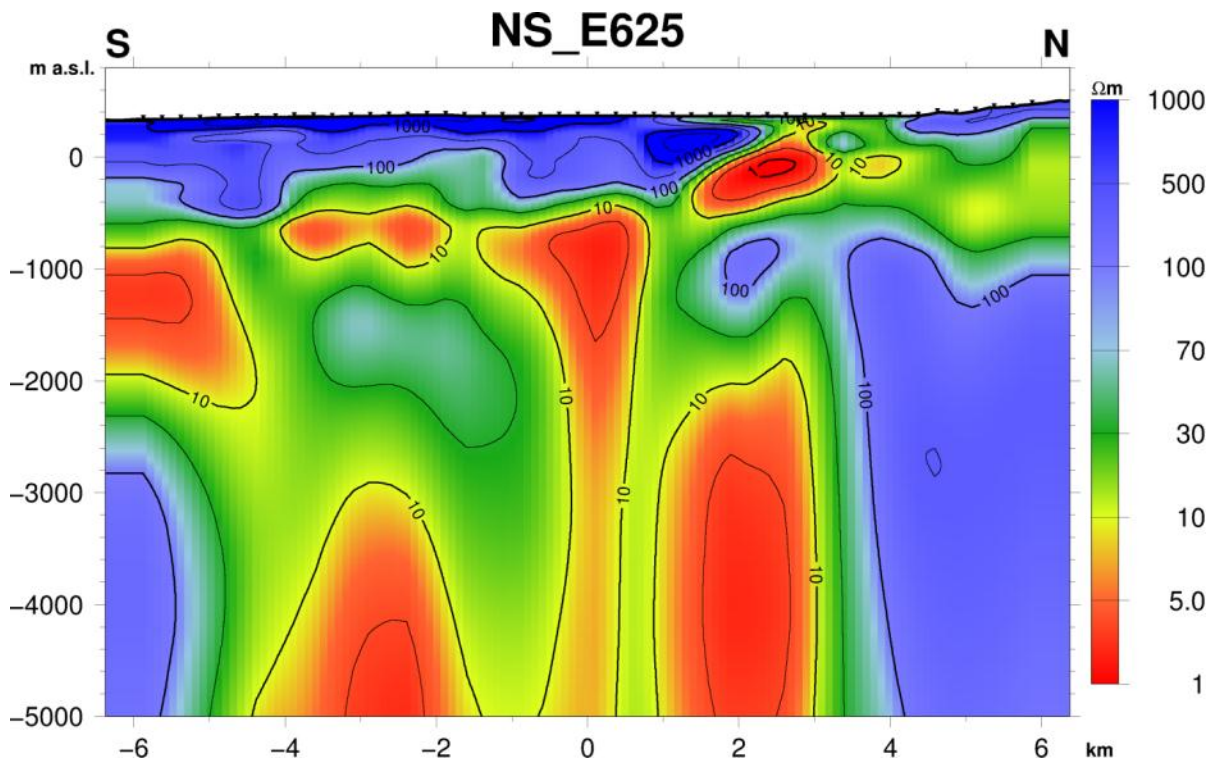


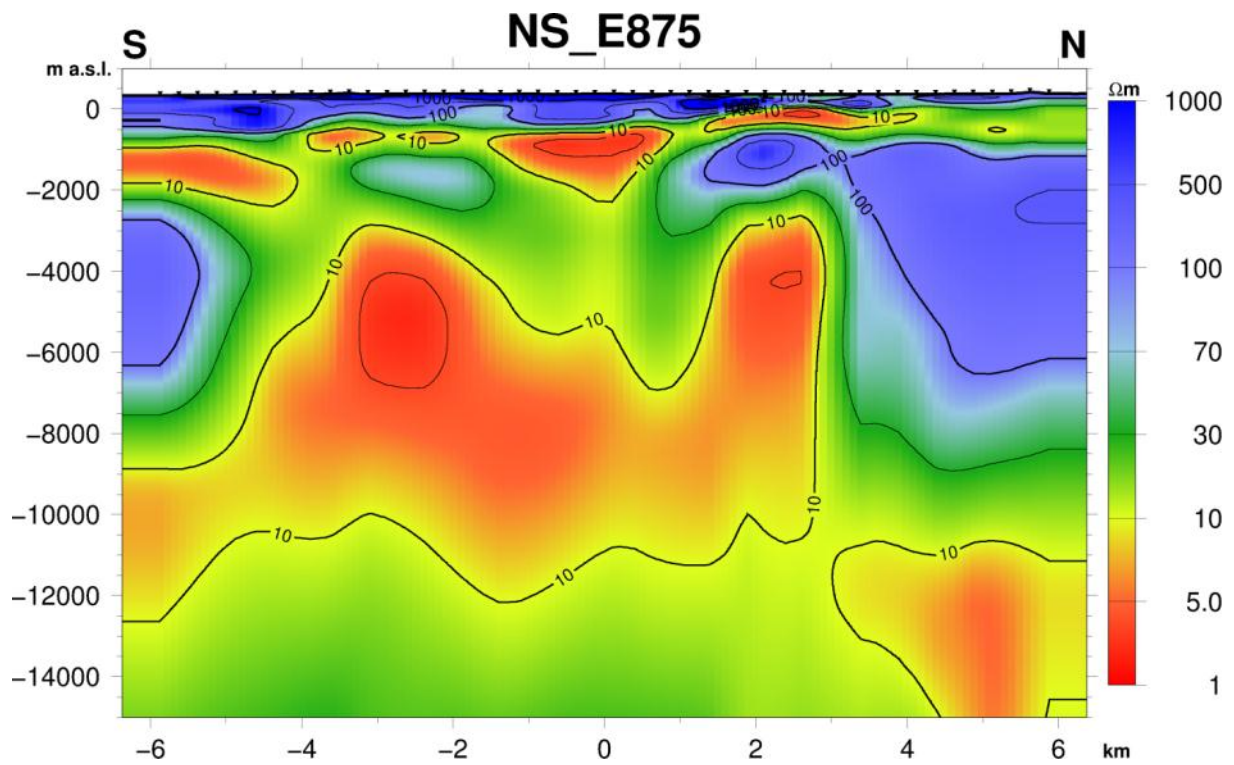
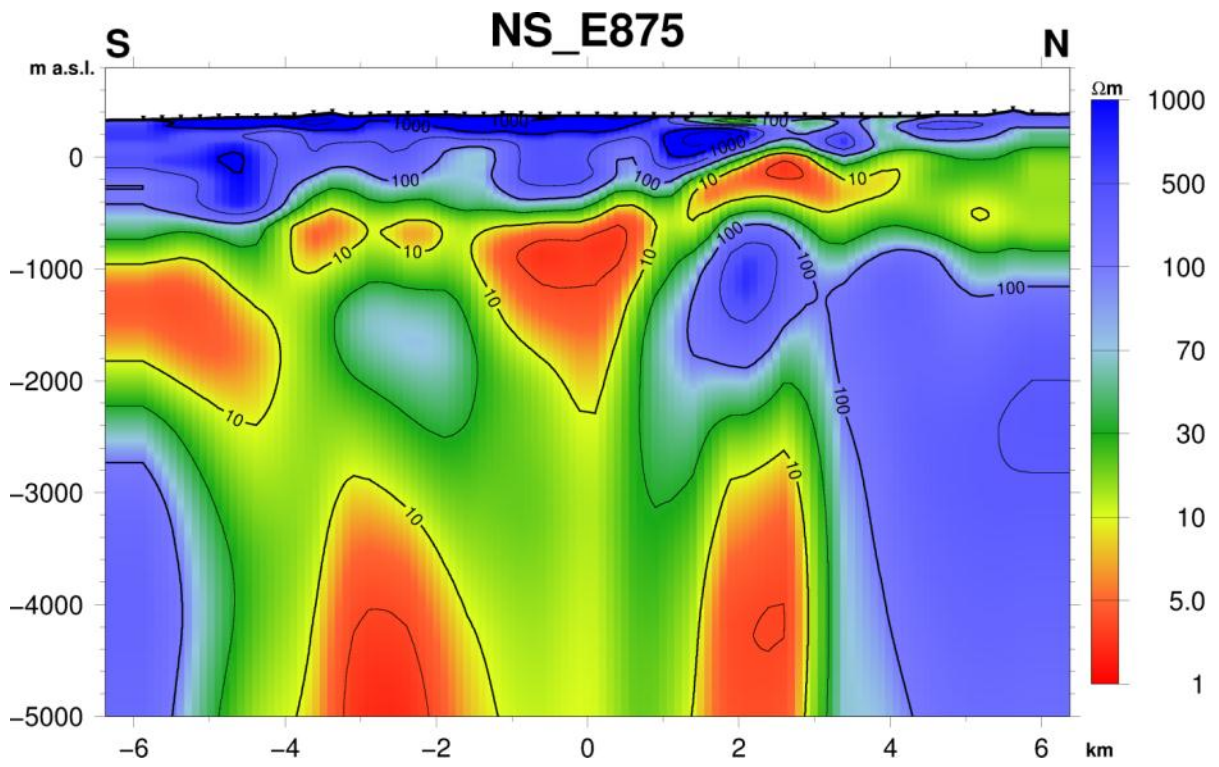


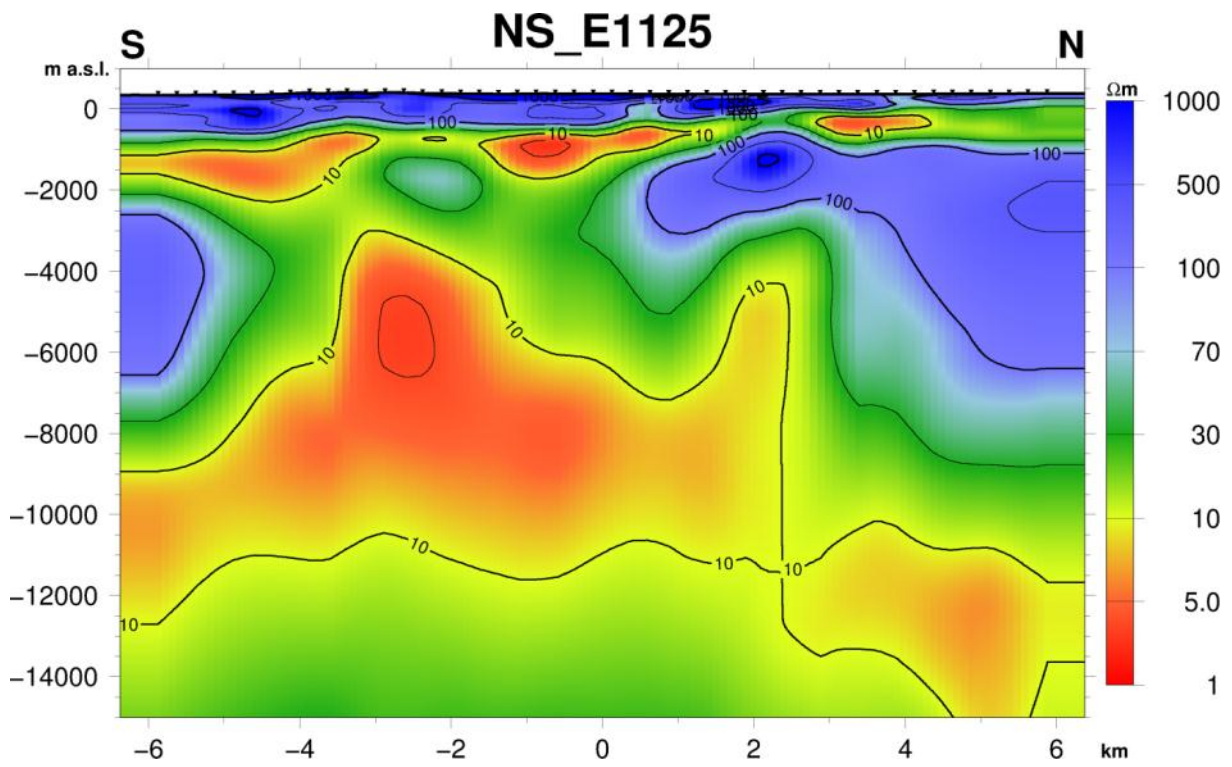
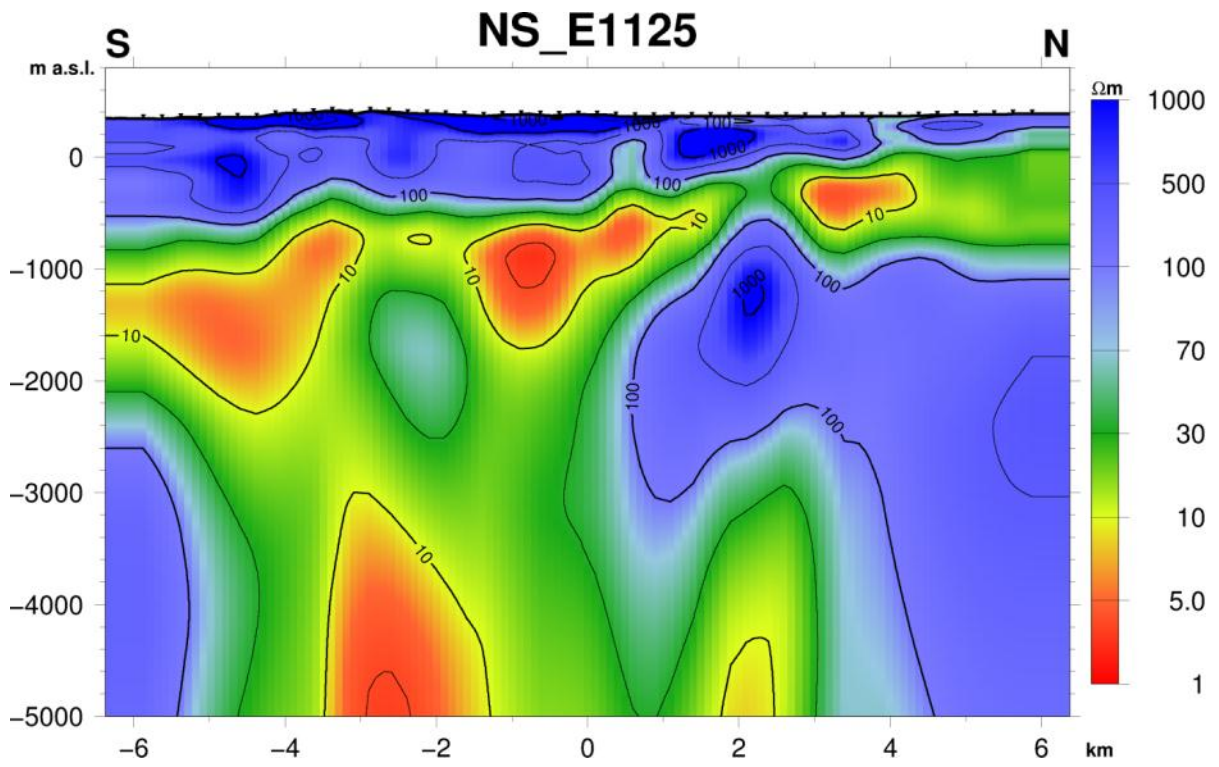


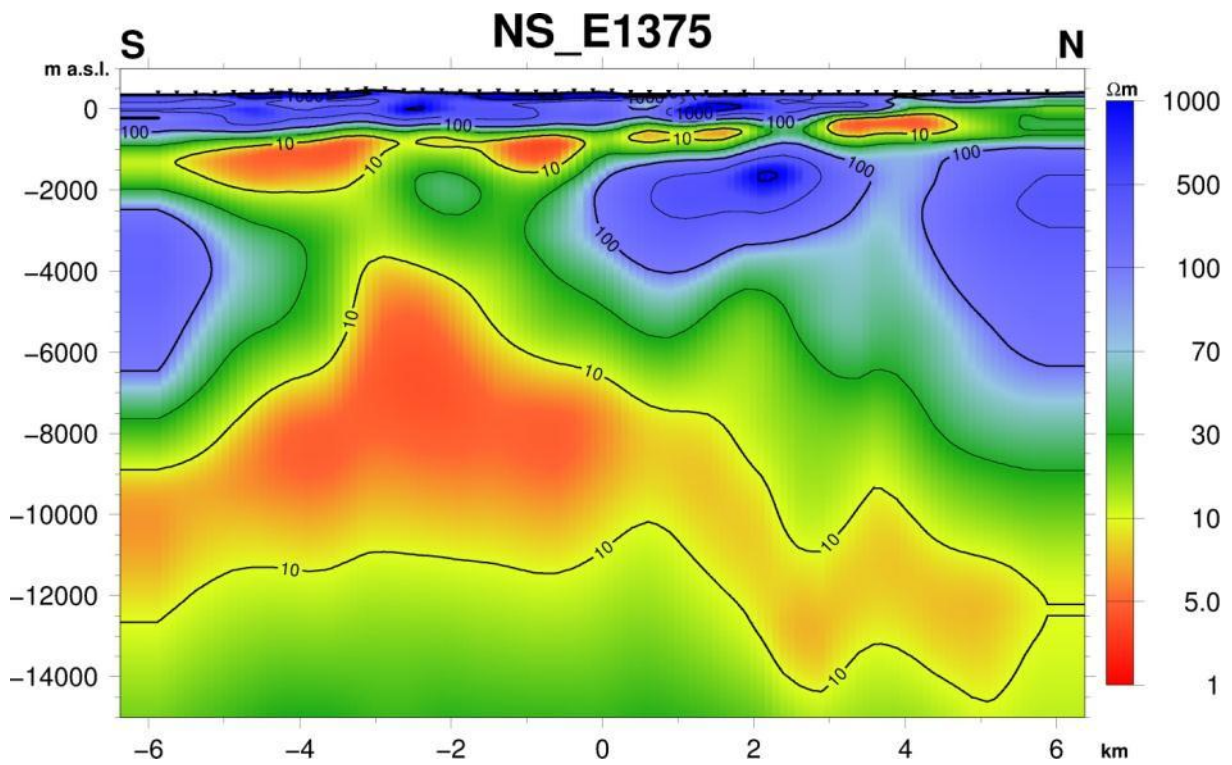
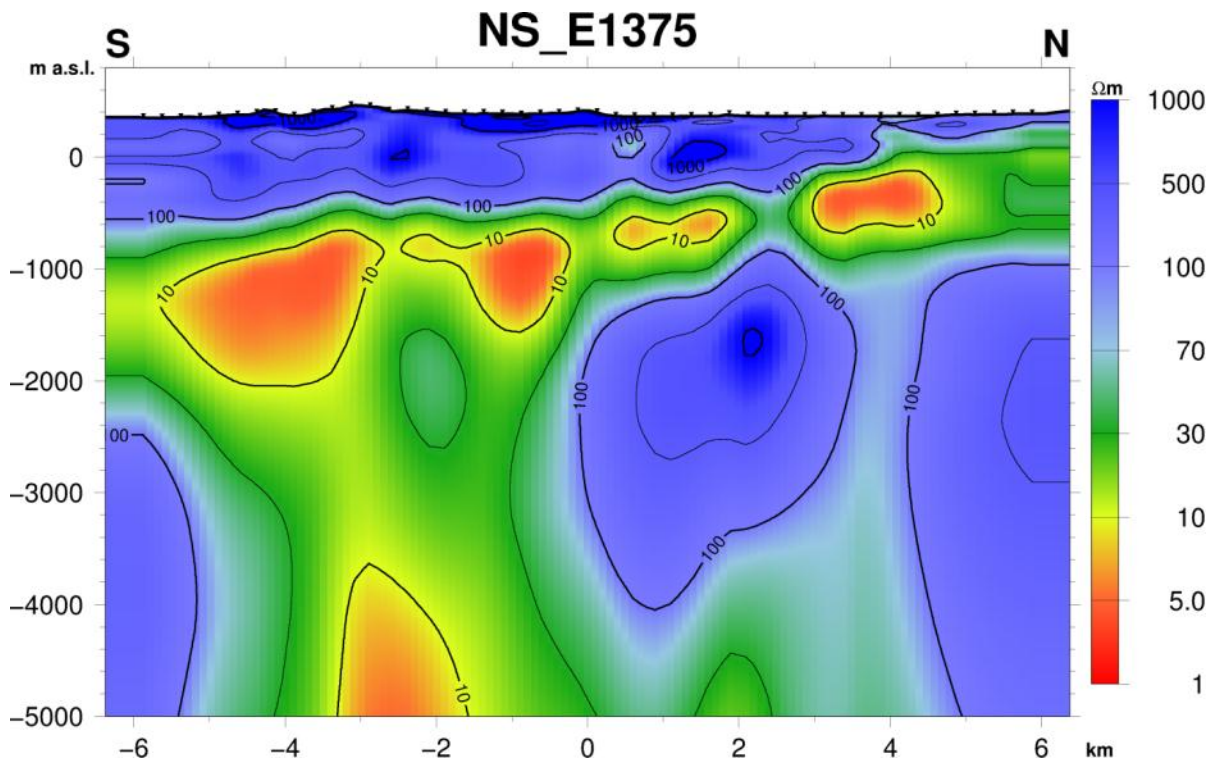


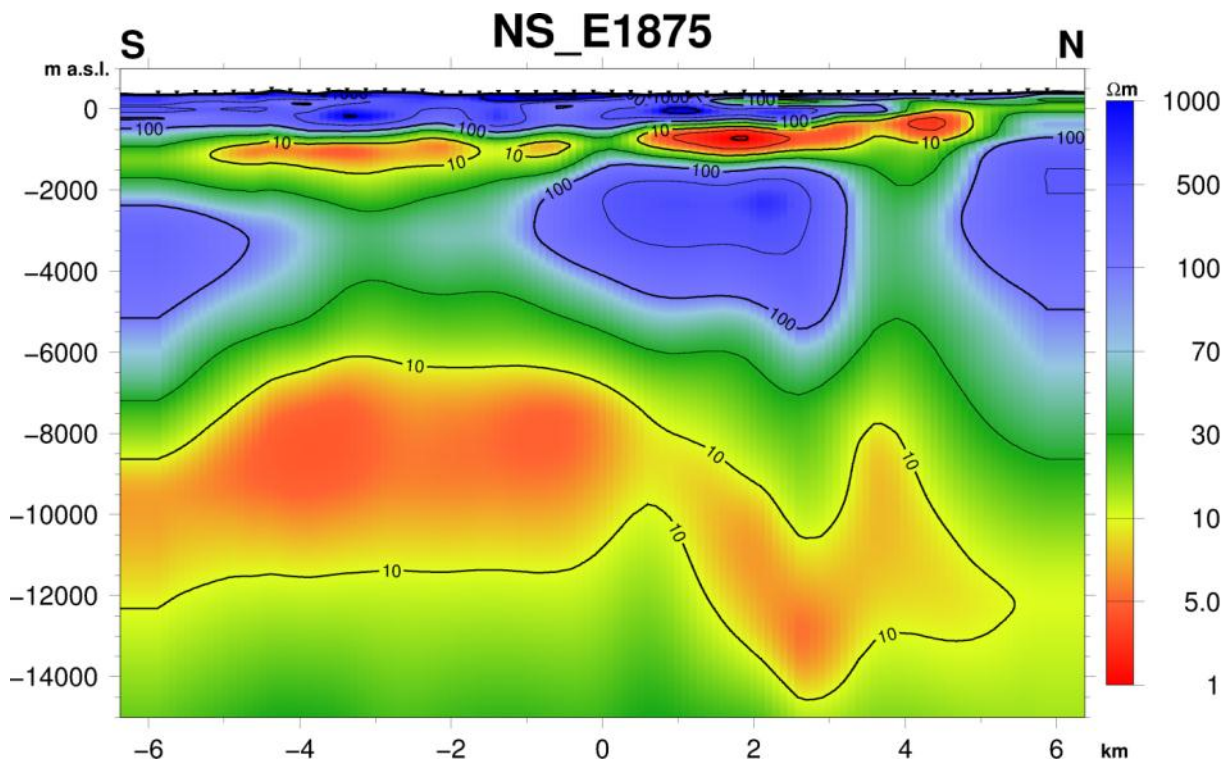
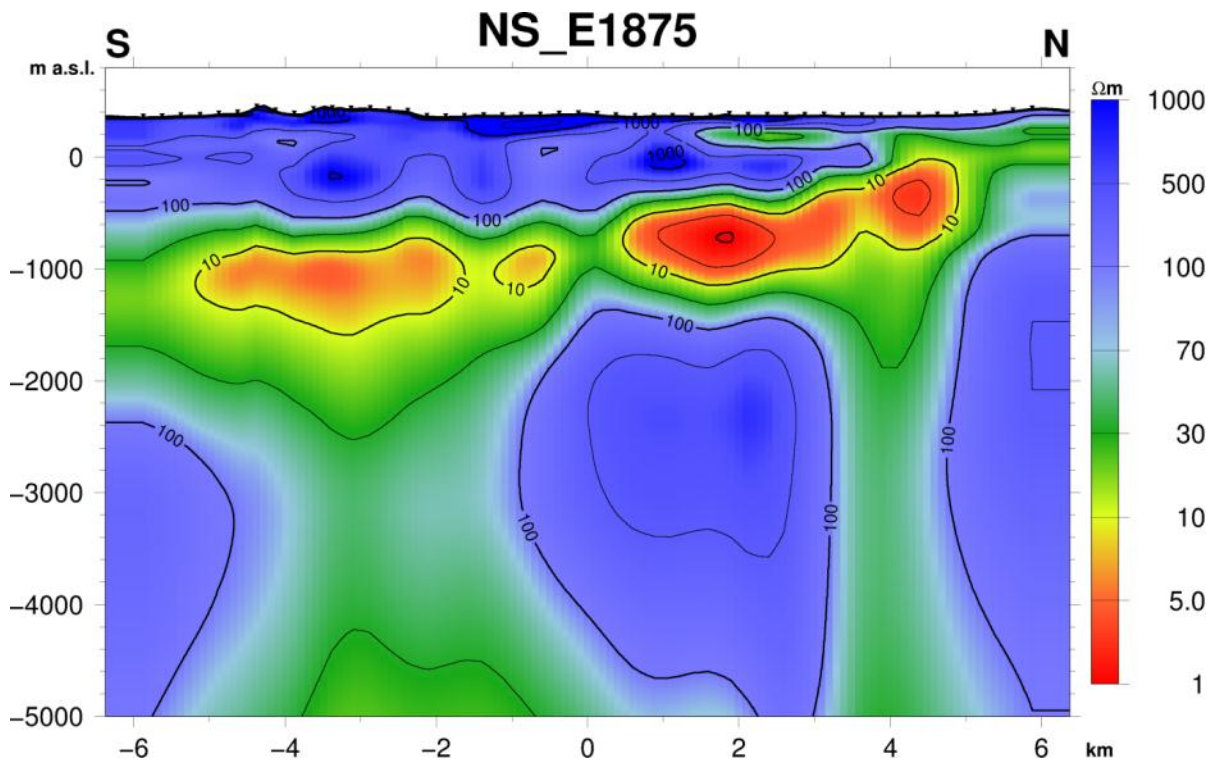


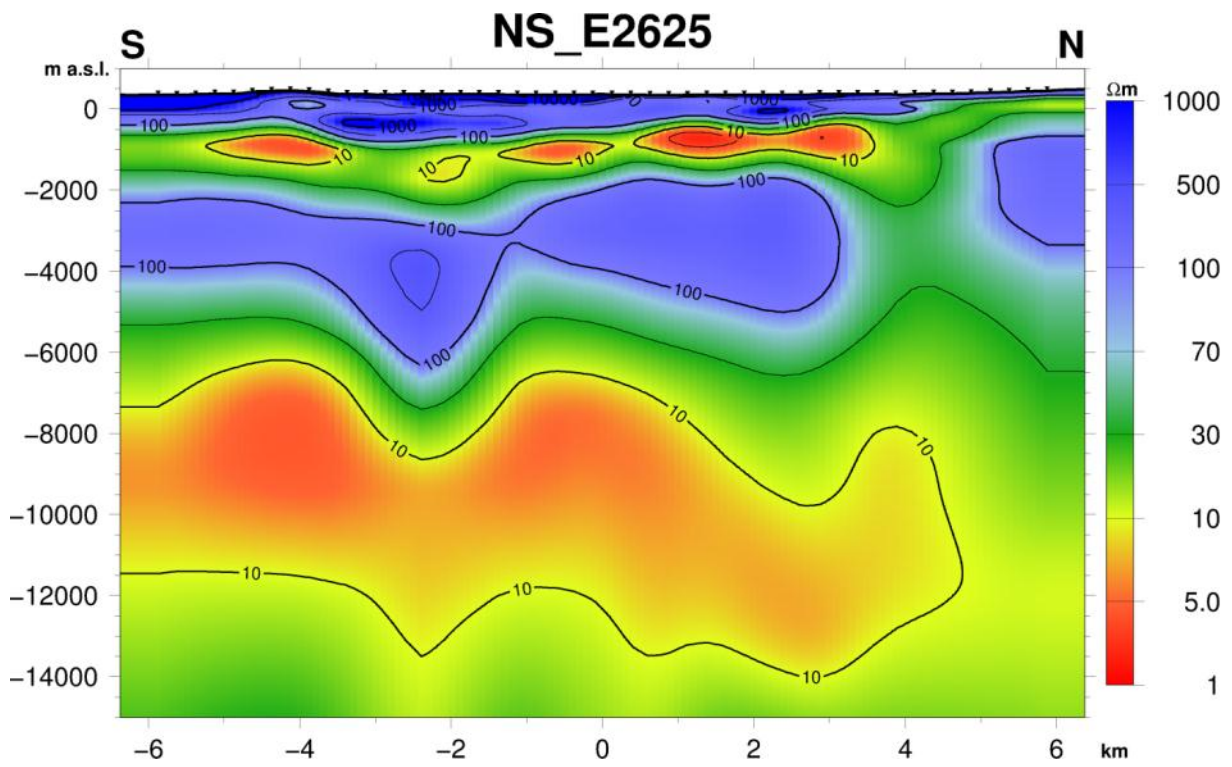
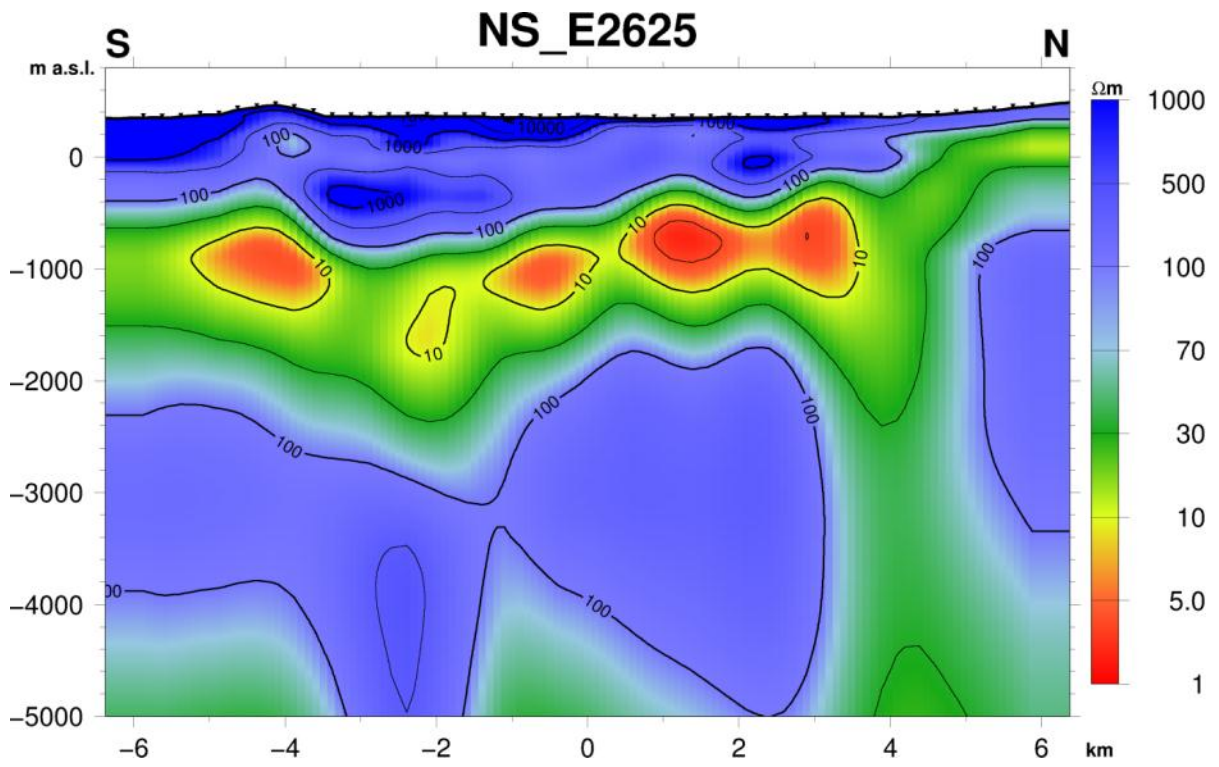






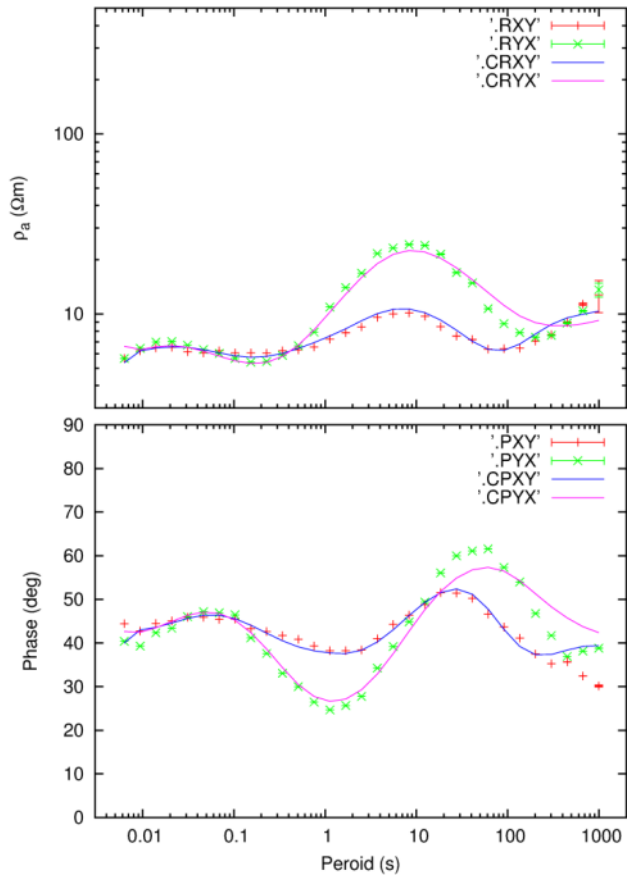
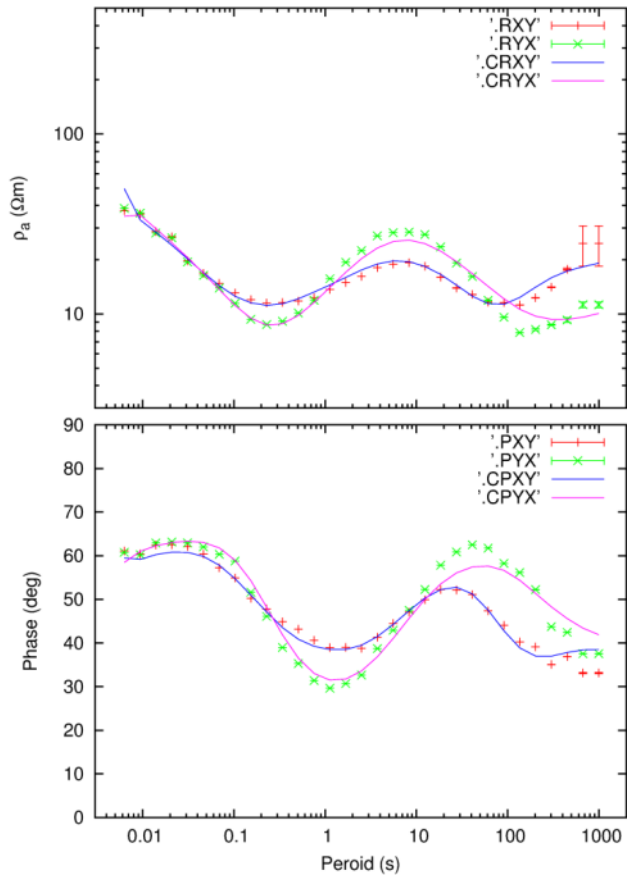
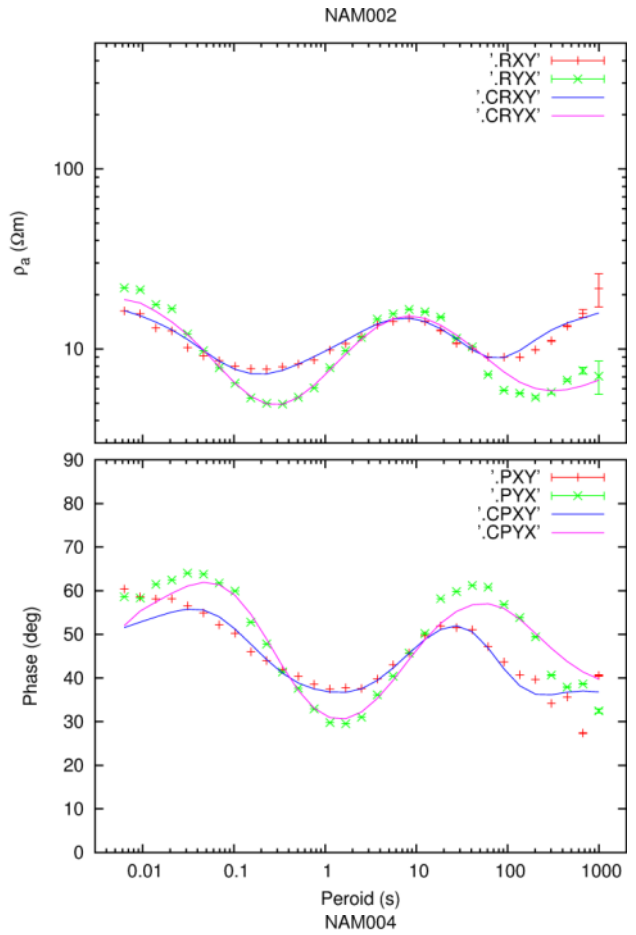
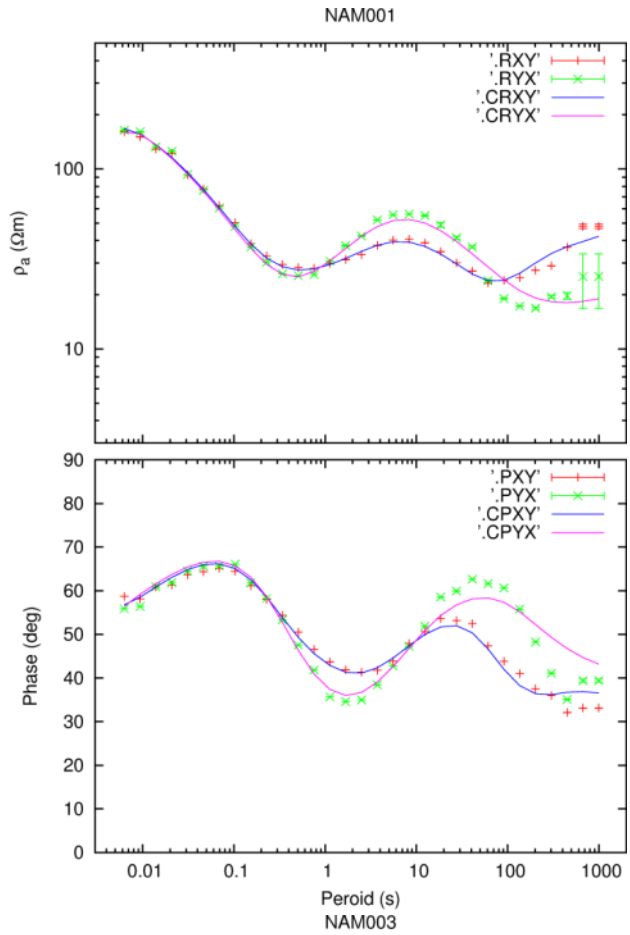


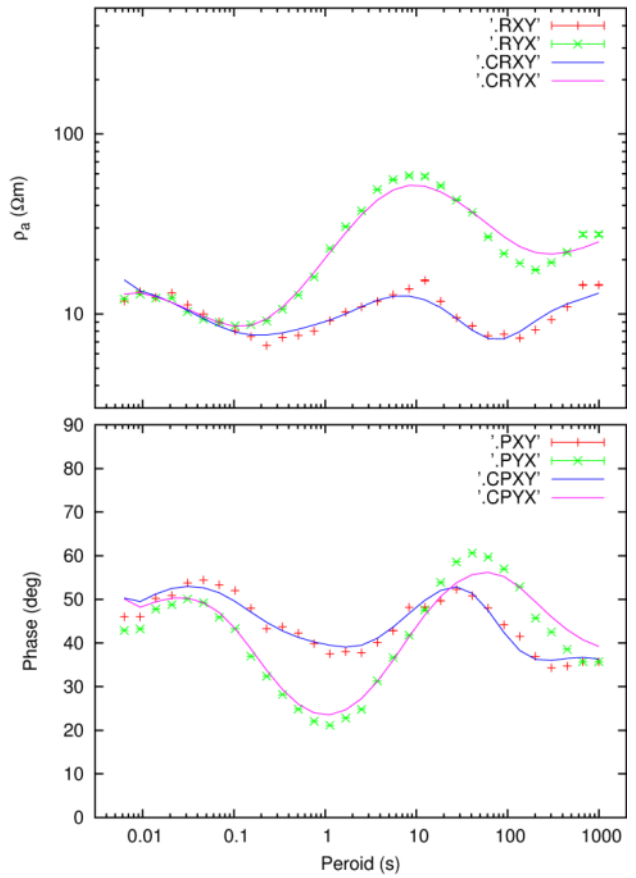
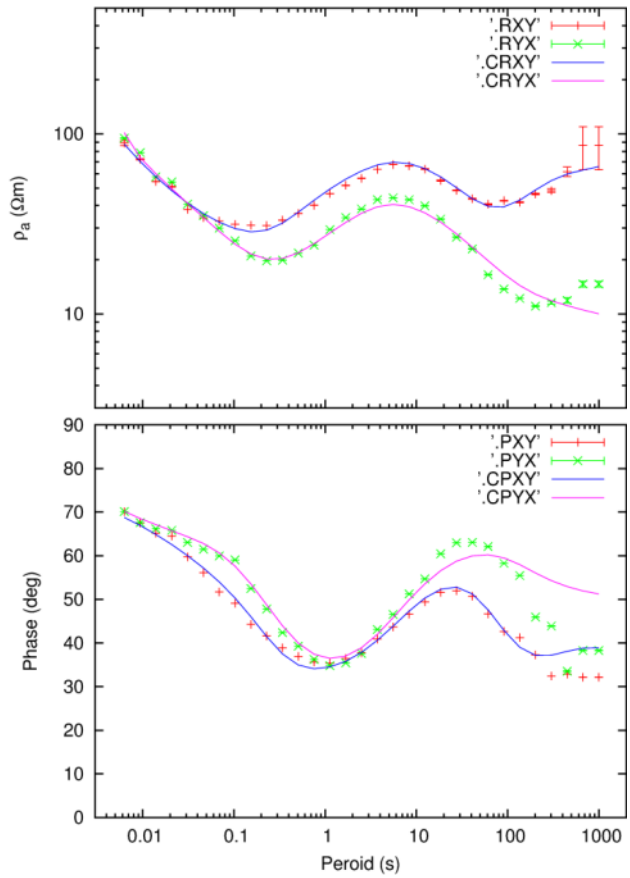
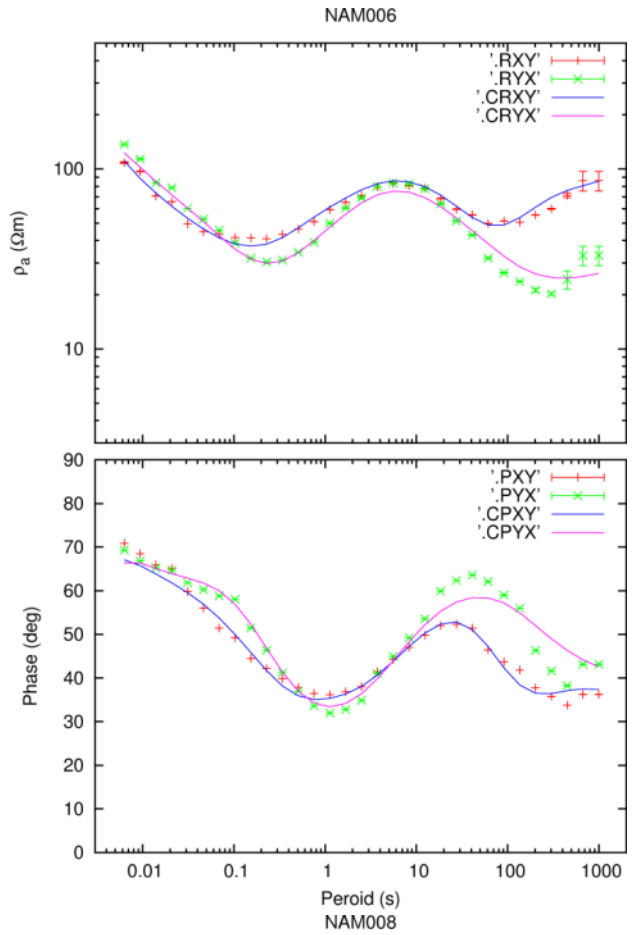
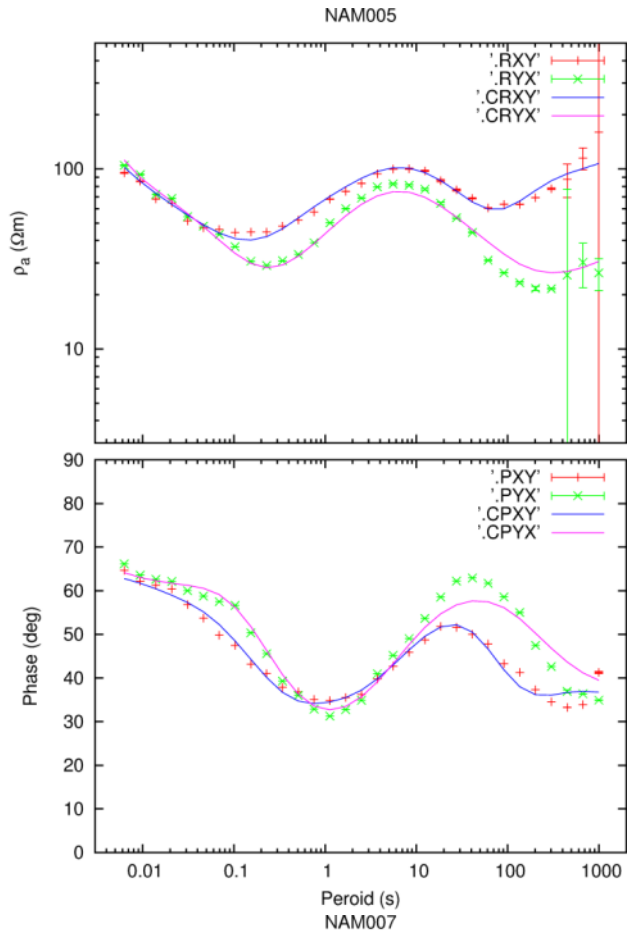


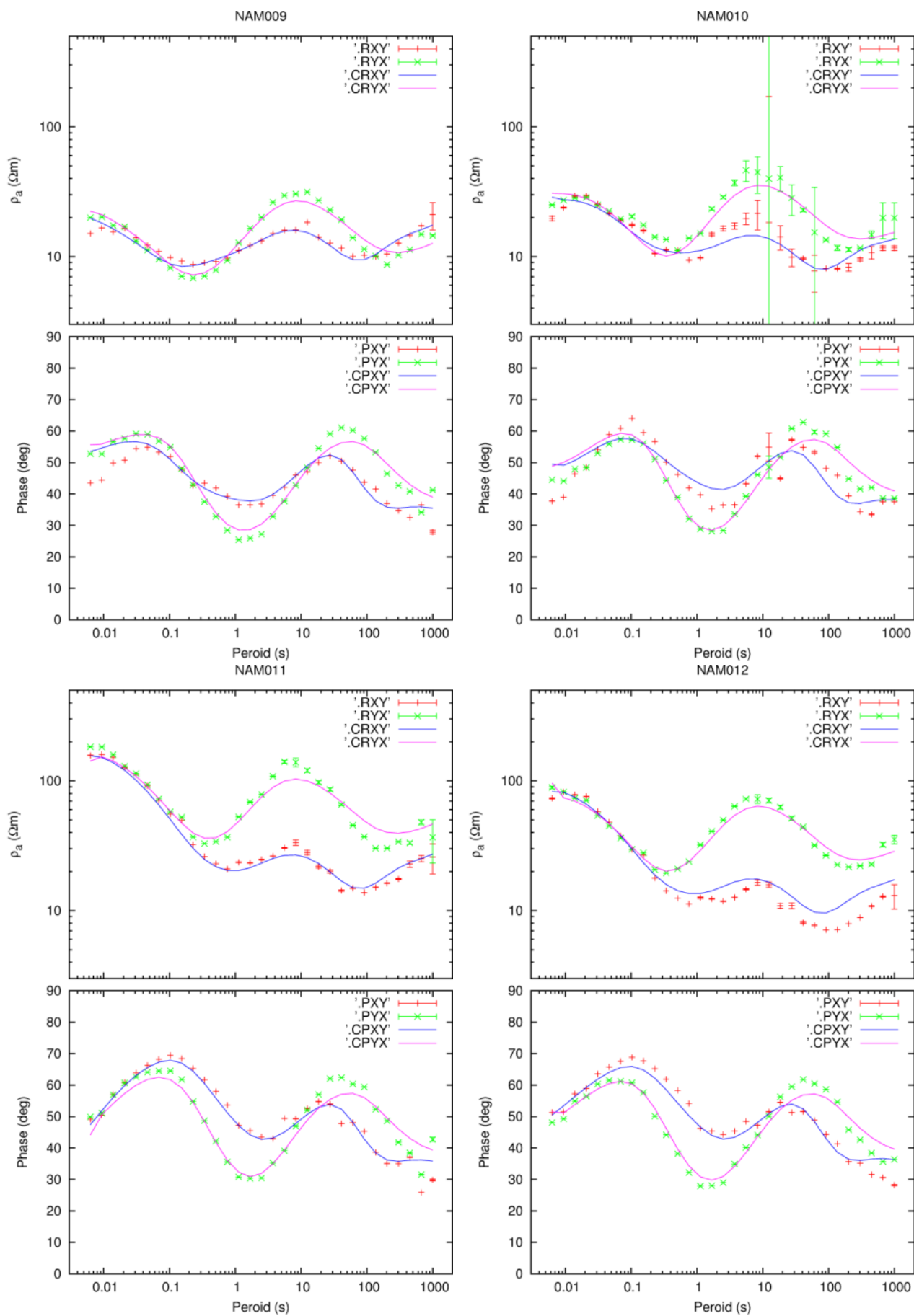


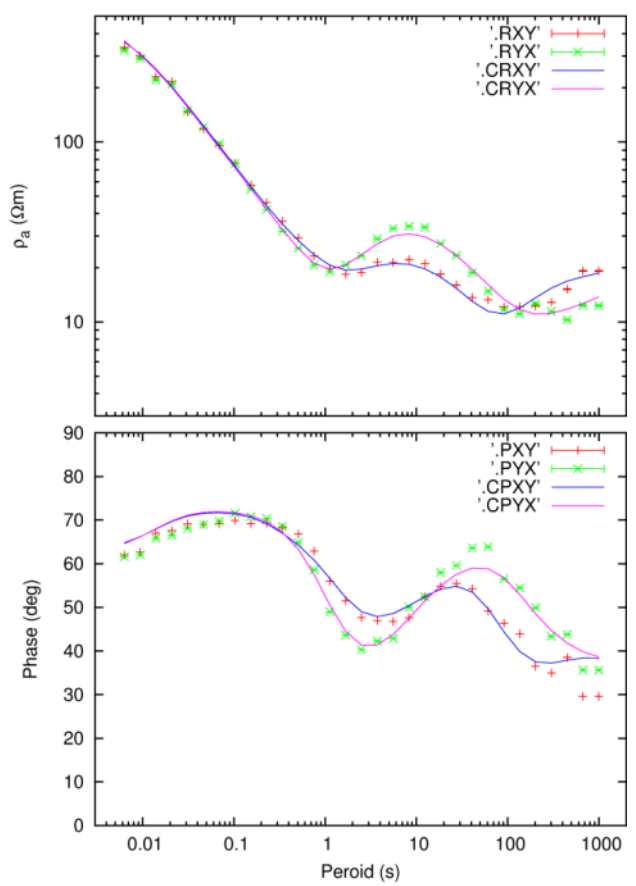
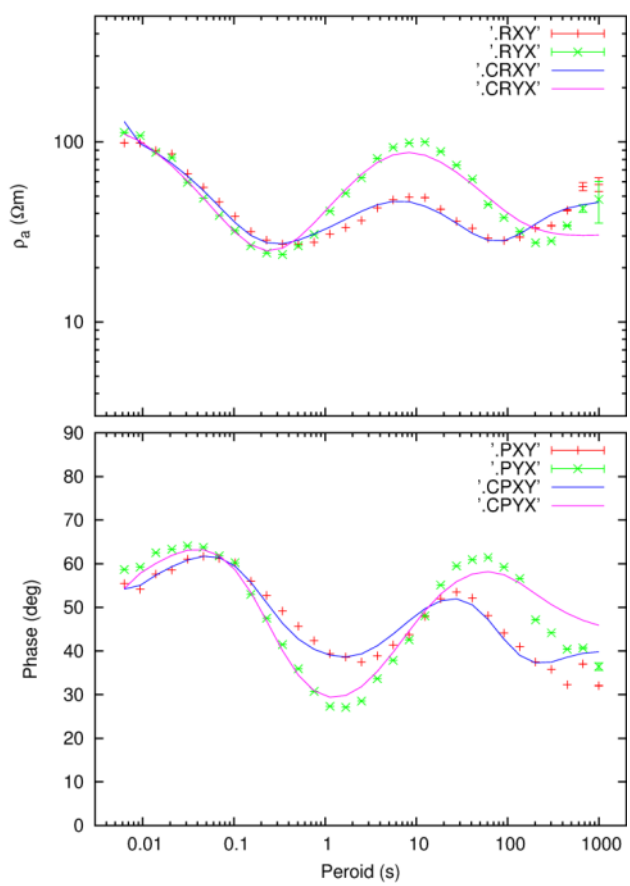
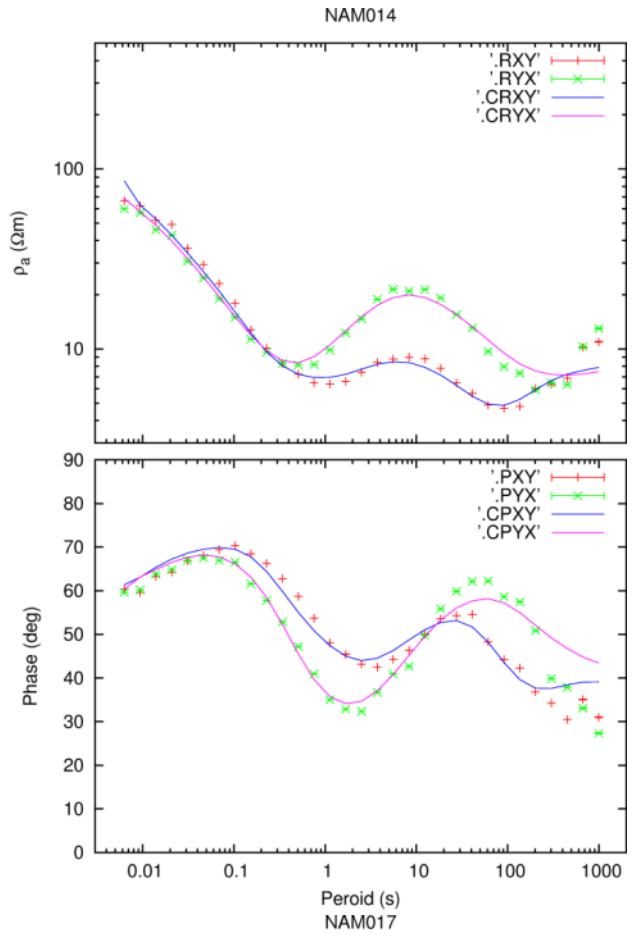
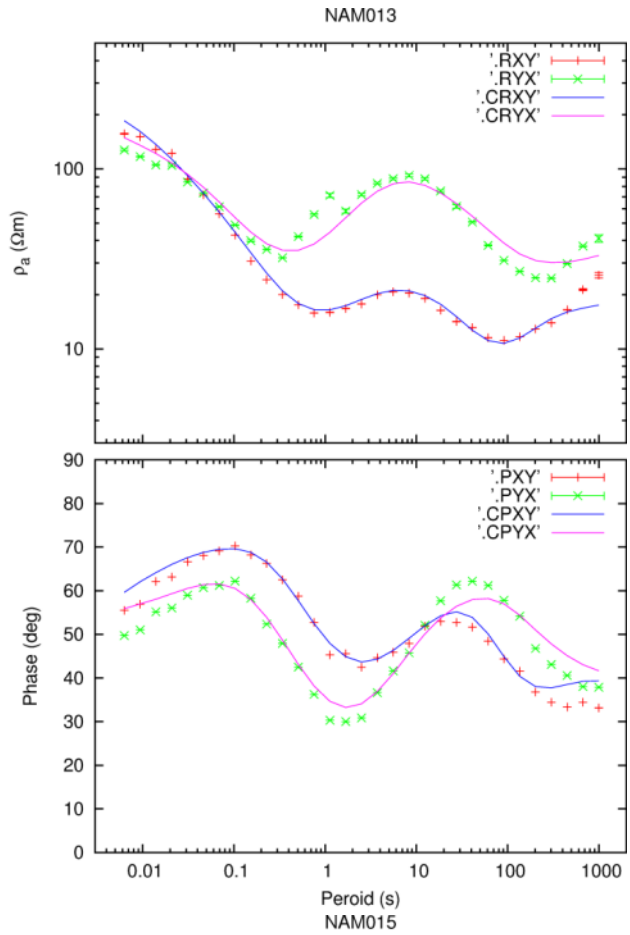
Appendix 4:

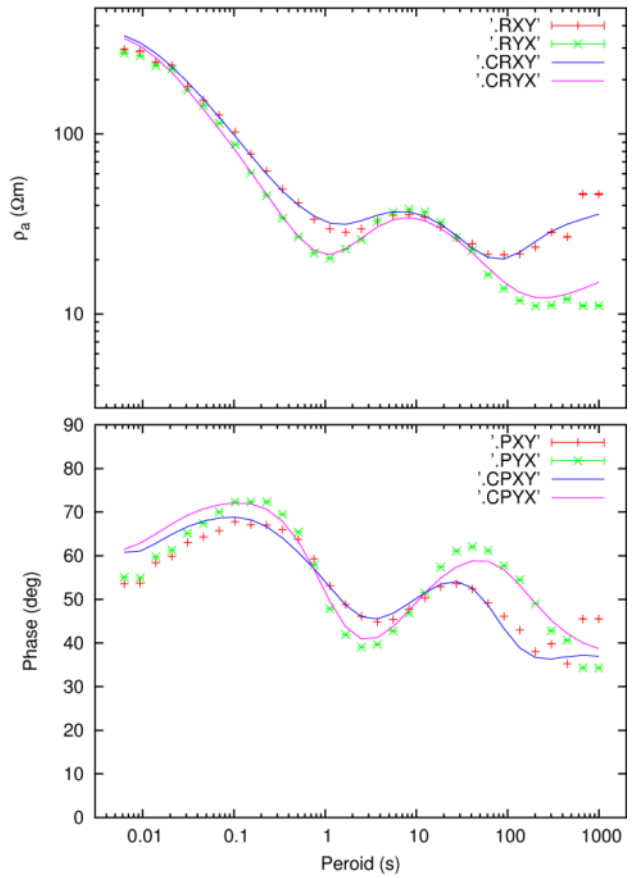
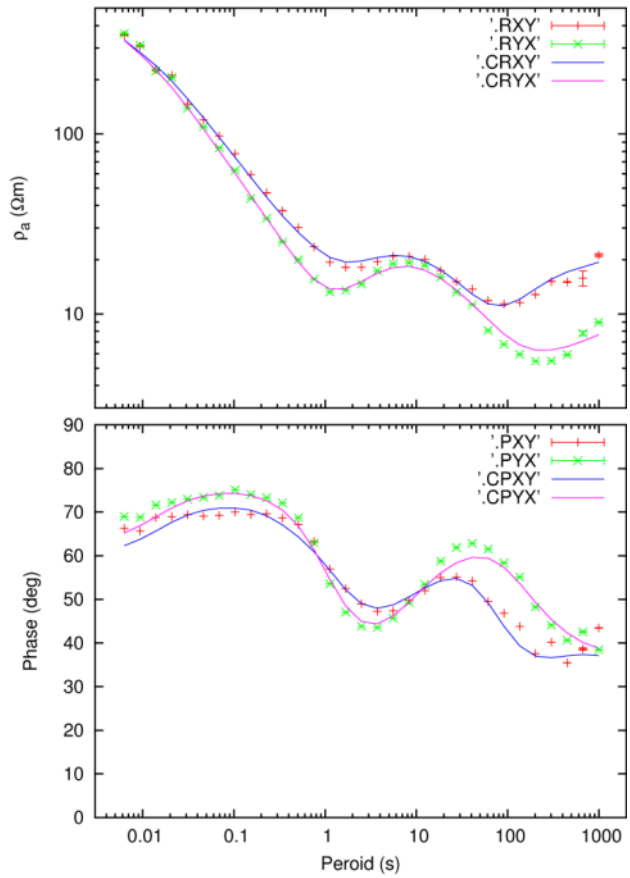
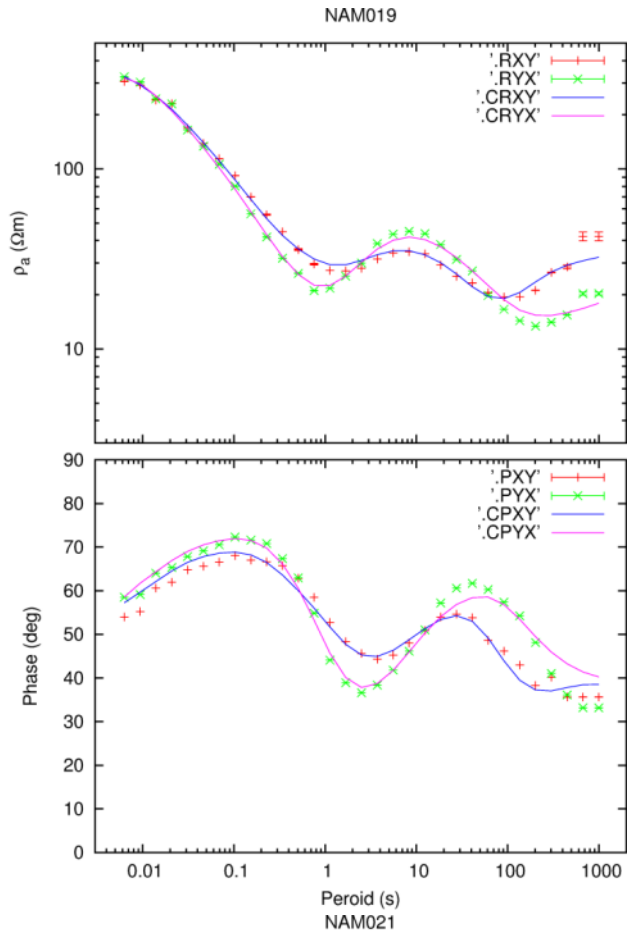
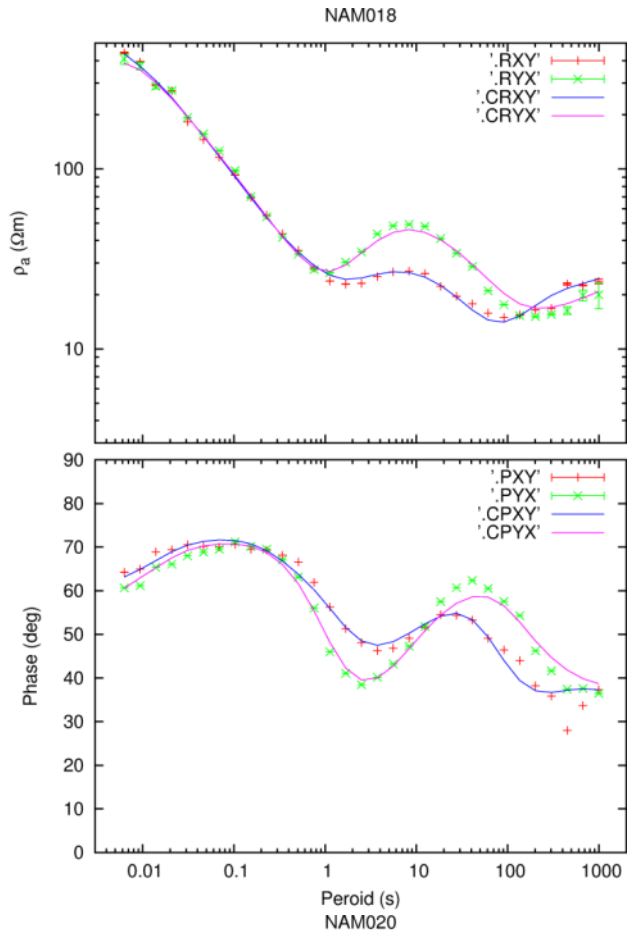
Datafit

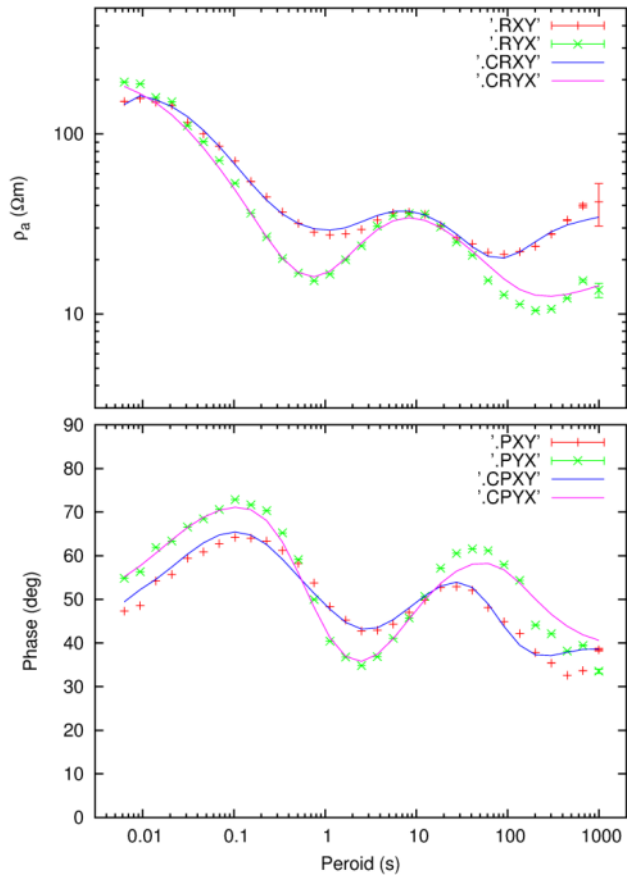
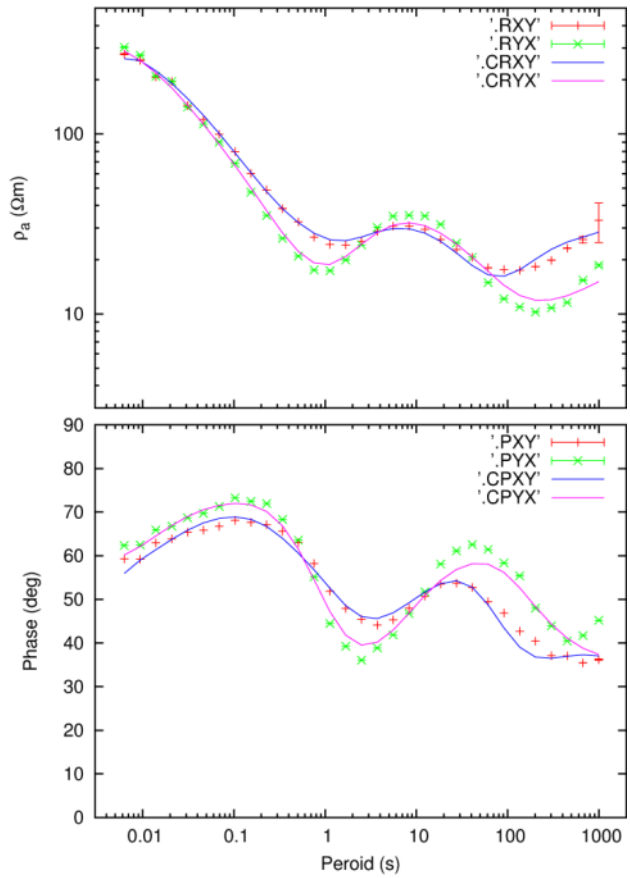
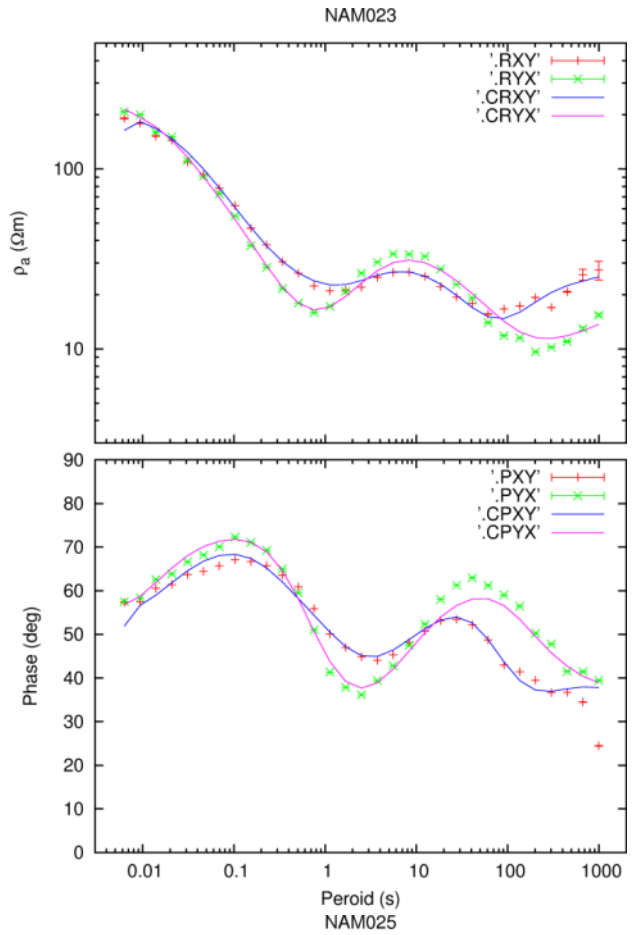
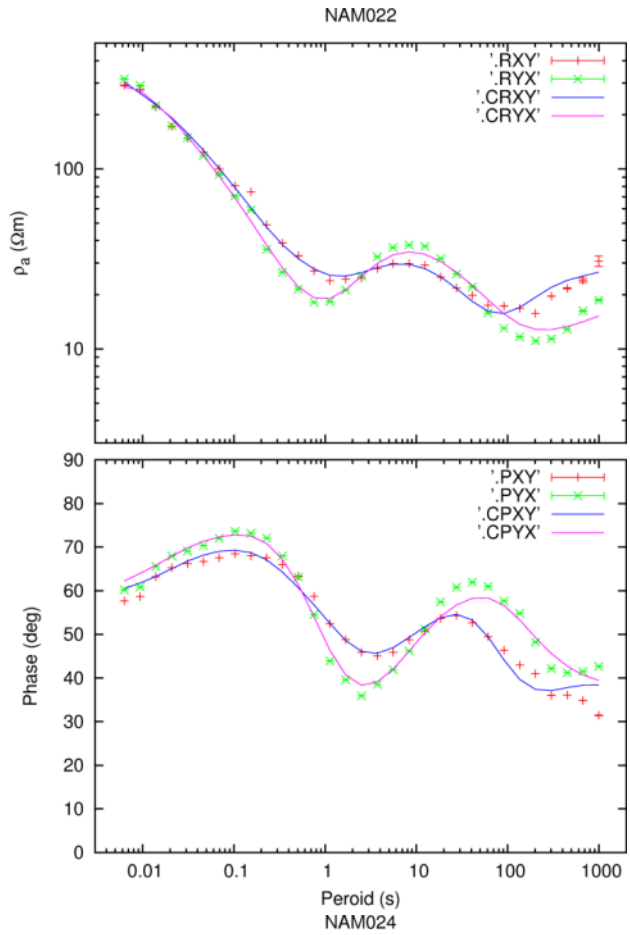


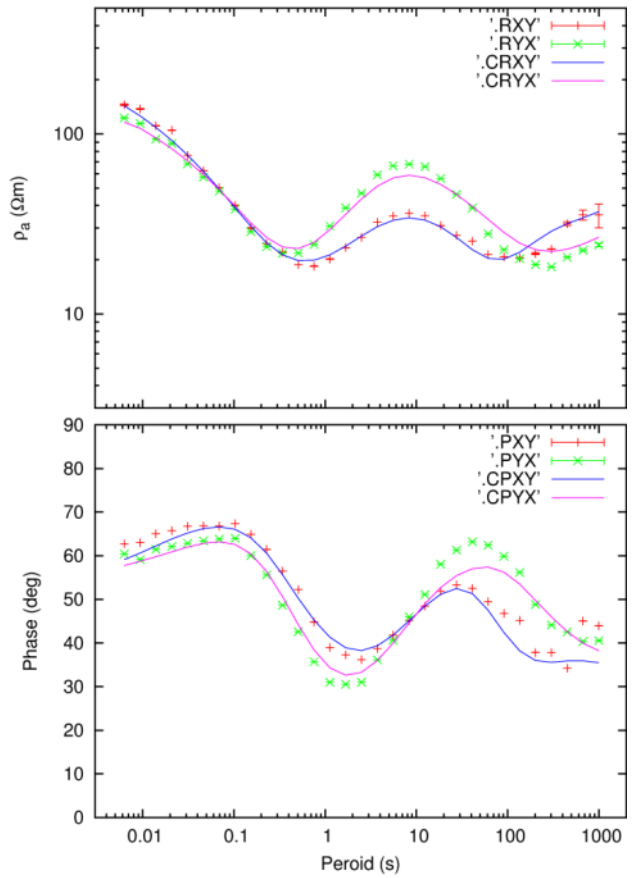
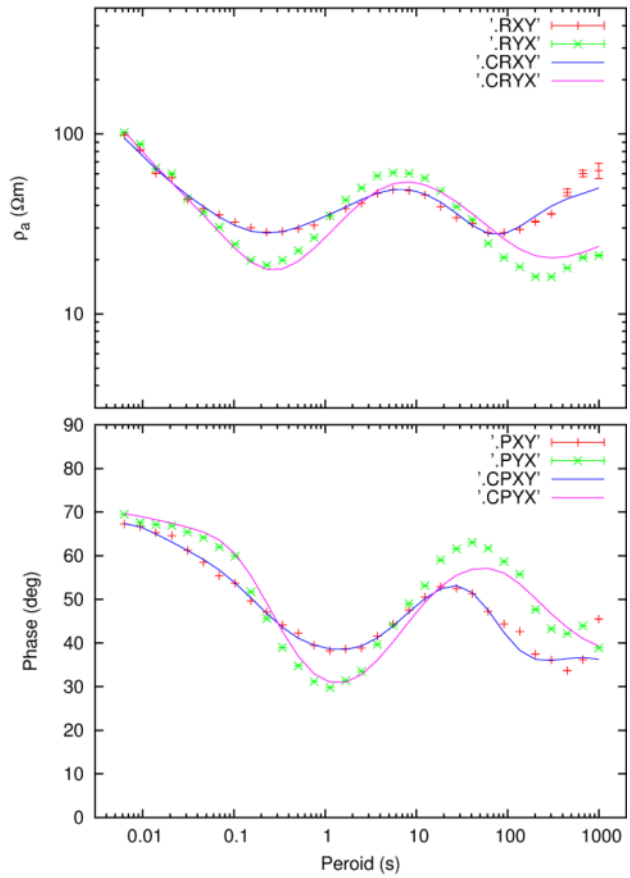
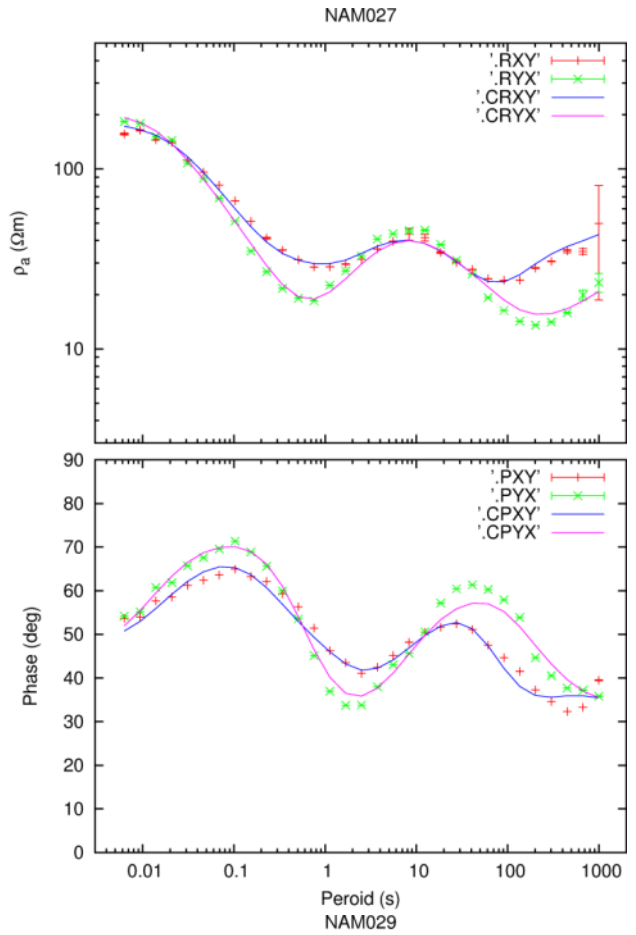
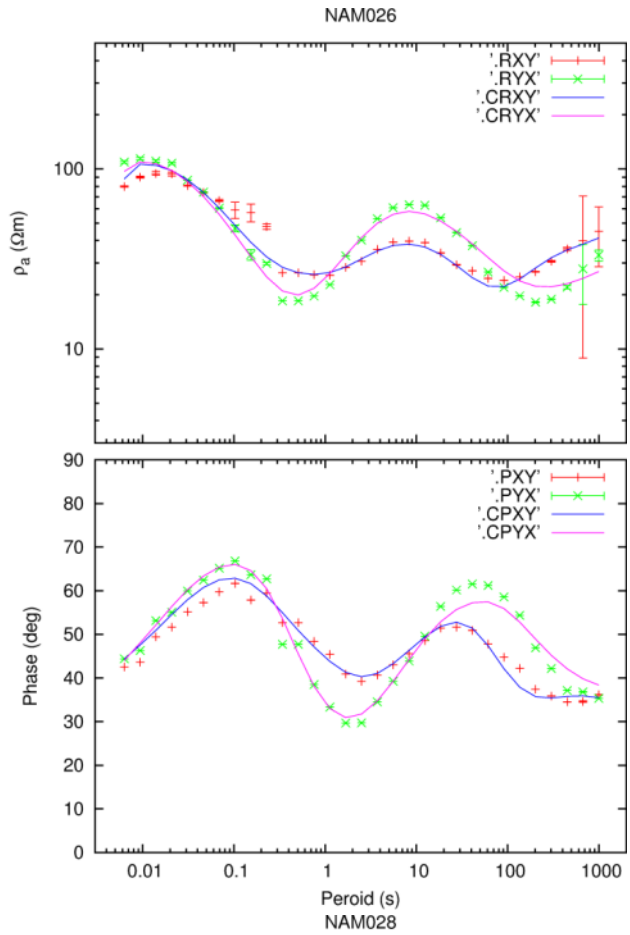


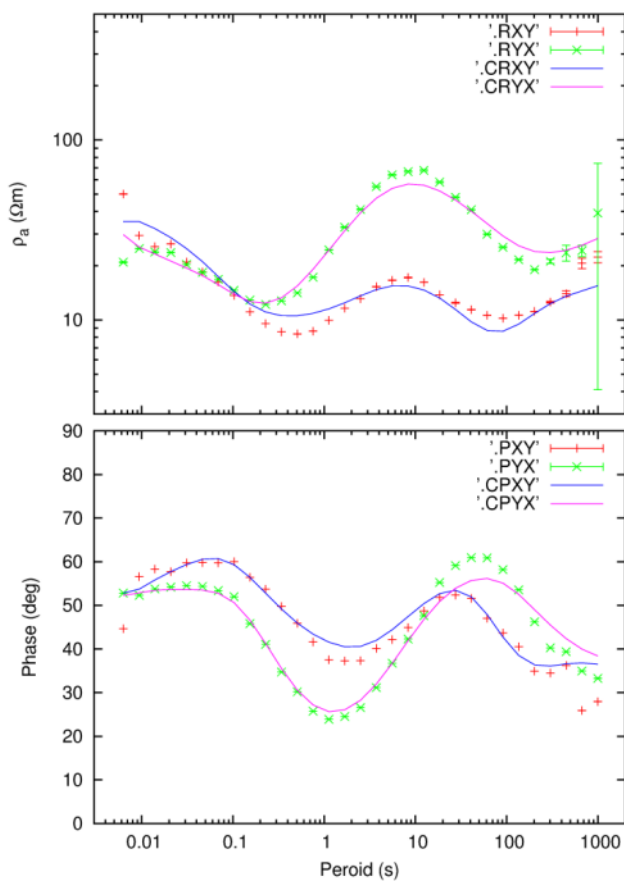
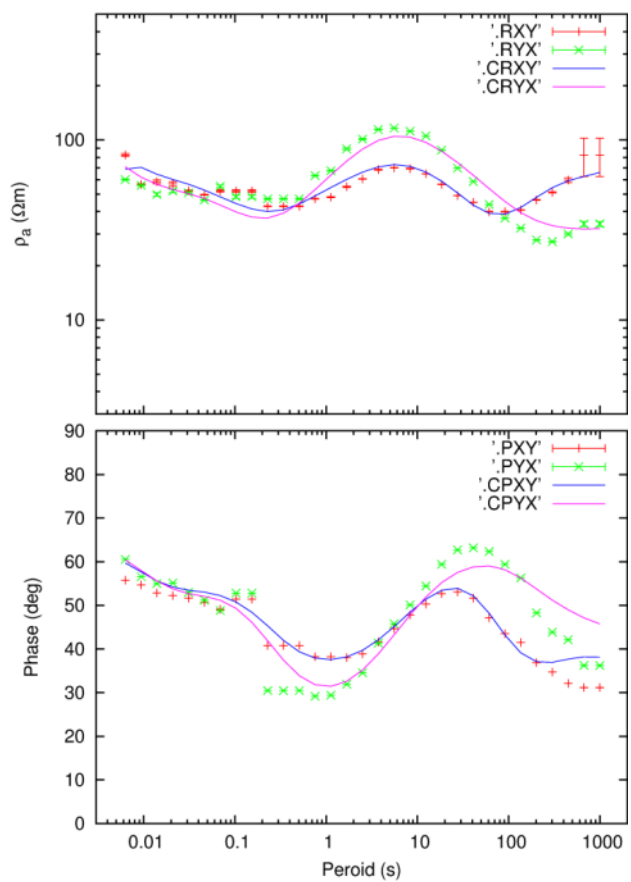
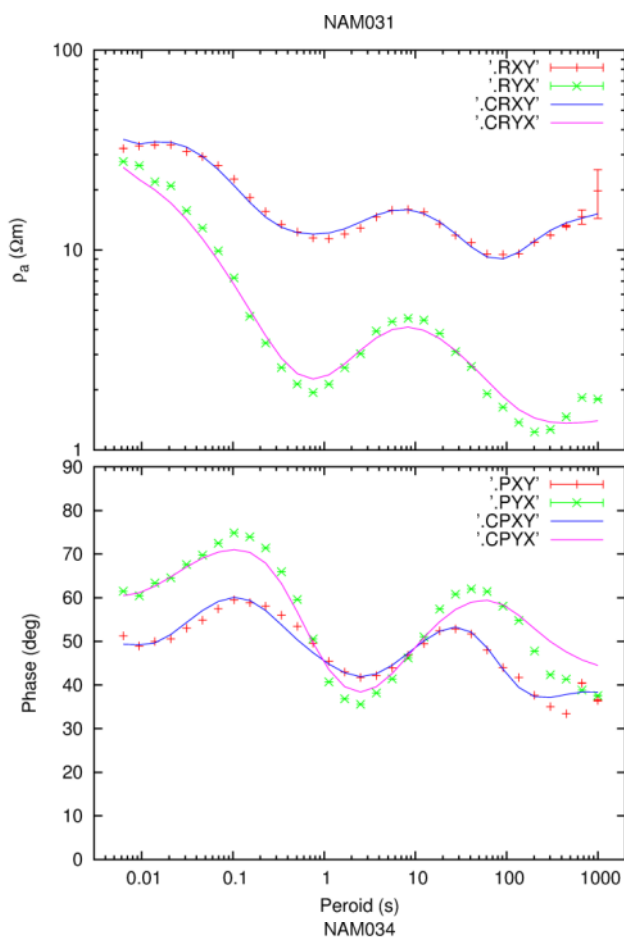
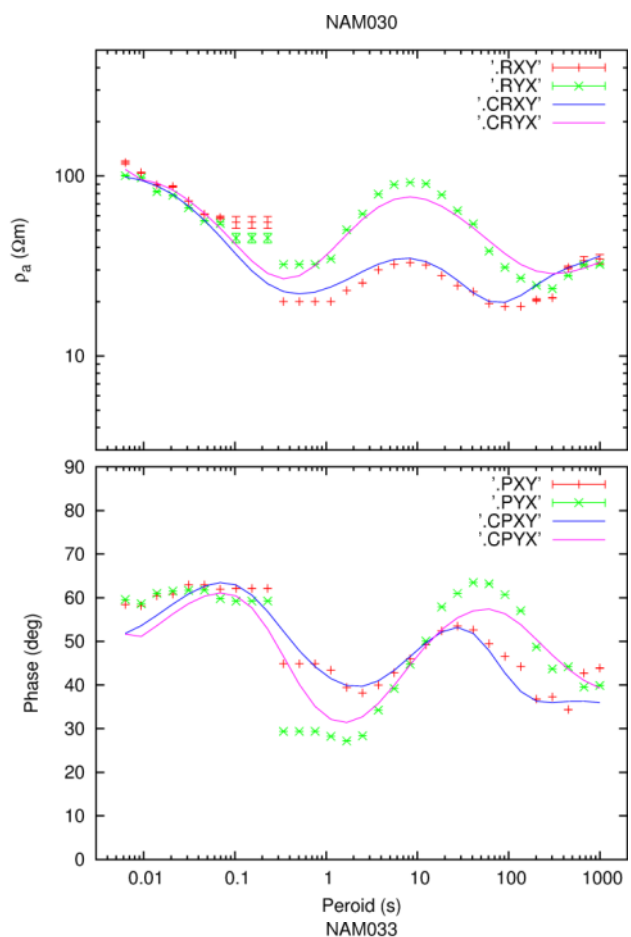


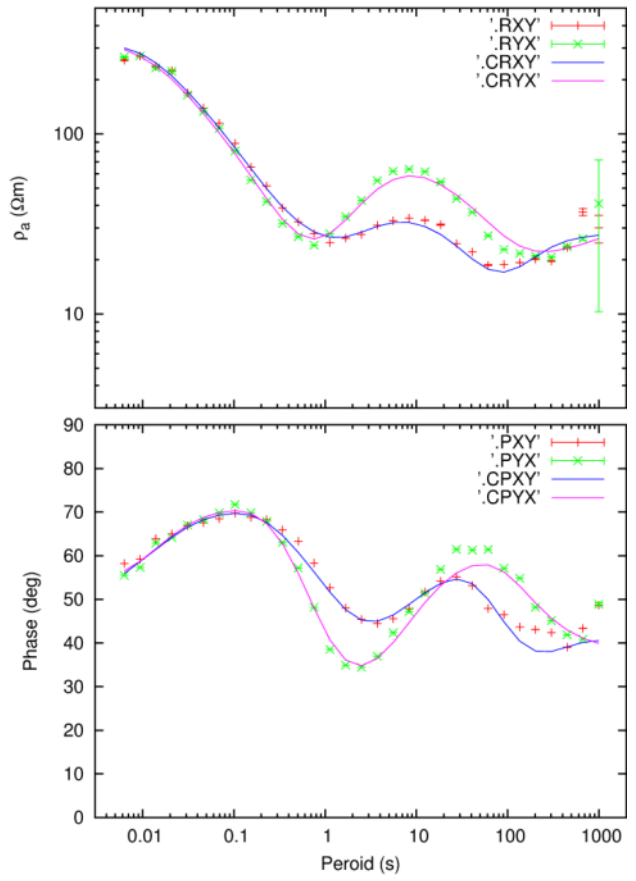
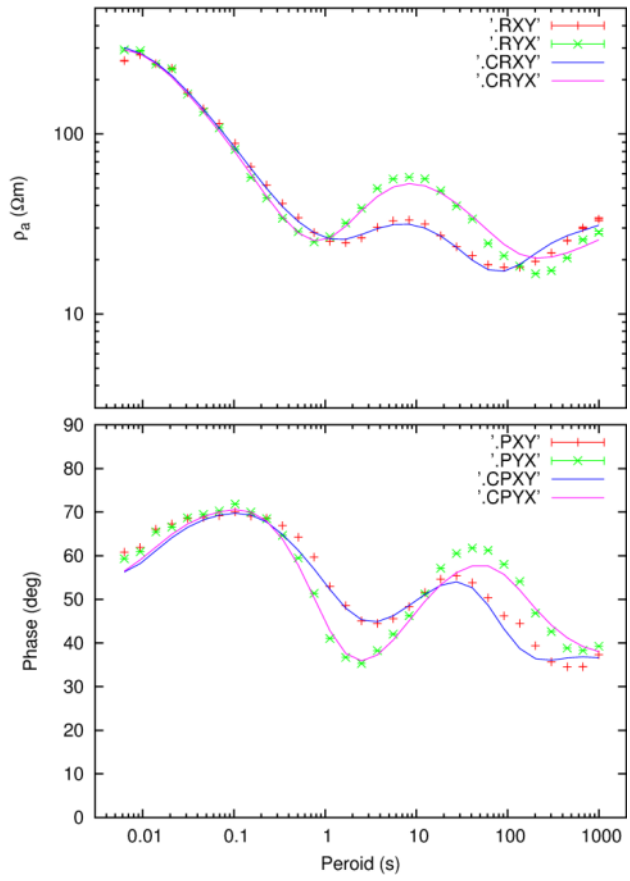
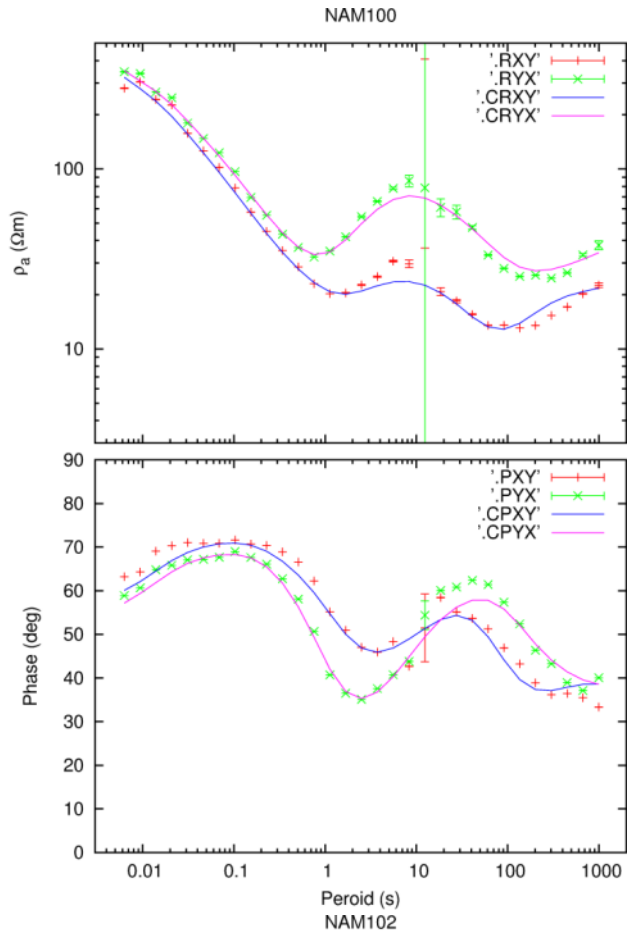
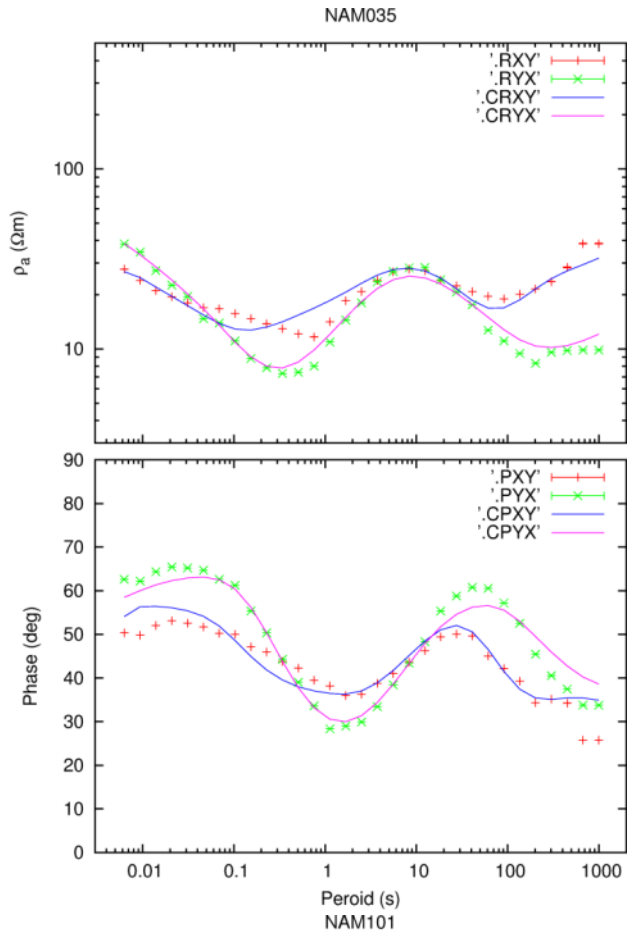


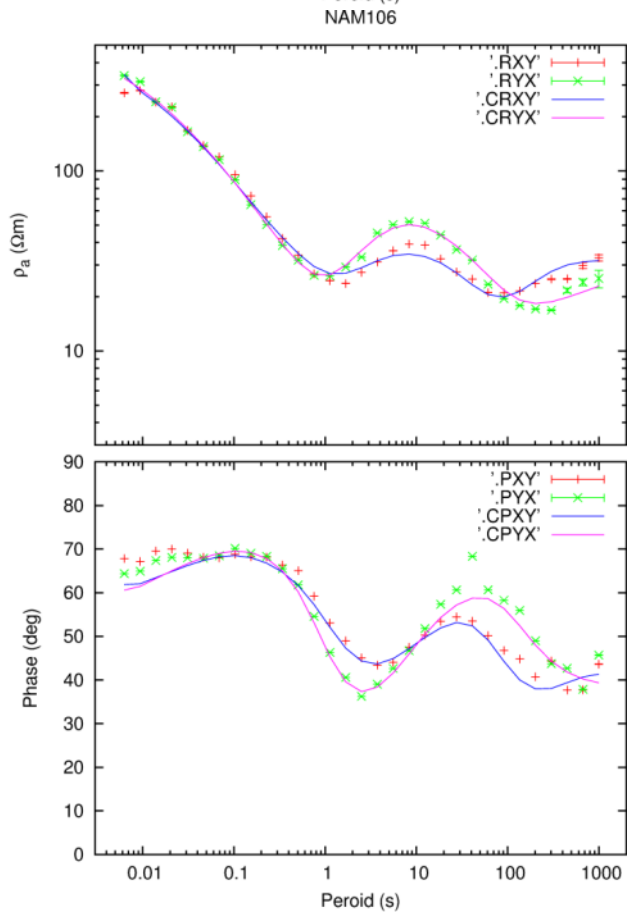
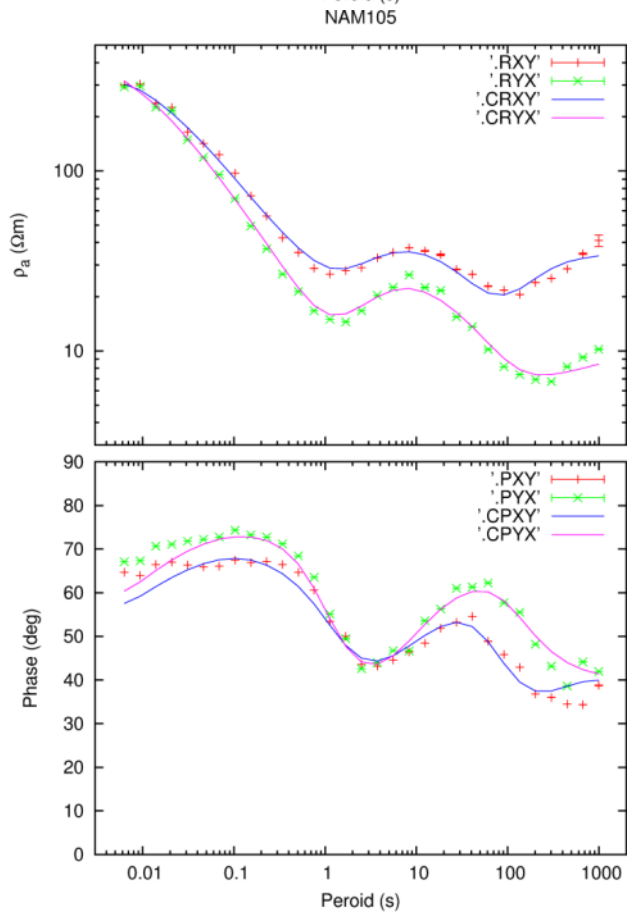
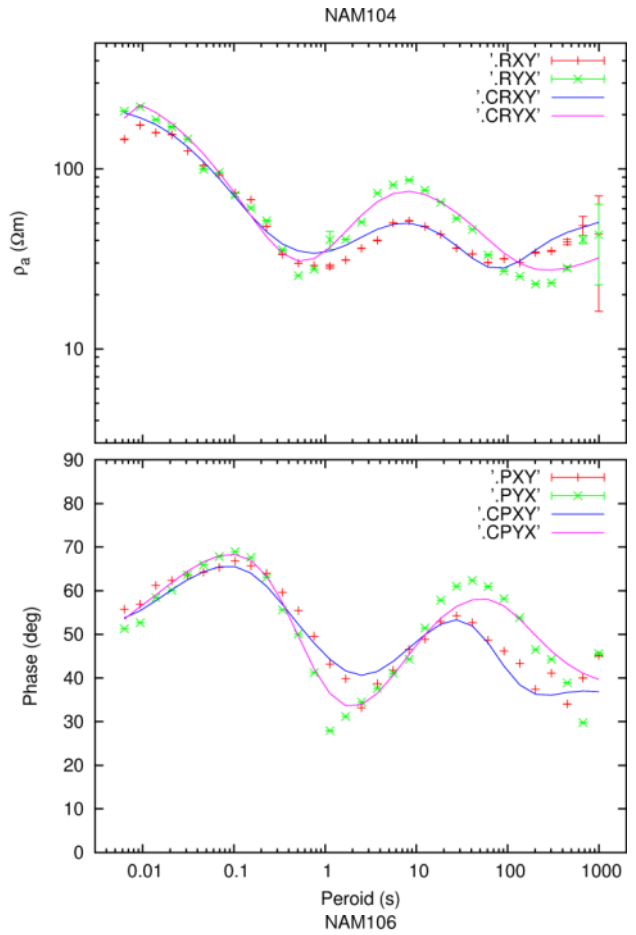
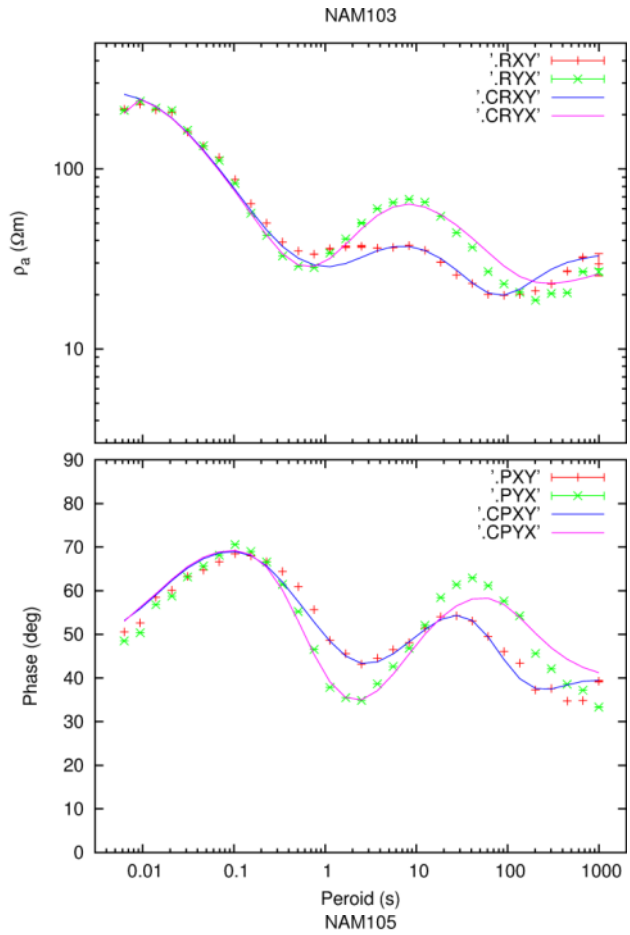


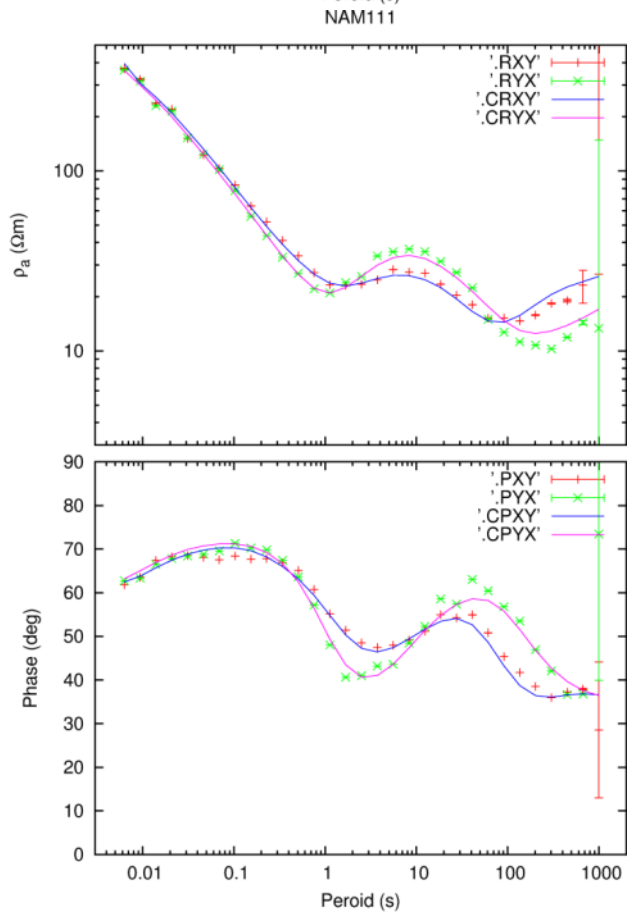
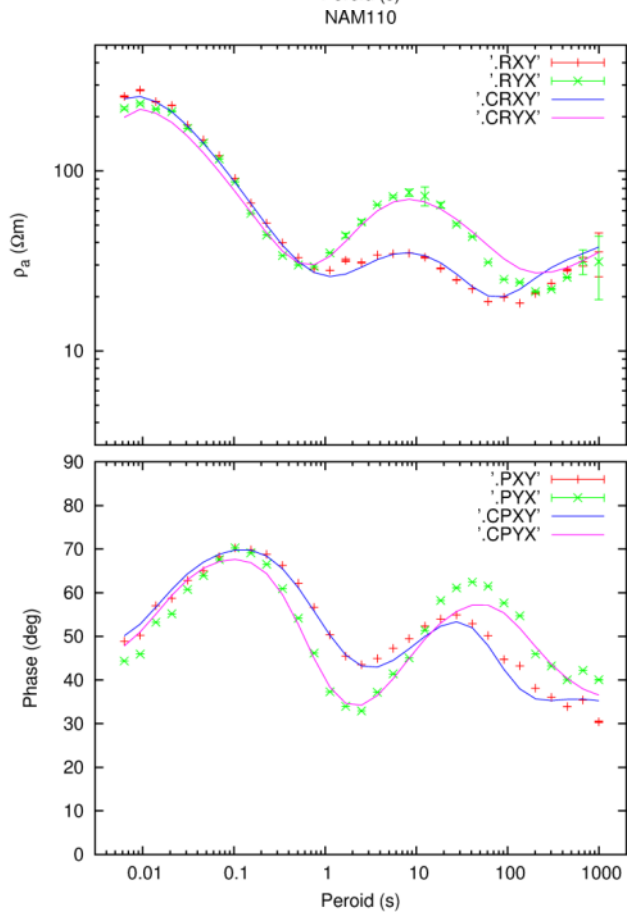
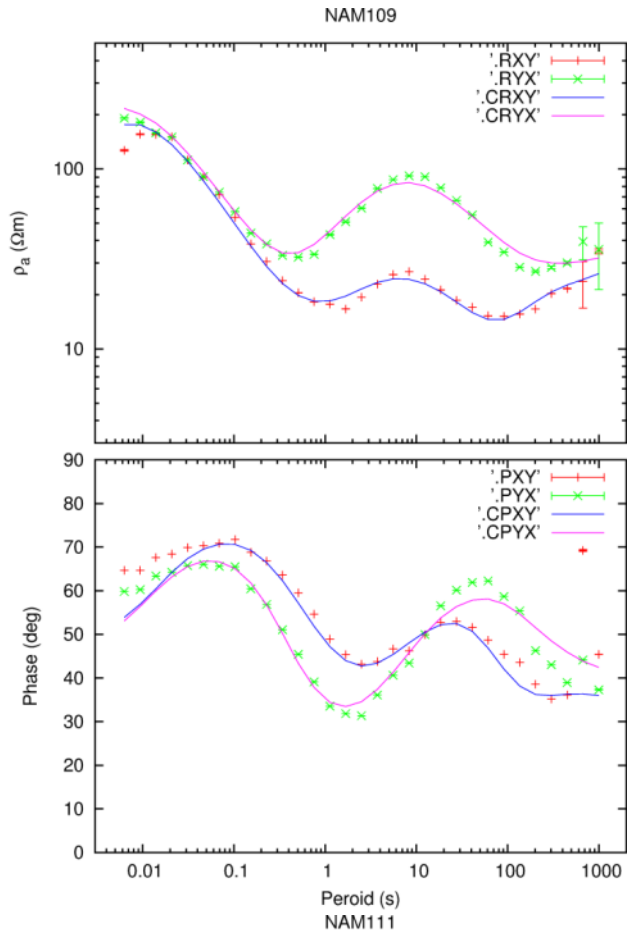
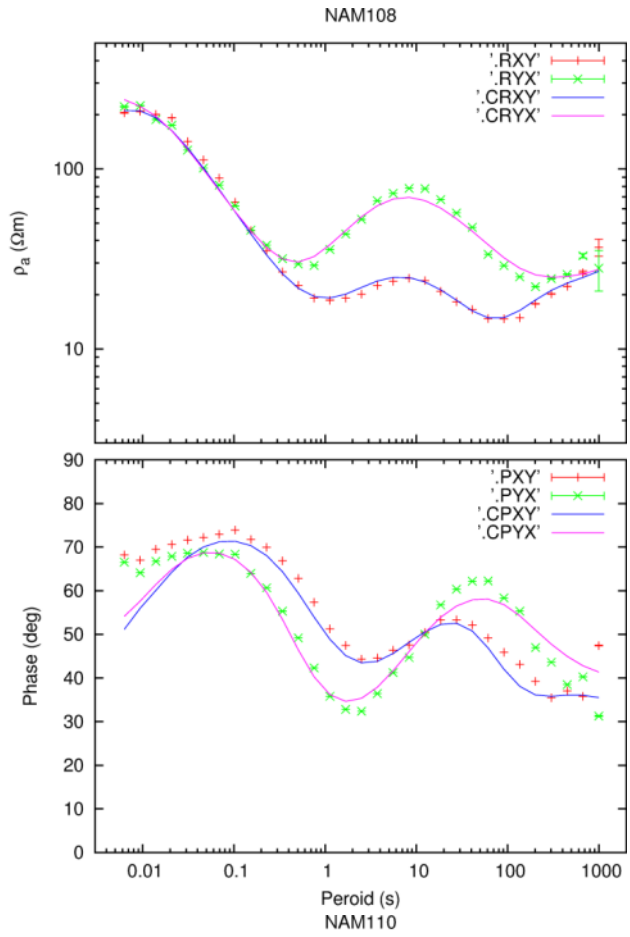


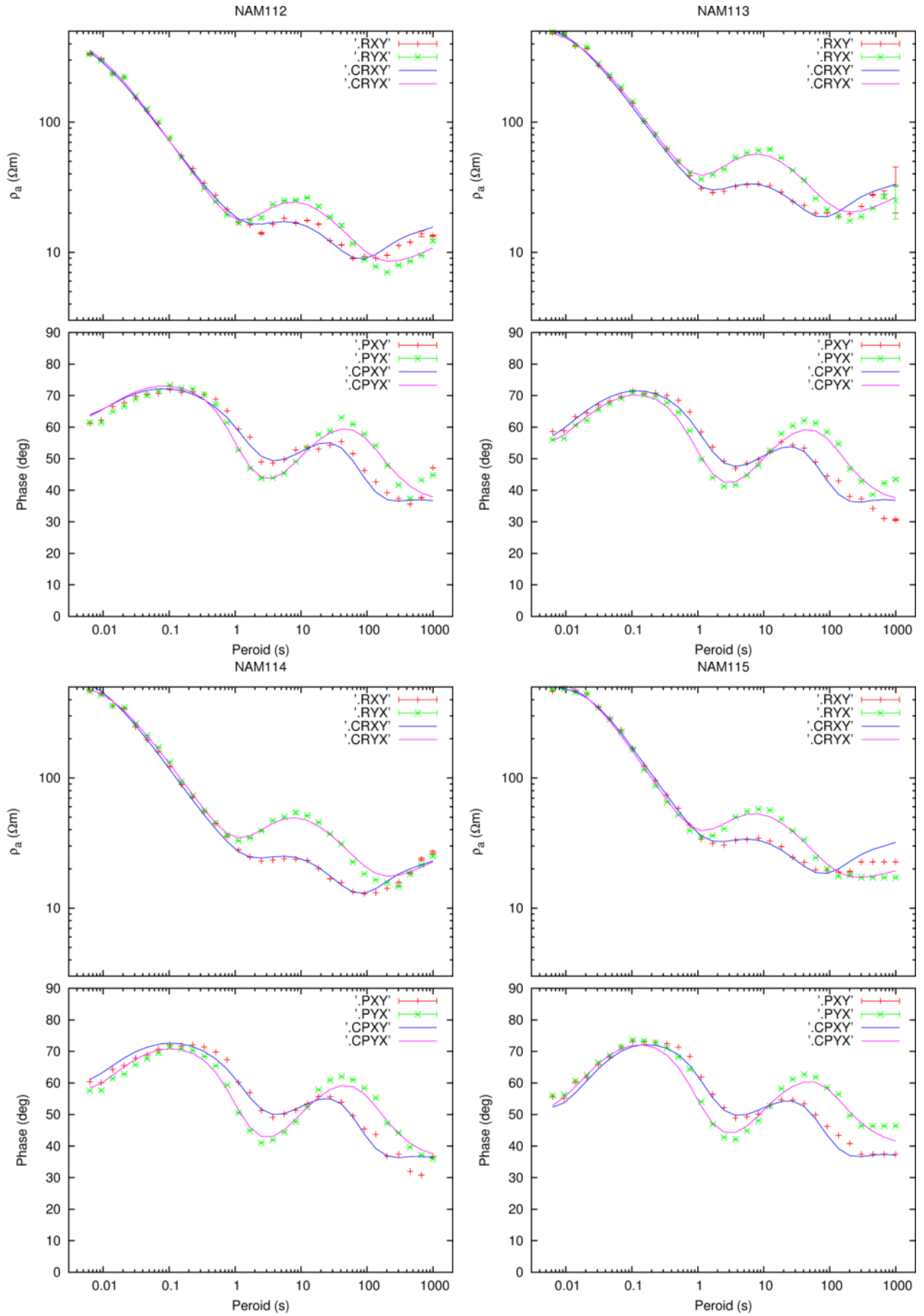


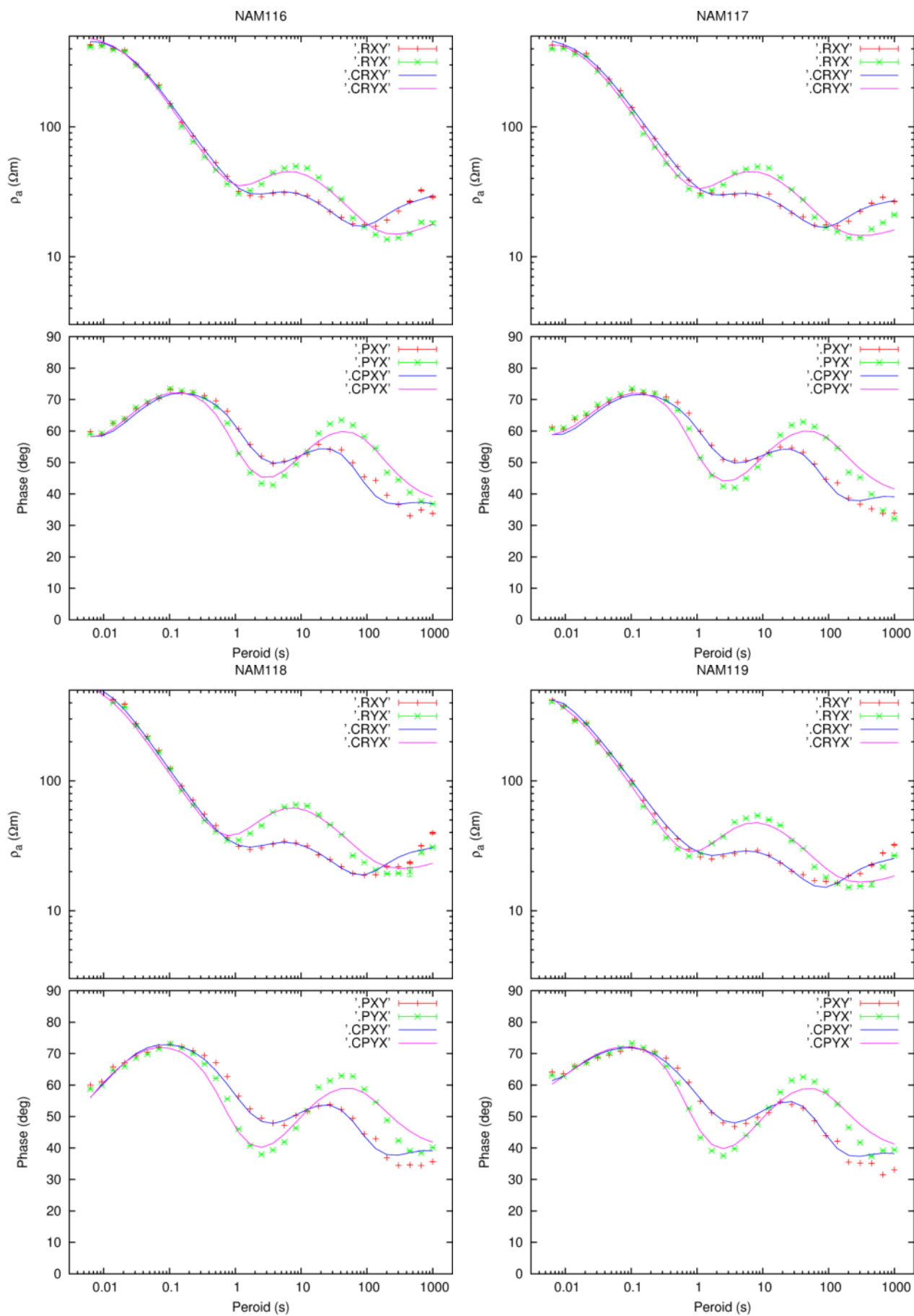


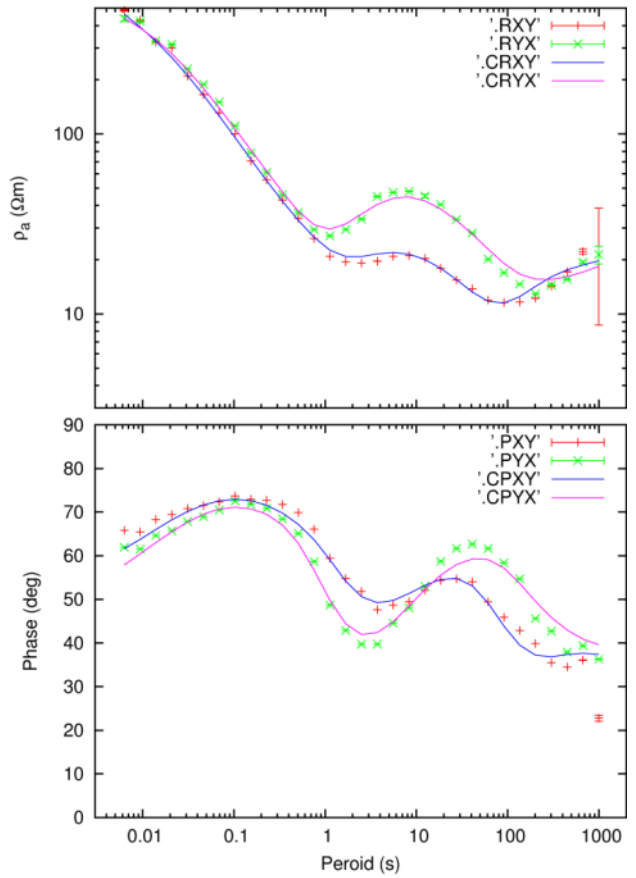
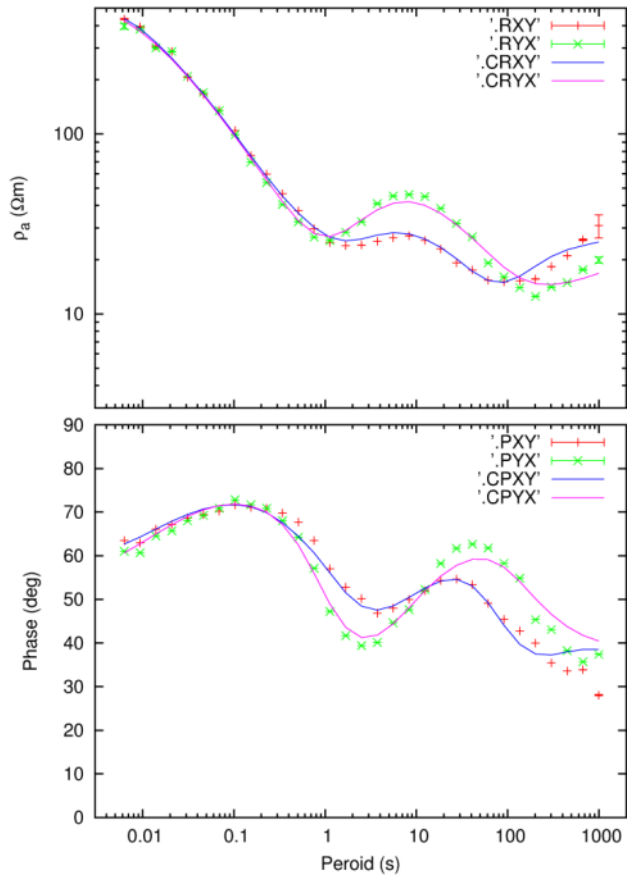
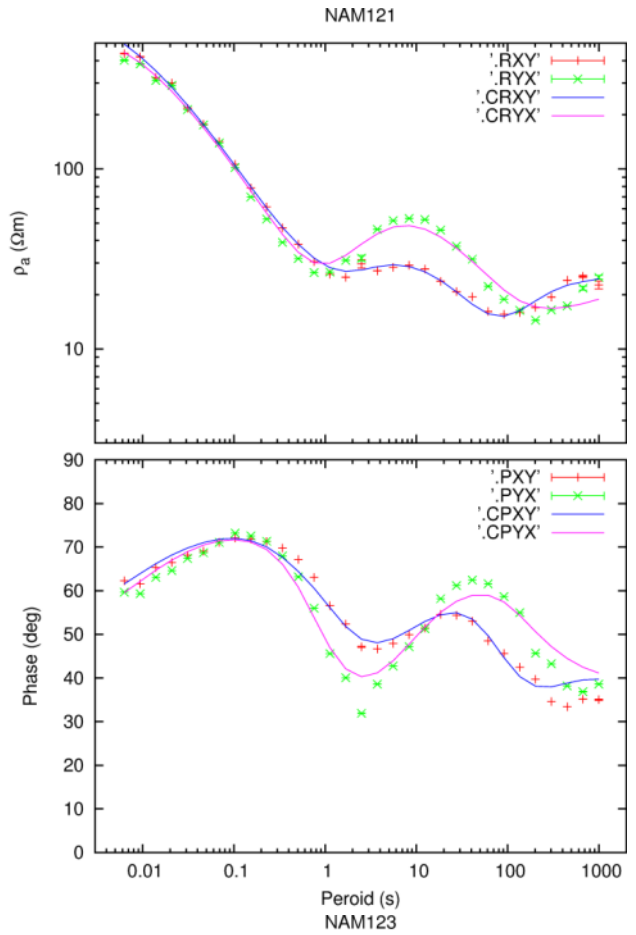
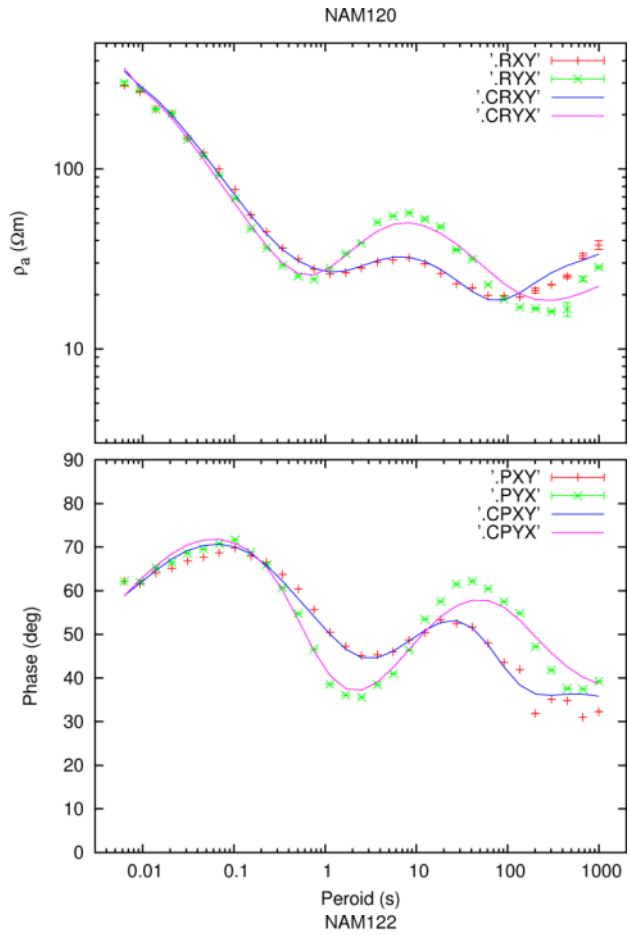


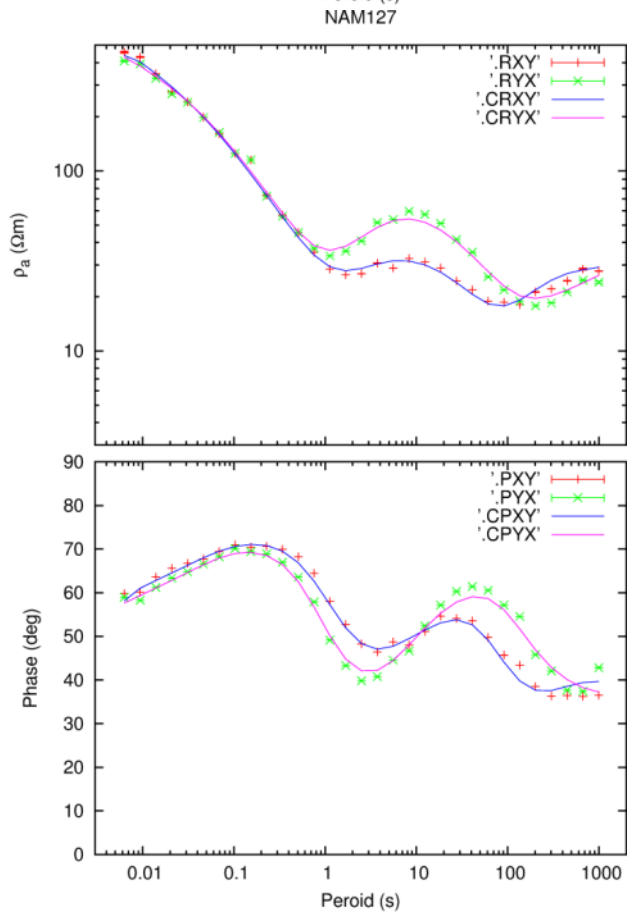
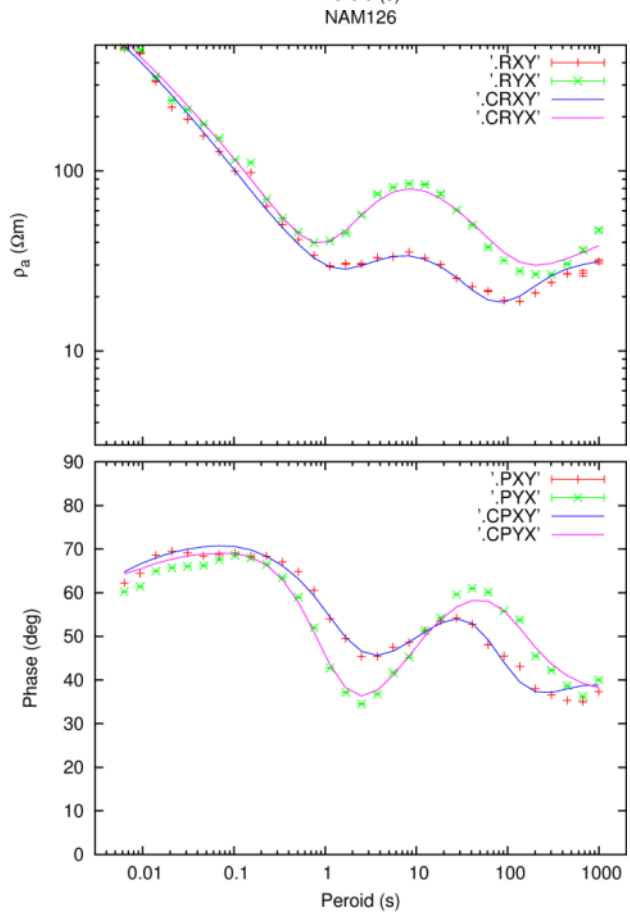
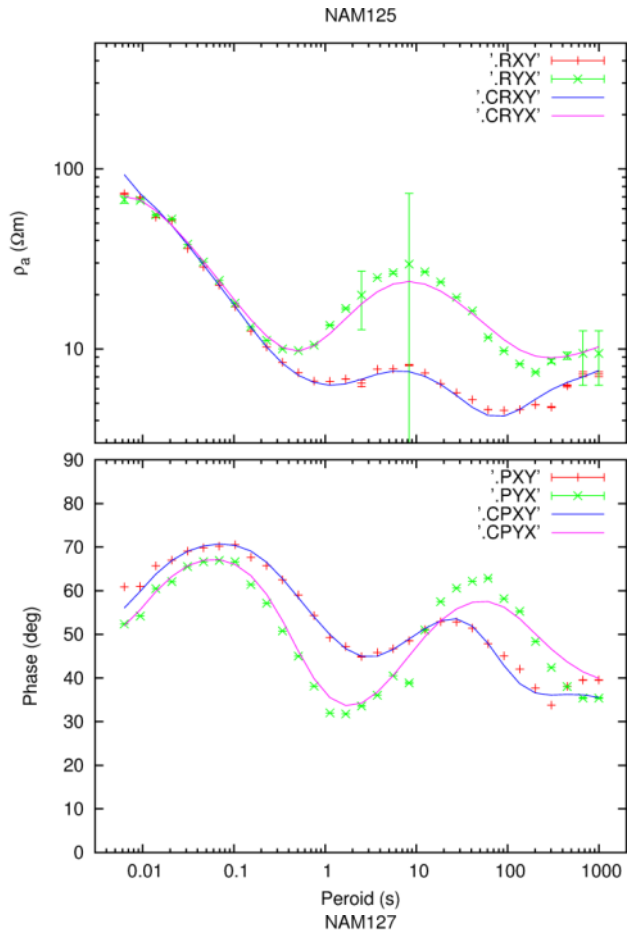
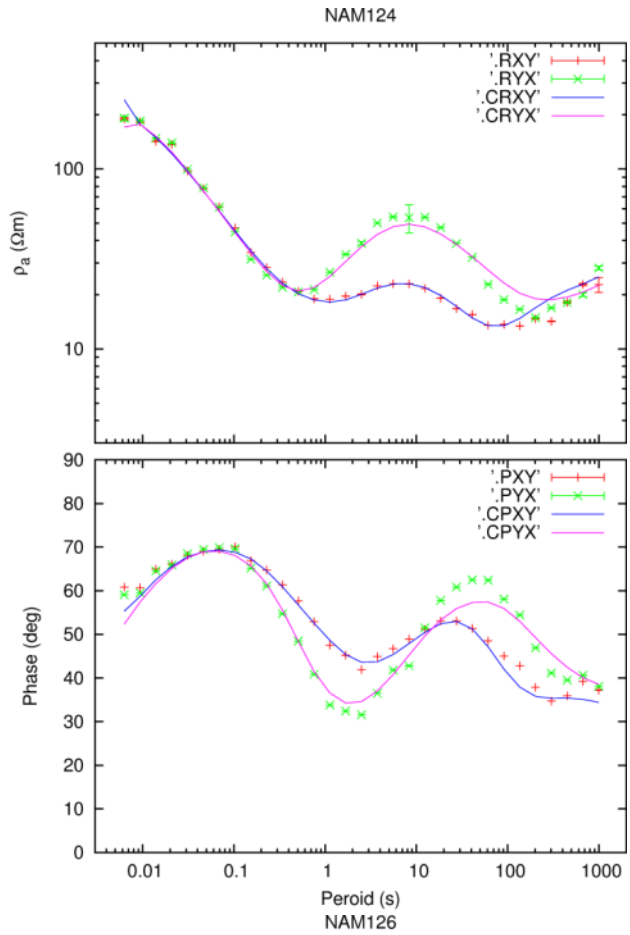


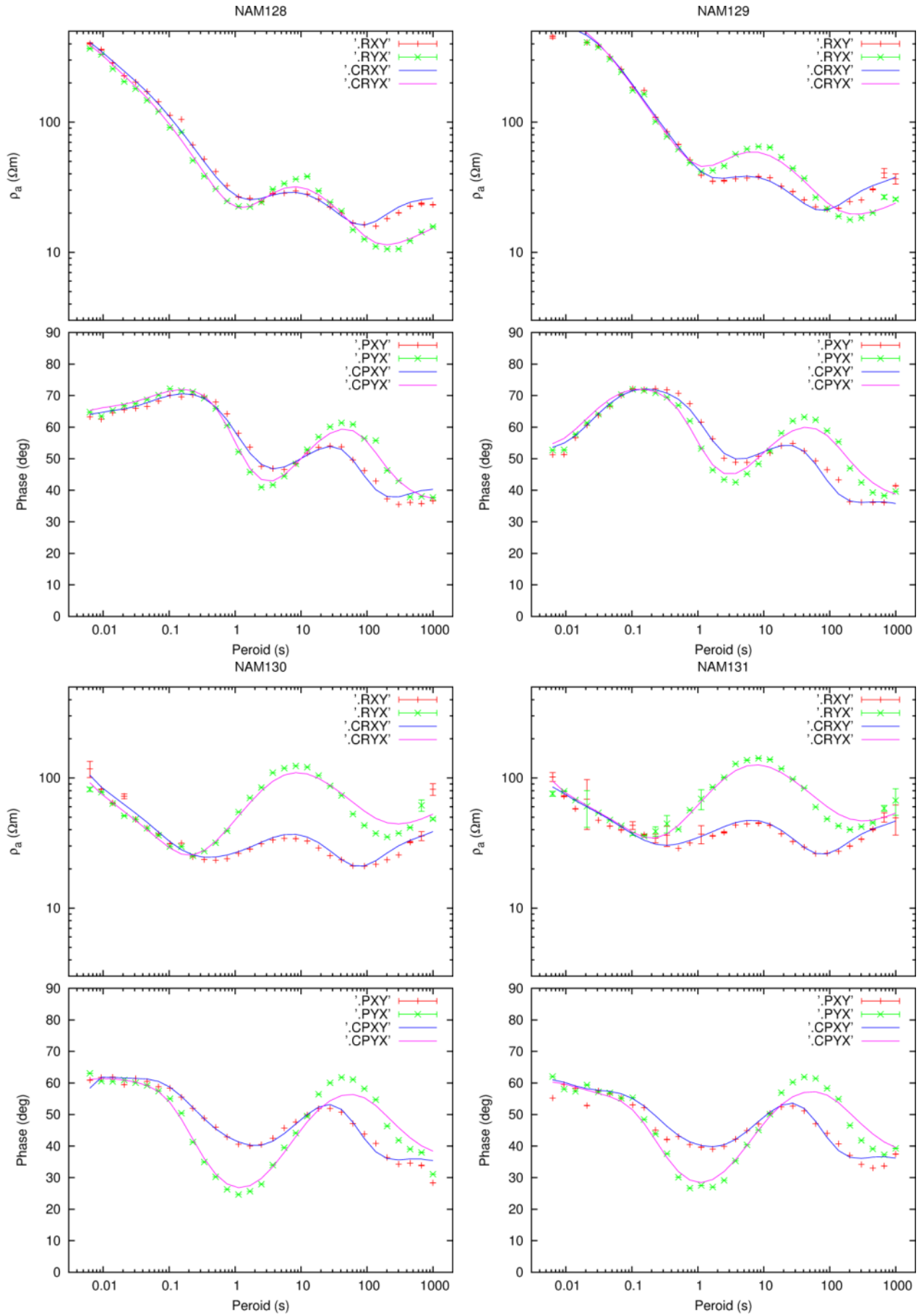


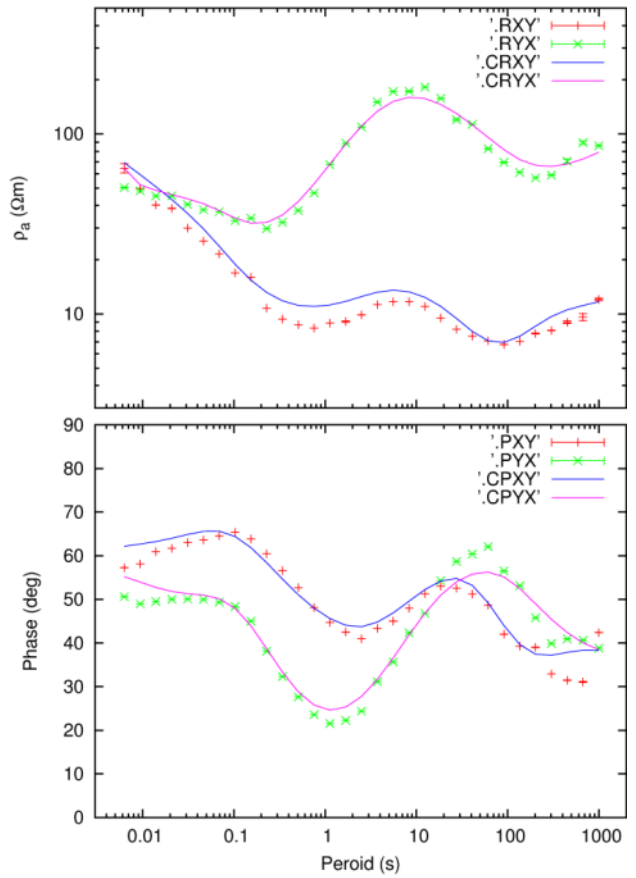
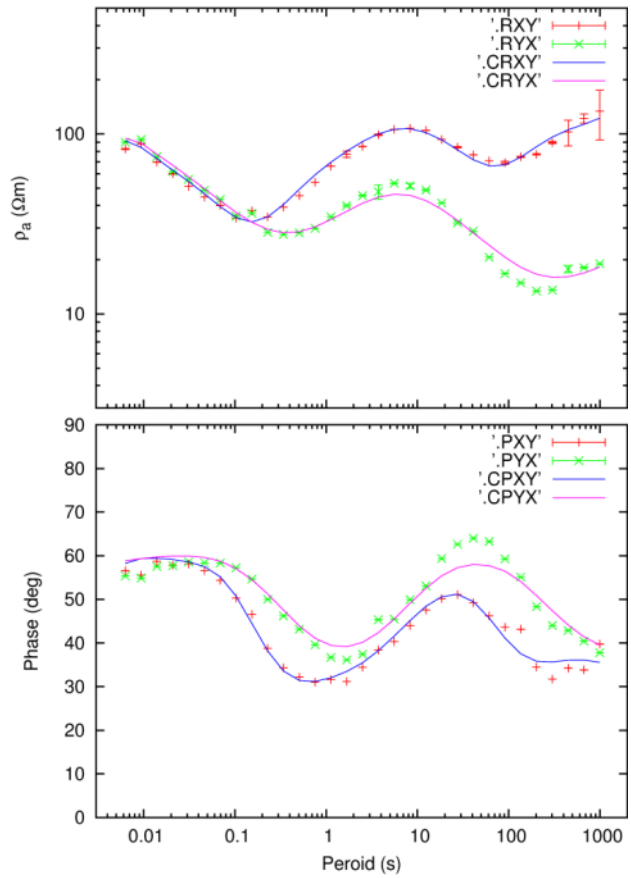
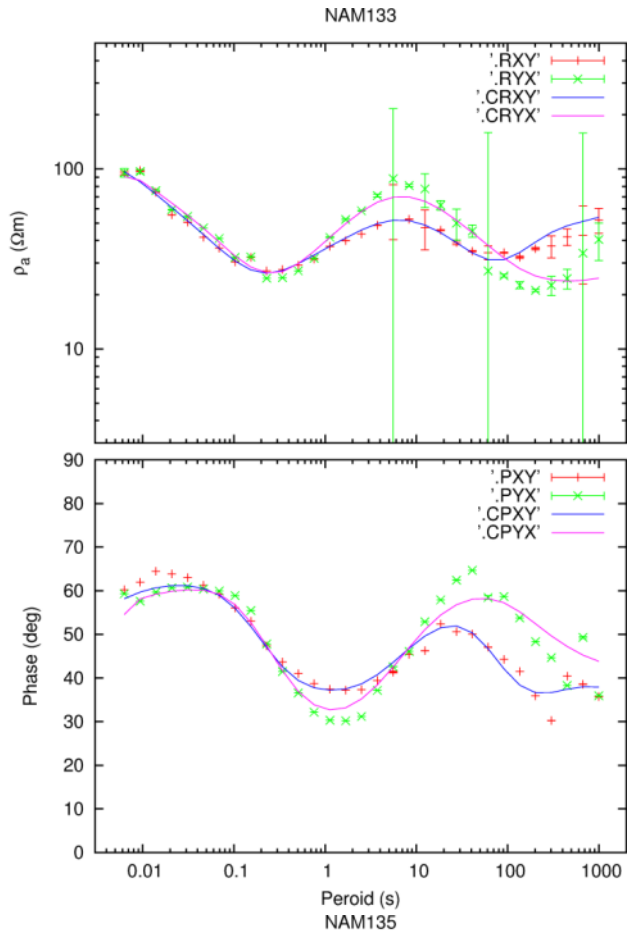
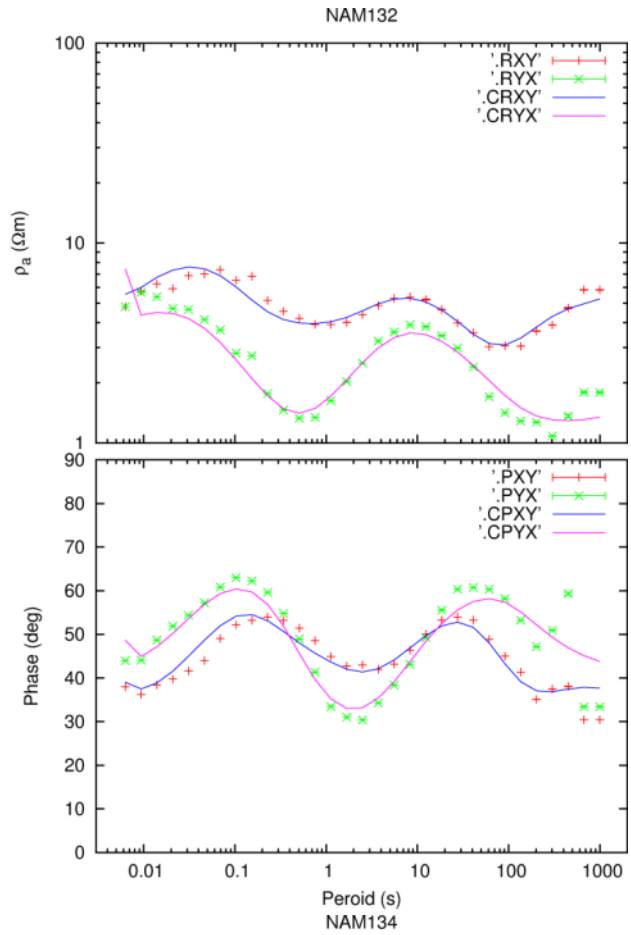




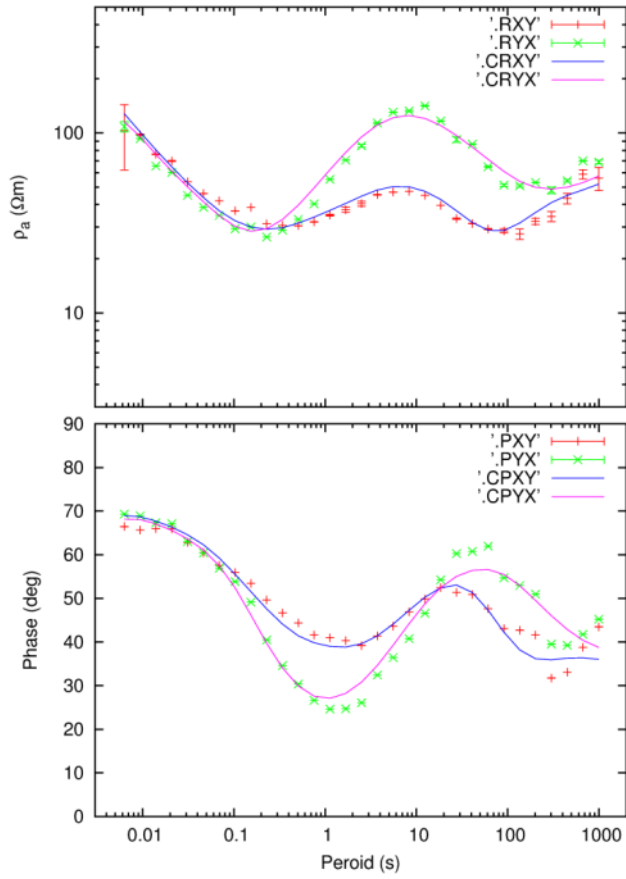








NAM136





Landsvirkjun

Háaleitisbraut 68
103 Reykjavík
landsvirkjun.is

landsvirkjun@lv.is
Sími: 515 90 00

